Fatigue Endurance of Steel Structures Subjected to Corrosion

By

Reza Rahgozar

A thesis submitted to the University of Bristol in accordance with the requirements for the degree of Doctor of Philosophy in the Faculty of Engineering, Department of Civil Engineering.

April 1998

Abstract

There are over a thousand steel girder bridges of short and medium span in the UK, many of which are more than 50 years old. Maintenance of these structures is not of a uniformly high standard and many examples may be found where the paint system has broken down and there is visible evidence of corrosion. Apart from fatigue, corrosion is the most important degradation mechanism in determining the remaining life of steel bridges. The results of this deterioration can range from progressive weakening of a bridge structure over a long period of time to sudden bridge collapse. Localized corrosion such as pitting can act as micro-notches which give rise to stress concentration and may reduce fatigue life severely compared with uniform corrosion. In this research, the effects of pitting corrosion are reviewed along with how this form of corrosion affects the fatigue endurance of steel bridges.

Existing methods of measurement and analysis of surface roughness of corroded specimens were reviewed. A technique for roughness measurement using a displacement transducer was developed. This has advantages in its accuracy and speed of measurement. A preliminary design of this system for use on site is presented.

In this investigation thirty four samples of severely corroded steelwork were measured carefully for their depth of corrosion and corrosion pitting, and were tested under cyclic load to obtain their fatigue capacity. Because of the irregularity of a corroded surface the measured roughness was expressed as maximum roughness, R_{max}, mean roughness, R_m, and the standard deviation of roughness, S_d. These measures were found to increase linearly with depth of corrosion. The fatigue endurance of the specimens correlated well with these measures of roughness. The results were compared with the fatigue endurance of various classes of structural detail in new steelwork construction.

In order to estimate the corrosion penetration of steel girders in long-term exposure time, the factors which may increase the corrosion penetration of steelwork have been identified. Several methods for determining the average corrosion penetration and

maximum roughness were investigated. Based on the corrosion penetration function two relationships have been developed for estimating the average corrosion penetration and maximum roughness in terms of exposure time. They compare favourably with existing methods. The main aspects that are associated with stress concentration created by corrosion are reviewed and separate functions are produced for fatigue notch factor in terms of average corrosion penetration and exposure time.

A procedure was developed for calculating the cumulative fatigue damage to steel bridges affected by corrosion. The method is illustrated by application to a simply supported composite welded plate girder bridge for different maintenance and re-painting scenarios during its life. In these calculations the vehicle load spectrum in BS 5400: Part 10 was modified to take account of changes in current heavy vehicle traffic. The analysis showed that a badly maintained class B detail would have a shorter fatigue life than a well maintained class D detail. This demonstrated the importance of continued maintenance of steel bridges. In addition, a procedure was developed for calculating the reliability index over the life of the bridge. In this way, the randomness inherent in corrosion pitting and in the results of fatigue tests could be taken into account.

Acknowledgements

First and foremost, thanks go to Allah for his mercy and guidance and peace be upon his messenger.

I would like to express my sincere thanks and appreciation to my advisor, Dr J W Smith for his guidance, inspiration, friendship and financial support throughout the course of this work. Special thanks go to Dr J R Stone for his advice, assistance and serving on the first year examination committees. I would also like to thank Mr Jim Hall for his co-operation and sparing time to answer my queries. Among the technical staff, I would also like to thank Mr Pete Whereat, Mr Alun Young and Mr Roy Sansom for their assistance in conducting the experiments.

I owe special thank you to my wife, Nahid, for her encouragement, unconditional support and for taking care of our children throughout my graduate studies during the past three years. My greatest thanks must go to my daughter Pegah and my son Peyman for their patience and being alone during my work. I am very grateful to my late parents and his family for their support.

I would also like to express my gratitude to the members of my wife's family. Especially her parents Mr Mohammed Hossein Saberzadeh and Mrs Ashraf Mirkazamei. They have continually encouraged and supported me throughout my study.

The financial support provided by University of Kerman through the Ministry of Culture and Higher Education is greatly appreciated. Finally, I would like to thank my friends in Bristol who have directly or indirectly helped me in accomplishing this research.

Dedication

To the memory of my parents, the late

Mr S Rahgozar

&

Mrs R Almase

Declaration

This thesis entitled "Fatigue Endurance of Steel Structures Subjected to Corrosion" is submitted for the degree of Doctor of Philosophy in the Faculty of Engineering, Department of Civil Engineering at the University of Bristol.

The research on which this thesis is based was carried out under the supervision of Dr. J W Smith from February 1995 to April 1998. It is entirely due to the author except where otherwise acknowledged in the text and has not formed the basis for a submission for any other degree.

The following paper is based on the work described in this thesis:

1. Rahgozar R and Smith J W (1997)
   Fatigue Endurance of Steel Structures Subjected to Pitting Corrosion, Proceedings of the Fourth International Conference on Civil Engineering, Sharif University of Technology, Tehran, Iran, Vol. 1, pp. 237-246.

Signed.....

Date.....27-04-1998.....

Table of Contents

VI. DEVELOPMENT OF FATIGUE NOTCH FACTOR DUE TO CORROSION

VII. REMAINING FATIGUE LIFE OF CORRODED STEEL STRUCTURES

List of Figures

List of Tables

Notation

Symbol	Meaning
A	Area of triangle
A	Corrosion loss in first year
A_a	Actual surface area
A_n	Nominal surface area
A_s	Total surface area
a	Crack length
B	Slope of the log-log plot of corrosion penetration versus time
C	Material constants
$C(\Delta)$	Autocovariance function for a profile measured in the x-direction
D	Density
$\bar{d}$	Mean thickness
d_c	Average corrosion penetration
d_i	Thickness reading
d_{max}	Maximum thickness
d_{min}	Minimum thickness
d_p	Average pit depth
da/dN	Crack length increment per cycle
e	Constant (2.718)
e_K	Error in a single test
e_{tfd}	Error in total fatigue damage
h	Distance from the reference of profile
h_w	Depth of web
ℓ	Line segment between points
K	Constant term relating to the mean-line of the statistical analysis results
K_c	Conversion constant
K_e	Environment factor
K_{max}	Maximum stress intensity factor

K_{min}	Minimum stress intensity factor
k_{eff}	Effective stress concentration factor
k_f	Fatigue notch factor
k_{fc}	Fatigue notch factor due to corrosion
k_t	Elastic or theoretical stress concentration factor
L	Profile length
M_{max}	Maximum bending moment
m	Inverse slope of the mean-line log σ_r - log N curve
N	Number of cycles to failure
$N(t)$	Number of cycles to failure in terms of exposure time
n	Total number of measurements
q	Notch-sensitive factor
R	Gas constant
R_a	Average roughness
R_ℓ	Roughness parameter
R_L	Large radius of the ellipse
R_m	Mean roughness
R_{max}	Maximum roughness
$\overline{R_{max}}$	Mean of maximum roughness
R_o	Radius at the end of major axis
R_S	Smaller radius of the ellipse
$R(\tau)$	Autocovariance function normalised by the profile sample variance
R_z	Average difference between the highest and lowest peaks on the profile
r	Number of load application per year
P	Perimeter of triangle
$P(\omega)$	Power spectrum of the profile
S	Standard root-mean-square
S_1	Root-mean-square of the first derivative of the surface profile
S_2	Root-mean-square of the second derivative of the surface profile
S_3	Sum of the distances along the profile
S^2	Square of the r.m.s roughness
S'	Slope of root-mean-square

S''	Curvature root-mean-square
S_d	Standard deviation of roughness
S_K	Standard deviation of log K
S_M	Standard deviation of the margin
S_R	Standard deviation of resistance
S_S	Standard deviation of stress
S_{tfd}	Standard deviation of total fatigue damage
T	Time interval
T	Geometric mean panel temperature when wet
t	Time of exposure
$\bar{t}$	Mean thickness
t_i	Thickness measurement
t_o	Original thickness
t_{wet}	Time of panel wetness
W	Mass loss
w	Width of the specimen
Y	Geometrical factor
Z	Level of adjacent pixels
z	Surface height from the mean line
$z(x)$	Surface profile in the x- direction
β	Reliability index
μ_M	Mean margin between resistance and applied stress
μ_R	Mean resistance
μ_S	Mean stress
μ_{tfd}	Mean of total fatigue damage
σ_a	Stress amplitude
σ_m	Mean stress
σ_{max}	Maximum stress
σ_{min}	Minimum stress
σ_r	Stress range
$\sigma_{r,B}$	Stress range for class B

$\sigma_{r,x}$	Stress range for class x
$(\sigma_{r,x})_c$	Stress range applied to the corroded specimen in the plane of crack
σ_u	Ultimate stress at maximum load achieved.
σ_y	Yield stress
Δ	Delayed interval
ΔK	Range of the stress intensity factor
ΔK_{eff}	Effective stress intensity factor range
ω	Frequency
ω_h	High frequency
ω_L	Low frequency

Abbreviations

Symbol	Meaning
AASHTO	American Association of State Highway and Transportation Officials
ASM	American Society for Metals
ASTM	American Society for Testing and Materials
FD	Fatigue Damage
HSLA	High Strength Low Alloy
LVDT	Linear Variable Differential Transducers
TFD	Total Fatigue Damage
TRRL	Transport and Road Research Laboratory
UB	Universal Beam

CHAPTER I

INTRODUCTION

1.1 Problem statement

Corrosion of steel structures is a serious problem throughout the world. Kayser et al (1987)[1] pointed out that a large number of the approximately 570,000 United States bridges are constructed with steel superstructures. Many of these bridges are undergoing deterioration due to corrosion. This corrosion is caused by an aggressive environment and inadequate maintenance. The maintenance of steel bridges around the world is not of a uniformly high standard and many examples may be found where the paint system has broken down and there is visible evidence of corrosion as shown in Figure 1.1.

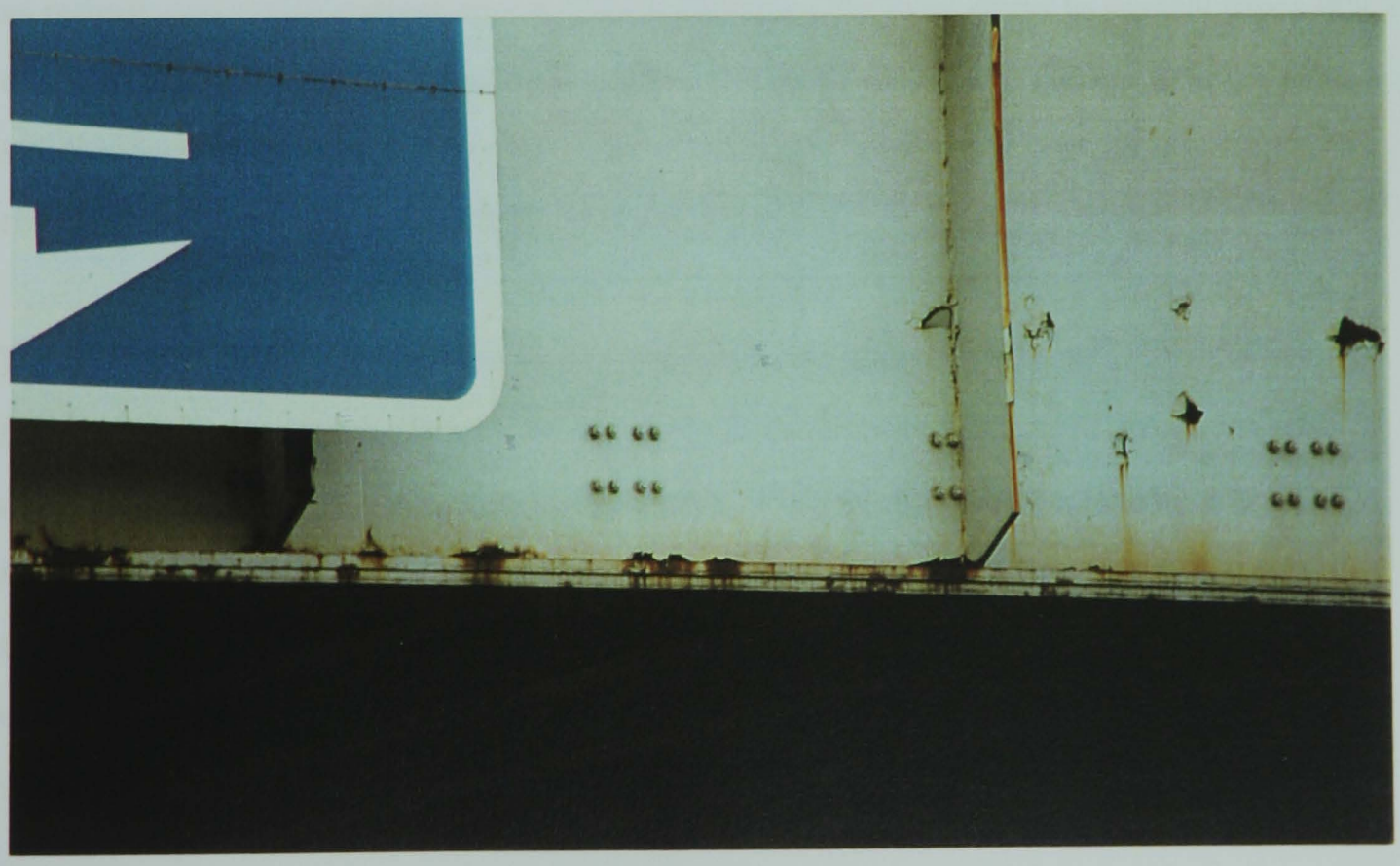

Figure 1.1 Photograph showing how the paint system has broken down.

The monetary costs of bridge rehabilitation and replacement due to unabated corrosion on the entire transportation network are very high and will become even more so in the future. In both the United States and in the United Kingdom, for example, the cost of corrosion has been estimated to be around 3% of the gross national product, if all the costs are included (Scully 1990). At the same time, in most countries government resources available for the infrastructure are severely limited. It is estimated that in the United States alone it will cost about 50 billion dollars to upgrade all the bridges to an adequate condition (Federal Highway Administration 1984).

Apart from fatigue, corrosion in steel bridges appears to be the most important degradation mechanism in determining the remaining life of these structures. Many steel bridges have exceeded 50 years of service life and are often in a severely deteriorated condition. Corrosion can have many detrimental effects on steel bridges. The most common effect of corrosion is the general weakening of structural members through loss of metal, which can be worse in aggressive environments such as industrial and marine areas. Recently, a bridge inspector in the UK reported that the corrosion in steel bridges tends to be worst on the bearing seats, at the webs and bottom flanges where water runs through from the road surface (Cygnus Instruments 1996). Localized corrosion, such as pitting, can create a stress concentration elevating the local stress to several times that of the global stress field. It has been pointed out by Smith (1993) that corrosion causes a small reduction in the ductility of the material and the presence of corrosion pitting reduces the effective yield strength by about 3 percent.

Deterioration of a steel structure due to corrosion can alter its stiffness and behaviour (Hearn and Testa 1991). Therefore, the analysis of corrosion damaged structures may differ from analysis of a structure under design. For example, the thinner webs and flanges may affect the critical failure mode. Some of the assumptions made in design may no longer be true and other failure mechanisms may become significant. The damage resulting from corrosion can have catastrophic effects on the performance of individual steel bridges.

Corrosion can produce other severe effects such as: locking of pinned joints which may cause unintended bending moments in members; locking of bearings which may lead to large forces in piers, abutments, and other members; and the build up of corrosion products causing local forces and distortions transverse to the normal load carrying direction. This last effect has been blamed for the Mianus River Bridge failure in the United States (Anon 1984)[1].

Matsumoto and Okada (1994) reported that the effectiveness of the paint system to protect steel bridges from corrosion depends on the paint system material and environmental factors. Dutems (1987) in France indicated that bridges should be painted every 7 years, and that long painting-cycles (greater than 15 years) could result in major corrosion damage. He also indicated that on the average a bridge is painted every 22 years. These painting cycles in France are comparable to the typical painting cycles of bridges in Michigan. Up to 1986, the State of Michigan was on a one hundred year paint-cycle (Burrill 1986). For all practical purposes, no painting was provided for steel bridges during their service life.

Apart from painting-cycles, in most specifications there are no established procedures for taking into account corrosion effects in steel and reinforced concrete bridges. The assessment of corrosion deterioration and the related remaining fatigue life of steel bridges are evidently important for the evaluation of bridge safety and reliability. The necessity to determine the remaining fatigue life of existing bridges has been spurred by catastrophic failures such as the collapses in the United States of the Point Pleasant Bridge over the Ohio River in 1967 (Hopwood and Havens 1984) and the Mianus River Bridge on Interstate 95 in Connecticut in 1983 (Kulicki et al 1990).

Presently, highway bridge engineers are handicapped by not having at their disposal a means to assess the extent to which ageing and long-term exposure have affected the remaining life in steel bridges. To date, evaluating the remaining fatigue life of existing steel bridges is considered a serious problem. The research reported herein addresses these issues.

1.2 Importance of the problem

The assessment of deteriorated steel structures has been achieved by widely varying procedures. Grattesat (1982) concluded that average life expectation is not sufficient to evaluate remaining life and commented that the present state of knowledge is insufficient to evaluate precisely the remaining life of bridges. Hirt (1982) emphasized that no unique or generally applicable evaluation method exists or has been agreed upon and more work is needed to establish such methods. Lichtenstein (1983) has stated that no scientific methods or formulas are available to assess remaining useful life.

Loss of thickness due to corrosion, and its effect on static capacity has been noted by Kayser and Nowak (1987)[2] in the USA and by Sarveswaran (1996) in the UK. The effect of corrosion on the fatigue capacity of steel bridge beams was considered by Albrecht et al (1990). Experimental studies have been carried out on the fatigue behaviour of corroded bridge girders (Zuraski 1986) and extensive research has gone into the performance of weathering steel (Albrecht and Naeemi 1984). Kulicki et al (1990) have suggested a method by which the remaining fatigue life of corroded structural members may be estimated on the basis of visual inspection. This visual estimation is in terms of percentage loss in the cross sectional area of the member. Note that the fatigue life may not be estimated accurately from the results of visual examination alone. The amount of pitting extending under the dense oxide cannot be evaluated accurately visually. He also mentioned the possibility of removing minor non-critical specimens for testing etc. Even in case of removing minor specimens from an existing bridge, they may not have the same condition as the specimens have at the critical regions. Another visual observation was carried out by Matsumoto and Okada (1994) in order to evaluate the corroded states and residual life of steel bridges by considering several environmental factors such as temperature, humidity, precipitation, SO_2 density and sea-salt particles.

The need to evaluate remaining fatigue life of bridges will become more acute because leaders in the field of bridge engineering and construction foresee that the rehabilitation of old bridges is a feasible alternative to new construction, primarily due to cost. Elliott

(1969) said that "the sizeable reserve of strength that has been built into our older structures provides a basis for a glimmer of optimism with regard to their future performance in the face of higher loads and material deterioration". In any event, there is probably no choice with regard to allowing deteriorating bridges to remain in service. Economists Choate et al (1981) and engineers from National Cooperative Highway Research Program (1982) and Federal Highway Administration (1982) agree that it will be impossible to replace all the deficient bridges in the near future. Effective decisions will be required.

1.3 Proposed study and layout of the thesis

The work of Albrecht was a useful introduction to research on the problem which was explained in the previous section. However, as yet there is no simple relationship between the magnitude of structural defects due to corrosion (e.g. corrosion pitting) and the corresponding reduction in fatigue life. There is an urgent need for this information in order to prevent damage and collapse of corroded steel bridges. Therefore, work has yet to be done on determining the performance and behaviour of corroded steel structures. As a consequence, the study of remaining fatigue life of corroded steel bridges has now become an important issue.

It is important to extend the previous researches which employed specimens weathered for several years to the studies of specimens that were weathered for several decades. At present, fatigue test data are available for small scale tensile specimens that were weathered in the USA for a maximum of eight years under ideal conditions (Albrecht and Sidani 1987). They show large reductions in fatigue life. Because of the short exposure time one cannot yet predict the reduction in fatigue strength that may occur towards the end of design life of a steel structure. Long-term exposure data are needed and these can be generated by steel beams in existing structures that have already been weathered for long periods.

The overall aim of this thesis is to examine and investigate the effect of fatigue and corrosion during decades of service history on the remaining fatigue life of steel bridges. The specific objectives are as follows:

1. To understand the nature of corrosion, more specifically corrosion pitting, and to study its effects on steel structures particularly steel bridges (Chapter 2).

2. To review surface roughness; to discuss the existing techniques for its measurement and analysis; to propose and investigate the accuracy of the method adopted in this study; to measure surface roughness of corrosion damaged specimens in the laboratory; to determine the relationships between pitting and overall depth of corrosion by expressing the irregularity of the corroded surfaces in terms of maximum roughness, R_{max}, mean roughness, R_m, and the standard deviation of roughness, S_d (Chapter 3).

3. To enhance understanding of the factors which may have an effect on the corrosion penetration of steelwork; to investigate and determine the parametric values of the corrosion penetration function from previous research carried out in the UK; to develop a function for corrosion penetration due to pitting corrosion on the basis of pit depth measurements obtained from corroded steelwork in this study; to make a comparison between the results of the empirical formula produced in this study and the relationships developed by Copson (1960) and Albrecht et al (1990) for average maximum roughness and to carry out a statistical analysis of the maximum roughness measurements (Chapter 4).

4. To review the fatigue concepts; to carry out fatigue tests on the corroded specimens; to investigate the fatigue capacity of corroded steelwork compared with the normal fatigue life of various classes of structural detail as classified in BS 5400, the UK code for fatigue design, and to consider the application of the results for existing corroded steel bridges (Chapter 5).

5. To develop functions which could represent the fatigue notch factor in terms of average corrosion penetration and exposure time by using different detailed thickness measurements such as the maximum roughness and the standard deviation of roughness (Chapter 6).

6. To develop separate relations for fatigue life of members or components subjected to corrosion in terms of maximum roughness and exposure time; to develop a procedure for estimating the cumulative fatigue damage of a bridge subjected to realistic traffic loading during its life and subject to intermittent paint protection; to consider the application of structural reliability analysis to the assessment of corrosion damaged steelwork (Chapter 7).

7. To summarise the outcomes of this research project (Chapter 8).

CHAPTER II

CORROSION OF STEEL STRUCTURES

2.1 Introduction

Refined metals are used extensively throughout the modern world. They serve as the skeletons on which we build our bridges, buildings and factories (Kayser 1988). The most frequently used metals (iron, aluminium and zinc) are found in nature in the form of ore. A great deal of energy must be expended to release or reduce the ore to the metallic state, and this energy is essentially stored in the metal. Because of the fact that all configurations in nature tend to spontaneously change to lower states of energy, refined metal will deteriorate. Corrosion of metals could be considered as extractive metallurgy in reverse as illustrated by Figure 2.1. Extractive metallurgy is concerned primarily with winning of the metal from the ore and refining or alloying the metal for use. Most iron ores contain oxides of iron, and rusting of steel by water and oxygen results in a hydrated iron oxide. Rusting is a term reserved for steel and iron corrosion, although many other metals form their oxides when corrosion occurs.

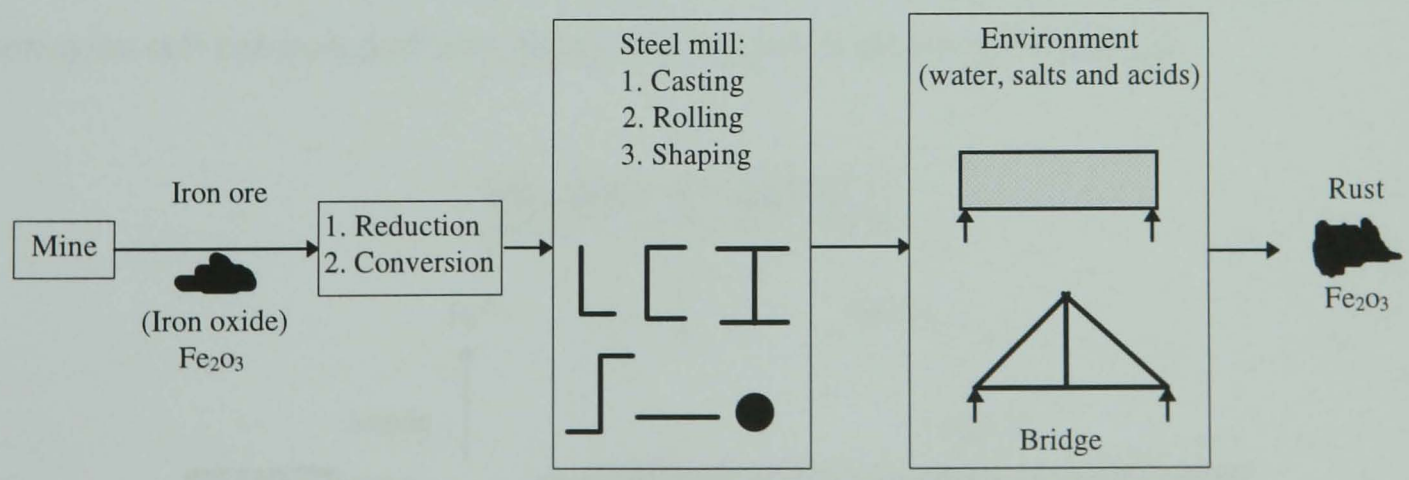

Figure 2.1 Steel life cycle.

In the atmosphere any metal will cover itself with a thin, usually invisible, film of condensed water, even at relative humidities of less than 100%. The moisture film enables the transport of electrons and is called an electrolyte. Corrosion may start when the relative humidity of the air exceeds around 65% (Stewart et al 1968 and Knoefel 1978). This chapter will discuss the mechanism and consequences of corrosion.

The specific objectives of this chapter are:

1. To review the case histories of corrosion on steel bridges.
2. To investigate the deterioration process of steel.
3. To study the various types of corrosion and their characterisations.
4. To consider the effects of corrosion on steel structures such as bridges.

2.2 Electrochemical reaction

The corrosion of steel is an electrochemical process which involves the movement of electrons and ions in a reaction. It requires steel, an electrolyte, and current flow. An electrolyte which allows current flow must be in contact with the anode and cathode for corrosion to occur. On bridges, this electrolyte is usually water with additional contaminants such as salt or acid. Electrons flow through the base metal from the anode to the cathode. Corrosion occurs at the anode as negative charges leave the anode, positively charged ions of the anode metal are released into the electrolyte. These ions can react with other materials to form the "corrosion product". A simple example of a corrosion cell composed of iron, water, and oxygen is shown in Figure 2.2.

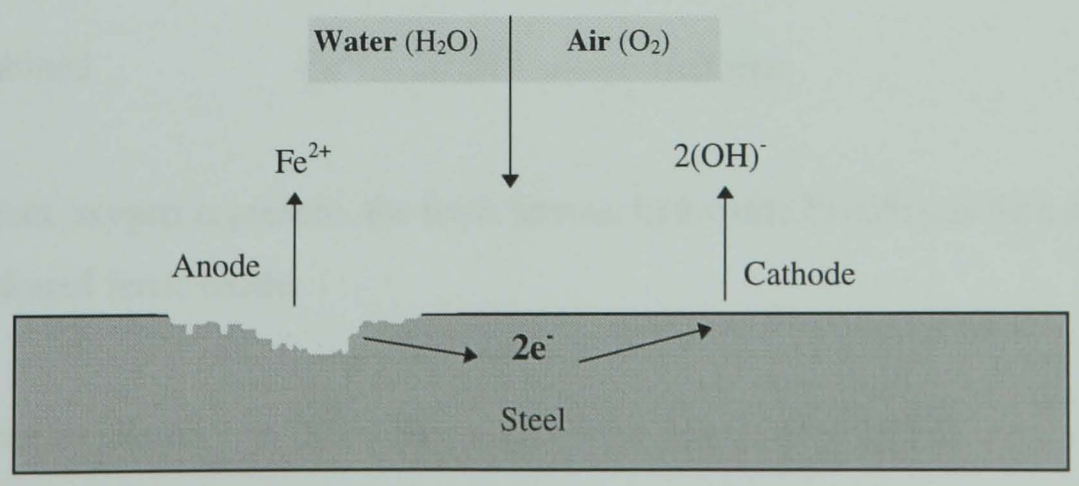

Figure 2.2 Simple process of the corrosion of steel.

Metal loss occurs at the anode, while the cathode is undamaged. Usually different areas on the same steel member can serve as anodes or cathodes because of differences in chemical or metallurgical structure, stresses, or the presence of corrosive deposits. It is possible for an area that is initially cathodic to become anodic, and even reverse back to cathodic again.

In the initial attack under humid conditions in a clean rural atmosphere, the first oxidation product is ferrous ion (Fe^{2+}) in the lowest oxidation state. Because of the presence of air dissolved in moisture, ferrous hydroxide $Fe(OH)_2$ can be quickly oxidised further to the ferric state (Fe^{3+}), to give the gelatinous precipitate of ferric hydroxide. This series of reactions can be expressed in a way suggested by Albrecht et al (1984) such as:

1) The anodic iron dissolves in the condensed moisture film.

at the anode $\quad Fe \longrightarrow Fe^{2+} + 2e^{-}$ $\quad (2.1)$

To counter-balance this reaction, the cathode accept the electrons and passes them on to the oxygen which is converted to the hydroxyl ion $(OH)^{-}$.

at the cathode $\quad O_2 + 2H_2O + 4e^{-} \longrightarrow 4(OH)^{-}$ $\quad (2.2)$

2) With free ferrous ions (Fe^{2+}) and free hydroxyl ions $(OH)^{-}$ in solution, the following reaction occurs:

combined $\quad Fe^{2+} + 2(OH)^{-} \longrightarrow Fe(OH)_2$ $\quad (2.3)$

3) If sufficient oxygen is present, the fresh ferrous hydroxide $Fe(OH)_2$ is then oxidised to produce hydrated ferric oxide.

further oxidation $\quad 2Fe(OH)_2 + O_2 \longrightarrow 2FeOOH + 2(OH)^{-}$ $\quad (2.4)$

The following reactions may take place instead of those listed in steps 2 and 3. The final product in both cases is hydrated ferric oxide.

combined $\quad Fe^{3+} + 3(OH)^{-} \longrightarrow Fe(OH)_3 \qquad (2.5)$

dehydration $\quad 2Fe(OH)_3 \longrightarrow 2FeOOH + 2H_2O \qquad (2.6)$

Where 2FeOOH can also be written as $Fe_2O_3.H_2O$, and this form of corrosion product is commonly known as yellow rust which contains entrained water.

4) When the supply of oxygen is not sufficient, the reaction take place according to equation (2.7) instead of equation (2.4):

further oxidation $\quad 6Fe(OH)_2 + O_2 \longrightarrow 2Fe_3O_4 + 6H_2O \qquad (2.7)$

Where Fe_3O_4 is another type of corrosion product which consists of black anhydrous magnetite.

Pearce (1997) pointed out that gradually a scab of rust ($Fe_2O_3.H_2O$) may form over the top of the pit but this is too porous to completely block the anodic area and the corrosion process will continue, resulting in deeper attack and a widening of the anodic area as the surface oxide film breaks away due to undermining, or is dissolved due to local increases in hydrogen ion concentration as hydroxyl ions become associated with ferrous ions.

If the pH of the solution in contact with the steel is low, for example dilute solution, then the surface oxide film will be removed and the cathodic reaction will be different; hydrogen gas will be liberated as gradual dissolution of the steel occurs:

$$H_2 \longrightarrow 2H^{+} + 2e \qquad (2.8)$$

With oxidising acids, a number of alternate cathodic reactions may take place (Evans 1963). In all cases of corrosion, as shown in reactions, two important points emerge:

i) for iron or steel to corrode it is necessary to have the simultaneous presence of water and oxygen; in the absence of either, corrosion does not occur.

ii) all corrosion occurs at the anode; no corrosion occurs at the cathode.

2.3 Types of corrosion

Corrosion may appear in many forms. These types are classified according to how the corrosion attacks the metal. Corrosion ranges from uniform corrosion, which can be identified visually, to stress corrosion, which cannot be identified without the microscope. In general, several types of corrosion may be present simultaneously on the surface of a steel member. The types of metal corrosion which occur in steel bridges are uniform corrosion, pitting corrosion, crevice corrosion, stress corrosion, corrosion fatigue, and galvanic corrosion. These forms are not listed in any particular order of importance. However, valuable information for the solution of a corrosion problem can often be obtained through careful observation of the test specimen, corroded members, or failed structures.

2.3.1 Uniform corrosion

Uniform corrosion or general corrosion is the most common type of corrosion, where metal oxidation take place uniformly over the complete exposed surface. This form of corrosion, accounts for the greatest destruction of metal (Fontana 1987). The process of this type of corrosion involves the formation of microscopic corrosion cells, distributed uniformly on the surface. It has been pointed out by Kulicki et al (1990) that uniform corrosion of steel typically consists of many small pits joined together. A typical example of general corrosion is the brown rust which develops on exposed unpainted steel. On steel bridges, it can observed as a uniform rust over the entire surface. With the thinning of a paint system, the peaks of metal are exposed and a coating of rust or corrosion occurs.

Usually uniform corrosion results in reduction of member cross-section, hence increased stresses and consequently reduced fatigue life. The rates of corrosion may seem negligible on a yearly basis, although over the lifetime of a bridge significant material loss can occur. This type of corrosion can be a specially serious problem when it occurs on a compression member such as beam web near a support because the critical mode of failure may change. Uniform corrosion is most commonly found on steel bridges or plates and shapes with large surface areas that can be uniformly attacked or oxidised, which may dry quickly, and preventing other forms of corrosion attack. Such members include webs of steel girders, vertical stiffeners, and truss verticals and diagonal members of bridges. The rate of uniform loss is highly variable, depending on conditions such as temperature, time of wetness, and chemistry (Guttman et al 1968). These conditions themselves depend upon local industrial activity and micro-climates. This type of corrosion from the technical standpoint can be accurately evaluated by the methods of weight loss for a specimen or thickness measurement for a member.

Uniform corrosion can be prevented or reduced by applying a number of methods:

(1) using proper materials with coatings,

(2) using cathodic protection,

(3) using inhibitors.

Uniform corrosion has become a particular problem with weathering steel bridges (McKenzie 1978, Albrecht et al 1984, and McCrum et al 1985). Weathering steel utilises the alloying effect of copper, phosphorus and nickel to resist corrosion. In order for the weathering steel to be effective, the following conditions must be present:

1) no salt or acid contamination,

2) periodic wetting and drying,

3) occasional washing of the surface with clean water.

Under ideal conditions, weathering steel will form a dense adherent rust or patina. This dense oxide will impede further ingress of oxygenated water. Unfortunately, the

conditions under which weathering steel are suited for bridge construction do not exist in many countries (Albrecht et al 1984). In the countries where a cold wet winter occurs, salt (NaCl) is often used on the roads as a de-icer. The wet salty conditions prevent formation of the patina surface. Salt also has the effect of lowering the relative humidity level at which the surface of the metal is microscopically wet. This limits the amount of drying that can take place, increasing the length of time while wet. Chloride ions, Cl^-, also promote the electrochemical dissolution of iron (Uhlig 1973). The net effect has been that weathering steel bridges are corroding at rates comparable to unpainted carbon steel bridges. Urea is now generally recommended as a de-icing agent for steel bridges.

2.3.2 Pitting corrosion

2.3.2.1 Overview

Pitting is a complex corrosion phenomenon. In pitting corrosion, initially corrosion takes place in a relatively uniform manner over the entire surface of unprotected steel that is exposed to moisture. The reaction tends to slow down as the film of corrosion products thickens. However, small variations caused by impurities can promote nucleation of corrosion attack. Potential difference over the surface results in faster corrosion at the more anodic areas leading eventually to concentration of corrosion in the form of small pits. The process accelerates as corrosion products trap moisture in the pits, acidity increases and the rate of attack increases within the depth of pit. Hence, once pits are initiated they continue to grow by a perpetuating mechanism and are difficult to detect because of their small size and concealment beneath corrosion products. Pits can be dangerous because they extend into the metal, showing little evidence of their existence. However, pitting is a type of extremely localized corrosion that takes the form of cavities in the metal surface which are confined to a point or small area. These cavities may have various shapes and sizes in diameter, but in most cases they are relatively small. The depth and shape of pits are significantly affected by the nature of the steel and by the chemical conditions in which corrosion takes place.

It has been found by Albrecht et al (1990) during a test that the pits in weathering steel beams had steeper walls and at the same times flat bottoms, while those in the carbon steel beams had a more rounded profile. Pits are sometimes isolated or so close together that they look like a rough surface (Fontana 1987). In addition, it is difficult to measure quantitatively and compare the extent of pitting because of the varied depths and numbers of pits that may occur under identical conditions. Pitting is also difficult to predict by laboratory tests because sometimes it needs a long time to show up in actual service. Moreover, corrosion pits can act as micro notches and therefore give rise to stress concentration which can reduce fatigue life severely comparing with uniform corrosion. Lindley et al (1982) pointed out that pits will form imperfections on the metal surface. These imperfections will act as stress concentrators, reducing the fatigue capacity of the metal and increasing the metal's sensitivity to cracking. Even an individual pit can perforate steel in a relatively short time. Pitting is particularly vicious because it is a localized and intense form of corrosion, and failure often occurs with extreme suddenness. However, due to the importance of this subject the following characteristics for pitting corrosion are investigated:

2.3.2.2 Pit shape & growth

A pit may be described as a cavity with the surface diameter about the same as or less than the depth. It has been noted by Fontana (1987) that pits usually grow in the direction of gravity. Therefore, most pits develop and grow downward from horizontal surfaces. Fewer start on vertical surfaces, and only rarely do pits grow upward from the bottom of horizontal surfaces. Pitting usually requires an extended initiation period before visible pits appear. This period may range from months to years, depending on both the specific metal and the corrosive electrolyte. However, once pits have started they tend to penetrate, undermine or undercut the surface of the metal as they grow. A visual examination of the metal surface may show round, elongated, or irregular openings, but it seldom provides an accurate indication of corrosion beneath the surface. Several variations in the cross-sectioned shape of pits have been taken from ASTM, G46 (1981) as shown in Figure 2.3.

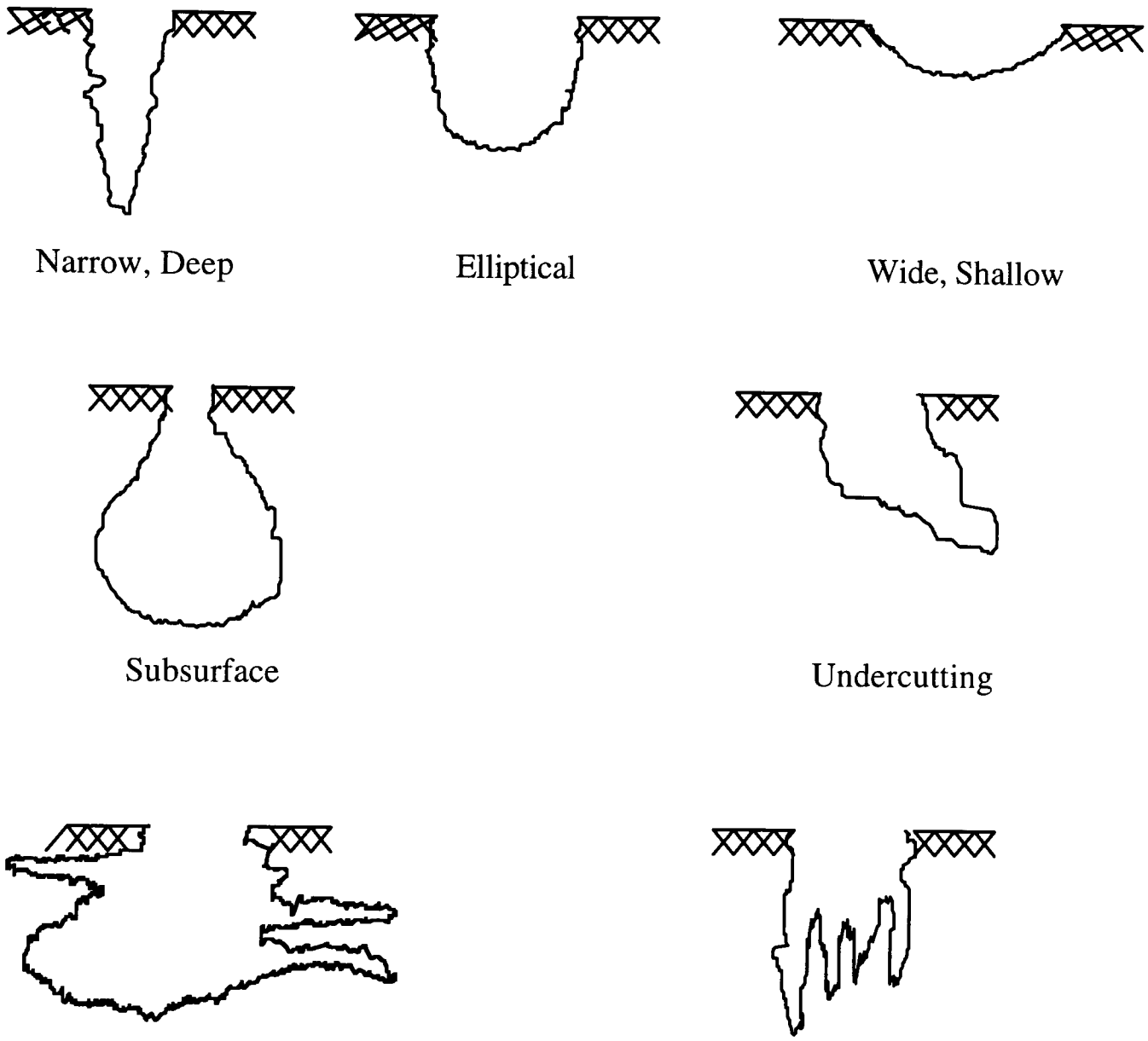

Figure 2.3 Variation in the cross-sectional shape of pits (ASTM, G46 1981).

2.3.2.3 Effect of electrolyte composition

From a practical standpoint, most pitting failures are caused by chloride and chlorine containing ions. Chlorides are present in varying degrees in most solutions made with water. In all instances, the chloride ions from de-icing salt or seawater spray are primary stimulants that accelerate pitting. Differential aeration cells, resulting from scattered deposits of damp, dirt, leaves, and oil, likewise stimulate pitting of the surface of all steels, from carbon through to stainless.

An experiment for many steel specimens has been carried out for 17 years under industrial and marine environments by Copson (1960). He used two different types of steels, these being weathering (copper steel) and carbon (low alloy steel). For all steels tested, pit depths after 17 years were two to three times the average penetration calculated from weight loss. The pitting factor which is the ratio of pit depths to average corrosion penetration for the low alloy steels was about three. Pit depths tended to increase with time in a manner similar to that of average corrosion penetration. In saltwater immersion, mill scale can cause galvanic and pitting corrosion at breaks in the mill scale (Coburn 1974). Under conditions of alternate wetting and drying, the mill scale slowly disappears due to undercutting of the scale in the cracked areas. To avoid deep pitting in locations that are continuously damp, the mill scale should be removed before the particular component of a structure is placed in service.

Pitting is commonly found on bridges where debris of any type shelters moisture on a surface, such as deposits of dirt, or bird excrement. Also it may be found where the paint protection is scratched, nicked from flying debris from vehicles, or at imperfections in the application of the paint. De-icing salt can lead to extensive pitting. Pitting can even take place under deposits of corrosion product such as packed rust. Moreover, the probability that pits will initiate on a metal surface is dependent on a number of factors, such as the pitting tendency of the metal, the corrosivity of the solution, the environmental factors of area, and the time of exposure.

2.3.2.4 Evaluation of pitting

Since pitting is a localized form of corrosion, metal mass loss cannot be used ordinarily for evaluation or comparison purposes. Metal loss is very small and does not indicate the depth of pits. Therefore, pitting damage cannot be determined accurately from mass loss. In any case, mass loss can only provide information about total metal loss due to pitting but nothing about depth of penetration.

As mentioned in ASTM, G46 (1981) there are several ways in which pitting can be described quantitatively such as metal penetration, statistical method, standard chart, and

loss in mechanical properties. Information on the use of standard chart and mechanical properties can be found in Rowe (1974) and ASTM G46 (1981). However, the two most commonly used methods are:

1) Metal penetration which can be expressed in terms of a pitting factor. It described the ratio of deepest metal penetration to the average metal penetration, determined from weight loss which can be expressed by the following relationship:

$$\text{pitting factor} = \frac{\text{deepest metal penetration}}{\text{average metal penetration}}$$

A pitting factor of one represents uniform corrosion; the larger the number, the greater the depth of penetration.

2) Statistical method: the application of statistics to the analysis of corrosion data is covered in Recommended Practice ASTM, G16 (1981). The procedures which were adopted by different authors will be explained in detail in Chapter 3 (section 3.3).

2.3.2.5 Prevention

The methods which can be used to combat pitting corrosion are:

a) using alloys with special additions to increase the resistant of metal to pitting,
b) using cathodic protection
c) avoiding re-entrant corners,
d) designing details for easy discharge of water,
e) sloping horizontal surfaces longitudinally or transversely,
f) using solid non-absorbent gaskets, such as Teflon, wherever possible,
g) filling up all crevices in steel with red lead paste (Evans 1981),
h) closing crevices in existing lap joints by continuous welding,
i) inspecting structures and removing deposits frequently,
j) using welded butt joints instead of riveted or bolted joints in steel structures.

2.3.3 Crevice corrosion

Crevice corrosion is a type of localized corrosion which frequently occurs within crevices and other shielded sites in steel bridges where two metal surfaces are in close proximity such as overlapping surfaces, lap splices, and crevices under bolt and rivet heads. Also in steel bridges it may appear between back to back angles used for bracing members, between lacing bars and adjoining components, between closely spaced eyebars, and between steel and other materials such as timber decks or concrete slabs. The mechanism of crevice corrosion involves electrochemical reactions that take place between the surfaces within the crevice, or between the surfaces of the crevice and those freely exposed to the environment outside the crevice (Ellis et al 1951). A typical example of crevice corrosion is shown in Figure 2.4, for a riveted lap splice.

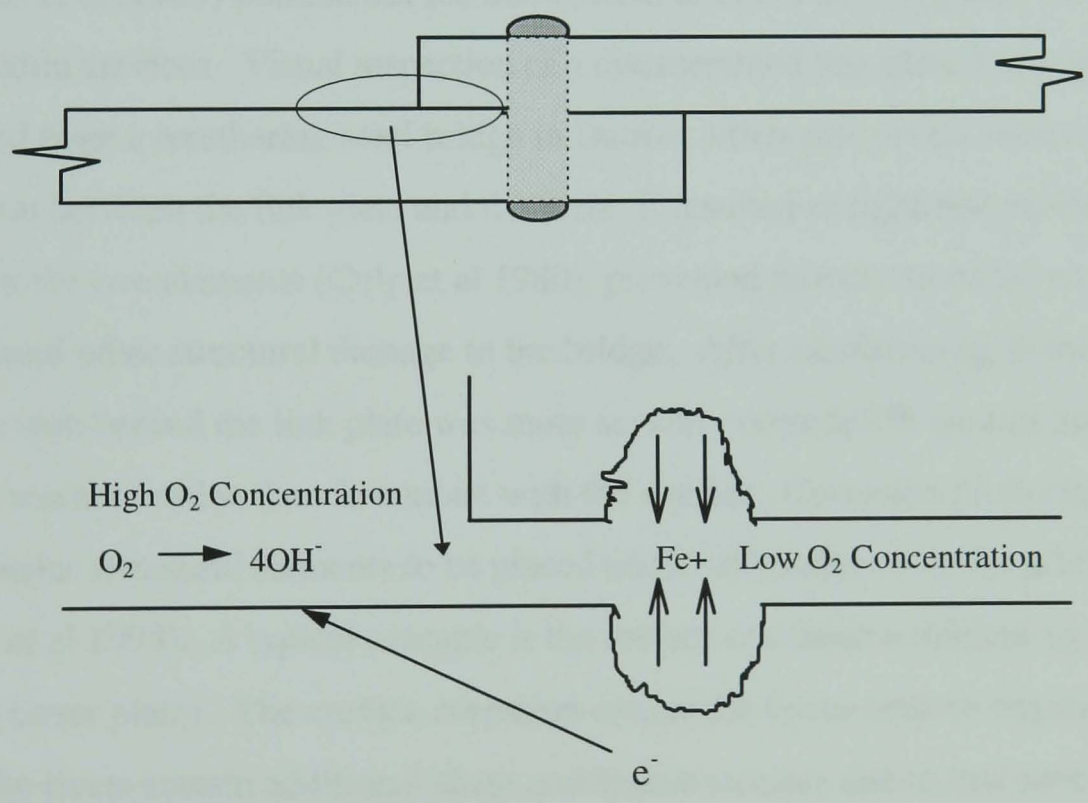

Figure 2.4 Lap splice undergoing crevice corrosion (France 1972).

In the example of the lap splice, moisture is present at the exterior surface of the splice and within the crevice. The concentration of dissolved oxygen is higher outside of the splice than inside. Therefore, the variation in the concentration of reactants and products can create a driving electromotive force. In the situation of the lap splice, the crevice

becomes the anode while the metal surface outside and adjacent to the crevice becomes the cathode. Once the dissolved oxygen is depleted within the crevice, the build-up of positive metal ions will attract negative ions in order to maintain electrical neutrality. Often chloride ions diffuse into the crevice, leading to the formation of hydrochloric acid. With a low pH, the dissolution of metal ions becomes even faster. Under certain conditions the hydrogen ions, H^+, can be reduced to hydrogen gas, H_2. This situation can lead to metal deterioration due to hydrogen embrittlement (Briant 1985).

The corrosion rates inside the crevices are much higher than on exposed surfaces of the structure. The presence of chlorides can promote the tendency towards crevice corrosion. It has been mentioned by IJsseling (1980) that the effect of crevice corrosion can range from pitting to uniform corrosion of the metal surface within the crevice.

Albrecht et al (1984) pointed out the detrimental effect of de-icing salts on corrosion of steel within crevices. Visual inspection of a disassembled link plate in an expansion joint removed from a weathering steel bridge in Detroit, Michigan, reveal severe crevice corrosion between the link plate and the web. It resulted in tight rust packing of the gap between the two elements (Culp et al 1980), prevented movement of the expansion joint and caused other structural damage to the bridge. After sandblasting, it became apparent that the web behind the link plate was more severely corroded in an area around the bronze washer outline than in contact with the washer. Corrosion products can also cause major structural elements to be placed under additional strain by actual expansion (Hahin et al 1993). A typical example is the crevice corrosion exhibited by beams with riveted cover plates. The crevice corrosion causes the cover plate to expand and yield. Also, the rivets sustain additional shear and tensile stresses due to this cover plate expansion.

The accumulation of rust products can lead to other forms of deterioration besides corrosion. Expansive rust can exert substantial outward pressure, estimated at 1200 psi (Brockenbrough 1983). This outward prying is known as oxide wedging. Crevice corrosion can cause member stresses and distortion. Wedging may also influence the growth of cracks (Hudak et al 1983).

Methods which may minimise the crevice corrosion are as follows:

a) using welded butt joint instead of riveted or bolted joints in steel structures,
b) using solid non-absorbent gaskets, such as Teflon, wherever possible,
c) filling up all crevices in steel with red lead paste,
d) closing crevices in existing lap joints by continuous welding.

2.3.4 Stress corrosion

Stress corrosion usually appears when metal in a corrosive environment is subjected to static tensile or residual stress which may be well below the yield strength. It has been pointed out by Scully (1966) that stress corrosion requires both an acting tensile stress and the presence of a specific corroding medium. Removal of either will prevent the initiation of cracking or stop cracks that are already propagating. Corrosion plays an important part in the initiation of cracks. A pit, trench, or other discontinuity on the surface of the metal acts as a stress raiser. Stress concentration at the tip of the notch increases rapidly as the radius of notch decreases. Cracks due to stress corrosion often start at the base of a pit and plastic deformation may also occurs. It has been observed that cracks proceed generally perpendicular to the applied stress (Fontana 1987).

Once a crack has started, the tip of the advancing crack has a small radius and the attendant stress concentration is great. Using audio amplification methods, Pardue et al (1961) showed that a mechanical step or jump can occur during crack propagation. In fact, "pings" were clearly audible. In general, the adjacent metal surface does not show any evidence of damage, but upon microscopic examination, the corrosion product can be found in the cracks.

The criteria for the stresses are simply that they be tensile as mentioned above and of sufficient magnitude. These stresses may be due to any source such as applied, residual, thermal, or from welding. In fact, numerous cases of stress corrosion have happened in which there is no externally applied stress. For example, welded steels contain residual stresses near the yield point. Corrosion products have been shown to be another source

of stress. Hudak et al (1983) show that highly localized stresses of about 2000 MPa, may be achieved.

The most general explanation for stress corrosion is the slip dissolution model (Briant 1985). The model is explained in the following discussion and in Figure 2.5. Small surface cracks can form stress concentrations when tensile stress is applied to a metal member. Under tensile strain, the passive film at the tip of a crack can break or slip apart. This slip causes a freshly exposed surface of metal at the crack tip. If the applied strain is low, and a corrosive medium is present, the passive film will reform. If the strain level is high, the passive film will reform but then re-break due to the high strain. The process of film growth and breakage will continue, causing the crack tip to grow, even though it would remain stable in a non-corrosive environment.

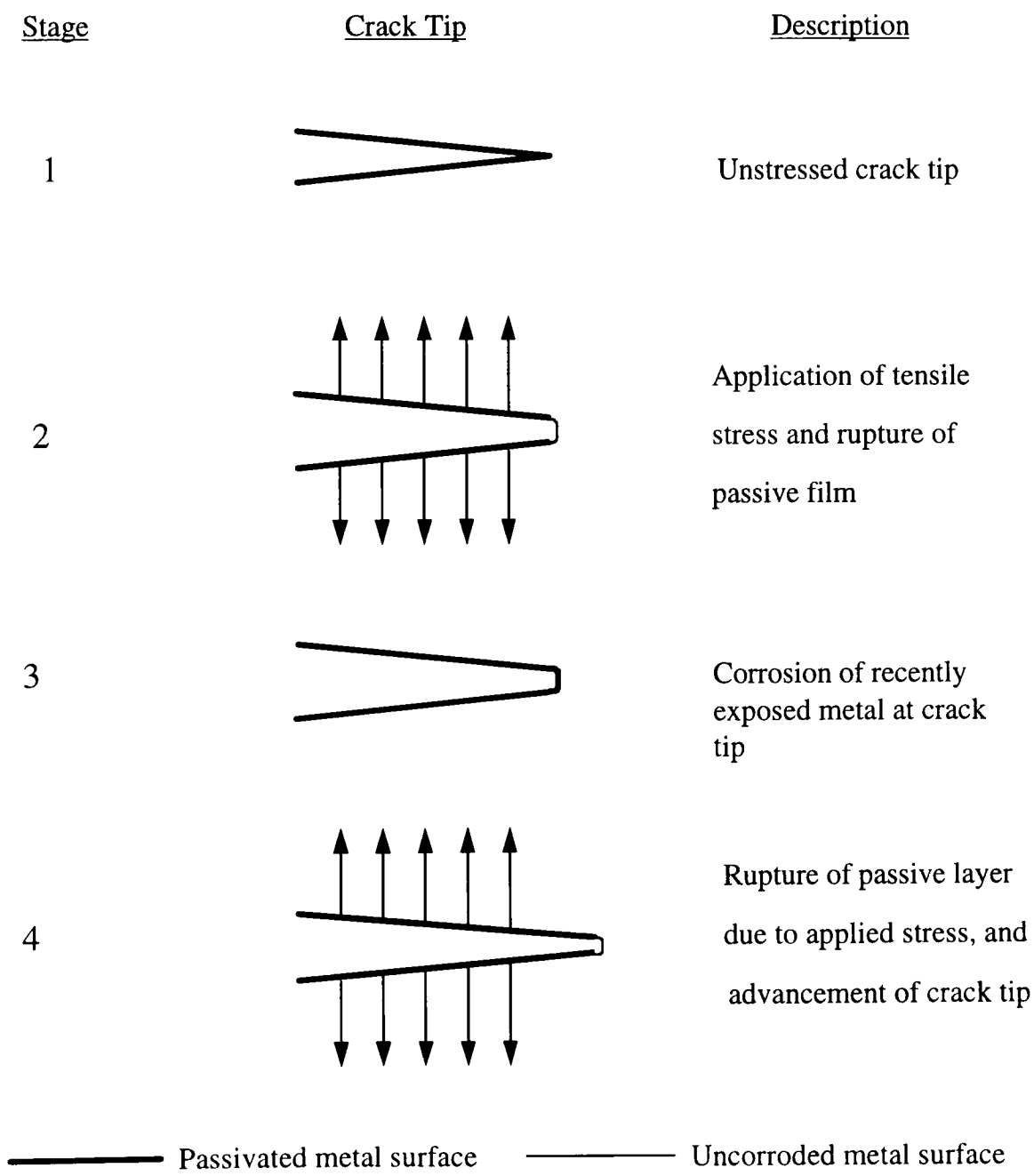

Figure 2.5 Stress corrosion and slip dissolution model (Knot 1982).

Stress corrosion occurs in bridges under severe environmental conditions, such as industrial areas or marine environments. Kulicki et al (1990) observed stress corrosion cracking in a structure in a corrosive environment where high strength bolts failed while the connected members showed no indication of corrosion. The tension in the bolts increased, due to expansion of corrosion products, until the bolts cracked transversely, hence reducing their cross section area, until failure occurred. Stress corrosion cracking has also been observed on wires and strands in the main cables of suspension bridges.

Chen et al (1976) pointed out that it is possible for crevice corrosion, pitting corrosion and stress corrosion cracking to occur simultaneously in a test assembly. It is also possible that one mode, say crevice corrosion, will initiate first and suppress pitting or stress corrosion elsewhere on the specimen as the result of providing cathodic protection to the exposed area.

The important variables affecting stress corrosion cracking are temperature, metal composition, time of cracking, solution composition, stress, and metal structure. In most chemical reactions, stress corrosion cracking is accelerated by increasing temperature. This type of corrosion may be exhibited in mild carbon steel in the presence of nitrates or in highly alkaline solutions, but not in a chloride environment. In general, the lower the fracture resistance of a metal, the higher its susceptibility to stress corrosion (Karpenko et al 1979). However, high strength low alloy steel is susceptible to stress corrosion in a chloride environment. The presence of oxidisers often has a pronounced influence on crack tendencies (the combined effects of chloride and dissolved oxygen). Also cracks may occur in the presence of certain liquid metals, fused salts, and non-aqueous inorganic liquids. In stress corrosion, time is an important parameter since the major physical damage during stress corrosion cracking occurs during the later stages. As stress corrosion cracks penetrate the material, the cross-sectional area is reduced and the final cracking failure results entirely from mechanical action. The criteria for the stresses are simply that they be tensile and of sufficient magnitude. These stresses may be due to any source such as applied, residual, thermal, or from welding.

Stress corrosion cracking may be reduced or prevented by application of one or more of the following methods which may be applicable:

a) using inhibitors such as phosphates and other inorganic and organic compounds,
b) lowering the applied stress below the value of critical stress,
c) using an alloy which may not be susceptible to stress corrosion,
d) applying cathodic protection to the structure,
e) coatings.

2.3.5 Corrosion fatigue

Corrosion fatigue is a complex phenomenon which occurs in metal due to cyclic stresses in a corrosive environment. In general, fatigue failures occur at stress levels below the yield point and after many cyclic applications of this stress. Corrosion fatigue is not defined in terms of the appearance of the failure, but in terms of mechanical properties. Usually in corrosion fatigue failure, a relatively large area is covered with corrosion products and a small roughened area results from the final brittle fracture as shown in Figure 2.6. It is important to realise that the presence of corrosion products at a fatigue fracture point does not necessarily indicate corrosion fatigue. Indeed, corrosion may occur during ordinary fatigue fracture, and the presence of rust or other corrosion products does not necessarily mean that fatigue life has been affected. This may be identified by a corrosion fatigue test.

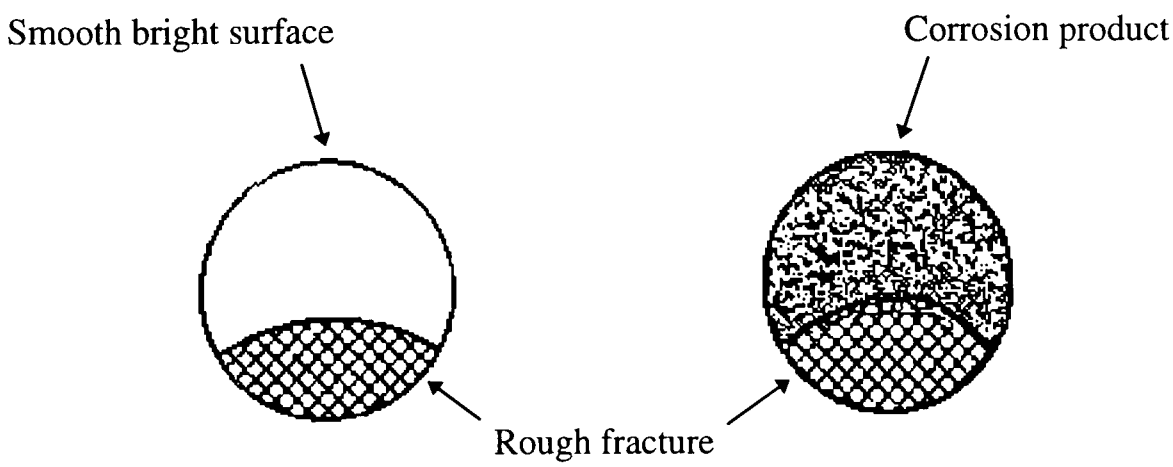

Figure 2.6 Schematic illustration of fatigue and corrosion fatigue failure.

Corrosion fatigue is similar to stress corrosion in that when a metal is under stress, local yielding of slip surfaces can provide sites for corrosion to occur. In addition, the cyclic slip behaviour of the metal will affect the accumulation of corrosion damage over time (Herbsleb et al 1985).

In corrosion fatigue, it has often been observed that surface pitting occurs, so it is conceivable that the pits act as geometric stress concentrators similar to mechanical notches (Congleton et al 1982). It has been observed by Kitagawa et al (1978) that very small, randomly distributed cracks often occur on the surfaces of unnotched specimens and parts broken in service, which were or could have been subjected to corrosion fatigue. Of course these cracks are affected by various environmental, metallurgical, and mechanical factors. The occurrence of corrosion fatigue on steel bridges is limited to fatigue sensitive members in a corrosive environment.

In the past decades, renewed attention has been given to corrosion fatigue due to some catastrophic failures in different fields such as offshore structures, aerospace, and nuclear. The mechanism of this form of failure still is not very clear, but it is known that crack initiation and crack growth respond differently to environmental factors.

Environmental factors strongly influence corrosion fatigue behaviour. Corrosion fatigue is most significant at low stress frequencies. This dependence is readily understood since low frequency cycles result in greater contact time between metal and corrosion. Corrosion fatigue is also influenced by the conditions to which the metal is exposed. Oxygen content, solution composition, temperature, and pH influence corrosion fatigue.

It is well known that the presence of an aqueous environment is likely to lower the fatigue resistance of metals (Congleton et al 1982). However, the most characteristic of this type of corrosion in a corrosive environment is a reduction in fatigue life of a metal compared with a non-corrosive environment. The size and shape of pits are enhanced during the tensile stress portion of the fatigue cycles and this tends to keep them open to corrosive environment. It has been pointed out by Kitagawa et al (1983) that increases in the cyclic stress level or the number of load cycles bring about corrosion pits on the

surface. In corrosion fatigue, corroded pits act as stress raisers and initiate cracks. It is most likely that the corrosion is most intense at the crack tip, and as a consequence there is no stable pit radius, since the pit radius continuously decreases due to simultaneous mechanical and electrochemical effects.

Ramachandra et al (1994) have shown by an experimental test on offshore structures that multiple cracks developed under corrosion fatigue resulting in accelerated crack growth and consequent reduction in fatigue life. Also it has been pointed out by Gaythwaite (1981) that structural steel corrodes at an average rate of around 0.13 mm/year (0.005 in/year) in quiet seawater (marine area), but due to corrosion fatigue, pit growth may be up to 10 times as great.

The major variables that influence the long life corrosion fatigue behaviour of low and medium strength structural steels in marine environments (seawater) are stress ratio, residual stresses, cyclic frequency, cathodic potential, seawater characteristics, and hot-spot stress range (Jaske et al 1978).

It has been pointed out by Evans (1981) that the applied frequency decisively influences the fatigue strength in corrosion fatigue. In structural parts subjected to a high frequency the damage done by corrosion diminishes during each cycle. Therefore the structural part can sustain more cycles in comparison with low frequency conditions where the corrosion can progress.

Usually alloys with high tensile strength resist the formation of nucleating cracks. However, once a crack starts in a high tensile strength material, it usually progresses more rapidly than in a material with lower strength. During corrosion fatigue a crack is readily initiated by corrosive action, and as a result the resistance of high tensile strength material is quite low. Therefore, from the standpoint of corrosion fatigue, high tensile strength metals are not suitable.

Corrosion fatigue can be minimized or prevented by applying a number of methods:

a) using coatings such as zinc, chromium, nickel, copper, and nitride,

b) avoiding high tensile strength steel,

c) reducing the stress in component.

2.3.6 Galvanic corrosion

Galvanic corrosion occurs when two different metals are in contact in a moist or immersed environment. The intensity of this type of corrosion depends on (a) the difference in their corrosive potential which produces electron flow, with one of the metals as the anode and one as the cathode, and (b) the ratio of exposed area of the metals and their specific corrosion behaviour. This form of corrosion mostly appears on steel bridges in bolted or welded connections, and where aluminium light poles, handrails, or electrical conduits are in contact with steel or where galvanised steel is in contact with bare steel such as weathering steel. Galvanic corrosion can be local, leading to pit formation (Kayser et al 1989).

The nature and aggressiveness of the environment determine to a large extent the degree of two metal corrosion. Usually the metal with lesser resistance to the given environment becomes the anodic member of the couple. Sometimes the potential reverses for a given couple in different environments. Usually both steel and zinc may corroded by themselves, but when they are coupled, the zinc is corroded and steel is protected. In the exceptional case, such as some domestic waters at temperatures over 180° F, the couple reverses and steel becomes anodic (Fontana 1987).

Usually the driving force due to the galvanic corrosion depends on the nature of the dissimilar material coupled with the reference metal (Harries 1990). Materials that provide additional anodic area are called "active" relative to the reference metal and those that provide more cathodic area are called "noble" relative to the reference metal. The coupling of weathering steel with more active metals, such as zinc or ordinary steel, results in accelerated attack of the active metals. Therefore, the coupling with more noble metals such as copper alloys, stainless steel, or bronze, results in accelerated attack on the weathering steel (Albrecht et al 1989). Galvanic corrosion is limited by the

conductivity of the corrosion medium. Thus, the effects of galvanic corrosion are not as destructive in air as under immersed conditions. However, the combination of galvanic and crevice corrosion, as with a bronze washer forming a crevice with a weathering steel member, can be destructive.

Another factor which may control the extent of galvanic corrosion concerns the relative areas of the anode and cathode. Whenever the cathodic area greatly exceeds the anodic area, the loss of metal from the anodic area required to balance the reaction of the corrosion on the cathodic area, can lead to unacceptably high corrosion rates (Ellis et al 1951).

For structures which are composed of different metals, galvanic cell formation can be a serious problem. Accelerated corrosion due to galvanic effects is usually greatest near the junction, with attack decreasing with increasing distance from that point. This form of corrosion is readily recognised by the localized attack near the junction of two metals. Several possible locations for galvanic cells exist on steel bridges. A common location is at pin and hanger or bolted connections (McCrum et al 1985). Variations between the base and weld metal composition can cause corrosion to occur at weldments also. Surface variations or imperfections in the girder metal can form microscopic galvanic cells, leading to localized pitting and crevice corrosion. The rate of galvanic corrosion is difficult to predict under field conditions. However, like crevice corrosion, the location of where galvanic cells will occur can be predicted, if variations in material are known.

A number of procedures can be used for minimising the rate of galvanic corrosion. Sometimes one is sufficient, but a combination of one or more may be required. These procedures are as follows:

a) adding inhibitors to decrease the aggressiveness of the environment,
b) avoiding the unfavourable area effect of a small anode and a large cathode,
c) insulating dissimilar metals wherever practicable,
d) installing a third metal that is anodic to both metals in the galvanic contact,
e) using a combination of metals as close together as possible in the galvanic series,

f) using a coating is the best way to minimise the galvanic corrosion,
g) designing for the use of readily replaceable anodic parts or make them thicker for longer life.

When organic coatings are used it is necessary to coat both the active and noble areas. This is because the driving force for galvanic corrosion can be so high that coating only the active metal usually leads to breakdown of the coating and subsequent corrosion of the active metal.

2.4 Corrosion case histories

Over the past decades a number of localized failures have occurred in components of steel bridges in the world. The sudden failure of bridges, with loss of life, is probably the most publicised aspect of bridge corrosion. Collapses of the Point Pleasant Bridge over the Ohio River in 1967 (Hopwood et al 1984) and the Mianus River Bridge on Interstate 95 in Connecticut in 1983 (Kulicki et al 1990) are two widely known bridge failures in the USA.

The Point Pleasant Bridge was an eyebar chain suspended structure. It failed because of stress corrosion cracks at the pin hole in an eyebar (Fisher 1984). The main cause of collapse was traced back to the unstable extension or brittle fracture of two corrosion cracks located at the pin hole of one of the four eyebars (Ballard et al 1969 and Scheffey et al 1974). Of course it is necessary to mention that the design of the chain was unique in that only two eyebars were used in each chain segment, and the chain also formed a portion of the top chord of the stiffening trusses. Thus failure of any one eyebar in the bridge would cause the complete collapse of the structure.

The Mianus River Bridge failure is attributed to corrosion of components of a pin-and-hanger assembly (Kulicki et al 1990). It was suggested that, over a relatively long period of time, accumulation of corrosion products from an underlying washer shifted the hanger transversely on the pin causing a misalignment of the hanger. This misalignment,

with the hanger now bearing nearer the end of the pin, increased the stress range in the pin resulting in a fatigue crack leading to failure of the pin.

In Detroit, there was a near collapse of a bridge because stirrups supporting a girder had rusted through and broken (Anon 1983). The girder and presumably the stirrups had been encased in concrete for protection against exhaust fumes from locomotives passing below.

The Harvard Bridge in Cambridge, Massachusetts, was approximately 100 years old. Its hangers were wrought iron eyebars that had locked at the pins because of corrosion, which caused a redistribution of forces sufficient to initiate fatigue cracks (Broderick 1985).

A broken hanger was found on the Yankee Doodle Bridge over the Norwalk River, on Interstate 95 in Connecticut. After blast cleaning the overlying corrosion products, 16 other hangers were found with cracks (Anon 1984). Although the cracks were not attributed to significant metal loss due to corrosion, corrosion products between the pin and hanger may have caused the joint to lock. In any case, corrosion had obscured serious structural damage that might well have gone undetected during a normal bridge inspection.

In Philadelphia, severe deterioration caused failure of a main load carrying member of a south-eastern Pennsylvania Transportation Authority Bridge which had been hidden from view by wall and ceiling panels of a station building (Kulicki et al 1990). Cracks were discovered in beams of a Virginia Bridge by a nearby work crew (Parsons 1978). These cracks were reported to be a result of bearings locked by rust. This damage occurred apparently within a 2-year inspection interval.

It has been noted by Stanley et al (1995) that in 1962 corroded buckled plates were replaced on London's Tower Bridge. Further work was carried out in 1992 for its centenary in 1994. Corrosion was observed and the removal of steel plating exposed internal voids and areas of corroded steelwork which had probably not been observed for

100 years. The corroded section of steelwork supporting the balustrades and deck under the bascule footway were subjected to extensive reconstruction work. It was noted by Hill (1985) that the majority of corrosion occurred where water collected near structural members, either by seepage through the deck or as a result of pockets in its design features.

2.5 Effects of corrosion on steel bridges

Corrosion may have many deleterious effects such as appearance, maintenance and operating cost, plant shutdown (for repair), contamination of product, loss of valuable products, product liability, and safety and reliability. The effect of corrosion on steel bridges varies from need of maintenance of non-structural elements to catastrophic failure. Some types of corrosion, such as stress corrosion or corrosion fatigue, can cause damage that is not easily identifiable and can lead to unexpected failures. The conditions created by corrosion can reduce the static, fatigue, fracture, or buckling strength of bridge members, affect the structural behaviour, and reduce overall fatigue life of bridge structural elements. The effects of various types of corrosion and their influence on steel bridge components are summarised in Table 2.1.

Table 2.1 Types of corrosion, bridge components effected and types of deterioration (Kayser et al 1987)[2].

Bridge component	Uniform corrosion	Pitting corrosion	Crevice corrosion	Stress corrosion	Galvanic corrosion
Web	S, I	S, I, F			
Flange	S, I	S, I, F			
Stiffeners	S, I	S, I, F			
Splice	S	F	W	F	S
Connection		F	W	F	S
Weld		S, F		F	S, F
Bolt		F	W	F	S
Hanger	S	S, F	W	F	S
Pin		S, F	W	F	S
Bearing			W		W

Types of deterioration: F Fatigue and cracking I Reduction in stiffness
W Oxide Wedging S Reduction in Strength

Kayser et al (1987)[2] pointed out that this Table 2.1 can serve as a guide, relating steel bridge components to the typical forms of corrosion damage which may occur. However, due to the subject of this study the following effects are considered on steel structural members of bridges:

1. Loss of thickness. Several types of corrosion lead to loss of thickness. Section loss may take place over a large area (uniform corrosion) or within a small area (pitting corrosion). The main effect of section loss is a reduction in section properties of member such as area, moment of inertia, radius of gyration, and etc. Those changes will occur in a non-linear manner because the geometric properties are related to the square or cube of the dimensions. Furthermore, the position of the neutral axis may change. The reduction in member section dimensions leads to lower bending, shear, and axial capacity. This effect should be evaluated based on its location on the member. Buckling

capacity of members will be critically affected by the reduction in metal thickness. The fatigue life of the member decreases because of the increase in stress range due to the reduction in section properties.

2. Stress concentration due to the corroded pits. Pitting will increase the sensitivity of a member to cracking due to local stress concentration in the region around the pit. Localized deterioration can cause increased nominal stresses, stress concentrations, and localized yielding or buckling, and thus result in a local reduction in strength. The effect of localized deterioration on the overall behaviour of a member will depend on the type of member and the location, nature, and extent of deterioration. The formation of pits which act as micro-notches due to corrosion create stress concentration in the region around the pit and can initiate cracks. This effect tends to reduce fatigue life severely. The effects of pitting are more prevalent for structural details which are not susceptible to fatigue damage, such as class A and B details (Albrecht and Naeemi 1984).

3. Unintentional fixity due to corrosion. Corrosion may lock moving parts of a bridge, such as joints, hangers, bearings, and expansion devices. Hence, the structure may behave differently from the way it was designed and the structural members can be subjected to unexpected stresses. Some accumulation of corrosion products in constricted areas like pin-and-hanger details can generate considerable pressure which may bend or move bridge components with damaging effects, such as the Mianus River Bridge (Kulicki et al 1990). Brockenbrough (1983) found that the resulting stress can exceed 1200 psi.

Normally bridge bearings are designed to transmit the weight of the superstructure and the loads it supports to the substructure. They are also designed to accommodate changes in the geometry of the superstructure which result from the load, temperature variations, and possible foundation settlements. Some bearings are designed to allow only rotation at the end supports, while others are designed to allow both rotation and longitudinal displacement. It has been reported by Hsiong (1978) that locked rocker bearings and structural damage such as web cracking, web buckling and separation between the bottom flange of girders and the top bearing plate, were found on the

elevated approach ramps to the Poplar Street Bridge, crossing the Mississippi River in St. Louis. The investigations concluded the locking of the rocker bearings was the primary cause of the web buckling. The seized bearing pin forced the girder to bend in order to accommodate the thermal movement and rotation. The bending of the girder lifted the bottom flange off of the bearing shoe, and shifted the reaction from the bearing shoe to behind the bearing stiffeners, thus causing the end of the girder web to buckle. It has been noted by Bakht et al (1979) that the seizure of the pin-supported bearing was caused by the formation of pack rust between the contact surfaces of the pin and the supporting saddles. Salt and air pollution were thought to have contributed to the locking of bearings.

Temperature induced stresses caused by a malfunctioning expansion bearing on the Perley Bridge across the Ottawa River in Canada resulted in failure of connecting angles of a girder column-connection. It has been mentioned by Bellenoit et al (1984) that the formation of "pack" rust around a bearing or hinges can lock the mechanism in place. The non-functional mechanism will cause unintended stresses in the structure.

2.6 Corrosion patterns

Corrosion occurs wherever water can leak onto the superstructure or areas where water and debris can accumulate. The corrosion of the steel can be particularly severe where road salt and dust are present in the water. The places most commonly found with corrosion are on the bottom flange where water collects from dew or splash, and on the webs near the abutments and joints. For instance, the examination of four bridges in Alaska by Albrecht et al (1984) showed that the most significant amount of corrosion occurred on the bottom flange of the seaward girders. This location on the steel would have the greatest amount of condensed water blown inland from the sea. The corrosion under moist conditions is related to the time of wetness.

Figure 2.7 illustrates the typical locations where corrosion is likely to occur in I-girder members of a simple span bridge. The pattern developed will be the corrosion of the webs at ends of girders, and the corrosion of the bottom portion of the girder, along the

entire length. Fontana (1987) pointed out that pitting corrosion mostly develops and grows downward from horizontal surfaces of the members. Usually the top surface of the bottom flange is the most vulnerable part for accumulation of the electrolytes. Apart from the regions mentioned above, Kayser and O'Neil (1987)[3] pointed out that severe corrosion may take place on the bottom one quarter of the web as shown in Figure 2.7. Visual examination and measurement of the thickness of three samples of severely corroded I-beams obtained from a chemical works also indicated that the corrosion pattern is similar to what is described above (see Chapter 3).

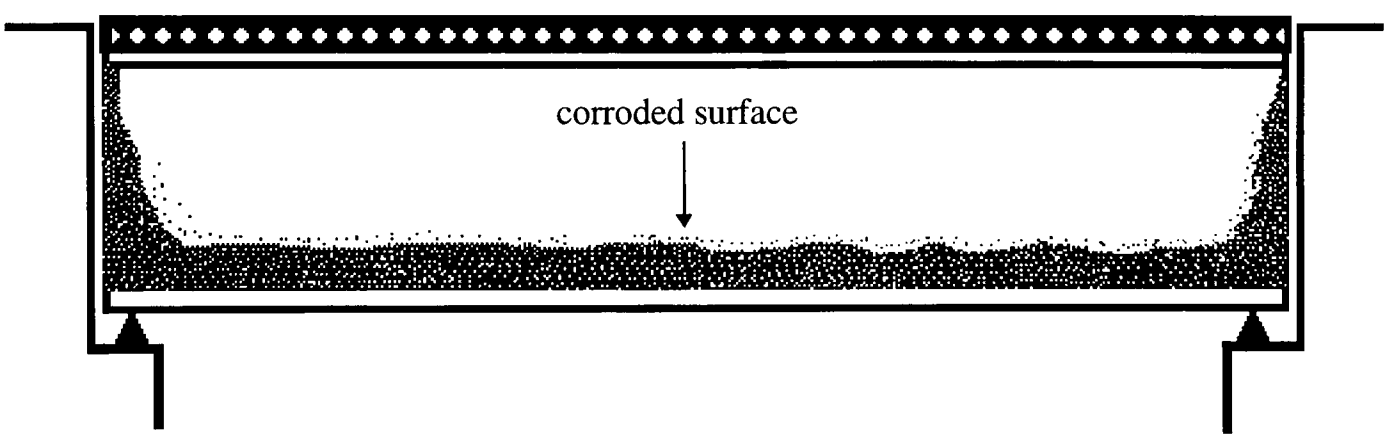

Figure 2.7 Typical locations where corrosion can occur on a steel girder bridge.

Of course the corrosion of the bottom flange and the bottom one quarter of the web are most likely to occur on the outside girder facing oncoming traffic. The outside girder on the other side of the bridge will have less corrosion. This difference in loss is caused by the pattern of spray and dust created by underpass traffic as shown in Figure 2.8. If traffic flow is in two directions below a bridge, a more even distribution of flange loss will occur among the girders. Web loss near the supports will occur equally among the girders, because it is caused by deck leakage from above.

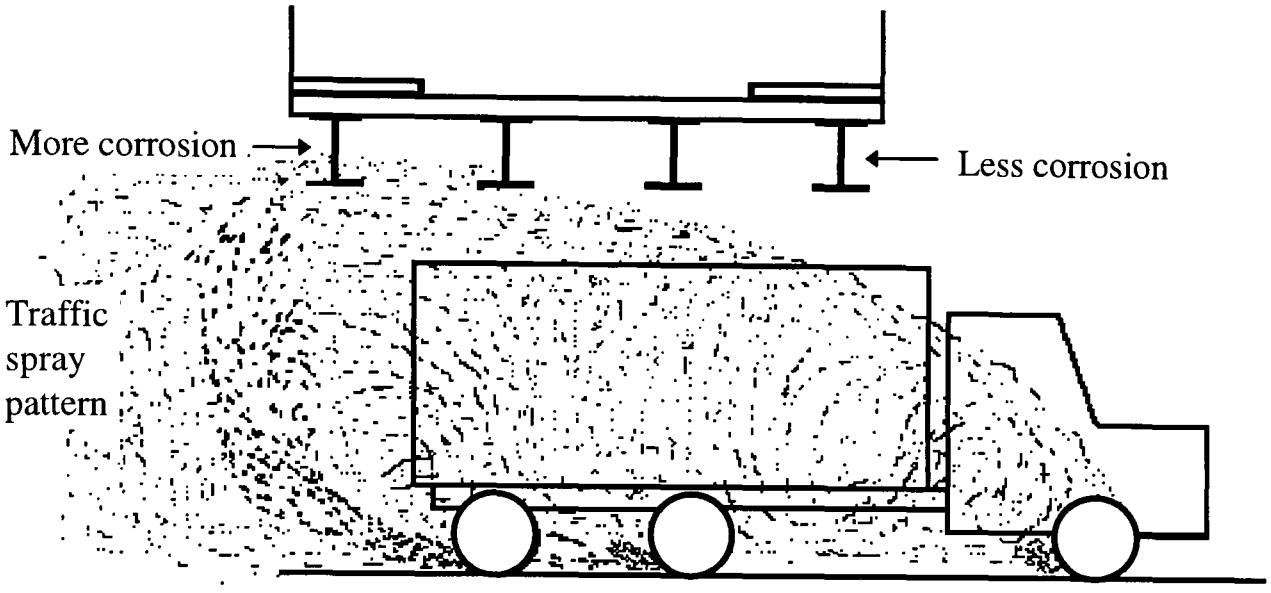

Figure 2.8 The traffic spray accumulation on girder flanges and webs.

2.7 Summary and conclusions

The main aspects that are associated with corrosion of steel have been discussed in this chapter. The electrochemical process of corrosion has been outlined. The various forms of corrosion have been explained along with how these occur on steel bridges and what factors contribute to their occurrence and prevention. The effects of corrosion on steel bridges were identified.

It can be concluded from the discussion of various forms of corrosion and their effects that corrosion at the initial stage may be taken as uniform. As the exposure time increases, pitting corrosion may occur on top surface of the bottom flange where water and contaminants can accumulate due to the leakage from expansion joints or the spray created by underpass traffic. We have seen that one of the effects of pitting corrosion in a corrosive environment is a reduction in fatigue life of a metal compared with a non-corrosive environment.

CHAPTER III

MEASUREMENT AND ANALYSIS OF SURFACE ROUGHNESS

3.1 Introduction

It is known that pitting corrosion gives rise to a notch factor affecting the fatigue life of corroded steel bridges. Therefore, it is important to have methods for the measurement and characterisation of corroded surfaces. The purpose of this chapter is to review surface roughness, discuss existing techniques for its measurement and analysis, to describe the method adopted in this study and to determine the relationships between pitting and overall depth of corrosion.

Typically, roughness between 1 cm to about 10 μm is measured by stylus profilometers, between 500 to 1 μm by optical interferometry and between 100 μm to 1 Å by scanning tunnelling or atomic force microscopy (Bhushan 1995). The overlap in length scales between these instruments are used to corroborate the roughness measurement techniques.

Surface roughness studies have come a very long way from the day when Bowden (1950) said that 'Putting two solids together is rather like turning Switzerland upside down on the top of Austria- the area of intimate contact will be small.' The development of early concepts of the role of surface topography in tribology (friction, lubrication and wear) has been reviewed by Dowson (1979). Most of the discussion was related to the period from the sixteenth to the late nineteenth century. Some of the concepts are quaint, some purposeful and accurate, but practically all are interesting. It seems quite remarkable that the concepts of surface topography, the modelling of rough surfaces for analytical purposes and the development of understanding of the influence of surface

roughness upon friction, lubrication and wear could have advanced so far before surface measuring instruments emerged in the present century.

In recent years the importance of tribology calls for much greater research on better surface quantification because it has been realised that most manufactured surfaces are very rough on an atomic scale, with asperity heights being 10^2-10^4 times larger than the atoms which form the features (Dyson 1978). Also Bhushan (1995) has pointed out that almost all surfaces that are prepared by mechanical techniques contain surface damage, resulting from plastic deformation and heating.

The quality of surface finishes produced by standard operations such as honing and grinding can be assessed by a variety of instruments, in particular by stylus techniques and by interferometry. Greenwood et al (1977) pointed out that surface roughness in tribology received great attention from about 1960 onwards. Various physical methods have been developed to yield information on surface topography, including oblique sectioning, optical interferometry, optical and electron microscopy and profilometry. Good introductions to these procedures can be found in Bowden et al (1950), Halliday (1955), Barwell (1956), BS 1134 (1961), Williamson (1967), Moore (1969), Thomas (1975), Halling (1975), Binning et al (1982), Lee et al (1990), Bennett et al (1989 and 1993), Slomba et al (1992), Cohen et al (1992), Caber (1993), Jolic et al (1994) and Bhushan (1995).

In this study only the surface roughness which is related to corrosion will be investigated. In the case of corrosion, it would be expected that pitting corrosion would cause a rougher surface compared with other types of corrosion. The aim is to review the physical principles of roughness measurement methods for corroded steel structures. The literature may be classified broadly as follows:

i) methods for examining the quality of manufacture or fabrication; in particular the surface finish of any object often leads to improved performance or increased life.

ii) methods for measuring and evaluating the surface roughness due to corrosion in structures such as steel bridges.

There is an extensive survey of roughness measurement methods in existence relevant to methods (i). The methods used for examining the quality of surface profiles e.g. in production and machining industries are divided into a number of categories as has been mentioned previously. Also some of those techniques were specifically developed for measuring roughness of corroded surfaces.

At present roughness measurements are generally carried out at right angles to the surface and may be characterised by some kind of height. The methods described in the following sections are considered to be relevant to the roughness measurement of steel structures. Each of the methods will be discussed with a view to the adoption and development of a method capable of improving the ability to measure surface roughness due to pitting corrosion on steel structures at the site or in the laboratory. A short review of methods which can be used in the identification and examination of pits and in the evaluation of pitting corrosion to determine the extent of its effect is given in ASTM G46 (1981).

The main objectives of this chapter are:

1. To review the existing techniques for measurement and analysis of surface roughness.
2. To develop a technique for measurement of surface roughness in the laboratory.
3. To propose a method of roughness measurement on site.
4. To compare the results of roughness measurement of the methods used in this study.
5. To investigate the relationships between pitting corrosion and overall depth of corrosion.

3.2 Review of techniques to measure surface roughness

Measurement techniques for surfaces have progressed rapidly during the last decade because roughness of surfaces is of interest to a wide range of researchers in materials

science (Underwood 1989). A number of methods for roughness measurements will be reviewed in the following sections and the selection of method often depends upon the desired resolution. For instance, roughness on an atomic scale might be best measured on an atomic force microscope while the roughness of a mountain range may measured by a stereophotography technique.

3.2.1 Visual inspection and fingernail methods

Visual inspection is probably the most widely used non-destructive testing method for the inspection of steel structures and assemblies, for quality control and in the field. It is usually used to give an initial appraisal before a more detailed examination by another method. It has been pointed out by ASTM G46 (1981) that the visual examination of corroded metal surfaces is usually beneficial and this can be done under ordinary light with or without the use of a low-power magnifying glass to determine the extent of roughness due to corrosion and apparent location of pits. It might be useful to photograph the corroded surface so that it can be compared with the clean surface after the removal of corrosion products. This method was adopted by Culp (1980) for 50 unpainted weathering steel bridges at different environments and severe corrosion problems including pitting of beams were identified.

Kulicki et al (1990) suggested that members and components of steel bridges are visually inspected with three levels of attention, these being: cursory, general and detailed inspection. According to Kulicki et al (1990) the cursory inspection provides an overview of corrosion condition without detailed examination or the use of sophisticated tools and equipment, by using visual observation and experience to evaluate the condition. General inspection provides random or spot measurements of worst case conditions. Estimating and measuring to determine the extent of corrosion damage is achieved by using calipers or ultrasonic measurements. Detailed inspection may follow, covering all corrosion aspects of all bridge elements. Close observation is needed for detailed measurements of all members. In this method steelwork surface cleaning is performed, as required, to make accurate surface measurements by using caliper readings or one of the methods explained in the following sections.

However, there are several limitations to the use of visual inspection as the only method of structural examination. Visual inspection is inherently subjective because it relies on the judgement of different individuals and one inspector may spot something that another does not or may classify the same fault differently. Since there is a limit to the resolution of the eye, there is an associated limit to the size of defect that can be detected. Another common problem is the inability to see corrosion that is hidden by paint or concealed between the interfaces of a joint. But it might be useful for a preliminary estimation of surface roughness. Further information on this method can be found in LeDoux et al (1983) and Halmshaw (1991).

It has been pointed out by Abbott et al (1937) that the simplest and cheapest method for preliminary estimation of surface roughness can be the human fingernail which in practice is suprisingly effective. He found that the human fingernail is more sensitive to some frequencies than others, so there is presumably an optimum speed with which it should be drawn along the surface. Haesing (1961) performed some careful tests in which subjects were asked to differentiate between pairs of test pieces of increasingly different roughness. The main finding of the study was that the fingernail test was much more effective than visual inspection. This method is not, however, able to give a quantitative measure of roughness. Furthermore, it may not be suitable for roughness on the scale found in bridges.

3.2.2 Optical methods

Optical techniques are important as they are so often used. It has been pointed out by Whitehouse (1997) that some optical methods mimic the eye whereas some mimic the profile produced by a stylus instrument. The benefits of optical surface profilometry include the ability to perform non-contact measurements of delicate surfaces, increased height resolution and high measurement speed (Caber 1993). In contrast, optical systems also scan a relatively two-dimensional area rather than along a line. Owing to the much smaller wavelengths involved (compared with ultrasonic), optical methods are highly suited for roughness assessment and detection of very small defects.

Optical methods applied to linear measurement may be divided into general types as follows: (1) very accurate measurement of small dimensions or displacement by methods using light-wave interference or image magnification and (2) measurement of large dimensions by use of alignment telescope with accessories and projection systems (Beckwith et al 1993).

All optical methods involve projecting light on to a surface. Sometimes the light is focused but often it is not. Also the light can pass by an obstruction on the way to the surface or after scattering. In addition the light can be used coherently or in an incoherent mode and finally polarization properties can be used (Beckmann et al 1963, Bass et al 1963 and Ogilvy 1991). More practical assessment by optical means have been treated thoroughly in the books by Bennett (1994) and Whitehouse (1996).

Schmaltz in 1927 was the first person to use optical techniques (Schlesinger 1942). He projected a collimated beam of light past a knife edge, the shadow of which was made to intersect the surface at an angle. When viewed from a different angle a profile of the surface roughness was apparent. In this method there is no horizontal magnification. The vertical magnification is provided by the obliquity angle of the projected edge. The magnification is only about ×20 so that the method is restricted to viewing rough surfaces. The roughness measurement is made by eye using the graticule in the viewing optics.

Surface roughness and imperfections in smooth materials such as metal can be detected by optical methods as they produce marked changes in the reflection, scattered or transmitted light levels (Owen 1990). Optical profilometers give an accurate non-contact method, but they provide slow measurement in the form of one-dimensional profiles that are not truly representative of the surface (Dovey 1991). It has been reported by Jacobson et al (1992) that, just as with mechanical probes, the high-frequency response of some optical profilometers have also been shown to be non-linear.

The optical method is a major aid to visual inspection as it allows clear observation of the cavities on the surface of steelwork. The image produced may be viewed directly or

recorded by photography or television. There is a voluminous literature in the field of optical methods but mostly relating to applications which are not relevant to the current study.

Various methods of optical profiling have evolved recently including phase-shifting interferometry, the measurement of local slope using laser techniques and the dynamic detection of focus (Stedman 1988). Phase-shifting interferometers can be used to obtain fast, three-dimensional profiles of very smooth surfaces with resolutions of the order of 1/100 of a wavelength of light or better (Creath 1988). However, these methods are typically limited to measurements of smooth, polished and homogeneous surfaces. Caber (1993) has found that when rough surfaces are measured severe errors can arise. Thus in this review many forms of optical examination have been excluded because of their limitations when applied to rough surfaces. Further general information on different optical methods can be found in Davidson et al (1987), Lee et al (1990) and Cohen et al (1992).

One possible method of optical measurement is simply to use the light beam as a non-contact stylus for profile measurement (Dupuy 1968). It has been found by Luk et al (1989) that the stylus techniques are not suitable for real-time quality control due to the time taken for measurements. He developed a computer vision system for roughness measurement. Further detail on the use of this technique can be found in Ho et al (1990).

A commercial automatic optical system using a video camera has been developed by Reece (1995), which is able to scan the surface texture. This system is particularly suited to those applications requiring fast, accurate measurement, real-time tracking and monitoring capabilities. This method has not been used widely in the field of surface roughness measurement of corroded steel structures because it is expensive compared to the other methods. Further information on the use of this technique can be found in Williams (1996).

Lange et al (1993) developed a new technique for measurement and analysis of roughness of fracture surfaces using confocal microscopy. A confocal microscope is an optical microscope which has the unique capability of creating a bright image of in-focus region of the specimen while causing all out-of-focus regions to appear dark. One of the major limitations of optical microscopy is an inherent narrow depth of field. However, by using a confocal microscope to assemble a series of optical sections, each taken at a different focal plane, a "through-focus" image can be created which has "infinite" depth of field. This ability to overcome the limitation of a narrow depth of field has allowed the confocal microscope to find a unique role imaging non-flat or translucent specimens (Yatchmenoff et al 1990).

Through the construction of an image from a series of optical sections taken of a rough surface, confocal microscopy also has ability to create topographic maps. The topographic map is a digital image in which each pixel is assigned a value that represents the z-level. Each pixel may be though of as an x-y-z coordinate in the three-dimensional surface. The actual surface area of the specimen can be estimated by geometric construction of the surface represented by the topographic map. Once the surface area is computed, roughness of the surface can be characterised. The analytical details of this method are given in section 3.3.2.7.

The manual optical method using a microscope is particularly valuable when pits are too narrow or difficult to penetrate with a probe type of instrument. The method is amenable to use as long as light can be focused on the base of the pit. Kitagawa et al (1983) used microscopy in his study of how the cyclic stresses can promote pitting and irregularity of the surface configuration in corrosion fatigue.

The simplest way of performing roughness measurement is by using a calibrated focal depth scale. Measurement must be carried out on a point-by-point basis. This technique is relatively simple in operation but in practice involves much tedious labour in gathering the data and is not recommended for site measurement. It requires small specimens and the microscope apparatus cannot be used effectively to measure steel members in-situ.

However, it was used in this study for laboratory measurement of corroded samples, as outlined in detail in section 3.5.1.

3.2.3 Ultrasonic method

The ultrasonic method is a non-destructive technique and has a role in the evaluation of surface roughness in particular applications. A short review of non-destructive testing methods for welded structural steelwork is given by Burdekin (1993). Recent research in the field of corrosion monitoring showed that ultrasonic techniques will consistently under-estimate the depth of corrosion pits (Drury 1997). This is because measurement is averaged over the area of the probe and small local variations cannot be resolved. Consequently, ultrasonic techniques are unsuitable for measuring roughness directly but can be used to measure thickness and therefore roughness indirectly using the method developed during this research.

In the ultrasonic method a travelling wave is passed into the structure under examination using a transmitter. This produces stress waves that propagate through the material and are reflected from any interfaces encountered. These might be due to the presence of cracks, changes of phase or composition within the material, or a material to air boundary. The modifications in the frequency content of the reflected signal are detected by a receiver placed at another location on the surface.

The oldest application of this method was the determination of material transmission properties by manual tuning of a conventional impulse echo instrument (Roderick et al 1952). The use of sound and ultrasound to assess surface topography, with principal application to macroscopic features in ocean environments, began to receive special attention in the early 1950's (Blessing et al 1993). The method was later refined and applied in different fields from the simple checking of machined parts where it is not possible to apply a caliper or micrometer, to the measurement of pipelines in situ, to detect corrosion on the inner surface, with access from the outside only (Halmshaw 1991). The other applications of this method are to determine those physical properties of a material that depend on microscopic structure such as elastic moduli, tensile strength

and hardness. Ultrasonic testing also can be used in the identification of cracks in structures and components.

An extensive survey was given by Porter (1996) and Charlton (1996) on the accuracy of ultrasonics in corrosion measurement. Porter (1997) has pointed out that the ultrasonic gauges are known from previous experience to be accurate to within one decimal place of a millimetre on uncoated, uncorroded steel with parallel surfaces. The reliability of the ultrasonic method as a non-destructive technique has been investigated by Silk et al (1987). The following advantages have been concluded: (a) the relative ease of penetration into materials with engineering applications such as steel and aluminium; (b) the sensitivity and comparative accuracy; (c) the ability to test from only one surface and to detect defects at substantial depth; and (d) the presence of no significant radiation hazard requiring operational precautions.

The Unit Inspection Section of the British Steel Corporation have developed a novel ultrasonic gauge which measures residual steel thickness through the rust (Mckenzie 1981). It requires no couplant and gives only the steel thickness not the steel plus a layer of rust. This instrument is known as the electromagnetic-acoustic induction ultrasonic thickness tester and is manufactured under licence by Wells Krautkramer. The electromagnetic-acoustic induction ultrasonic thickness tester consists of three parts, a control and power unit, a transducer, the probe itself and an ultrasonic instrument type. This combined equipment is quite heavy and bulky and two people are required to operate it. Thickness is measured by inducing high frequency eddy currents into the steel surface in the presence of a magnetic field. The eddy current and magnetic field interact with the material to produce an ultrasonic shear wave normal to the surface of the material. Ultrasonic pulses reflected from the other surface are detected by the reverse process and displayed on the oscilloscope screen of the ultrasonic instrument type. From the time interval between echoes, the material thickness may be obtained after suitable calibration of the instrument. As this method does not necessitate contact between the probe and test material, it is suitable for measuring the residual steel thickness of structures covered by a layer of rust.

British Steel Corporation carried out some laboratory work and this showed that the instrument could accurately measure steel thickness but indicated that there was a limit to the thickness of rust that could be tolerated (Mckenzie 1981). As rust thickness increases, there should be no change in thickness readings but the signal strength will be reduced, eventually becoming too low to give any readings.

McKenzie (1981) from the Transport and Road Research Laboratory investigated the accuracy of the instrument by measuring the residual steel thickness of I beam samples of weathering steel which had been exposed under simulated bridge decks for five years in different environments such as rural, industrial and marine areas. The only problem occurred when thick, tenacious rust layers were present. The rust layer reduced the signal strength and no reading could be taken until some of the rust had been removed by scraping. In fact, the immediate concern at a particular time is the thickness of steel remaining at any point on a structure. The induction ultrasonic probe provides a suitable means of measuring thickness provided that the corrosion is generally uniform. He pointed out that when the electromagnetic-acoustic induction ultrasonic thickness tester probe was used over the areas of simulated pitting, there was no change in the thickness reading, the only effect being some reduction in signal strength. Clearly, the instrument does not detect pitting of the type simulated. The instrument does not detect minimum and maximum thickness since the given value is the average of thickness under the contact area of the probe. Therefore, this method may not be suitable for roughness measurement of corroded steelwork. General information can be found in Krautkramer et al (1975), American Society for Metals (1976), Silk (1984), Blessing et al (1988) and Stanke et al (1991).

The Cygnus instrument is an advanced type of ultrasonic thickness gauge which uses the impulse echo technique, and allows the testing of steel beneath thick protective coatings and corrosion products. For the purpose of thickness measurement of corroded steel structures at the site it has been found by the Department of Transport in the UK that Cygnus instrument is the most accurate and reliable method compared with conventional ultrasonic methods. The Cygnus ultrasonic instrument uses the pulse echo technique

with a single transducer. Its signal processor measures and compares the time intervals between successive pairs of backwall echoes for reliability.

Figure 3.1 shows a schematic diagram of the technique used by the Cygnus multiple echo technique. It can be seen that the timing between any two successive backwall echoes gives a true indication of thickness of the metal only. The time interval T_2 will equal T_3 for only true backwall echoes. This type of instrument ignores the first transit time which will include the time taken to pass twice through any coating (at very different speeds and time delays to metal). The gauge then measures the time delay between each of three successive echoes where the time taken for a part of the ultrasound energy to pass back through the surface coating and be detected by probe, becomes a constant, and therefore does not alter the time delay between the detection of each of those successive echoes. Therefore, by using the three echoes the Cygnus ensures good accuracy. The accuracy and resolution of the instrument are claimed by the manufactures to be ±0.05 mm.

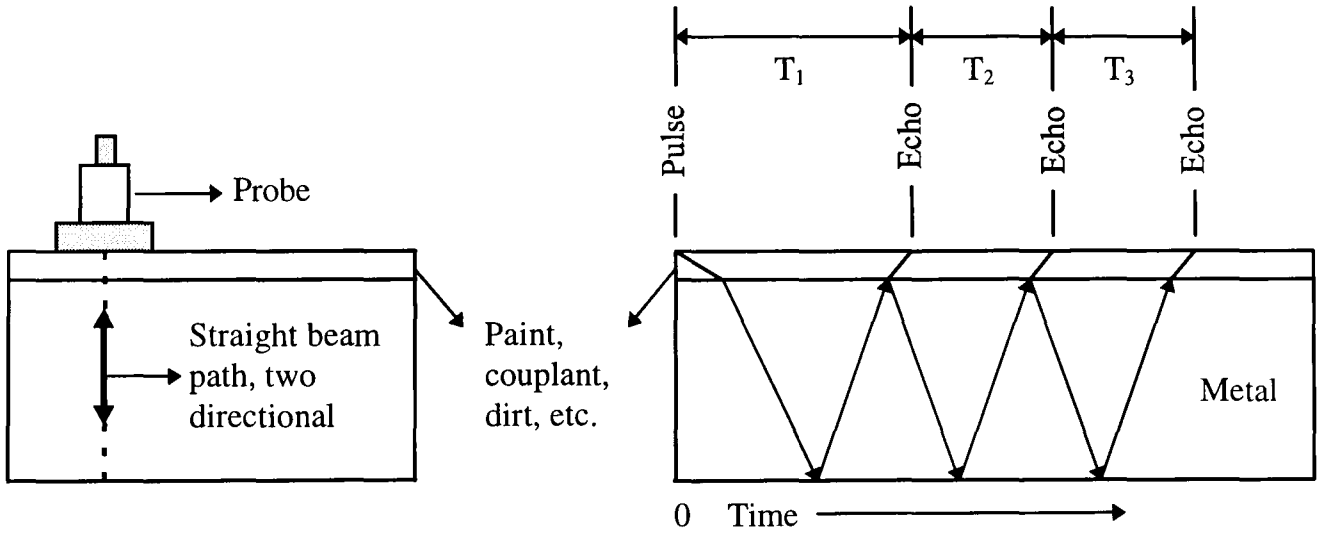

Figure 3.1 Multiple echo single probe.

It has been pointed out by Cygnus Instruments (1996) that the speed of measurement is an advantage of the method because on many bridges, the inspectors prefer to use a mobile underbridge unit, which gives working access to the underside but needs lane closures on the top. It has been reported by one of the bridge inspectors of the Department of Transport in the UK that the Cygnus gauge was able to measure web and

flange thickness on a 23 m span bridge located in Guildford, Surrey in just a few hours. Previously it took two days to obtain the necessary measurements. Also it has been mentioned by Cygnus Instruments (1996) that the bridge inspectors believed that the Cygnus instrument minimizes the time spent near dangerous and busy carriageways.

The main disadvantage of this instrument is that when the surface corrosion causes pitting, these areas when filled with couplant return echoes that will give false readings because the echo is received in advance of the echo from the rear-wall (Cygnus Instruments 1992). However, this method is not suitable for roughness measurement since the probe is not sharp enough and the given value is the average of the thickness under the contact area of the probe.

3.2.4 Grinding method

The grinding method was first introduced by Bengough et al (1935) and Champion (1965). The American Society for Testing and Materials, ASTM G46 (1981) carried out some modification of this method so that it could be used to evaluate the extent of pitting corrosion. Albrecht et al (1988) used the method to measure surface roughness (pit depth) of some corroded steel beams from a railway bridge in the laboratory. An electrically powered disk grinder and an ultrasonic thickness gauge are needed to measure the roughness of corroded surfaces. The procedure for measurement is as follows:

1. A 25 mm wide strip is ground across one side of the tension flange in areas of high stress range and severe corrosion where cracks are likely to initiate until bare metal is exposed on the highest points of the corroded surface, leaving the pits filled with dense oxide. Approximately 30 percent of the surface should have a metallic appearance.

2. The thickness is measured with the ultrasonic thickness gauge at 20 mm intervals along the ground strips. At each measurement point, the ultrasonic probe should be moved slightly around each measurement point and the smallest reading retained. This peak-to-valley reading gives a good estimate of the thickness.

3. The strip is ground further until only traces of corrosion product remain.

4. The thickness is measured again with the ultrasonic thickness gauge and the smallest reading is retained. This represents the valley-to-valley thickness.

5. The valley-to-valley thickness is subtracted from the peak-to-valley thickness measured in step 2 to obtain the maximum roughness of surface (maximum pit depth).

However, this method is not widely used, because it is slow and damages the structure. Moreover, a local area on the existing structure has to be ground and polished which is inconvenient and can adversely affect the behaviour of the structure. Therefore, in the absence of an obvious way of improving the performance of the grinding method in the present application, it was decided to explore other methods. Further information on the use of this method can be found in ASTM E797 (1983).

3.2.5 Stylus method

The most widely used and reliable surface measuring instruments currently used today are mechanical profilometers such as stylus instruments (Kohon et al 1988). For example Talysurf is a type of stylus instrument with very light contact which can be used for assessing surface texture. This technique was first introduced by Abbott and Firestone (1933). This method is based on traversing a diamond stylus across a surface profile to produce an electrical signal which can be plotted as a surface profile on a chart or an average reading meter. The stylus moves up and down as it moves across the surface. This up and down motion effectively replicates the texture of the surface. The instrument consists of two separate units: the traverse unit with a pick-up and the amplifier-recorder.

The principle of the Talysurf is illustrated schematically in Figure 3.2. The pick-up is driven slowly across the surface and a sharply-pointed stylus follows the profile of the surface irregularities. The pick-up has an optical transducer and vertical movements of

the stylus are sensed photo-electrically. The signal is processed for display either on the recorder or on the roughness average meter.

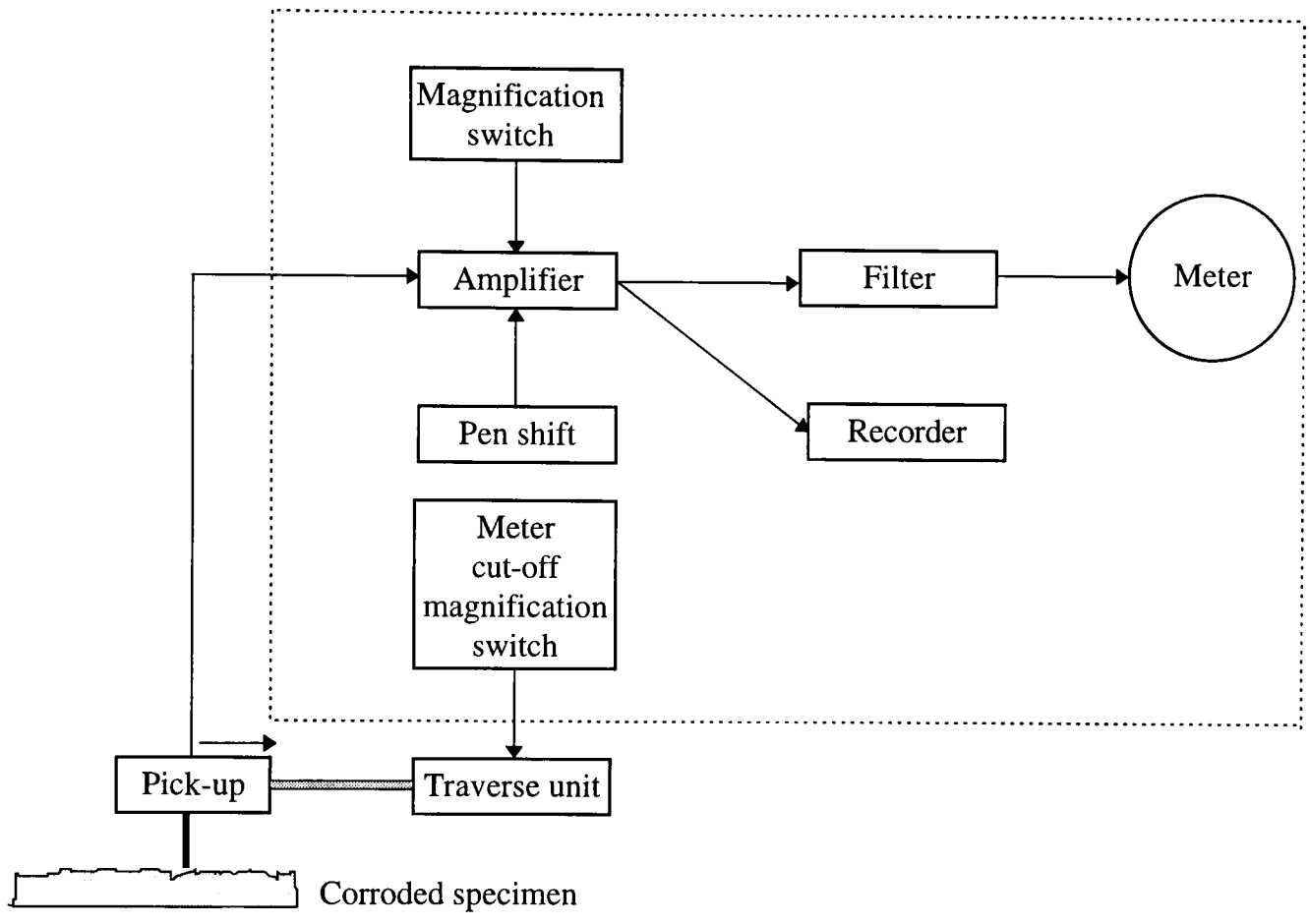

Figure 3.2 Schematic arrangement of Talysurf (Talysurf handbook).

The optical transducer system comprises: (a) a pivoted beam which carries the stylus and slotted flag; (b) light guide and lamp assembly; and (c) beam splitter and photocell. In the balanced position, the slit in the flag is in line with the centre of the beam splitter; and light passing through the slit falls equally on the upper and lower elements. Thus, the electrical signals from the photocells balance. When the stylus moves up or down, the corresponding movement of the flag across the beam splitter causes more light to fall on one photocell than on the other. As a result there is a decrease in signal from one which is accompanied by a corresponding increase in signal from the other. This change in signal is proportional to the deflection of the stylus. The signals from the photocells are amplified before being fed to the amplifier-recorder for display graphically or for further processing before being display on the meter.

In order to get a true measure of the roughness of a surface it is necessary to choose a sampling length which should be long enough to include the various roughness crest spacings exhibited by the surface. In electrical integrating instruments the meter cut-off values are made equal to the sampling lengths. When the instrument is switched to the desired meter cut-off, the pick-up will traverse the surface to give average results from several (normally 5) consecutive sampling lengths.

The operation of the Talysurf is simple and may provide rapid analysis in the workshop or laboratory with high resolution and accuracy, because the probe of the pick-up is made of diamond material with a tip diameter of 0.8 mm. This method is believed to be most useful in the field of finishing and manufacturing processes (Bhushan 1995). However, the instrument is designed for measuring smooth surfaces (with roughness measured in microns). Moreover, the other problems associated with this type of instrument for site measurement are manifest: its bulk, its relative fragility, its high cost and the limitation of traversing length (2 to 50 millimetre). Therefore, this method may not be recommended for the purpose of measuring roughness of corroded steelwork with very rough surfaces. Further detail on the use of this technique can be found in Greenwood et al (1966) and Hondros (1971).

3.2.6 Large scale profilometers

Numerous methods have been developed for measurement of uneven surfaces of roads under the wheel paths. Although this work is not directly relevant to corrosion roughness, the principles may be of interest if there is no fixed reference point. The development of rutting in road surfaces is an important factor because of its implication for road safety and its significance as an indicator of structural conditions (Alm 1977). A study was performed for measurement of rut depths in road surfaces by Jordan et al (1982) using the Transport and Road Research Laboratory (TRRL) high-speed profilometer. The method of measurement and the evaluation of the factors affecting the accuracy of measurement have been described and discussed. Also Cooper (1983) used the same instrument to monitor the surface geometry of the Humber bridge.

The wheels of the trailer ride in the ruts and the height of the axle from the road surface is measured by the laser sensors, along a line centred between the wheel paths. The difference between the axle height on a deformed surface and that obtained on a plane surface gives the rut depth averaged over both wheel paths as shown in Figure 3.3.

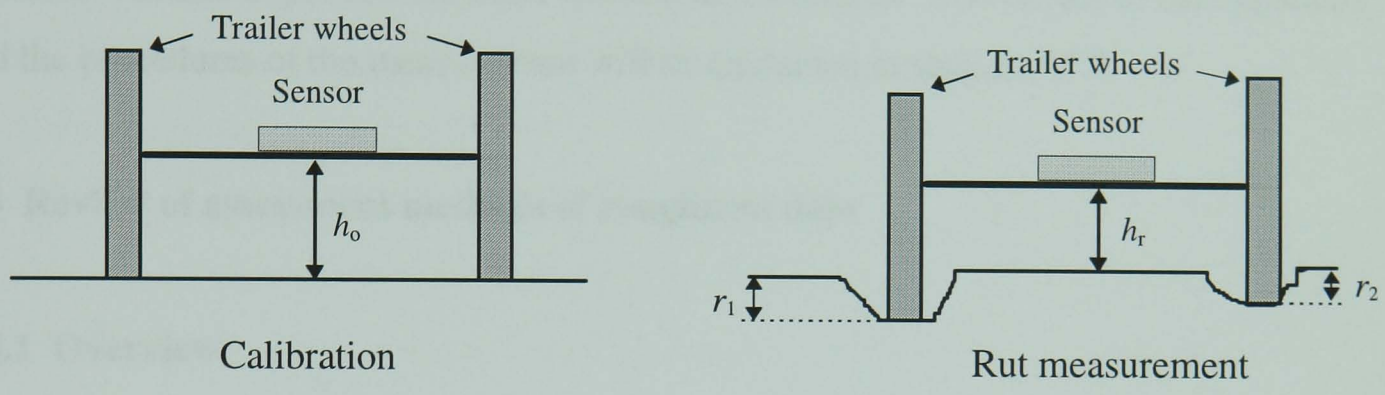

Figure 3.3 Rut depth measurement.

The profilometer consists of a two-wheel trailer supporting a 4.5 meter long beam on to which four laser sensors are mounted. On the profilometer beam the configuration of sensors is such that none of the sensors are positioned on the line of the axle. Consequently the axle height is obtained, as described in Jordan et al (1982), from a linear interpolation of the height measurements made by sensors positioned on either side of the axle.

A description of the use of high-speed profilometer can be found in Dickerson et al (1976) and Still et al (1980). Further experiments were carried out using of this technique by Henry et al (1975), Lister et al (1978) and Chaka (1979).

Although the type of profilometers that are used on highways are not directly suitable for corroded surfaces, the principle of operation may be relevant to site measurements. This is because measurements of roughness on site do not have an available reference point, in general, as is the case of highway profiles.

3.2.7 Longitudinal profile system using displacement transducer

A technique was developed in this study based on direct physical measurement of depth with a displacement transducer which was moved over the surface to be scanned. The system consists of two linear variable differential transformers (LVDT), one of which measures vertical depth and the other horizontal movement. The details of the apparatus and the procedures of the measurement will be explained in section 3.5.2.

3.3 Review of assessment methods of roughness data

3.3.1 Overview

Courtel et al (1963) pointed out that little is known about the publications of Belidor in the eighteenth century, but he was one of the first to conclude that the surfaces of solids are uneven and consist of a multitude of hemispherical peaks and valleys. He derived an elementary expression for force required to surmount these obstacles and permit relative motion between surfaces. Later, Coulomb investigated further the effect of surface finish for lubricated and unlubricated surfaces. Ernst and Merchant (1940) advanced a hypothetical two-term expression for friction, showing the adhesion and surface roughness contributions as separate entities. It was Bowden (1950), however, who performed the most outstanding work on the physics of rubbing surfaces and surface roughness, which gave rise to his classic friction-welding theory for metals.

It has been pointed out by Posey (1946) that the scientific measurement of roughness presents a difficult problem. With sufficient care and ingenuity, it is possible to record the profile of a surface accurately. The difficulty lies in deciding what is to be done with this record. Posey suggested that three parameters (histograms of the profile itself and its slope and curvature) for a representative length of profile, give sufficient information to permit a complete characterisation of the texture. Moore (1969) has mentioned that Posey was well aware some twenty three years ago of the inadequacy of single numerical parameters to define texture (i.e., the root-mean-square of deviations from the average as used in the USA, or the British concept of arithmetic average height measured outward

from the centre-line). Myers (1962) listed a new series of single elementary parameters to define texture (these will be described later), but he carefully indicated that depending on the particular application each of the new parameters might be considered more useful than the others. Thus, to determine the degree of wear which a surface has undergone, the root-mean-square of the second derivative of the profile (i.e., its degree of curvature at peaks or sharpness) would be most appropriate, or perhaps the light scattering properties of a surface would best be described by determining the root-mean-square of the profile itself or its first derivative.

The statistical nature of surface profiles has been studied by many investigators. Moore (1969) has shown that whereas the required autocorrelation function or dispersion spectrum of a surface profile may be too complex an undertaking for practical applications, the standard deviation of the slope and the mean thickness of profile (parameters which may be readily computed) are definite numbers which correlate well with the autocorrelation function. Prior to the work, autocorrelation functions or dispersion spectra had been used by Papoulis et al (1965) and Press et al (1992) to describe surface roughness. A common assumption is that the height distribution curve obtained from the profile is normal or approximately normal (Tsukizoe et al 1968). Bendat et al (1986) clearly distinguished between stationary and non-stationary random profiles. He showed that the basic statistical properties of importance for describing stationary random records are: probability density distributions, and autocorrelation and power spectral density functions. For stationary profiles taken in pairs, cross-correlation and cross-spectral density functions and frequency response parameters are significant. Hasunuma (1966) reviewed Japanese research results on the statistical characterisation of surface profiles.

At one time measurement of the surface was considered largely irrelevant but it soon became apparent that the finish on the surface was extremely sensitive to any changes in the process (Whitehouse 1997). Hence it became logical to assume that measurement of the surface could be used to control the process of manufacture. The argument was that, if the surface parameter being measured remained constant from workpiece to workpiece, then the process must be under control. Any change in the surface parameter

should initiate a review of the process parameters. In the UK and USA the average roughness was used as the control parameter whereas in Germany and USSR peak parameters were used (Schlesinger 1942 and Schorsch 1958). The UK approach was pragmatic in the sense that the parameter specified on the drawing had to be measurable. In Germany the approach was to use parameters such as the maximum peak-to-valley height on the surface, in an attempt to impose functional constraints on the surface as well as manufacturing control. The peak parameters, however, are inherently divergent, they become larger as the sample size increases. Also, sometimes the maximum values of parameter are difficult to find over a large area of the surface. Extreme peak-valley measures soon degenerated into measurements of average peak-valley height and so on simply in order to make them reliable.

Although the use of a single parameter of the surface roughness could be used to indicate a change in the manufacturing process, it is not sufficiently discriminating to pinpoint where the changes in the process have occurred. Even using a number of simple parameters rather than just one fails to provide the necessary discrimination. It is only recently that surface metrology has become comprehensive enough to be used as a diagnostic tool. This capability arose because of the advent of random-process analysis. That is, the use of autocorrelation, power spectra and probability density functions.

3.3.2 Characterisation of surface roughness

Surface profile is generally divided arbitrarily into three classifications according to its scale such as roughness, waviness and errors of form (Tsukizoe 1970). Roughness shows closely spaced irregularities, the height, width and direction of which create the predominate surface pattern. Roughness includes those surface features intrinsic to the production process. Waviness shows surface irregularities of greater spacing than roughness. Errors of form are gross deviations from the nominal or ideal shape. They are not normally considered part of the surface textures.

Thomas (1975) pointed out that a large number of parameters have been defined and used to describe roughness, which are explained in the following sections.

3.3.2.1 Peak-to-valley height

Peak-to-valley height, R_{max} is defined as the distance between the highest peak and lowest valley on the profile as shown in Figure 3.4.

$$R_{max} = h_3 - h_6 \tag{3.1}$$

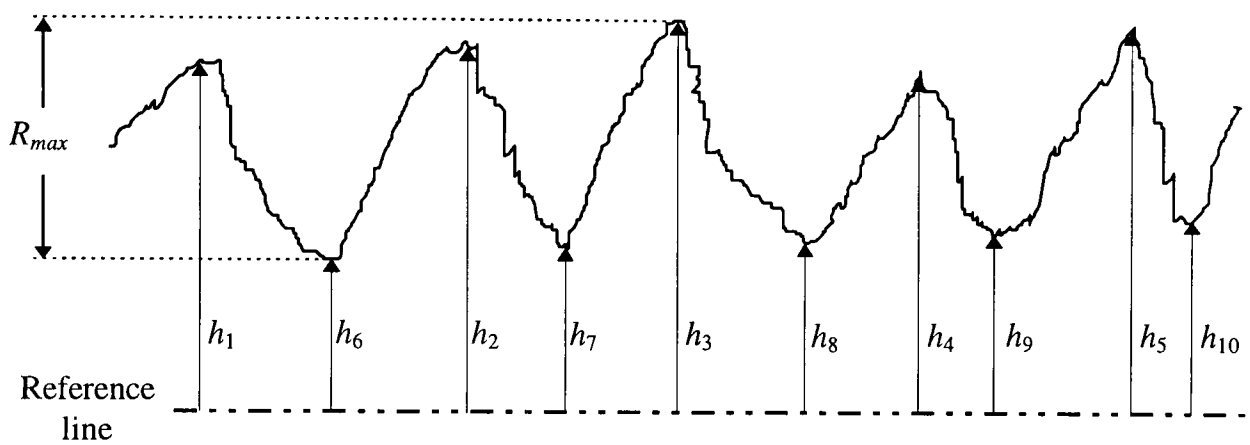

Figure 3.4 Randomly rough profile showing ten-point height.

where h is the distance from the reference of profile. Its sole advantage is ease of definition and it is inconveniently sensitive to typical surface events such as scratches.

3.3.2.2 Ten-point height

This is the difference in height between the average of the 5 highest peaks on the profile and the 5 lowest valleys. It is free from the disadvantages of peak-to-valley height but has no particular advantage. Figure 3.4 shows how the following equation can be used for obtain ten-point height, R_z.

$$R_z = \frac{1}{5}\left\{\sum_{i=1}^{5} h_i - \sum_{i=6}^{10} h_i\right\} \tag{3.2}$$

3.3.2.3 Centre-line average

It has become common to digitise the surface profile, to give a record which is more amenable to statistical analysis and to separation of its periodic and random elements. In this technique the analogue output from the amplifier is digitised at discrete intervals, as shown in Figure 3.5, to give a sequence of height readings relative to the profile centre line.

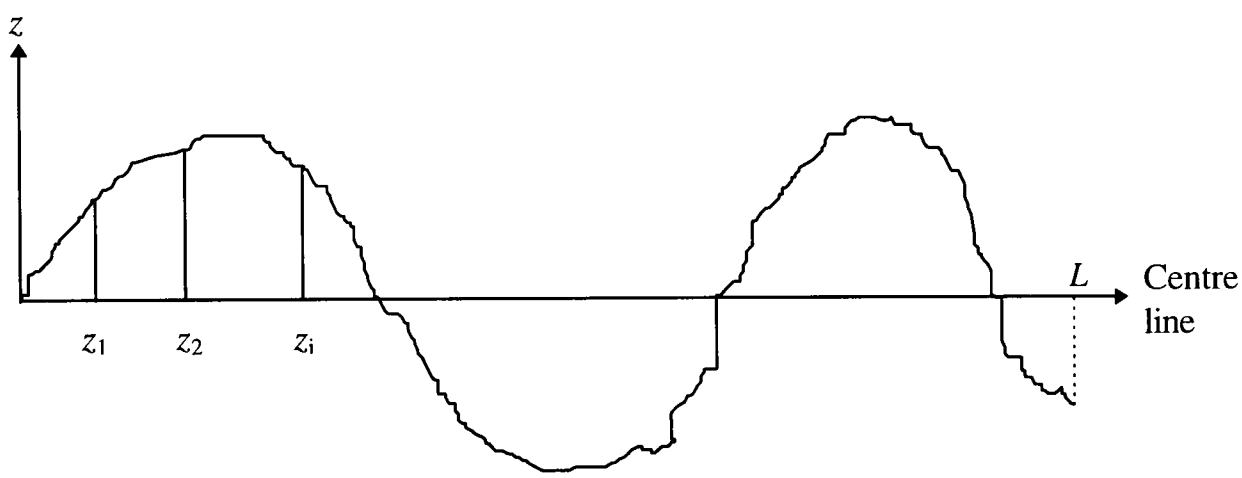

Figure 3.5 Surface height readings taken at discrete intervals.

The most universally used roughness parameter because of its ease of measurement is defined for a profile of length, L in the x-direction is centre-line average, R_a which can be defined by the following relations.

The mean-line is defined by

$$\int_0^L z\,dx = 0 \tag{3.3}$$

The average roughness is

$$R_a = \frac{1}{n}\sum_{i=1}^{n} |z_i| \tag{3.4}$$

For a continuous profile, equation (3.4) can be rewritten as

$$R_a = \frac{1}{L}\int_0^L |z|\,dx \tag{3.5}$$

where z is surface height measured from the mean line. Alternatively, the centre-line average mean line is defined as the line such that the area above is equal to the area of void below. However, the centre-line average has no particular physical significance.

3.3.2.4 Root-mean-square

A well known numerical evaluation for characterising surface roughness is the root-mean-square (r.m.s), S, of the deviations from the centre-line average (Myers 1962). Although this characteristic is useful for the measuring gross roughness, it does not meet all of the requirements of today's high technological standards. Many different surfaces may all have the same r.m.s value even though their geometrical properties differ greatly.

Formerly in use in the USA, the r.m.s roughness has now almost dropped out of practical usage although it has attained considerable circulation in the theoretical work (Thomas 1975). It is defined by

$$S = \sqrt{\frac{1}{n}\sum_{i=1}^{n}(z_i)^2} \tag{3.6}$$

For a continuous profile, equation (3.6) can be rewritten as

$$S = \sqrt{\frac{1}{L}\int_0^L z^2\,dx} \tag{3.7}$$

As it is weighted by the square of the heights it tends to be more sensitive than centre-line average, R_a, to large deviations from the mean line, but this is not necessarily a disadvantage. The r.m.s roughness is the only roughness parameter with any fundamental significance; it is the standard deviation of the distribution of surface heights

and as such it is of fundamental importance in any attempt to describe surface roughness by statistical methods.

Papoulis (1965) has pointed out that a rough surface is often assumed to be a statistically random process. This means that the measured roughness sample is a true statistical representation of the entire rough surface. Therefore, the probability distribution and the standard deviation of the measured roughness should remain unchanged, except for fluctuations, if the sample size or the location on the surface is altered. The properties derived from the distribution and the standard deviation are therefore unique to the surface, thus justifying the use of such roughness characterisation techniques.

Due to the simplicity in calculation and its physical meaning as a reference height scale for a rough surface, the r.m.s height of the surface is used extensively in tribology. However, it was shown by Sayles and Thomas (1978) that variance of the height distribution is a function of the sample length and in fact, suggested that the variance varied as

$$S^2 \approx L \tag{3.8}$$

where L is the length of the sample. This behaviour implies that any length of the surface cannot fully represent the surface in a statistical sense. This proposition was based on the fact that beyond a certain length, L, the surface heights of the same surface were un-correlated such that the sum of the variances of two regions of lengths L_1 and L_2 can be added up as

$$S^2(L_1 + L_2) = S^2(L_1) + S^2(L_2) \tag{3.9}$$

They gathered roughness measurements of a wide range of surfaces to show that the surfaces follow the non-stationary behaviour of equation 3.8. However, Berry and Hannay (1978) suggested that the variance can be represented in a more general way as follows:

$$S^2 \approx L^n \tag{3.10}$$

where n varies between 0 to 2.

If the exponent n in equation 3.10 is not equal to zero for a particular surface, then the standard deviation or the r.m.s, S, is scale dependent, thus making a rough surface a non-stationary random process. This basically arises from the multi-scale structure of surface roughness where the probability distribution of a small region of the surface may be different from that of the larger surface region.

Nayak (1973) has pointed out the other statistical parameters that are also used in tribology are the first and second derivatives of equation 3.7 which gives the r.m.s slope, S', and r.m.s curvature, S'', respectively.

3.3.2.5 Statistical features of the surface profile

Bendat et al (1986) has mentioned the basic statistical properties of importance for describing single, stationary random profiles as

(a) mean and root-mean-square values,
(b) probability density and distribution functions,
(c) autocorrelation functions and
(d) power spectral density functions.

These can be conveniently derived from the profile of the surface under consideration. The mean and r.m.s values have been described in previous section. The probability density distribution function for a single random profile has the familiar bell shape in probability theory, the total area under this curve from $-\infty$ to $+\infty$ being unity. This simply indicates the certainty that the amplitude must fall in this range. The partial area under the probability function from $-\infty$ to some given value represents the probability that the amplitude values will fall below this given value (Bendat et al 1986). Further detail on the use of probability density distribution function can be found in Papoulis (1965), Thomas (1982) and Bhushan (1990).

The autocorrelation function for a single record is obtained by delaying the record relative to itself by some fixed interval, then multiplying the original record by the

delayed profile and averaging the product values over a representative length of profile. This technique with the exception of the structure function, is well documented in standard textbooks e.g., Bendat and Piersol (1986) and only a brief description will be given here.

With reference to Figure 3.6, $C(\Delta)$ denotes the autocovariance function for a profile measured in the x-direction with an amplitude variation described by $z = f(x)$.

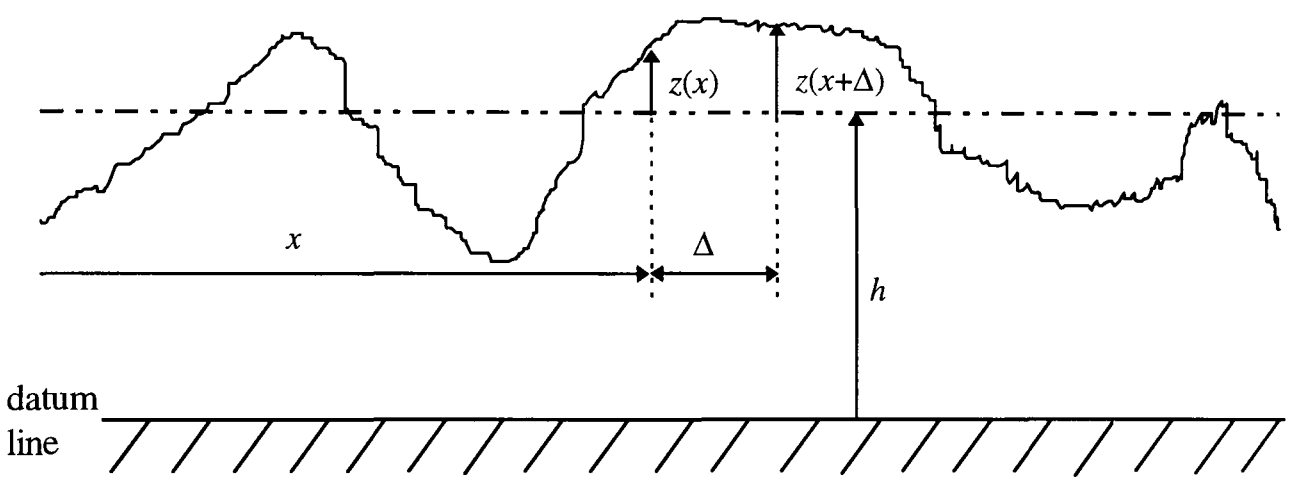

Figure 3.6 Height distribution of randomly rough profile.

Thus for a continuous profile

$$C(\Delta) = \lim_{L\to\infty} \frac{1}{L} \int_0^L z(x)\, z(x+\Delta)\, dx \tag{3.11}$$

where L is the sample length and Δ is the delayed interval.

Equation 3.11 can be written in a more statistical form;

$$C(\Delta) = E\left[z(x)\, z(x+\Delta)\right] \tag{3.12}$$

where $E[\ ]$ denotes an expectation, i.e. an average value of $[z(x)\ z(x+\Delta)]$ over an ensemble of values covering the sample length. It is observed from equations 3.11 and 3.12 that when $\Delta = 0$ the autocorrelation function is identical with the variance or mean

square value of the profile. The autocorrelation function, $R(\tau)$ is simply the autocovariance function normalised by the profile sample variance, S^2 (i.e. the square of the r.m.s roughness). Thus

$$R(\tau) = \frac{C(\Delta)}{S^2} \tag{3.13}$$

An interesting observation by Greenwood (1966) is that the mean and autocorrelation functions completely characterise the profile in a statistical sense, provided that the profile function $z(x)$ is both stationary and Gaussian. Indeed, it assures us that the assumption of Gaussian or normal distribution of asperity heights in a profile is valid.

The power spectral density function for a single record represents the rate of change of mean square value with frequency, where the mean square value is taken in a narrow frequency band at various centre frequencies. If $z(x)$ is the surface profile in the x-direction, the power spectrum of the profile can be found by the following relation (Papoulis 1965 and Blackman et al 1958)

$$P(\omega) = \frac{1}{L}\left|\int_0^L z(x)\exp(i\omega x)\,dx\right|^2 \tag{3.14}$$

where the coordinate x ranges from 0 to L. The power spectrum can be obtained from a measured roughness profile by a fast Fourier transform routine (Press et al 1992). The square of the amplitude of $z(x)$ or the power at a frequency ω is equal to $P(\omega)d\omega$. The r.m.s height, the r.m.s slope, and the r.m.s curvature can be obtained from the power spectrum (McCool 1987 and Majumdar et al 1990).

$$S = \sqrt{\int_{\omega_L}^{\omega_h} P(\omega)\,d\omega} \tag{3.15}$$

$$S' = \sqrt{\int_{\omega_L}^{\omega_h} \omega^2 P(\omega)\, d\omega} \tag{3.16}$$

$$S'' = \sqrt{\int_{\omega_L}^{\omega_h} \omega^4 P(\omega)\, d\omega} \tag{3.17}$$

where ω_L and ω_h are the low frequency and the high frequency cut-offs, respectively. For a roughness measurement, the low frequency cut-off is equal to the reciprocal of the sample length, $\omega_L = 1/L$ and the high frequency cut-off is equal to the Nyquist frequency or equal to $\omega_h = 1/2\Delta$ where Δ is the distance between two adjacent points of the data sample. It is evident that the power spectrum is a more fundamental quantity than the r.m.s values since the r.m.s values can be obtained from the spectrum and not vice versa.

3.3.2.6 Other mathematical approaches

Early investigators considered that one parameter would suffice to characterise surface texture, the choice depending on the application and field of research in question. A direct mathematical approach was presented for obtaining numerical values for the main components of surface geometries by Myers (1962). He developed three new characteristics that are useful in giving numerical values to certain components of surface roughness. For a more representative description of surface texture he recognised the necessity of combining at least two of these new parameters.

These new characteristics are valuable in identifying the physical geometry of surfaces and in studying the correlation between this geometry and other surface properties, such as friction and light reflection. They will also be useful in specifying surface geometries for fabrication or quality control. These new characteristics are derived from the first and second derivation of a surface profile and together with the standard r.m.s, provided a more complete description of surface roughness than any previous summation method (Posey 1946).

The American Standards Association (1955) pointed out that the standard r.m.s and three new characteristics are defined as follows:

Standard root-mean-square (S)

$$S = \sqrt{\frac{1}{L}\int_0^L z^2\,dx} \qquad \text{(units of length)} \qquad (3.18)$$

where z is the amplitude of roughness.

First new characteristic (S_1)

$$S_1 = \sqrt{\frac{1}{L}\int_0^L \left(\frac{dz}{dx}\right)^2 dx} \qquad \text{(dimensionless)} \qquad (3.19)$$

or the root-mean-square of the first derivative of the surface profile.

Second new characteristic (S_2)

$$S_2 = \sqrt{\frac{1}{L}\int_0^L \left(\frac{d^2z}{dx^2}\right)^2 dx} \qquad \text{(units of length}^{-1}\text{)} \qquad (3.20)$$

or the r.m.s of the second derivative of the surface profile.

Third new characteristic (S_3)

$$S_3 = \frac{\sum(\Delta x_i)_p - \sum(\Delta x_i)_n}{L} \qquad (3.21)$$

or the sum of the distances along the profile that the slope is positive, minus the sum of the distances where the slope is negative, divided by the total profile distance. where

$L = \sum(\Delta x_i)_p + \sum(\Delta x_i)_n$ = total profile distance

p = positive slope

n = negative slope.

Each of these characteristics may more useful than the other for a particular application. The parameter S_1 is perhaps more appropriate when considering the importance of the slopes of asperities (light scattering properties), S_2 is a sensitive indicator of the sharpness of the peaks. The directional parameter, S_3 represents the excess of the percentage of distance along the profile where the slopes of the asperities are positive over that where the slopes are negative. Although most descriptions of texture ignore the directional effect, it has important wear implications in cases where the relative velocity of sliding varies systematically. A typical application is pavement texture at the approach to a traffic signal, where the predominantly braking mode of vehicle behaviour introduces a positive S_3 and wears a symmetry into the pavement in the direction of travel. Also a series of tests was conducted by Myers (1962) to determine the values of these characteristics in predicting the frictional properties of surfaces.

3.3.2.7 Roughness parameter developed for confocal microscopy

As mentioned in section 3.2.2, this type of microscope optically sections the surface, and a computer transforms a series of sections into digital images and a topographic map. Using a straightforward algorithm, the computer analyses the topographic map to derive a roughness parameter that characterises the texture of the surface (Lange et al 1993). The algorithm approximates the surface area of a topographic map by calculation of the surface area of elements defined by four adjacent pixels and then summing the surface elements over the entire image. A roughness number, R_ℓ, is computed from the following equation

$$R_\ell = \frac{\text{actual surface area}}{\text{projected surface area}} \qquad (3.22)$$

Plane geometry is used to find the surface area of each element. A representative element of area is illustrated in Figure 3.7. The Z-levels of four adjacent pixels are

shown as Z_1, Z_2, Z_3 and Z_4. The line segments between points are shown as ℓ_{12}, ℓ_{23}, ℓ_{34}, ℓ_{41} and ℓ_{13}. The line segments create the sides of two triangles for which areas can be computed. The sum of the two triangular areas provides an approximation of actual surface bounded by the four adjacent pixels. The equations used for this procedure are explained below.

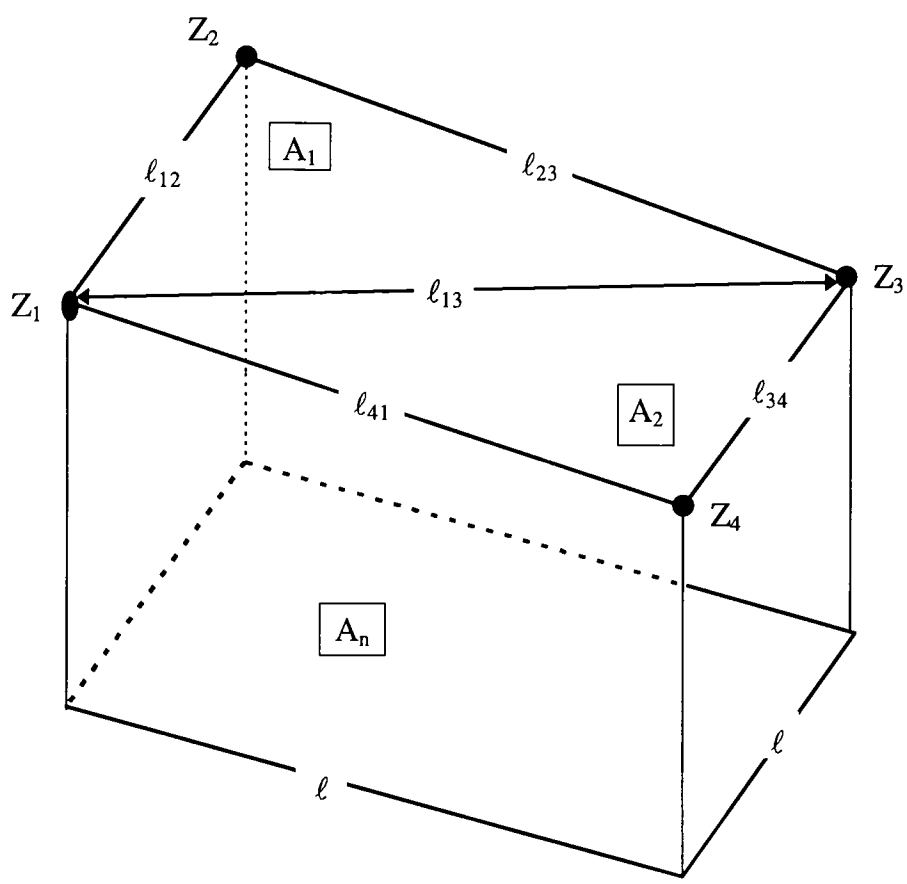

Figure 3.7 Representative area element bounded by four neighbouring pixels in the topographic map (Lange et al 1993).

Line segments are given by

$$\ell_{ij} = \sqrt{\left[\ell^2 + (Z_i - Z_j)^2\right]} \tag{3.23}$$

except for ℓ_{13} which is

$$\ell_{13} = \sqrt{\left[2\ell^2 + (Z_1 - Z_3)^2\right]} \tag{3.24}$$

Triangle perimeters are given by

$$2P_1 = \ell_{12} + \ell_{23} + \ell_{13} \tag{3.25}$$

$$2P_2 = \ell_{34} + \ell_{41} + \ell_{13} \tag{3.26}$$

Triangular areas are given by

$$A_1 = \sqrt{[P_1(P_1 - \ell_{12})(P_1 - \ell_{23})(P_1 - \ell_{13})]} \tag{3.27}$$

$$A_2 = \sqrt{[P_2(P_2 - \ell_{34})(P_2 - \ell_{41})(P_2 - \ell_{13})]} \tag{3.28}$$

Actual surface area is given by

$$A_a = A_1 + A_2 \tag{3.29}$$

Nominal surface area is given by

$$A_n = \ell^2 \tag{3.30}$$

Roughness parameter is given by

$$R_\ell = \frac{\text{actual surface area}}{\text{no min al surface area}} \tag{3.31}$$

Equation 3.31 can be written alternatively as:

$$R_\ell = \frac{\sum A_a}{\sum A_n} \tag{3.32}$$

The computed area of a specific element may vary depending on whether the algorithm makes two triangles by connecting points Z_1-Z_2-Z_3 and Z_1-Z_3-Z_4 instead of Z_1-Z_2-Z_4 and Z_2-Z_3-Z_4. However, such differences may be neglected when summing over 250,000 elements in an image (Lange et al 1993).

3.3.2.8 Roughness parameters used in this study

It has been mentioned in previous chapter that corrosion pits acts as micro-notches and therefore give rise to stress concentration which can reduce fatigue life severely. A corroded surface is random in its roughness and recourse to statistical evaluation is required as suggested by Kitagawa et al (1983). Therefore, for the purpose of this study three measures of surface roughness including maximum roughness, mean roughness and standard deviation of the roughness were investigated from the variation in thickness measurements. In order to calculate the above parameters the following steps were followed:

The first step is to determine the average depth of corrosion of each specimen. This was achieved by means of thickness measurements using an anvil micrometer. Hence, referring to Figure 3.8 the depth of corrosion of one exposed face is given by

$$d_c = \frac{1}{2}(t_o - \bar{t}) \tag{3.33}$$

where t_o = original thickness and mean thickness is given by

$$\bar{t} = \frac{1}{n}\sum_{i=1}^{n} t_i \tag{3.34}$$

where t_i is a thickness measurement and n is the number of measurements.

Figure 3.8 Detail thickness measurements of unmachined corroded specimen.

The next step was to machine each specimen flat on one face only, enabling accurate measurement of corrosion pitting to be achieved. The variation in thickness of each corroded specimen was measured over a specific grid at the centre of the specimen.

The parameters were calculated from the detailed thickness measurements (see Figure 3.9):

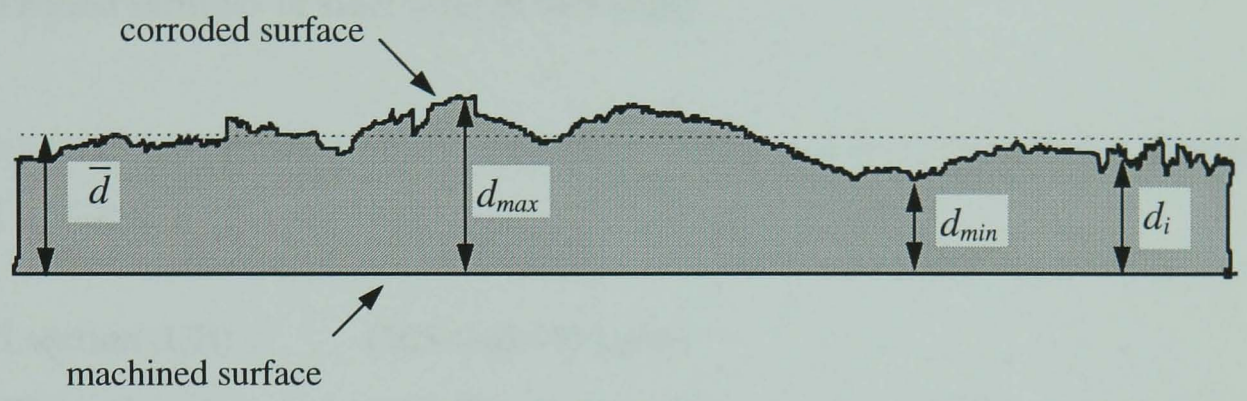

Figure 3.9 Detail thickness measurements of one face machined corroded specimen.

The parameters are described and identified as follows:

1. the maximum roughness R_{max}, defined as the difference between the highest and lowest measured points on the surface;

$$R_{max} = d_{max} - d_{min} \tag{3.35}$$

where d_{max} is the maximum thickness and d_{min} is the minimum thickness measured,

2. the mean roughness R_m, defined as the average deviation of points on the surface from the mean corrosion penetration;

$$R_m = \frac{1}{n}\sum_{i=1}^{n} \left| d_i - \bar{d} \right| \tag{3.36}$$

where $\bar{d}$ = mean thickness

d_i = thickness reading

n = total number of measurements

3. the standard deviation of the roughness S_d, which is the standard deviation of the surface from the mean corrosion penetration.

$$S_d = \sqrt{\frac{1}{n-1}\sum_{i=1}^{n}\left(d_i - \bar{d}\right)^2} \tag{3.37}$$

3.4 Corroded samples of steel used in this study

The basic materials provided were in the form of samples of severely corroded structural sections as follows:

A: I section (UB) (305×165×40 kg/m)

B: Channel section (305×89×41.69 kg/m)

The beams were mild steel and recovered from two different industrial plants undergoing demolition. In this experiment forty specimens were used. Twenty six of the specimens were cut from the flanges, the webs and the stiffeners of three universal beams and the remaining from the web of a channel beam. The paint system had completely broken down with only remnants of the paint on the webs. The beams were all in a severely corroded condition (nearly 40 years old) with the thickness diminishing almost to zero in places as can be seen in Figure 3.10. A diagram of the location of holes in beam 3 is shown in Figure 3.11.

The thickness of these beams were measured by an instrument which was designed specially for this purpose. The instrument, which was used together with a depth gauge, is shown in Figure 3.12. As many readings as possible (up to 150 readings for each beam) were taken in order to increase the accuracy of the measurements. Average measurements of the thicknesses are shown in Table 3.1. The loss of thickness on average was more significant in the flanges than in the webs or stiffeners. Standard test specimens were used as shown in Figure 3.13. The corrosion products were removed from the surface by using a chemical solution consisting of 2/3 volume of hydrochloric acid (66%), 1/3 volume of water and 10% weight hexamine.

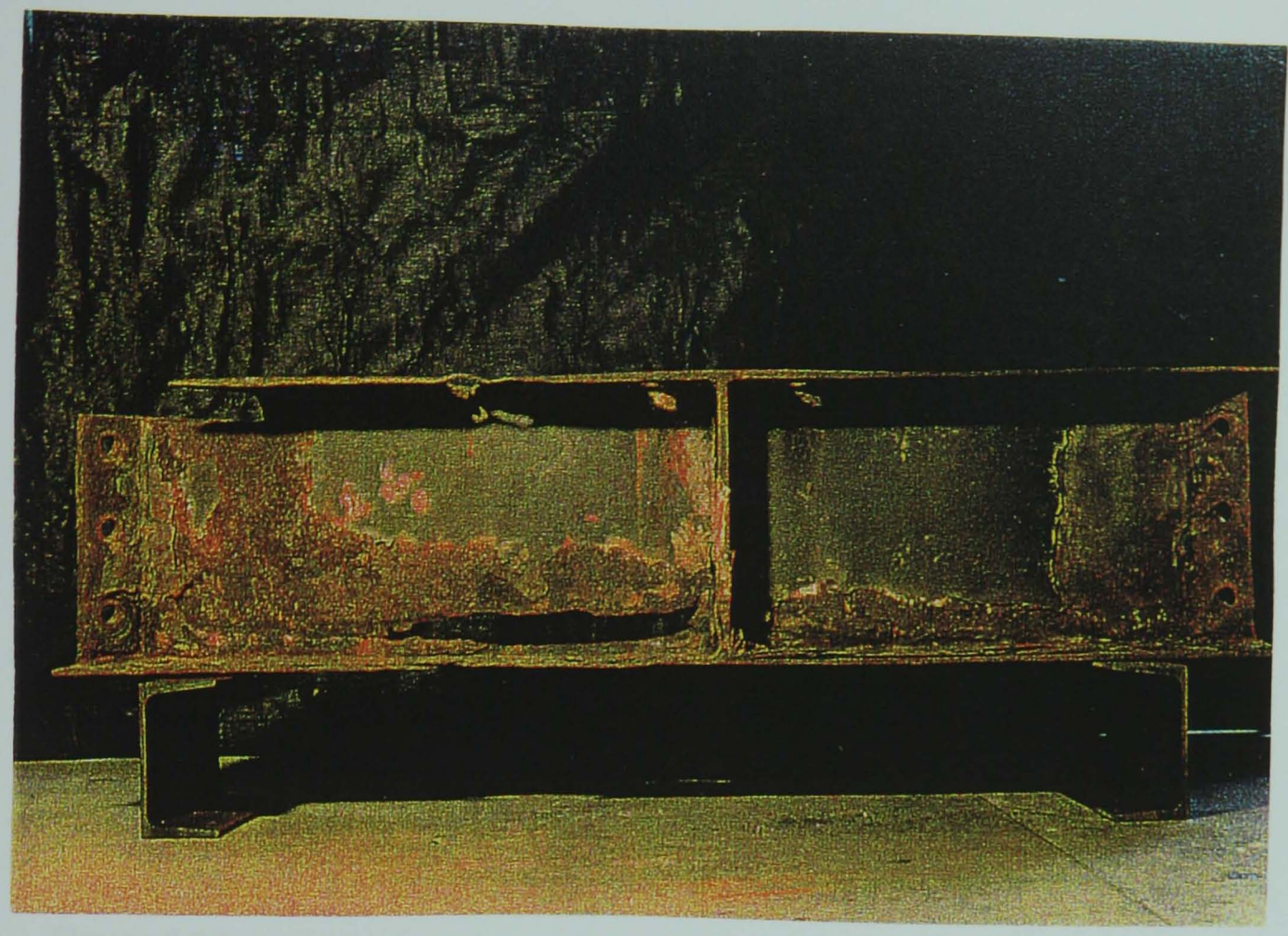

Figure 3.10 Corrosion damage of beam 3.

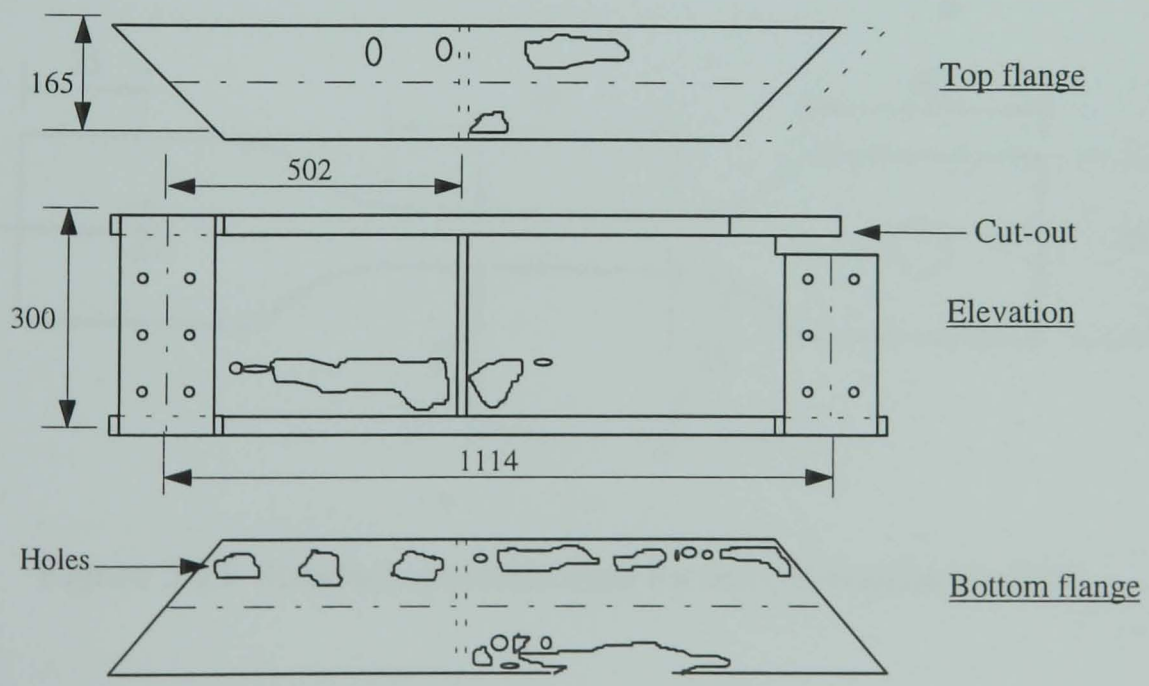

All measurements are in millimetres

Figure 3.11 Detail of holes in beam 3.

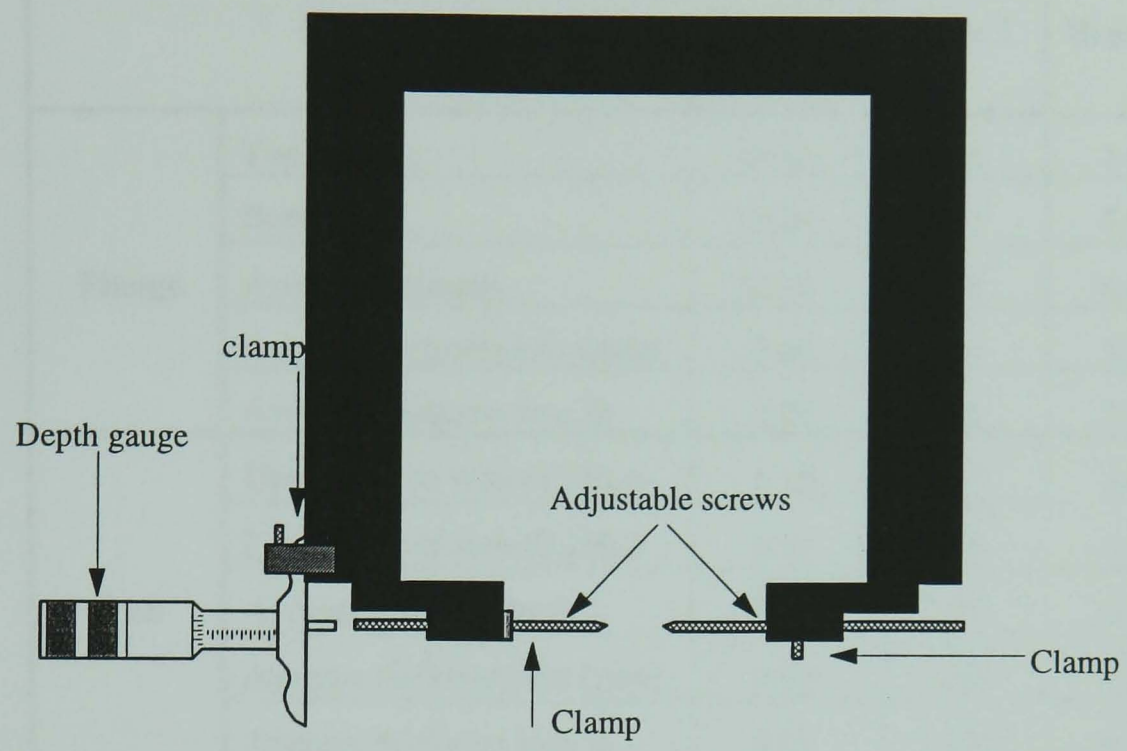

Figure 3.12 Instrument used for thickness measurements of sample beams.

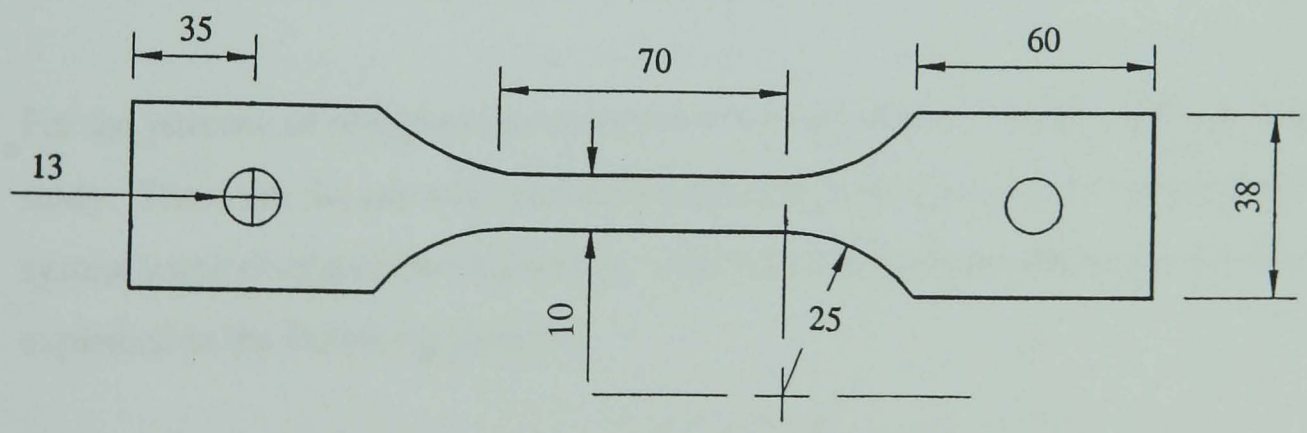

Figure 3.13 Standard specimen used for test (dimensions in mm).

Table 3.1 Average measured thicknesses of corroded beams.

Element		As new	Beam 1	Beam 2	Beam 3
Flange	Top	10.20	7.45	7.81	7.23
	Bottom	10.20	5.62	5.85	4.84
	Average thickness	10.20	6.54	6.83	6.04
	Average thickness loss (mm)	0.00	3.66	3.37	4.16
	Average thickness loss %	0.00	35.9	33.3	40.8
Web	Upper part of web ($0.75h_w$)	6.10	5.63	5.74	5.45
	Lower part of web ($0.25h_w$)	6.10	3.16	4.32	3.18
	Average web thickness	6.10	5.01	5.39	4.88
	Average thickness loss (mm)	0.00	1.09	0.71	1.22
	Average thickness loss %	0.00	17.8	11.7	20.0
Stiffener	Average stiffener thickness	9.50	8.55	8.66	8.63
	Average thickness loss (mm)	0.00	0.95	0.84	0.87
	Average thickness loss %	0.00	10.0	8.80	9.16

Note: h_w = depth of web, all measurements are in millimetres

3.5 Methods used in this study for measurement of roughness

For the purpose of roughness measurement two different methods have been used in this study. These are the manual optical method using a microscope and longitudinal profile system using displacement transducer. The measurement procedure of both methods are explained in the following sections.

3.5.1 Manual optical method using a microscope

3.5.1.1 Measurement procedure

As mentioned in section 3.2.2, the simplest way of performing roughness measurement is by using a calibrated focal depth scale. The variation in thickness of each corroded

specimen was measured over a 11×70 millimetre grid at the centre of the specimen. The thicknesses of twenty corroded specimens from three universal I beams were measured. The visual examination of the specimens showed that the pits had various sizes and shapes (round, elongated or irregular). Therefore, it was decided to improve the accuracy of results by taking measurements at every millimetre of surface.

The following procedure was used.

1. Each corroded specimen was machined on one face only in order to have a reference point for measurement (see Figure 3.9).

2. The microscope was focused on the platform where specimen was placed for measurement as the reference point.

3. The microscope was focused on the specimen. The difference in displacement caused by focusing on the stage and specimen will give the thickness at a certain position.

4. Step 3 was repeated for every millimetre over a grid of 11×70 along the length and width of each specimen.

5. Surface roughness were calculated from the detailed thickness measurements by using equations given in section 3.3.2.8.

3.5.1.2 Results of the measurement

It has been pointed out in the previous section that a large number of measurements were made on each specimen totalling 11×70=770 values. For example, the values for specimen No. 16 are listed in Table 3.2. Also its surface roughness profile is plotted in Figure 3.14. The results of the measurements by microscope and calculations of the roughness parameters (using the relations in section 3.3.2.8) for twenty of the specimens are recorded in Table 3.3.

Table 3.2 Results of variation in thickness of specimen No. 16 over a 11×70 millimetre grid at the centre of the specimen (the variations in thickness are in mm).

Spec # 16	1	2	3	4	5	6	7	8	9	10	11
1	3.34024	3.20666	3.01098	3.03414	3.00307	3.06194	3.37907	3.47372	3.57372	3.60731	3.85218
2	3.26794	3.39008	3.27329	3.06194	3.03446	3.20655	3.21243	3.35715	3.55715	3.51287	3.91876
3	3.37372	3.518	3.31778	3.20098	3.14024	3.22189	3.31276	3.32399	3.52399	3.60686	3.87994
4	3.36827	3.55137	3.45137	3.29553	3.24602	3.44046	3.32849	3.29073	3.69073	3.80881	3.98561
5	3.41254	3.67372	3.42367	3.36227	3.51795	3.32945	3.36838	3.22945	3.62945	3.77994	3.88005
6	3.21778	3.62923	3.57917	3.34602	3.39608	3.28068	3.69608	3.60164	3.70164	3.89673	3.91898
7	2.91734	3.30666	3.20098	3.20164	3.2626	3.48506	3.54024	3.55693	3.55693	3.70229	3.88026
8	2.60033	2.85616	2.80055	3.25137	3.1457	3.30666	3.21767	3.28441	3.28441	3.53544	3.92476
9	2.3723	2.50022	2.76162	3.34559	2.92312	2.91767	2.83981	2.96135	2.96205	3.67972	3.97352
10	2.27765	2.17765	2.45017	3.20098	2.76729	2.80644	2.88986	2.85638	2.95638	3.44057	3.81865
11	2.22529	2.1554	2.23326	2.8506	2.57274	2.78408	2.70644	2.61506	2.7506	2.99591	3.87394
12	2.00823	2.07198	2.2722	2.72269	2.53381	2.67841	2.71167	2.49466	2.49466	2.95693	3.79608
13	1.98497	2.06085	2.46685	2.62258	2.51135	2.6106	2.47252	2.39455	2.39455	2.97329	3.60698
14	2.01771	1.96631	2.31669	2.64482	2.45028	2.46696	2.33359	2.28332	2.28332	2.96194	3.5903
15	1.91047	2.09422	2.32781	2.57808	2.33915	2.41022	2.33904	2.57252	2.57252	2.94526	3.518
16	2.10491	1.97743	2.36118	2.35006	2.26663	2.35562	2.24995	2.1999	2.1999	2.98964	3.4012
17	2.14362	1.94406	2.36118	2.41124	2.32781	2.47776	2.32225	2.42792	2.42792	2.88953	3.15627
18	1.9609	2.01636	2.20546	2.39455	2.26107	2.34439	2.35562	2.46129	2.46129	2.41124	3.13622
19	2.08171	1.99412	2.26107	2.35006	2.4168	2.43904	2.45017	2.52247	2.52247	2.33337	3.10622
20	2.05529	2.04973	2.10535	2.42792	2.51691	2.55584	2.52247	2.76718	2.76718	2.42792	3.25104
21	2.10385	2.2277	2.30557	2.31669	2.68932	2.72825	2.76718	2.85616	2.85616	2.71156	3.71265
22	2.28888	2.35006	2.61145	2.5614	2.99521	2.8228	2.86173	3.02301	3.02301	3.30666	3.80164
23	2.55584	2.54471	2.72825	2.69488	2.9674	2.96184	2.95071	2.98964	2.98964	3.51243	3.74046
24	2.7783	2.76718	2.90066	2.96184	2.86173	2.90622	3.11756	3.39008	3.39008	3.51243	3.58474
25	2.97296	2.93959	2.87285	2.9229	2.81723	2.86729	3.16761	4.03523	4.03523	3.56249	3.77939
26	2.84504	2.8506	3.0397	2.8506	3.10644	3.20098	3.1843	4.15758	4.15758	3.56805	3.88506
27	2.74493	2.88953	3.03414	3.3228	3.35704	3.76827	3.90175	4.24101	4.24101	3.86282	4.19095
28	2.76718	2.77274	3.05082	3.25104	3.63479	3.80164	4.0964	4.27994	4.27994	3.89619	4.54133
29	2.91178	2.8506	2.98408	3.32334	3.52912	3.76827	4.01309	4.36892	4.36892	4.0686	4.647
30	2.90622	2.7783	2.91734	3.28997	3.58474	3.6626	4.04079	4.49128	4.49128	4.27438	4.62476
31	2.81167	2.93959	2.97852	3.28997	3.5458	3.6626	3.95736	4.79717	4.79717	4.58026	4.79717
32	2.85616	3.01745	3.0397	3.27329	3.56805	3.79052	4.17427	4.94733	4.94733	4.66925	4.9084
33	2.98408	3.4735	3.00633	3.16205	3.58474	4.05191	4.56358	4.84722	4.84722	4.75267	5.1253
34	3.38975	3.6626	3.07863	3.26772	3.79608	4.32999	4.66925	4.59139	4.59139	4.76936	5.27547
35	3.05104	3.62923	3.21767	3.31778	3.90175	4.24101	4.55246	4.45791	4.45791	4.93621	5.13643
36	3.50687	3.79608	3.69041	3.57361	4.05747	4.25213	4.37448	4.40229	4.40229	4.80873	5.05278
37	3.47907	3.89619	3.96293	3.77939	4.13533	4.29662	4.36336	4.3578	4.3578	4.84188	4.9948
38	3.70153	3.99073	4.00186	4.1687	4.01298	4.17983	4.36892	4.38561	4.38561	4.82498	4.95262
39	3.87394	3.98517	4.01854	4.1687	4.31887	4.26881	4.40785	4.43566	4.43566	4.65257	4.9192
40	3.95191	3.47983	4.0241	4.2132	4.53021	4.45235	4.44679	4.58026	4.58026	4.46903	4.98166
41	3.79095	3.86347	4.25769	4.40785	4.44166	4.81941	4.75824	4.94177	4.94177	4.81887	5.17547
42	3.85224	3.69192	4.50796	4.60807	4.39193	5.09749	5.15867	5.10894	4.90894	4.31331	5.1959
43	4.09128	3.76936	4.66925	4.88059	4.91985	5.11445	5.15355	5.13697	5.13697	4.40785	5.32938
44	4.27193	4.19739	4.88615	4.96402	4.81996	5.07557	5.14242	5.15922	5.15922	4.59695	5.31387
45	4.38059	4.33643	4.8253	4.99749	4.94777	5.19226	5.15911	5.17601	5.17601	5.053	5.23163
46	4.5053	4.62519	4.78659	4.9422	4.93108	5.22541	5.21472	5.27045	4.97045	5.18681	5.21494
47	4.39458	4.69193	4.51985	4.81044	4.96434	5.10338	5.15036	5.29815	5.19815	5.10927	5.19943
48	4.50306	4.32421	4.63664	4.74122	4.84231	5.04242	5.12585	5.13708	5.13708	5.18702	5.19831
49	4.43643	4.64755	4.87547	4.90144	4.90894	5.19237	5.06445	5.14242	5.14242	5.15387	5.15039
50	4.48075	4.79717	4.90338	5.11996	4.93097	5.13119	4.91461	5.11461	5.11461	5.18713	5.1036
51	4.63054	4.62476	4.93422	5.08125	4.98053	4.89226	4.97034	5.16478	5.16478	5.17601	5.07568
52	4.58583	4.54133	5.04199	4.98643	4.95311	4.95889	4.91996	5.00349	5.10349	5.1205	5.00125
53	4.47459	4.53021	4.91396	4.88648	4.91053	4.61976	4.88615	5.14755	5.14755	5.1205	5.0078
54	4.52465	4.50796	4.84166	4.92519	4.90306	4.89728	4.69706	4.86391	4.86391	4.95922	4.91974
55	4.36892	4.35224	4.78048	4.94733	4.66369	4.65257	4.46903	4.74155	4.74155	4.98135	4.94188
56	4.10229	4.30774	4.59139	4.94733	4.55802	4.30774	4.40229	4.60807	4.60807	4.9459	4.87503
57	3.98331	4.32443	4.44679	4.74711	4.3578	4.20764	4.22988	4.59695	4.59695	4.85344	4.5024
58	3.91331	4.03544	4.3578	4.49128	4.27994	4.20207	4.07416	4.4301	4.4301	4.83653	4.48572
59	3.98005	3.85246	4.12443	4.14111	4.15202	4.32443	4.08528	4.29662	4.29662	4.31053	4.32443
60	4.08015	4.1301	4.00673	3.72977	3.85758	3.91843	4.14646	3.97983	3.97182	4.04166	4.05191
61	4.06903	4.01331	4.09684	3.83555	3.86314	3.98517	4.1687	3.95213	3.85213	3.79374	4.0072
62	4.19117	4.04635	3.71352	3.71331	3.81298	3.90175	4.15202	3.87438	3.67438	3.54668	4.06271
63	3.76881	3.79619	3.65864	3.89095	3.96293	3.72934	4.03523	3.82999	3.82999	3.5855	4.01303
64	3.86881	3.55715	3.57394	3.71309	3.75158	3.57361	3.93512	3.65202	3.75202	3.77972	3.92301
65	3.75202	3.50142	3.45704	3.49619	3.5458	3.71821	4.07972	3.65769	3.85769	3.72388	3.91807
66	3.62388	3.25693	3.4012	3.62367	3.47907	3.91687	4.11865	3.92988	3.82988	3.75731	4.20785
67	3.60939	3.20131	3.46238	3.45682	3.30109	3.95235	4.07416	3.8855	4.1855	4.05191	4.08572
68	3.62956	3.30687	3.44013	3.46794	3.69041	3.94133	4.32999	4.13555	4.13555	4.11309	4.00459
69	3.81865	3.61349	3.65671	3.76227	3.96293	3.91301	3.99352	4.01909	4.01909	3.93192	4.23577
70	4.0687	3.87216	3.8735	3.99698	4.07972	4.03566	3.9747	4.15235	4.10235	4.44679	4.09139

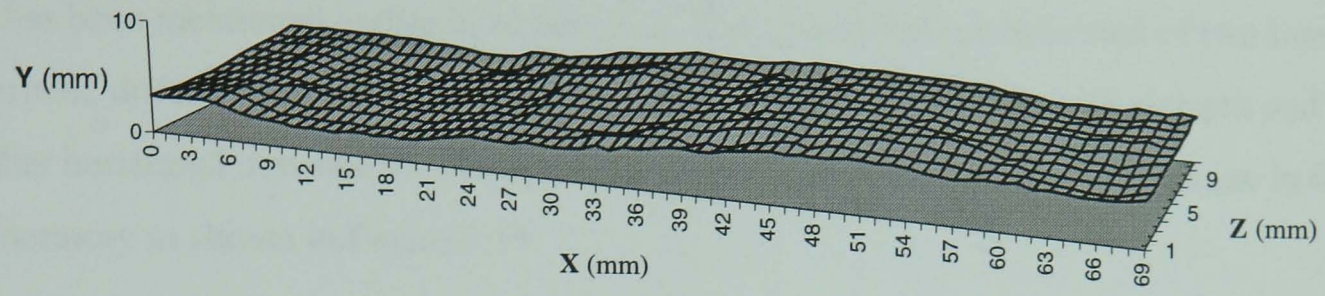

X = Length of specimen, Z = Width of specimen and Y = Variation in thickness of specimen

Figure 3.14 Surface roughness profile of specimen No. 16.

Table 3.3 Results of measurements.

Specimen number	Origin	t_o (mm)	$\bar{t}$ (mm)	d_c (mm)	$\bar{d}$ (mm)	d_{min} (mm)	d_{max} (mm)	R_{max} (mm)	R_m (mm)	S_d (mm)
1	web	6.1	5.85	0.13	5.64	5.45	5.79	0.34	0.056	0.067
2	flange	10.2	7.02	1.59	6.21	5.69	6.89	1.20	0.180	0.226
3	stiffener	9.5	9.12	0.19	8.39	7.99	8.93	0.94	0.087	0.112
4	flange	10.2	7.75	1.23	7.61	6.65	8.18	1.53	0.310	0.357
5	flange	10.2	6.78	1.71	6.42	5.98	6.71	0.73	0.085	0.110
6	flange	10.2	10.02	0.09	9.31	9.04	9.51	0.47	0.075	0.090
7	flange	10.2	5.64	2.28	4.27	3.18	4.96	1.75	0.258	0.324
8	flange	10.2	6.54	1.83	3.72	2.11	4.90	2.79	0.519	0.630
9	flange	10.2	7.70	1.25	6.20	4.26	6.88	2.62	0.303	0.465
10	web	6.1	5.84	0.13	5.67	5.43	5.82	0.39	0.052	0.064
11	stiffener	9.5	9.21	0.16	8.50	7.87	8.88	1.01	0.137	0.170
12	stiffener	9.5	8.78	0.38	8.11	7.43	8.58	1.15	0.234	0.271
13	flange	10.2	6.98	1.61	5.84	5.01	6.69	1.68	0.260	0.320
14	flange	10.2	5.58	2.31	4.74	3.76	5.54	1.78	0.282	0.349
15	flange	10.2	5.52	2.34	3.87	3.12	4.48	1.36	0.183	0.232
16	flange	10.2	4.85	2.68	3.59	1.84	5.21	3.37	0.640	0.780
17	flange	10.2	6.34	1.93	5.72	4.12	6.82	2.70	0.483	0.483
18	flange	10.2	7.04	1.58	6.78	6.45	7.05	0.60	0.082	0.101
19	flange	10.2	6.98	1.61	6.49	6.11	6.78	1.58	0.084	0.105
20	flange	10.2	8.08	1.06	7.96	7.60	8.16	0.56	0.079	0.098

3.5.2 Longitudinal profile system using displacement transducer

It has been mentioned earlier in section 3.2.7 that this technique consisted of two linear variable differential transformers (LVDT), one of which measured vertical depth and the other horizontal movement. The system was set up on a vertical milling machine in the laboratory as shown in Figure 3.15.

The outputs of the two LVDTs were read by an analogue to digital card on a PC. Simultaneous readings of vertical displacement and horizontal movement were made while the specimen was traversed laterally on the milling machine. The area was scanned by multiple passes of the system, each pass being offset by a fixed increment from the origin.

A computer program to read the data was written in Microsoft QuickBasic. The written computer program read the analogue data automatically at three second intervals from transducers, converted them to digital and wrote them to the screen and also into a file at the same time. The processing chart used for PC26AT on the computer is shown in Figure 3.16.

The variation in thickness (y) of corroded specimens was measured by the vertical LVDT whose probe had vertical travel of 15 mm. Its position (x) on the specimen was determined by the horizontal LVDT which had horizontal travel of 70 mm. The details of the LVDTs are given in Table 3.4.

Table 3.4 Details of LVDT.

LVDT	Range of travel	Range of voltage	Type of shaft
Horizontal	70	±4.9	spring loaded probe
Vertical	15	±6.5	spring loaded probe

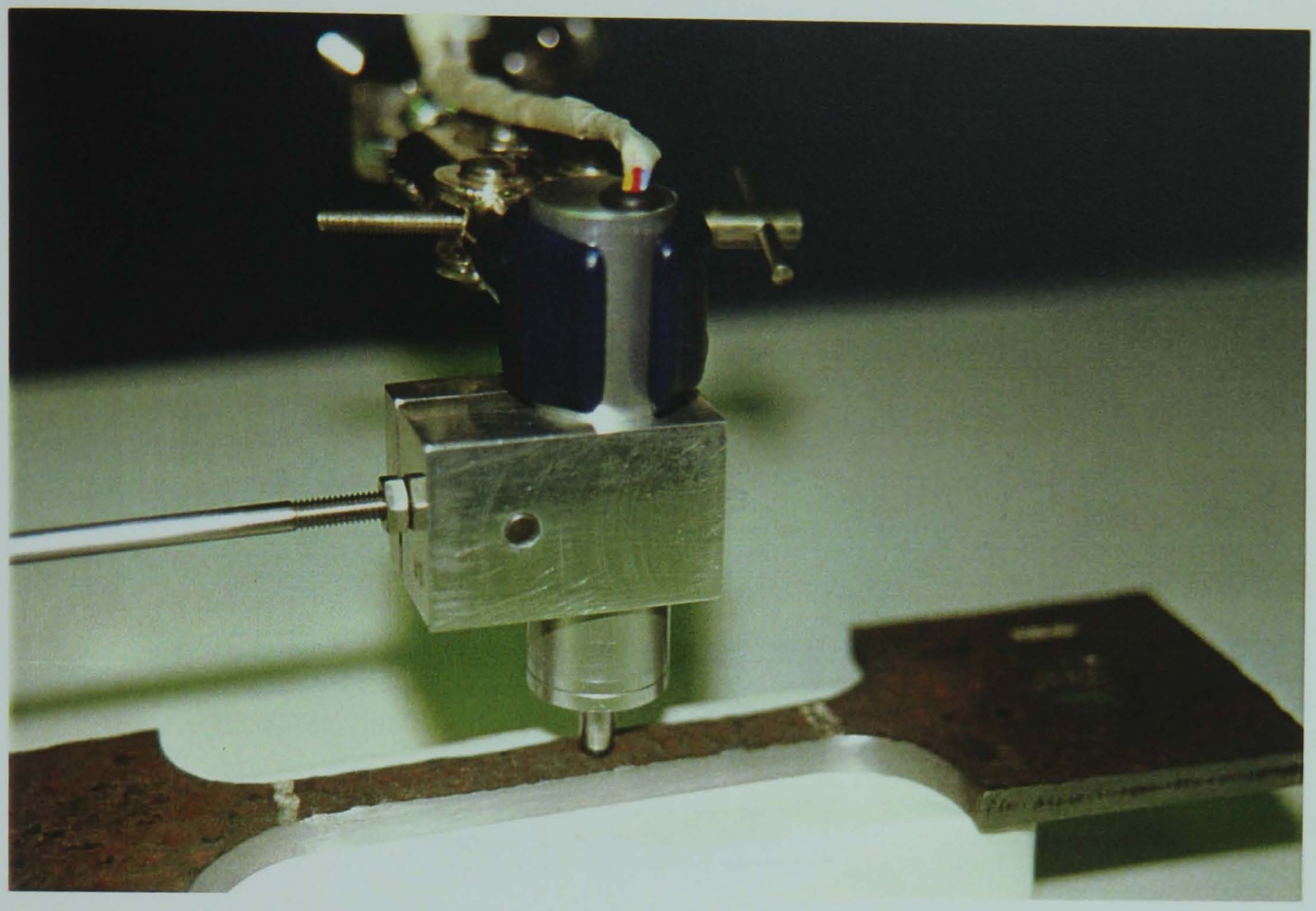

3.15 Set-up of system in the laboratory.

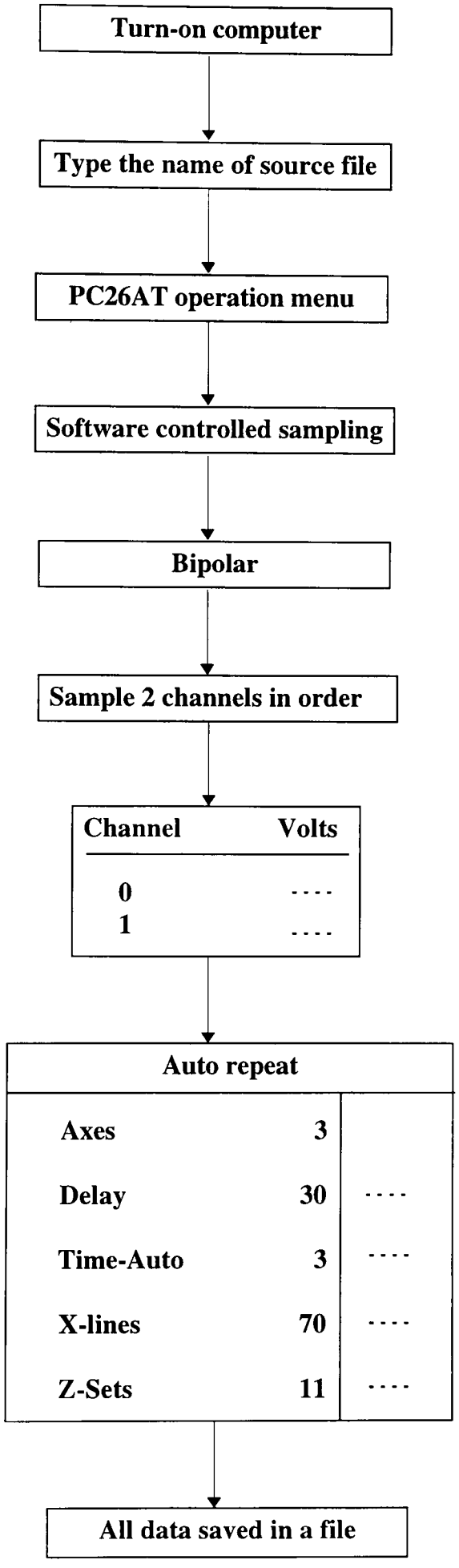

Figure 3.16 Processing chart of PC26AT.

3.5.2.1 Measurement procedure

As shown in Figure 3.15 the system was set up on a table of a vertical milling machine in the laboratory. The table could move in three directions x, y and z. The corroded specimen was mounted on a magnetic block which was itself mounted on the table of the milling machine. The vertical LVDT was fitted into an aluminium block clamped to the vertical head of the milling machine. The horizontal LVDT was mounted on the table and its probe was pushed against the aluminium block which held the vertical LVDT. The surface of magnetic block was chosen as a reference point for the probe of the vertical LVDT; in this case the free length of 15 mm showed zero displacement. Then the probe of the vertical LVDT was pushed up from surface of magnetic block and placed on the corroded surface of specimen. In this case the whole set-up was mounted on the table of the milling machine during the measurement so that it could just move in two directions (x and z) since the position of vertical LVDT had been adjusted before. The horizontal movement of the table was controlled by turning the calibrated handles. Consequently, the ball on the tip of the probe of the vertical LVDT was rolled and traversed over the portion of the surface to be measured. The area was measured by multiple passes of the system and each pass was offset by a fixed increment from the origin.

In this investigation the variation in thickness of each corroded specimen was measured over a 11×70 millimetre grid at the centre of the specimen. The thickness of fourteen corroded specimens from the channel beam were measured by this method.

3.5.2.2 Results of the measurement

In this section the same procedure and relations which were mentioned in section 3.5.1.2 have been used to calculate the roughness parameters. The results of the measurements by the longitudinal profile system using a displacement transducer for fourteen of the specimens from channel beam are recorded in Table 3.5.

Table 3.5 Results of measurements.

Specimen number	Origin	t_o (mm)	$\bar{t}$ (mm)	d_c (mm)	$\bar{d}$ (mm)	d_{min} (mm)	d_{max} (mm)	R_{max} (mm)	R_m (mm)	S_d (mm)
21	web	10.2	6.09	2.06	5.47	4.35	6.36	2.01	0.432	0.515
22	web	10.2	7.68	1.26	4.72	4.16	4.98	0.82	0.130	0.159
23	web	10.2	7.52	1.34	4.77	4.25	5.23	0.98	0.176	0.210
24	web	10.2	7.96	1.12	4.79	4.30	5.23	0.93	0.169	0.202
25	web	10.2	7.82	1.19	4.93	4.23	5.46	1.23	0.173	0.215
26	web	10.2	7.74	1.23	5.76	5.15	6.36	1.21	0.18	0.227
27	web	10.2	7.16	1.52	5.21	4.55	5.70	1.15	0.222	0.261
28	web	10.2	6.11	2.05	5.87	4.68	6.97	2.29	0.381	0.469
29	web	10.2	6.92	1.64	4.63	3.51	5.31	1.80	0.237	0.304
30	web	10.2	5.88	2.16	5.44	4.38	6.44	2.06	0.43	0.522
31	web	10.2	7.09	1.56	5.46	4.58	6.25	1.67	0.308	0.366
32	web	10.2	7.28	1.46	4.47	3.86	5.12	1.26	0.174	0.217
33	web	10.2	7.43	1.39	6.01	5.44	6.72	1.28	0.201	0.254
34	web	10.2	6.08	2.06	6.50	5.30	7.89	2.59	0.578	0.717

3.5.3 Comparisons between the results of two methods

The results of the longitudinal profile system using displacement transducer method was compared for accuracy with the microscope technique. A comparison of the major parameters for two of the specimens is given in Table 3.6, showing it to be generally satisfactory.

The small difference between the two methods is likely to be due to the large radius of the ball probe but may also be due to the noise and resolution of the analogue to digital interface card. However, compared to other techniques, longitudinal profile system using the displacement transducer has several advantages. The scanning and measuring process is semi-automatic and therefore rapid. The whole system is relatively simple to operate in the laboratory. It is inexpensive. It is believed that this system could be developed for roughness surveys on site.

Table 3.6 Comparison between the results of two methods.

Methods	Average thickness	Minimum thickness	Maximum thickness	Maximum roughness	Mean roughness	Standard deviation
LVDT	5.84	5.07	6.77	1.70	0.30	0.36
Microscope	5.84	5.01	6.69	1.68	0.26	0.32
% Difference	*0.0*	*1.20*	*1.20*	*1.20*	*13.30*	*11.1*
LVDT	3.79	1.91	5.33	3.42	0.74	0.88
Microscope	3.59	1.84	5.21	3.37	0.64	0.78
% Difference	*5.30*	*3.70*	*2.30*	*1.50*	*13.50*	*11.30*

3.6 Proposal for a method of roughness measurement on site

A preliminary design of longitudinal profile system using displacement transducers for use on site is illustrated in Figure 3.17. It consists of: (a) two magnetic blocks with the bottom release; (b) a rectangular slot steel plate; (c) two screws, one on each end to connect the magnetic block to the rectangular slot; (d) two aluminium clamps, one on each end; (e) four screws, two on each end to connect the rectangular slot steel plate to clamps; (f) two travelling bars; (g) an aluminium block to hold the vertical LVDT; (h) two LVDTs and (i) a handle connect to aluminium block to aid in moving the vertical LVDT.

The magnetic blocks with release bases can be used as stand bases of system on the steel surface. The aim of using release magnetic blocks is to remove the system from the steel surface smoothly and avoid any damage to the system. The rectangular slot steel plate is screwed to the magnetic block in order to secure the system from any rotation. The aluminium clamps at each end are screwed to the rectangular slot steel plate which are able to hold the travelling bars but one is placed on left end also holds the horizontal LVDT as well. The aluminium block holds the vertical LVDT and itself is supported by two travelling bars. Two travelling bars can be connected to the aluminium clamps at the ends and allow the aluminium block which is holding the vertical LVDT to move

horizontally. A handle is connected to aluminium block to aid in moving the vertical LVDT. The probe of the horizontal LVDT is connected to the aluminium block in order to record the movement of the vertical LVDT along the system on the corroded surface. The outputs of both LVDTs can be read by an analogue to digital card on a PC simultaneously.

The numbers in the boxes for Figure 3.17 are used for the following descriptions:

1. Magnetic block with the bottom release.
2. Magnetic release (to release magnetic block from steel surface).
3. Rectangular slot plate (used as a frame to secure system).
4. Clamp (used to hold the bars).
5. Two travelling bars (to allow the aluminium block to move horizontally).
6. Aluminium block holds vertical LVDT and itself is supported by two bars (see No. 5).
7. Vertical LVDT.
8. Probe of vertical LVDT.
9. Probe of horizontal LVDT which is screwed to number 6).
10. Clamp (which holds the travelling bars and horizontal LVDT).
11. Horizontal LVDT.
12. Handle (connected to aluminium block to aid in moving vertical LVDT).
13. Screws which have been used to connect the rectangular slot plate to clamps at both ends).
14. Screw which has been used to connect the magnetic block to the rectangular slot plate.

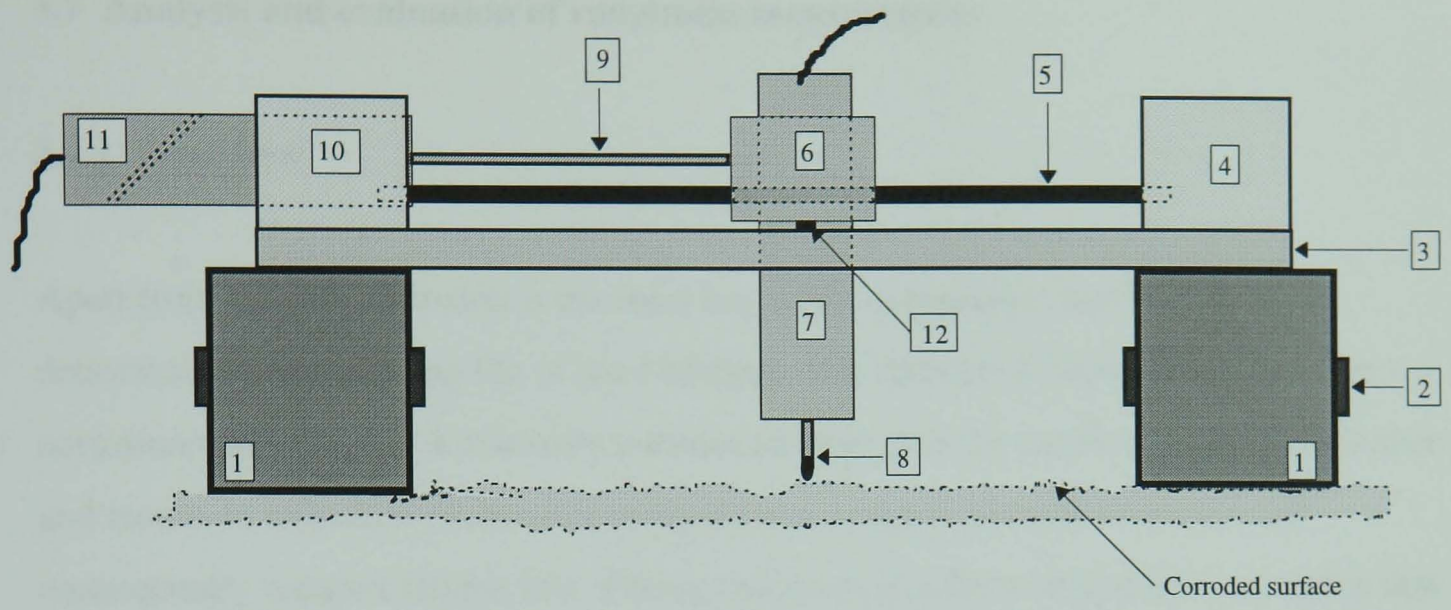

(a) Side elevation

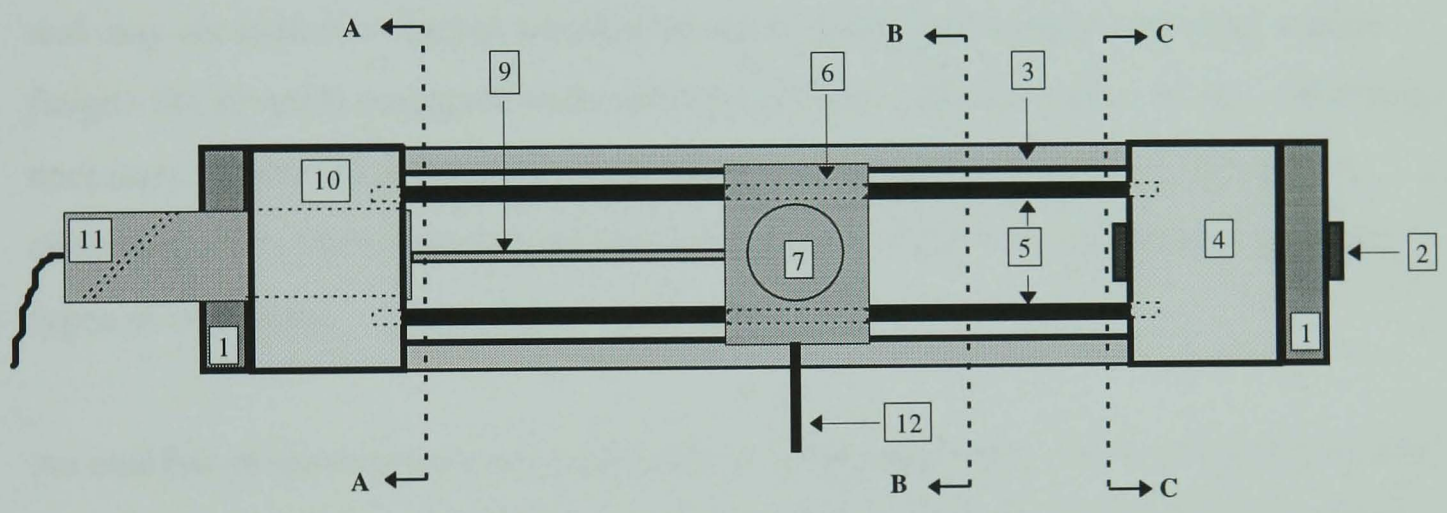

(b) Plan

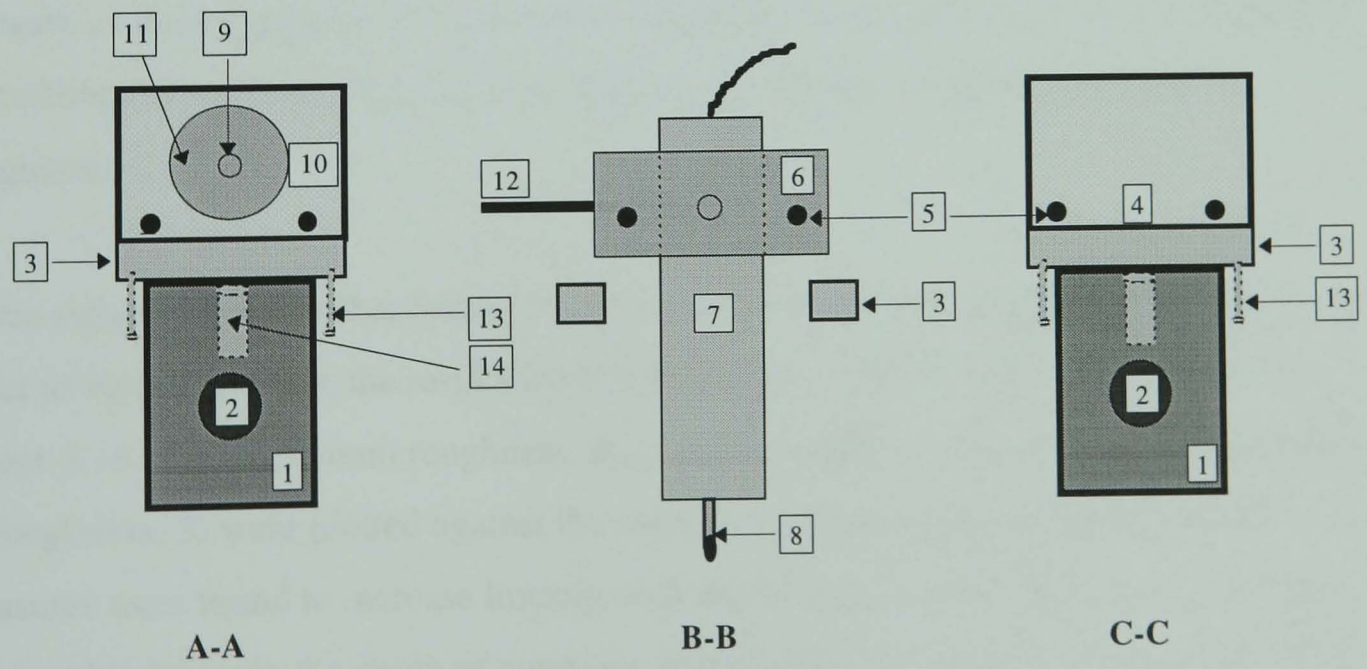

(c) Sections

Figure 3.17 Preliminary layout of the system for site measurement.

3.7 Analysis and evaluation of roughness measurement

3.7.1 Overview

Apart from fatigue, corrosion is the most important degradation mechanism in determining the remaining life of steel bridges. It is stated in Chapter 2 that uniform corrosion takes place in a relatively uniform manner over the entire surface of a member and results in reduction of member cross-section, henced increased stresses and consequently reduced fatigue life. Pitting corrosion is a form of localized corrosion that produces a pitted profile on the metal's surface. The profile of the pits can vary from broad and shallow to deep and narrow. Pits can act as initiation sites for fatigue cracks and may act as micro-notches which give rise to stress concentration and may reduce fatigue life severely compared with uniform corrosion. In order to assess this effect it is necessary to have some measure of pit depth and sharpness. Therefore, this type of corrosion needs more attention in measurement and analysis compared with the other types of corrosion.

An analysis of the experimental measurement work undertaken in the research project is provided in this chapter. In this investigation thirty four samples of severely corroded steelwork were measured carefully for their depth of corrosion and corrosion pitting. Because of the irregularity of a corroded surface the measured roughness was expressed as maximum roughness, R_{max}, mean roughness, R_m, and the standard deviation of roughness, S_d.

It was suggested earlier that pitting becomes more severe with progressive corrosion. In order to investigate this, the results from both Tables 3.3 and 3.5 have been plotted in Figure 3.18. The maximum roughness, R_{max}, mean roughness, R_m and standard deviation of roughness, S_d were plotted against the average corrosion penetration, d_c. These measures were found to increase linearly with depth of corrosion. This shows that the relationship between the depth of corrosion and roughness parameters for the corroded specimens from different sites is the same. A further investigation was carried out between the roughness parameters themselves which is described in next section.

3.7.2 Correlation between the roughness parameters

It may be seen from Figure 3.18(a), (b) and (c) that there is a distinct correlation between corrosion penetration and these measures of roughness although there is considerable scatter. A further comparison was made between maximum roughness, R_{max}, and the standard deviation of roughness, S_d. This is shown in Figure 3.19. In this case the correlation is very good. In most cases d_{max} and d_{min} could be identified with the deepest pit in a specimen, although in principle the maximum and minimum need not be in the same area. This result indicates that the standard deviation is closely correlated with the depth of pitting at the worst section. Therefore, this measure has considerable potential for correlating with fatigue endurance. Mean roughness was also compared with standard deviation and revealed a similar relationship as shown in Figure 3.20.

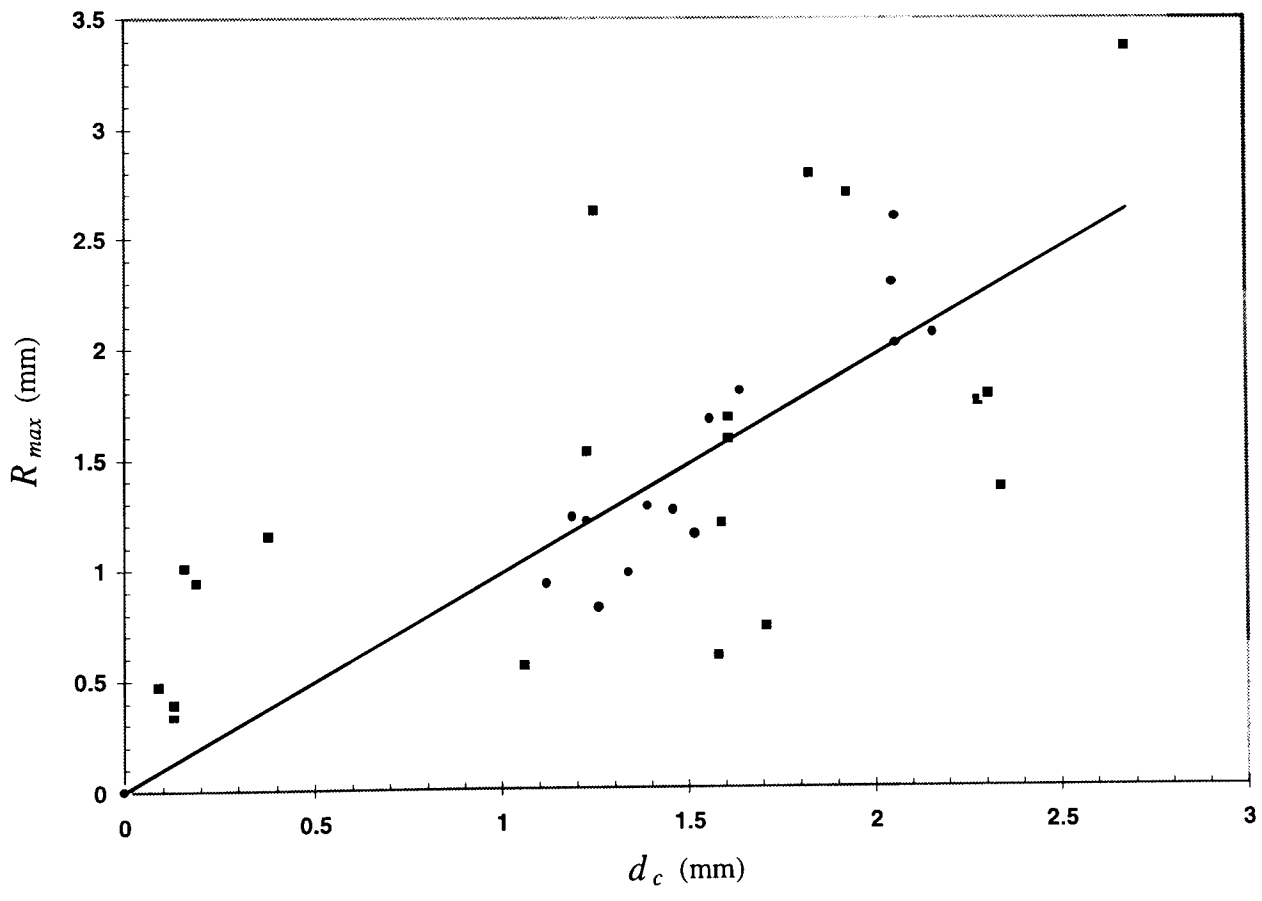

Figure 3.18(a) Depth of corrosion, d_c versus maximum roughness, R_{max} (correlation coefficient = 75%).

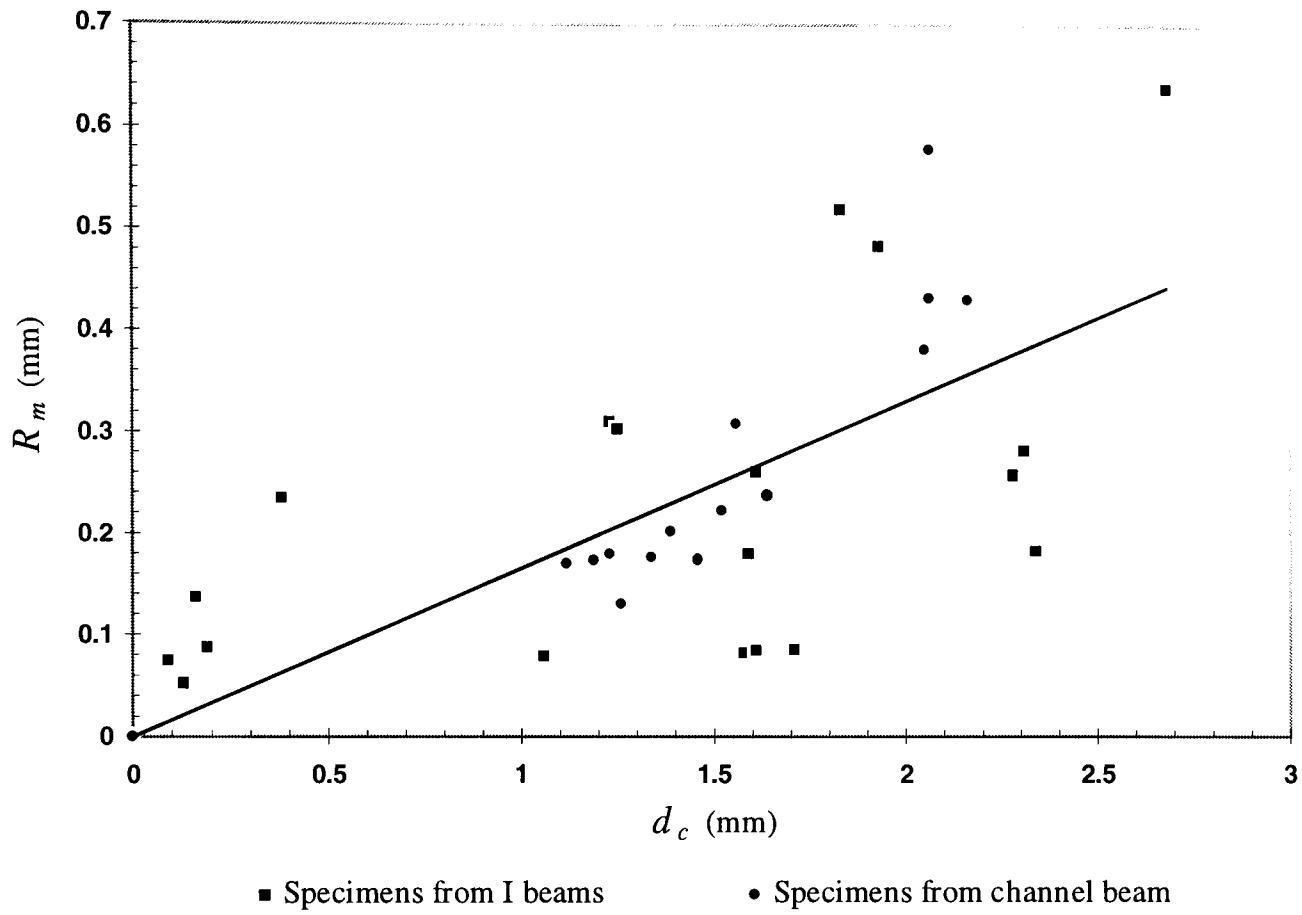

Figure 3.18(b) Depth of corrosion, d_c versus mean roughness, R_m (correlation coefficient = 72%).

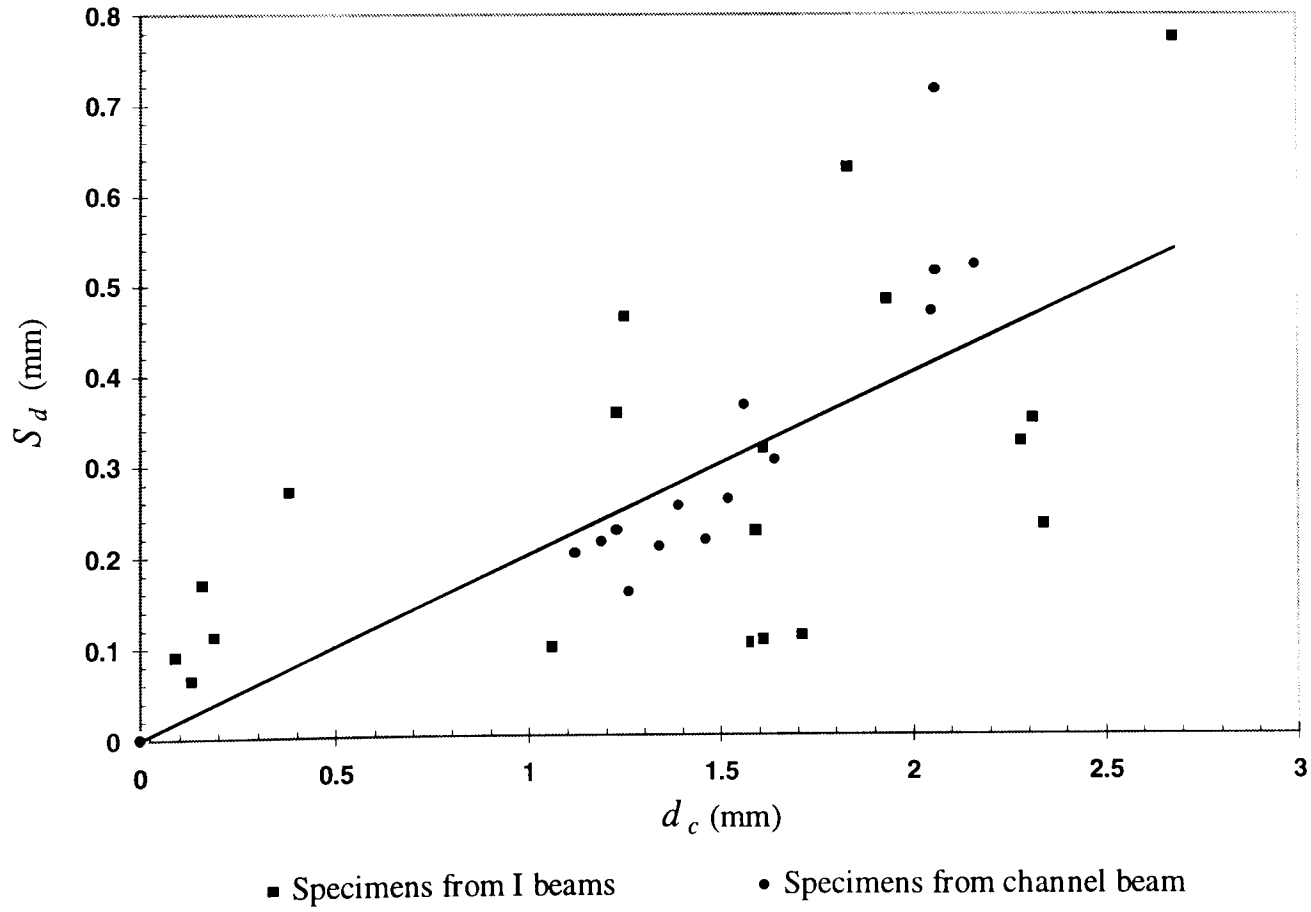

Figure 3.18(c) Depth of corrosion, d_c versus standard deviation, S_d (correlation coefficient = 72%).

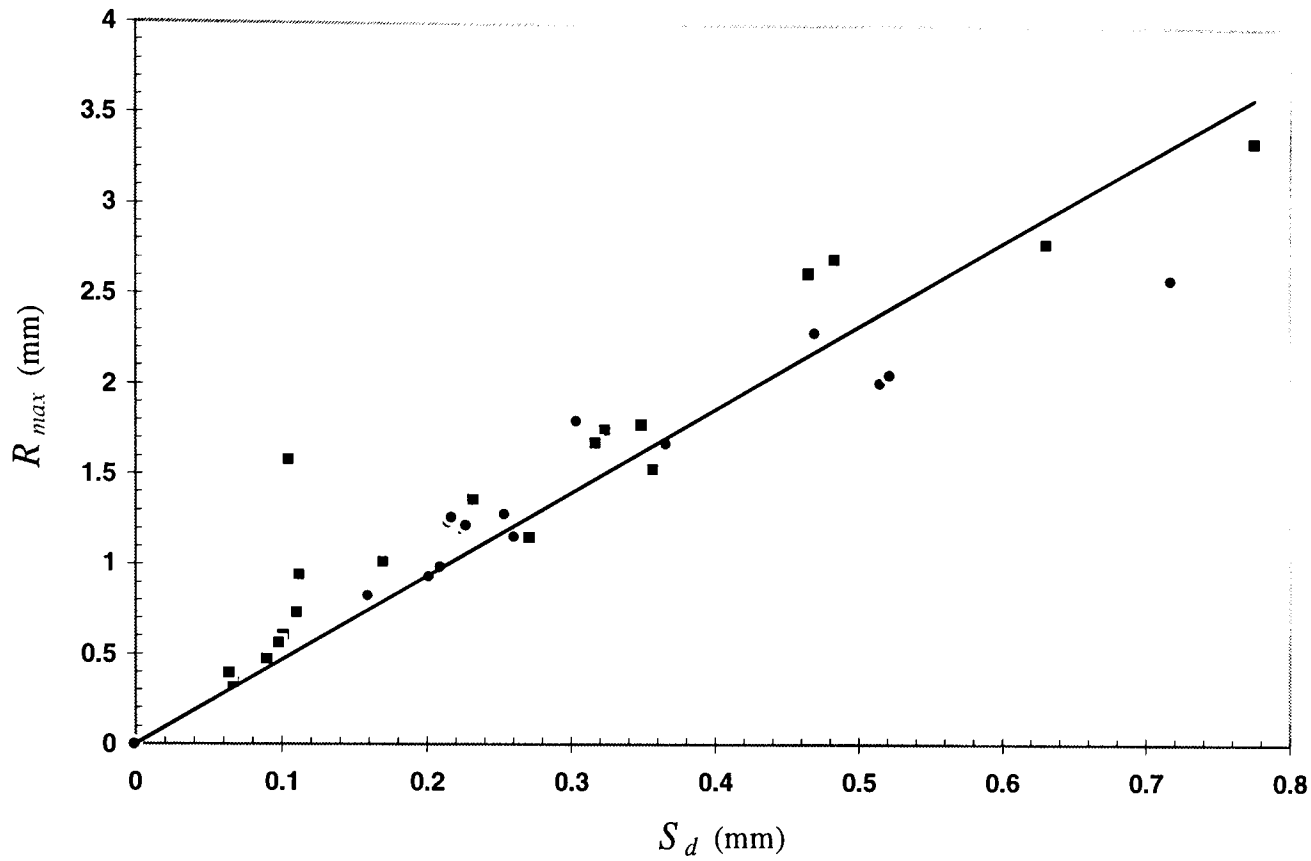

Figure 3.19 Standard deviation, S_d versus maximum roughness, R_{max} (correlation coefficient = 93%).

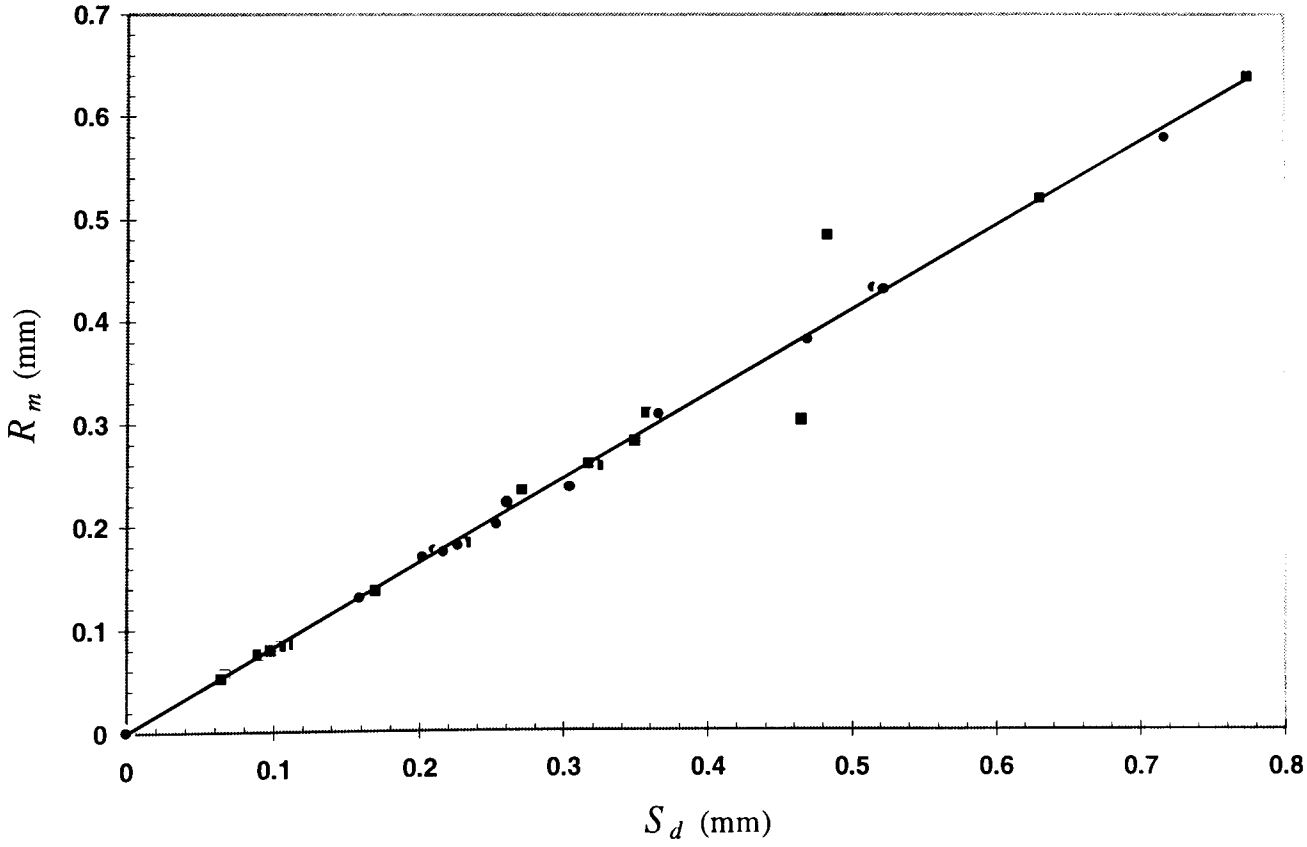

Figure 3.20 Standard deviation, S_d versus mean roughness, R_m (correlation coefficient = 99.2%).

3.8 Summary and conclusions

The main aspects that are associated with measurement and analysis of surface roughness have been explained. In this review existing methods have been discussed and a new technique for measurement of surface roughness is described. The discussion of different methods of measurement and analysis helped to identify the best methods from the point of view of operability, efficiency and accuracy. Each of the methods has its advantages and disadvantages.

It was found from the literature review that many statistical parameters were available to assess the surface irregularity. The autocorrelation function describes a surface and is particularly useful for looking at random surfaces. The power spectrum analysis would collect most of the information necessary to describe a surface and is more useful when looking at periodic surfaces. The method which provides a more straightforward mathematical procedure has been used in this study to calculate the surface roughness parameters such as the maximum roughness the mean roughness and the standard deviation of roughness.

For the purpose of thickness measurement of corroded steel structures at the site it has been found by Department of Transport that the Cygnus instrument is easiest and the most accurate, repeatable and reliable method. But it is not suitable for pitted areas because they can give high readings due to the influence of the layer of couplant trapped between the probe and the true top surface of the metal. Ultrasonic equipment will not give an accurate reading unless the point of contact has been ground smooth. The widespread use of disc grinding in steel bridges is unlikely to be acceptable.

None of the methods investigated are entirely satisfactory for roughness measurement of corroded steelwork directly but can be used to measure the variation in thickness and therefore roughness indirectly using the relation between roughness and corrosion depth presented in this chapter. The manual optical method using a microscope, and the longitudinal profile system using displacement transducers described in this chapter have been applied to the corroded specimens used in this study.

However, the longitudinal profile system using displacement transducers developed in this study appears to have some potential advantages in its accuracy and speed of measurement. The variation in thickness of corroded steelwork specimens can be measured much more rapidly than by using the manual optical method using a microscope. The results were very accurate compared to the microscopic method. The small difference between the two methods is more likely due to the large radius of the ball probe or due to the noise and resolution of the analogue / digital interface card and the problems experienced with the optical method. This technique is believed to have potential in terms of cost, time and accuracy for the measurement of roughness of existing corroded steel bridges on site.

The analysis of the data provided by roughness measurement showed that there is linear relation between the depth of corrosion and the degree of roughness or pitting such as maximum roughness, mean roughness and standard deviation of roughness. In particular, it has been found that the standard deviation of roughness correlates well with the largest corrosion pits. Furthermore, the linear relation between maximum roughness and overall corrosion depth provides a convenient tool for the assessment of corrosion damaged bridges. Its application will be explained in Chapter 5. A particular point of interest was to see how the depth of corrosion had correlated with roughness parameters for beams from different sites.

CHAPTER IV

CORROSION PENETRATION

4.1 Introduction

In the past decade, corrosion has received increased attention as a cause of structural damage and failure (Kulicki et al 1990). The results of corrosion deterioration can range from progressive weakening of a bridge over a long period of time to sudden bridge collapse. Due to the variety of parameters affecting the corrosion penetration, every steel structure behaves differently. Therefore, penetration of future corrosion is usually projected based on knowledge of prior corrosion penetrations on the same structure. However, even different locations on the same structure are likely to corrode at different rates, so each structure and detail should considered individually.

In Chapter 2, an overview of metal corrosion was presented. In this chapter the corrosion penetration of steel structures will be discussed. Corrosion penetration has a significant effect on fatigue life of steel structures. The most common form is overall loss of surface material. Such conditions will lead to the general thinning of members. It has been mentioned by Fontana (1987) that uniform corrosion accounts for the largest percentage of corrosion damage. Pitting corrosion is particularly important. Pits can produce early service failure because they may provide sites for crack initiation and may decrease the mechanical strength of a material. Kayser (1988) has pointed out that the prediction and measurement of pitting is difficult in practice because it is random in nature and occurs quickly. However, pits are serious in high stress regions because they cause local stress concentrations. Consequently, reducing the fatigue resistance of the members and components of the structures.

To date, the amount of published data on long-term corrosion penetration is limited. Currently, short-term corrosion penetration data are available for small scale specimens weathered under various types of environments. Because of the short exposure time, one cannot yet project the penetration of corrosion that may occur towards the end of the design life of a steel structure. Long-term exposure data are needed. They can be obtained from steel beams in existing structures that have already been weathered for several decades. In this study as mentioned in Chapter 3, corroded mild steel beams were recovered from the site of different industrial plant which have been exposed to precipitation and pollution for nearly 40 years. The main idea is to develop an empirical relationship for predicting the average penetration and maximum roughness of corroded steelwork based upon its exposure time.

The specific objectives of this chapter are:

1. To enhance understanding of the factors which may have an effect on the corrosion penetration of steelwork.
2. To review the relevant research and existing methods for predicting corrosion penetration and maximum roughness.
3. To review and develop the parametric values of the corrosion penetration function from previous research carried out in the UK.
4. To develop a relationship for maximum pit depth in terms of corrosion penetration on the basis of roughness measurements obtained from corroded specimens in Chapter 3.
5. To develop relationships for predicting average corrosion penetration and maximum pit depth in terms of exposure time.
6. To make a comparison between the results of empirical formulae produced in this study and the one which Copson (1960) developed.
7. To investigate the accuracy and reliability of the empirical formulae produced for average maximum roughness in this study by using Albrecht's (1990) data developed from other structures.
8. To carry out a statistical analysis of the maximum roughness measurements.

4.2 Factors effecting on corrosion penetration

The penetration and progress of corrosion on steel are affected by several factors such as environmental effects, type of structural details, type of steel, surface protection, de-icing materials, and other factors as the presence of pollutants, crevices, bacteria, clogged drains, deposits and stress (Kulicki et al 1990). Impurities such as sulphur dioxide, chlorine, ammonia, nitrogen dioxide, and hydrogen sulphide increase the corrosion penetration by additional reactions (Fontana 1987).

4.2.1 Environmental effects

The main environmental factors which affect the corrosion penetration are: initial exposure, wetness of climate, orientation and temperature. These effects are explained briefly in the following paragraphs.

The climatic conditions at initial exposure can produce large differences in corrosion penetration. These differences are much larger for mild steel than for weathering steel. Evidently, the initial reactivity of steel with its environment affects the long term corrosion behaviour (Larrabee 1966).

The wetness of the climate is very important to the penetration of corrosion because water serves as an electrolyte. It has been pointed out by Albrecht et al (1989) that rain or snow are not the only sources of wetness. Moisture can be deposited by (a) nightly condensation when the surface temperature of the steel falls below the dew point; (b) radiant cooling of the skyward deck surface in a clear night, causing moisture to condense on the upper portions of the steel girder and run down the web along drip lines; (c) capillary moisture absorption by the porous oxide coating and crevices in structural details; (d) adsorption by corrosion products particularly in the presence of salt; (e) leaking bridge deck joints; and (f) traffic spray kicked up in the wake of high-speed traffic and settling on the overhead members of a bridge. High relative humidity, nightly fog, moisture evaporating from bodies of water, and poor air circulation enhance the deposition of moisture. In arid regions, corrosion may be slow compared to regions with

above average precipitation. It should be noted that the areas exposed to wind or sun that can dry quickly are less prone to corrosion than sheltered areas where water can remain in contact with the metalwork.

In general, the corrosion penetration of steel structures on surfaces exposed to the ground is higher than it is on surfaces exposed to the sky and it is also higher on surfaces exposed to the north than it is on surfaces exposed to the south (Larrabee 1941). These effects can be attributed to the longer time of wetness of the groundward and northward orientations because the sun dries the steel exposed to these orientations less than it does to steel exposed to the sky and south.

Environmental effects include temperature, humidity, and the exposure of the material. The rate of almost all chemical reactions increases with temperature, therefore at elevated temperatures the rate of corrosion will be high. Fontana (1987) has pointed out that the corrosion rate at low temperature is very low and increases exponentially as temperature increases. This is usually not significant in bridges. In the UK the effect of temperature on the penetration of corrosion is less than elsewhere in the world (Owens et al 1992).

4.2.2 Effects of structural details

Structural details have an important effect on the corrosion penetration. Details that collect water or provide ideal nesting spots for birds should be carefully checked for corrosion. Deck joint leakage has been identified by Purvis et al (1983) as a source of moisture. The failure of deck joints is primarily due to improper installation and maintenance. A contributing factor is that deck joints undergo severe operating condition and have a limited service life. The leakage of water through the deck joints persistently wets the other structural members such as web, stiffeners, diaphragms, flanges, and bearings in the vicinity of the joint where it can migrate for long distances along the bottom flange and lower part of the web. An investigation was carried out by Byers (1979) on approximately 4,000 steel bridges. It was concluded that the main

reason for bridge corrosion is the accumulation of water on the steel. The primary cause noted was the leakage of water from the deck.

The National Cooperative Highway Research Program (1979) has suggested that the most susceptible locations are: the top surfaces of lower beam flanges and truss chords, gusset plates for horizontal bracing, bolted splices of horizontal and sloped members, bearing and intermediate stiffeners, and the interior of non-sealed box sections. To avoid water ponding and debris accumulation it is important to: (1) slope horizontal surfaces longitudinally or transversely; (2) avoid re-entrant corners; (3) seal box sections and provide drainage holes at the lowest point; (4) design details for easy discharge of water. To enhance the good performance of steel bridges, careful attention must be given to detailing. It is important to note that salty water causes the steel to develop a porous coating with high capillary action. As a result, water migrates to places it would not normally reach. This may reduce the effectiveness of some details designed to remove water from the surface. Further information on how to improve design details can be found in Yamada (1983), Manning (1984), Albrecht et al (1989) and Owens et al (1992).

4.2.3 Type and grade of steel

The type and grade of steel used can have a major effect on the rate of corrosion. In general, structural steels are "mild steels". They contain carbon as an alloying element to give strength and hardness. Copper as an additive to steel helps improve strength and gives a significant increase in corrosion resistance in atmospheric exposure. Silicon has a similar effect. Chromium increases the hardness and strength of steels, as well as its corrosion resistance. Nickel shows similar behaviour as an alloying element. Manganese is used to prevent brittleness and increase the toughness of steel. In the UK, steel grade 50 is often used for bridges as it offers a lower cost-to-strength ratio than grade 43 (BS 4360, 1990). According to ASTM the grades and characteristics of structural steel typically used for bridges are as follows:

A36 steel or mild steel: The main alloying agents are carbon and manganese. Copper may be added to increase corrosion resistance. This type of steel is inexpensive but is

particularly susceptible to atmospheric corrosion which is often greatest in marine and industrial environments. It requires coating for corrosion protection.

A572 steel: This is a higher strength grade than A36. Its main alloying agents are carbon, manganese, silicon and vanadium which give a fine grained structure. Its corrosion resistance is about twice that of mild steel, but also requires coating for protection.

A588 steel or weathering steel: This grade is one of the high strength, low alloy steels which are also known as weathering steels. Besides the alloying agents used in A572, it includes nickel, copper and chromium. Also it has about twice the atmospheric corrosion resistance of mild steel containing copper and four times the resistance of mild steel without copper (Naeemi et al 1984). This type of steel is used both with and without painting, when unpainted, its corrosion product forms a protective film on the steel surface that reduces further corrosion (Martin et al 1992).

4.2.4 Effects of surface protection

Surface protection is the most common type of corrosion defence. It has been noted by Johnson (1992) that painting is the principal method of protecting structural steelwork from corrosion. Typical forms of surface protection provide a barrier between the metal and its environment, particularly water, the common electrolyte for corrosion. Several investigators have examined the performance of paint systems applied to weathering and mild steels. Some have found certain paint systems to be more durable on a weathering steel (Copson 1959, Schmitt et al 1967 and Coburn 1978). Others have found comparable durability of the same paint systems applied to both weathering and mild steels (Nakayama 1972, Van Eijnsbergen 1979 and Scantlebury et al 1980). From the above studies data have been collected by Albrecht et al (1984) and they have mentioned that weathering steels enhance the service life of paint, because the protective oxide coating in scratches and thin spots is sufficiently thin to avoid undercutting the adjacent intact paint film. With mild steel, the voluminous rust continuously destroys the adhesive bond between the paint and the surface of the steel. On the other hand, when

environmental conditions are so bad that the weathering steel would have to be painted, A572 steel would be a preferred economic choice.

4.2.5 Effects of de-icing materials

Impurities such as salt can make water a more efficient electrolyte and speed corrosion. De-icing salts spread on highways and bridge decks during the winter can create a more corrosive environment for the bridge than that encountered at coastal sites. It has been found by Albrecht et al (1984) that the corrosive de-icing salt solution can leak through the bridge deck by way of expansion and construction joints and drain along girder and floor beam flanges leaving a corrosive salt residue that remains active throughout the year by absorbing moisture from the air. In the case of double deck bridges and overpasses, a salt mist or spray from moving traffic can be generated such that it splashes overhead girder structures leaving a salt residue that remains active throughout the year. Likewise, dried salt residue from the highway can blown into and on various bridge components where it can continue its aggressive action during humid periods. Evaporation of water leaves salt deposits, leading to accelerated pitting of the surface. It has been pointed out by Uhlig (1973) that chloride ions, Cl^-, also promote the electrochemistry dissolution of iron. However, one of the solutions to minimise the effect of de-icing material on the steel bridges is to wash them at the end of each winter season.

4.2.6 Effects of other factors

Other factors affecting penetration include the presence of pollutants in the atmosphere, the action of bacteria or other micro-organisms. Atmospheric pollutants can have similar effects to salt as discussed in de-icing section. Acids formed from gases in the atmosphere due to acid rain can also directly attack structural steel and increase the penetration of corrosion. Bacteria and other micro-organisms contribute to corrosion by destroying the protective film on metals, forming deposits on the surface and sometimes, even attacking the steel itself (Dexter 1986). The accumulation of corrosion products

(rust) on the surface of metal by their metabolism (generally acids) can directly increase the corrosion penetration.

Industrial, marine and rural atmospheres contain considerable amounts of impurities, the most important of which from the corrosion viewpoint will be dust, sulphur dioxide, and carbon dioxide. Dust appears to be important in initiating corrosion, and surface specks of carbonaceous material such as soot are efficient sites for hydrogen evolution because of the low hydrogen over potential of carbon. Chandler et al (1970) has mentioned that all the evidence indicates that sulphur is harmful. The presence of sulphur dioxide in the atmosphere has long been recognised as a major cause for concern to those interested in corrosion. The reasons why sulphur dioxide should cause such drastic increases in corrosion penetrations are still obscure, but it is probable that the classical theory that the sulphur dioxide oxidises and dissolves in water to form sulphuric acid is a simplification. The effect of sulphur dioxide on corrosion was investigated by Haynie et al (1978).

4.3 Review of relevant research

More recent studies have increasingly focused on quantitative and predictive methods of assessing corrosion resistance. This includes the classification and calibration of atmospheric corrosion test sites, the evaluation of the effects of micro-climate on corrosion, the prediction of long-term atmospheric corrosion from short-term experimental data and the measurement of time-of-wetness of the specimen.

Payer et al (1971) extensively described environmentally-induced localized penetration (pitting) which can occur at a metal surface. Sereda (1974) assessed weather factors in relation to corrosion of metals. Haynie et al (1974) presented a correlation between the corrosion behaviour of steel and atmospheric pollution data. The importance of time-of-wetness in assessing corrosion rates, as well as the composition and physical nature of corrosion products was emphasized. Knotkova et al (1982) presented basic atmospheric corrosion penetration data for weathering steel. Tests were conducted in configuration representative of actual service conditions, including steel girder models. Bragard et al (1982) suggested that the corrosiveness of a test site toward a grade of steel be

represented by one-year mass loss, and the further evaluation of corrosion be considered a function of the one-year mass loss and the relative humidity of the site. An extensive summary of corrosion mechanism and atmospheric corrosion penetration data for weathering steel was conducted by Albrecht et al (1984).

Methods for assessing the extent of corrosive attack on metal have been presented by Champion (1964). Classification by comparison with standard charts was illustrated. Maximum depth was considered to be an unreliable parameter to quantitatively described pitting and a performance factor, based on statistical considerations was presented along with other statistical methods. Deterioration in mechanical properties was also presented as a basis to assess the effect of corrosive attack. Crews (1976) proposed a means for obtaining quantitative estimates of service life and corrosion penetrations for buried pipes. Statistical methods were employed to extrapolate pit depth measurements beyond the exposure period of tests. Rowe (1974) discussed the measurement and evaluation of pitting corrosion. Maximum pit depth was considered a meaningful way to show the extent of pitting. Statistical methods were presented to show the relationship between depth and time of exposure, and to estimate the maximum pit depth based upon an examination of a portion of the exposed metal surface. Rating numbers for atmospheric corrosion resistance of weathering steel were investigated for 33 sets of domestic corrosion penetration data by Albrecht et al (1991). The results showed that the rating numbers calculated with both the ASTM and direct ASTM methods were inconsistent and misleading because it does not reflect the actual corrosion resistance of a steel in a given environment.

An eight-year atmospheric test was carried out by Townsend et al (1982) on weathering steel and steels with 0.21 and 0.021 percent copper for corrosion resistance in rural, marine, and two industrial environments. The results of these tests were fitted by a straight-line function (see equation 4.6).

An investigation of weathering steel bridges was conducted by the State of Michigan (McCrum et al 1985) to identify the extent and magnitude of corrosion. Fifty weathering steel bridges were surveyed for location and penetration of corrosion. The study showed

that significant surface corrosion was occurring on the bridges. The areas of corrosion were limited to places where deck leakage or road spray accumulated. It has been noted by McKenzie (1978) that both the existing rust layer and environment could influence the corrosion penetration. Also he has mentioned that the corrosion tests in the USA had shown that the corrosion penetration of weathering steel was much lower than the penetration for mild steel in the same environment. It has been found during a study by Kilcullen et al (1979) that the corrosion penetration in the UK was generally higher than those measured in the USA.

Long-term corrosion tests have been carried out on mild and weathering steels at a number of locations in the UK by McKenzie (1990). Test specimens were exposed under open and sheltered conditions on both real and simulated bridge decks. In some cases the test specimens were in close thermal contact with the bridge girders to check that small test specimens do give corrosion measurements representative of the steel in large structures. The results showed that small test specimens do provide relevant information and confirmed the difference between corrosion under sheltered and open exposure conditions. He has also concluded that the weathering steel corroded at a generally lower rate than mild steel but the difference was reduced under sheltered conditions. Sheltered marine environments led to high corrosion rates with localized corrosion and pitting and there were indications that similar problems might develop on over-bridges subjected to traffic spray sometimes containing salt from de-icing operations.

4.4 Methods for assessing corrosion penetration

It is vital to determine how fast corrosion will occur on steel structures. Some procedure is often needed to quantitatively describe or classify the extent of corrosion penetration. In the following sections several methods in which corrosion penetration can be evaluated are presented.

4.4.1 Mass loss method

Metal mass loss is not very satisfactory as a measure of the extent of pitting unless the overall corrosion is small and even provides no information about variations in depth of pitting. According to ASTM Standard Practice G1 (1981), whatever cleaning method is used, the average corrosion penetration per side of a specimen may be calculated from the mass lost during the time of exposure by the following equation:

$$d_c = K_c \left(\frac{W}{A_s D} \right) \tag{4.1}$$

where

d_c = average corrosion penetration per side (μm);

K_c = conversion constant;

W = mass loss (grams);

A_s = total surface area, all sides (cm^2); and

D = density (g/cm^3).

The constant, $K_c = 10^4$ when the other variables are substituted in the indicated units. The density of low-alloy steels is $D = 7.85$ g/cm^3. This method is believed to be most useful for small specimens with uniform corrosion. It should be noted that the corrosion penetration calculated from mass losses can be misleading when deterioration is highly localized, as in pitting or crevice corrosion. Therefore, this method may not be recommended for the purpose of evaluating penetration of corroded steelwork with very rough surfaces and in practice members and components in service cannot be removed for mass loss. However, this method has been used by several researchers to estimate the corrosion penetration of steelwork, as explained in the following paragraphs.

Legault et al (1974) derived three equations that allow one to estimate the 15.5 year corrosion penetration of weathering steel with a given chemical composition. The equations are based on the Larrabee et al (1961) data, they can apply in a strict sense, only to the environments comparable to those which tests have been done. However, the

regression equations for average corrosion penetration can be found in Albrecht et al (1984).

In developing a corrosion deterioration model for steel girder bridges, Albrecht et al (1987) calculated the projected corrosion penetration for bridges exposed to industrial environments in the United States with the following expression which came from Copson (1960):

$$d_c = (50 + 10t) \tag{4.2}$$

where d_c is the average corrosion penetration per side in micrometers and t is time of exposure in years. It has been noted by Albrecht et al (1989) that for bridges located in industrial sites, the examination of underlying steel shows that shallow pitting occurred in conjunction with uniform corrosion. Therefore, the use of the average penetration is adequate for many structural calculations.

For all steels tested by Copson (1960), the average depth of the four deepest pits after 17 years of exposure on the groundward and skyward surfaces of steel specimens having many different chemical compositions were two to three times the average corrosion penetration calculated from mass loss. The pitting factor which is the ratio of pit depths to average corrosion penetration for mild steel was about three. Accordingly, the following empirical formula was produced to estimate the average pit depth, d_p, for bridges exposed to high corrosive industrial environments.

$$d_p = 3(50 + 10t) \tag{4.3}$$

where d_p is the average pit depth in micrometers and t is the time of exposure in years. It is emphasized that the pits can be much deeper in crevices, along breaks in mill scale, and under deposits of debris that trap moisture and salts from any source.

The effect of sulphur dioxide on corrosion penetration was investigated by Haynie et al (1978). The results of the study are of interest in the sense that they showed

concentration of SO_2, relative humidity and temperature to be the important factors controlling corrosion. The following empirical equation accounted for 91 percent of the variability in the experimental data.

$$d_c = \left[5.64\,SO_2 + e\left(55.44 - \frac{31150}{RT} \right) \right] t_{wet} \qquad (4.4)$$

where

d_c = corrosion penetration (μm);

SO_2 = concentration of SO_2 (g/m^3);

e = constant (2.718);

R = gas constant (1.9872 cal/g-mol);

T = geometric mean panel temperature when wet (K°); and

t_{wet} = time of panel wetness (year).

4.4.2 Power function method

The rate of attack for each material must be expressed quantitatively. The corrosion penetration in different environments has been evaluated in several studies by Bohnenkamp (1973), Townsend et al (1982) and Albrecht et al (1984). It has been observed that the average corrosion penetration follows a power law function (Komp 1987). The form of this function is:

$$d_c = A\,t^B \qquad (4.5)$$

where d_c is average corrosion penetration in micrometers, t is exposure time in years, A is the intercept (equal to the corrosion loss in 1.0 year) and B is the slope of the log-log plot of corrosion penetration versus time whose values depend on the type of steel and the environment.

Equation 4.5 becomes a straight-line relationship in logarithmic form which was used by Townsend et al (1982) as mentioned in section 4.3 as follows:

$$\log d_c = \log A + B \log t \tag{4.6}$$

It is clear that A is numerically equivalent to the corrosion loss when time is unity. Accordingly, A is generally considered to be a measured of the initial reactivity of the materials with the environment prior to long-term changes, such as the accumulation of corrosion products.

Alternatively, equation 4.5 can be solved for t, the time required to reach a particular value of corrosion penetration, d_c.

$$t = \left(\frac{d_c}{A}\right)^{1/B} \tag{4.7}$$

4.4.3 Comparison between Copson's and power function methods

A comparison is made between equation 4.2, which has been developed by Copson, and the power function (equation 4.5) which has been used in this study for calculating the average corrosion penetration. In order to show how the results of these equations can be compared together, they have been plotted in Figure 4.1 for exposure time of 120 years. It can be seen that after the initial exposure time the curves are diverging as the exposure time increased. However, it can be concluded that the power function is on the safe side.

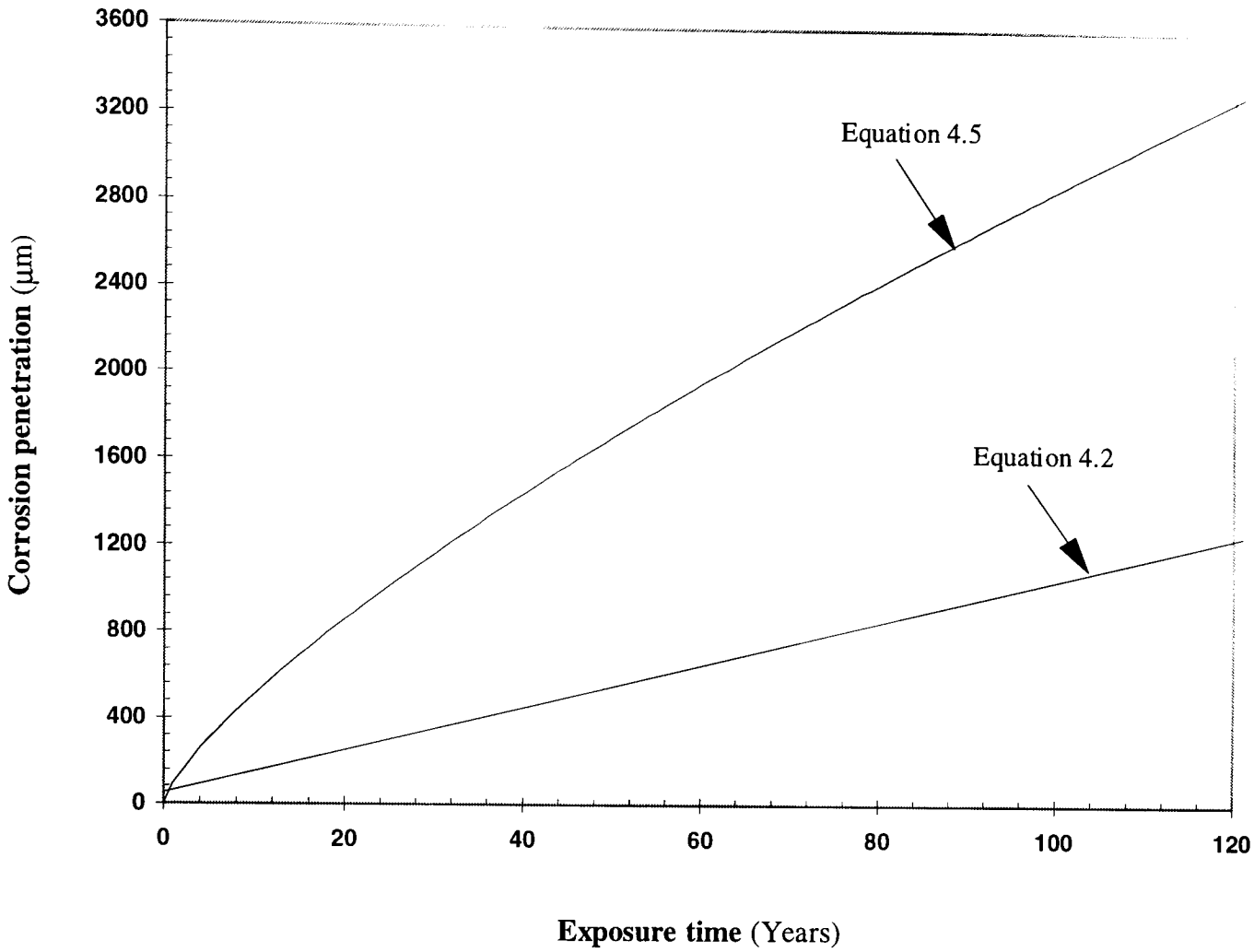

Figure 4.1 Comparison between the corrosion loss curves.

4.5 Evaluation of corrosion penetration parameters

The rate of corrosion penetration for different types of steels in different environments has been evaluated by experimental work in several ongoing studies by Copson (1960), Townsend et al (1982), Albrecht et al (1984), Komp (1987) and McKenzie (1978 and 1990). Albrecht and Naeemi (1984) collected data for both mild and weathering steels exposed at different environments over period of 3 to 17 years in the UK and USA. Uniform corrosion has been considered because it can be identified easily and there was no need to measure the pit depth. The power function has been used to represent the average corrosion penetration. The average values of A and B for mild and weathering steels exposed in the rural, marine and industrial environments in the USA are listed in Table 4.1.

Table 4.1 Statistics for corrosion parameters *A* and *B*, for mild and weathering steels exposed in different types of environments in the USA.

Environment	Mild Steel		Weathering Steel	
	A	*B*	*A*	*B*
Rural	31.9	0.69	27.1	0.48
Marine	74.2	0.85	28.0	0.62
Industrial	83.2	0.55	41.7	0.27

This study will consider only the experimental data which have been developed in the UK by McKenzie (1978) and in a joint study by the British Steel Corporation and the British government's Transport and Road Research Laboratory (Kilcullen et al 1979). In these studies, specimens of mild and weathering steels were exposed in the rural, marine and industrial environments for a period of five years. At each test site, the specimens were mounted vertically and boldly exposed to the prevailing wind direction. The specimens of each steel were removed to measure corrosion penetration from each exposure position annually for periods of up to five years. The corrosion penetration was estimated from the difference between the total corrosion at the end of the year minus the corrosion at the beginning. The locations of the experiments carried out in the UK are listed in Table 4.2.

Table 4.2 Locations of the experiments in the UK (Kilcullen et al 1979).

Site	Locations
Rural	Loudwater and Silverdale
Marine	Brixham, Eastney and Rye
Industrial	Tinsley, Middlesbrough, Portishead and Battersea

The regression coefficients *A* and *B* for all sets of rural, marine and industrial data are given in Table 4.3. As indicated by the high value of correlation coefficient ($R = 1.0$ means perfect correlation), equation 4.5 accurately represents the relationship between corrosion penetration and exposure time. From the statistical results in Table 4.3 it is

apparent that a wide variation can occur in both A and B from one environment to another. The average values of A and B for mild and weathering steels in the UK have been calculated from Table 4.3 and listed in Table 4.4.

Table 4.3 Regression analysis of corrosion penetration data for steels exposed to different environments in the UK.

Environment	**Location**	**Mild Steel**			**Weathering Steel**		
		A	*B*	*R*	*A*	*B*	*R*
Rural	Loudwater	51.7	0.600	1.00	50.7	0.494	0.99
	Silverdale	38.7	0.601	1.00	38.4	0.471	1.00
Marine	Brixham	39.1	0.530	0.98	28.6	0.574	0.98
	Eastney	53.6	0.669	1.00	42.9	0.511	1.00
	Rye	70.3	0.623	1.00	49.3	0.585	0.99
Industrial	Portishead	49.4	0.562	1.00	42.0	0.572	1.00
	Tinsley	65.4	0.872	1.00	71.2	0.709	1.00
	Middlesbrough	80.0	0.534	1.00	59.1	0.585	0.99
	Teesside	182.0	0.469	1.00	65.3	0.646	1.00
	Battersea	76.9	0.669	1.00	57.2	0.693	1.00

Table 4.4 Average values of parameters A and B for mild and weathering steels in the UK.

Environment	**Mild Steel**		**Weathering Steel**	
	A	*B*	*A*	*B*
Rural	45.20	0.60	44.55	0.48
Marine	54.33	0.61	40.30	0.56
Industrial	90.74	0.62	58.97	0.63

Results of the data collected from research carried out in the UK are substituted into the power function (equation 4.5) and are plotted as a function of time in Figure 4.2. This plot shows that the steels at different environments can be quantitatively ranked in terms of their corrosion penetration resistance.

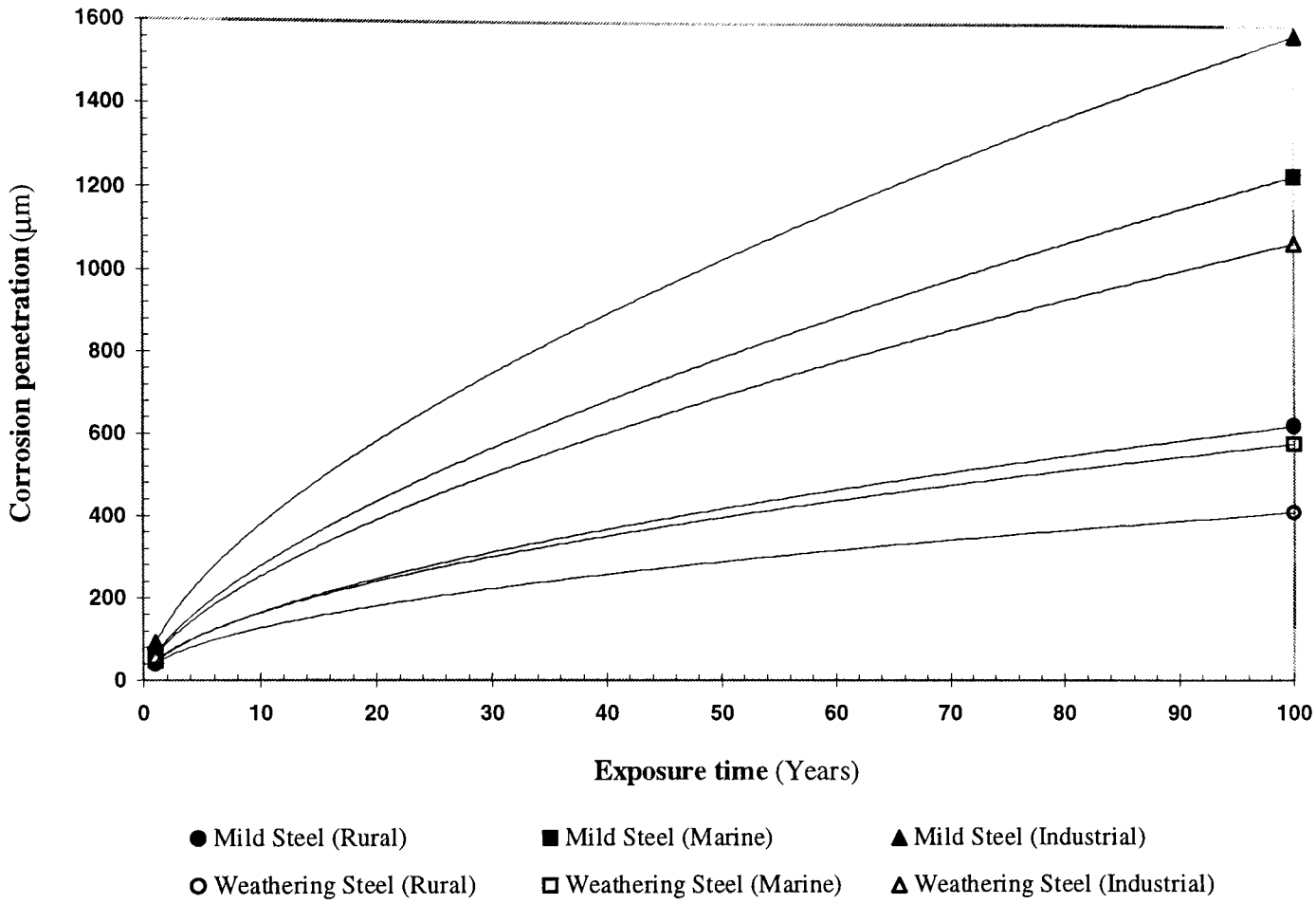

Figure 4.2 Corrosion penetration versus exposure time for different types of steels in various environments within the UK.

4.6 Corrosion penetration model used in this study

The value of *A* has been taken as 90.74 for industrial environments from Table 4.4. This value is the average value of the tests which have been carried out at different types of industrial sites in the UK. The main reasons for using this value is because the initial penetration of the specimens in the first year of exposure are not known.

The corroded specimens measured in Chapter 3 were obtained from an industrial structure approximately 40 years old. The corrosion penetration and maximum roughness of each specimen is given in Table 4.5. The value of *B* can be obtained by substituting the average value of mean corrosion into equation 4.5.

Table 4.5 Results of measurements.

Specimen number	d_c (mm)	R_{max} (mm)
1	0.13	0.34
2	1.59	1.20
3	0.19	0.94
4	1.23	1.53
5	1.71	0.73
6	0.09	0.47
7	2.28	1.75
8	1.83	2.79
9	1.25	2.62
10	0.13	0.39
11	0.16	1.01
12	0.38	1.15
13	1.61	1.68
14	2.31	1.78
15	2.34	1.36
16	2.68	3.37
17	1.93	2.70
18	1.58	0.60
19	1.61	1.58
20	1.06	0.56
21	2.06	2.01
22	1.26	0.82
23	1.34	0.98
24	1.12	0.93
25	1.19	1.23
26	1.23	1.21
27	1.52	1.15
28	2.05	2.29
29	1.64	1.80
30	2.16	2.06
31	1.56	1.67
32	1.46	1.26
33	1.39	1.28
34	2.06	2.59
Average	1.42	1.47

The following data have been used to calculate the exponent B from equation 4.5:

$A = 90.74$ (mild steel exposed at industrial site, Table 4.4);

$d_c = 1420$ μm (mean penetration of 34 corroded specimens per face, Table 4.5); and

$t = 40$ years (exposure time).

$$B = \frac{\log(1420) - \log(90.74)}{\log(40)}$$

$$B = 0.75 \tag{4.8}$$

Accordingly, by substituting the values of A and B into equation 4.5 gives the following relationship which represents the average corrosion penetration with time:

$$d_c = 90.74\, t^{0.75} \tag{4.9}$$

The relationship between the measurements of maximum roughness, R_{max}, and corrosion penetration, d_c, for all corroded specimens can be obtained from Figure 4.3 by plotting R_{max} against d_c. The mean regression line drawn through the data points leads to the following function:

$$R_{max} = 0.98\, d_c \tag{4.10}$$

By substituting d_c from equation 4.9 into equation 4.10, we can obtain R_{max} in terms of exposure time.

$$R_{max} = 88.90\, t^{0.75} \tag{4.11}$$

Equations 4.9 and 4.11 have been plotted in Figures 4.4 and 4.5 for 40 years exposure, respectively.

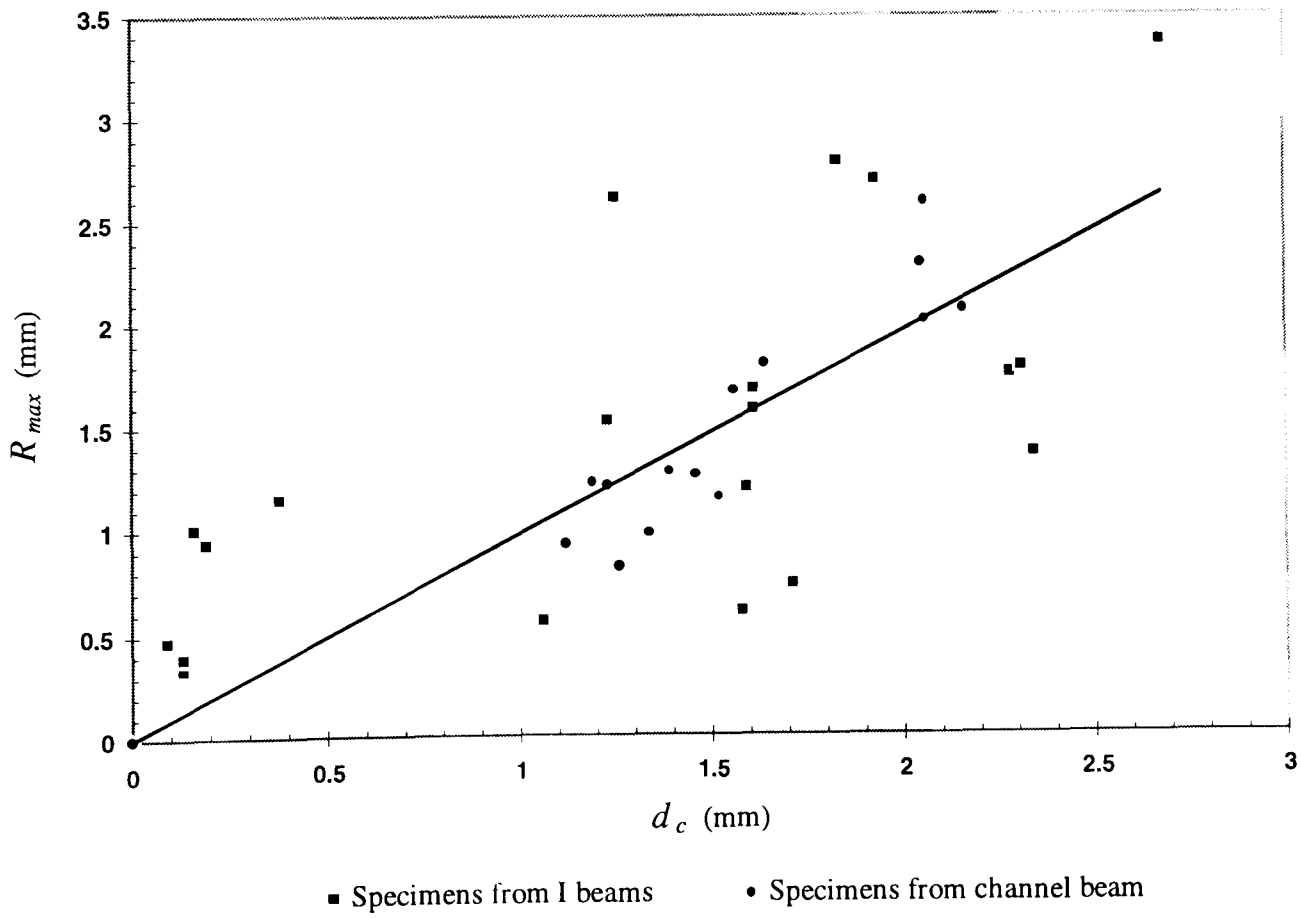

Figure 4.3 Depth of corrosion, d_c versus maximum roughness, R_{max} (correlation coefficient = 75%).

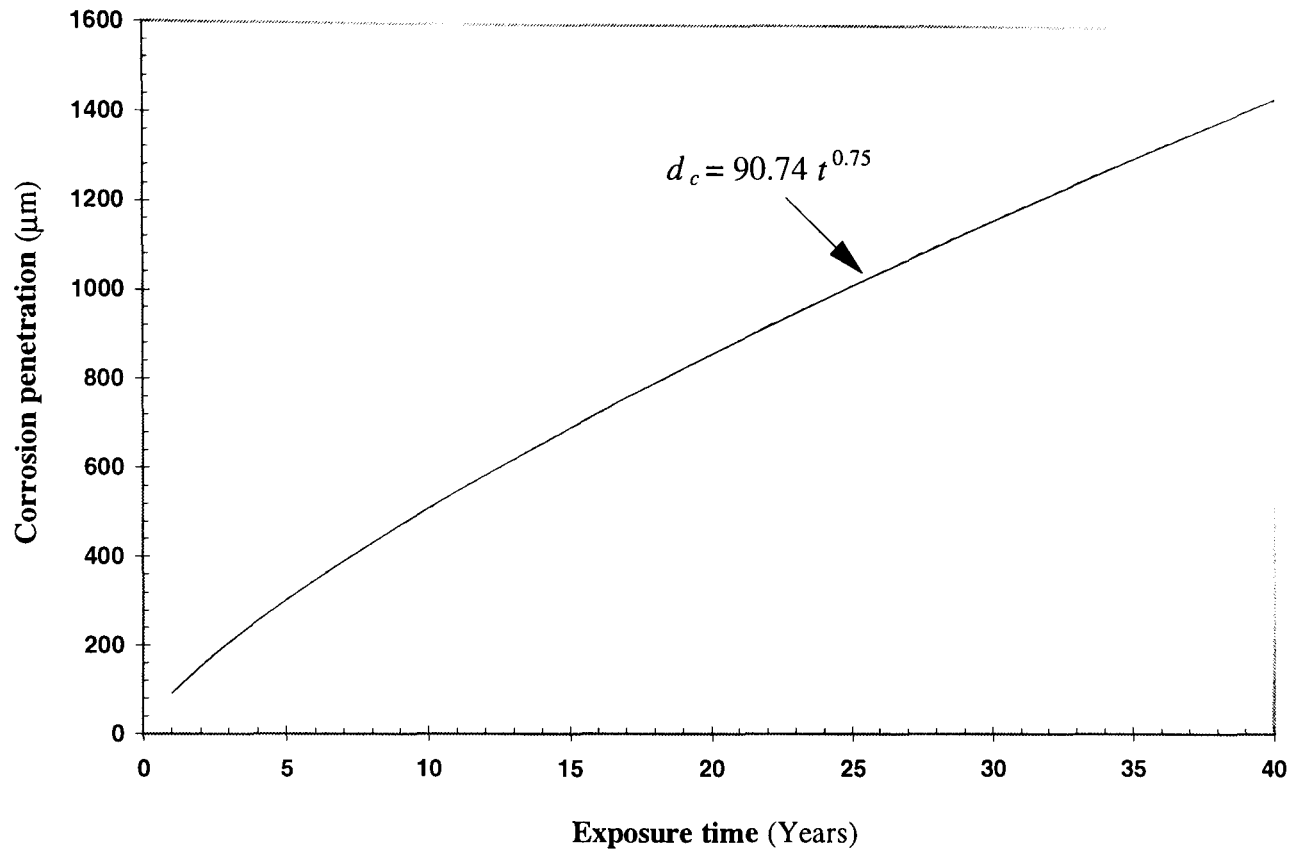

Figure 4.4 Corrosion penetration versus time of exposure.

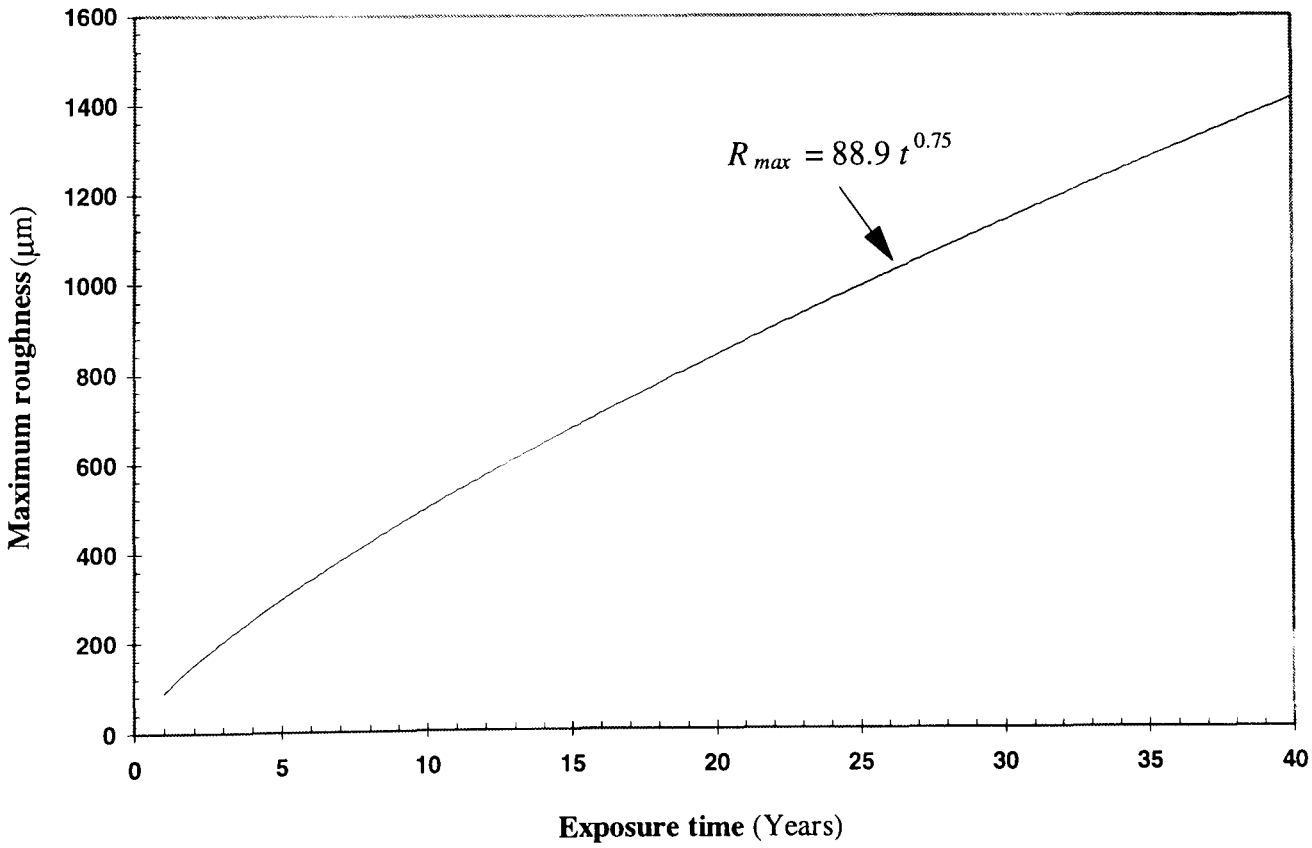

Figure 4.5 Average maximum roughness versus time of exposure.

4.7 Quantitative comparisons of the average maximum roughness

The result of the average maximum roughness obtained from the measurements of corroded specimens was compared for accuracy with the Copson's method and the empirical relation developed in this research. Albrecht's data was also used to investigation the accuracy and applicability of the empirical relation developed in this chapter for predicting pit depth.

4.7.1 Comparison with Copson's method

The calculated average maximum roughness from the measurements of the corroded specimens in this study was found to be 1.47 mm (see Table 4.5), whereas using equation 4.3 produced by Copson (1960) for 40 years exposure it is 1.35 mm.

4.7.2 Comparison with the Albrecht work

In order to investigate the applicability and the accuracy of the empirical formula developed for calculating average maximum roughness, Albrecht's (1988) data from other corroded steel structure is compared with equation 4.11. The data were generated by testing stringers from an existing railway bridge which were in service for 58 years. The stringers were directly exposed to precipitation and sunshine except for the partial shelter provided by the railway ties. It has been reported that the stringers were corroded severely at two locations: top of top flange where crevices formed between the railway ties; and top of bottom flange where the accumulated debris trapped moisture that wicked up the lower web by capillary action. The bridge was located in an environment of moderate corrosivity. The stringers were made from mild steel.

The following data have been used from Albrecht's work:

t = 58 years (exposure time) and

R_{max} = 1.88 mm (average maximum roughness of 18 stringers, as shown in Table 4.6).

Table 4.6 Results of measurements obtained by Albrecht (1988).

Stringer number	R_{max} (mm)
1	4.67
2	0.76
3	0.69
4	2.84
5	4.06
6	3.43
7	2.03
8	1.45
9	0.89
10	0.41
11	2.08
12	2.16
13	0.33
14	0.76
15	3.43
16	1.95
17	0.71
18	1.27
Average	1.88

The value of average maximum roughness, R_{max}, from the equation developed in this study (equation 4.11) has been calculated for exposure time of 58 years and found to be 1.87 mm. It is evident that the difference between the results is less than one percent. The small variation between the results clearly shows that the proposed empirical formula provides improved performance in prediction of pit depth. It can be seen from Figure 4.5 that as time of exposure increases the slope of the curve decreases. This result indicates that in the long-term exposure time the rate of change in the B exponent may not be significant. However, it can be stated that the relation which has been developed in this research is reliable and may be used for estimating the pit depth in practice for corroded existing steel structures.

4.8 Statistical analysis of maximum roughness

4.8.1 Statistical analysis of maximum roughness for all specimens

The results of maximum roughness measurements of 34 corroded specimens as listed in Table 4.5 showed that there is a large variation in the measured pit depth (0.34-3.37 mm). Therefore, special attention has to be given to the variability of the maximum

roughness, because the degree of corrosion may vary with location of members and components of steel structures. The objective is to define the probability of the maximum roughness which has a 5% chance of exceedance.

The easiest starting point is to construct a histogram for the maximum roughness. A suitable class-interval of 0.25 mm has been chosen and the results are recorded in Table 4.7. The histogram in terms of equivalent probability density function and maximum roughness interval is plotted in Figure 4.6. The histogram is not particularly smooth, because it relates to only 34 samples. An increased sample size would be expected to generate a smoother histogram.

Table 4.7 Frequency of maximum roughness measurements.

Interval (mm)	Frequency
0.0-0.24	0
0.25-0.49	3
0.5-0.74	3
0.75-0.99	4
1.0-1.24	6
1.25-1.49	3
1.5-1.74	4
1.75-1.99	3
2.0-2.24	2
2.25-2.49	1
2.5-2.74	3
2.75-2.99	1
3.0-3.24	0
3.25-3.49	1

In this study variation in roughness has been modelled by normal and log-normal distributions. In order to calculate the normal probability distribution function, the mean ($\overline{R}_{max}$ = 1.47 mm) and standard deviation (S_d = 0.75 mm) of maximum roughness of the corroded specimens has been computed. For log-normal distribution function the mean ($ln\ \overline{R}_{max}$ = 0.24 mm) and the standard deviation ($ln\ S_d$ = 0.57 mm) have been calculated. The resulting normal and log-normal distribution probability density functions are superimposed on the equivalent histogram as shown in Figure 4.6. It can be observed

that the log-normal distribution function fits the experimental data more closely than the normal distribution function.

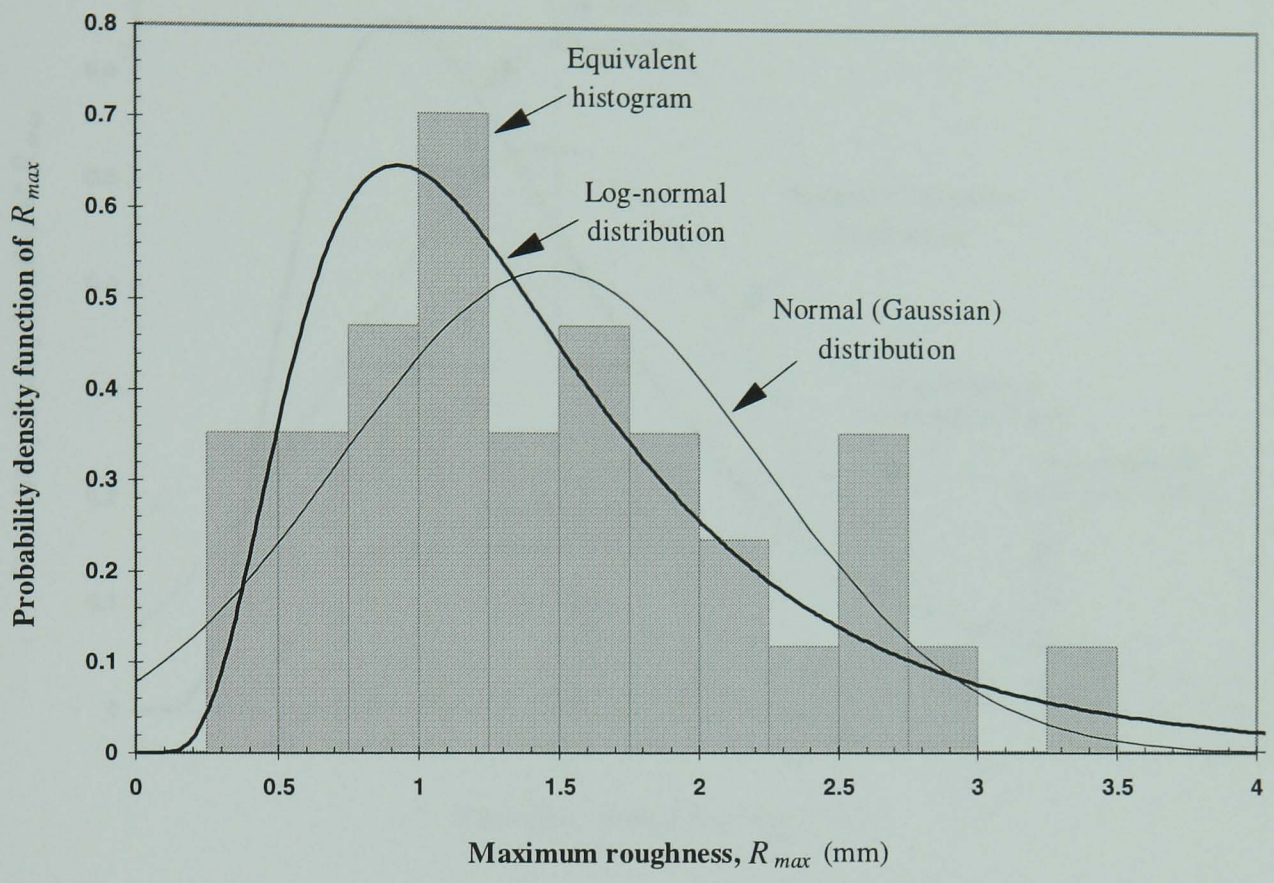

Figure 4.6 Probability function and the equivalent histogram of maximum roughness, R_{max}.

Using the two distributions the following values of maximum roughness are obtained for a probability of exceedance of 5% (see Figure 4.7):

R_{max} = 2.70 mm (normal distribution function)

R_{max} = 3.24 mm (log-normal distribution function)

The value obtained from the log-normal distribution is preferable because the distribution fits the experimental data more closely.

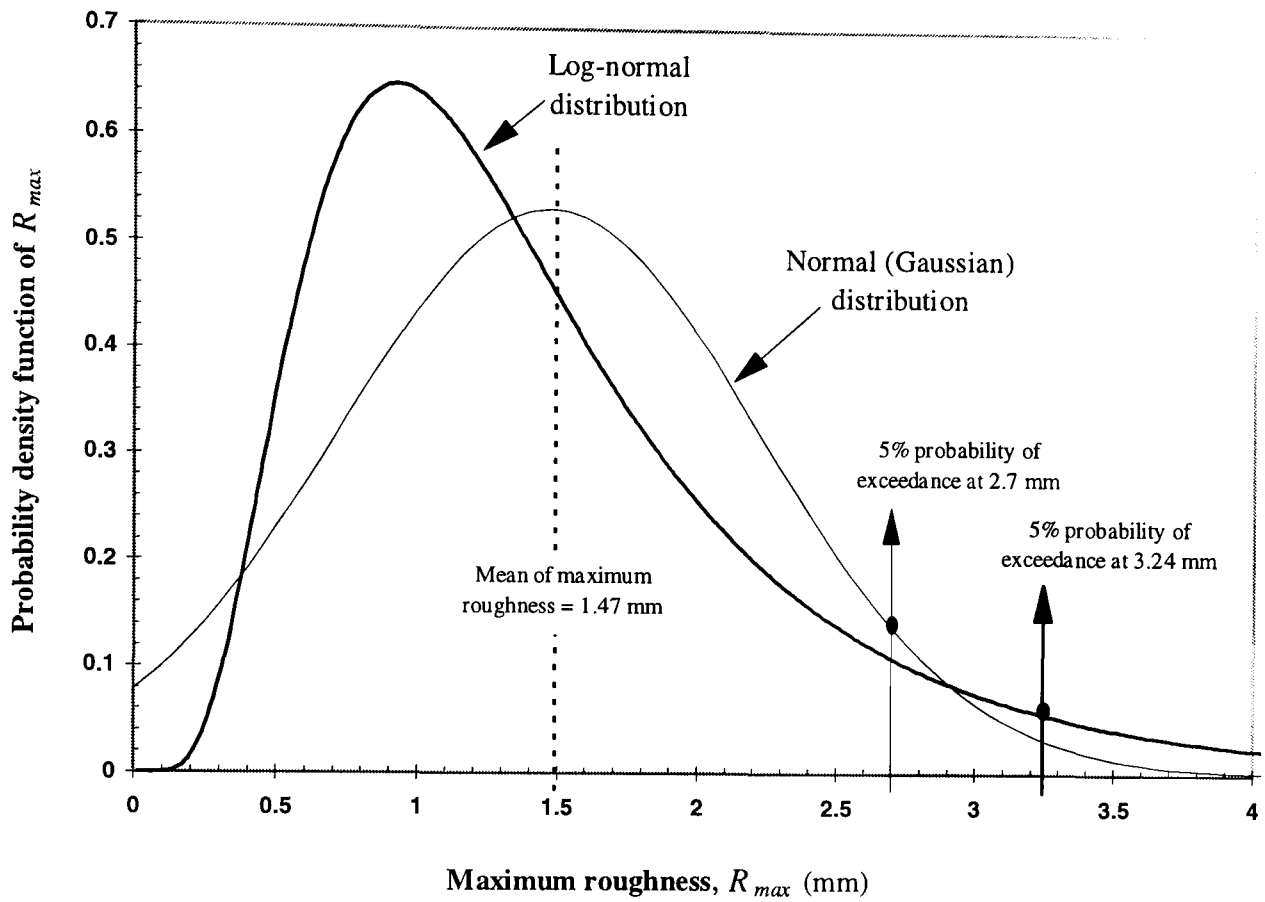

Figure 4.7 Probability function of maximum roughness, R_{max}.

4.8.2 Statistical analysis of maximum roughness for each specimen

It was observed in Chapter 3 that a large variation existed in the roughness measurements of each individual corroded specimen. Therefore, it was decided to carry out the same statistical analysis for each individual specimen as was done for the corroded specimens collectively in previous section. The 5% probability of exceedance of each corroded specimen was calculated and is listed in Table 4.8. Furthermore, the maximum roughness of each specimen is plotted against the 5% probability of exceedance of each corroded specimen in Figure 4.8. It can be seen from the plot that there is a good correlation between maximum roughness and the 5% probability of exceedance.

Table 4.8 Results of 5% probability of exceedance of roughness for each corroded specimen.

Specimen number	5% probability of exceedance of maximum roughness (mm)
1	0.45
2	1.57
3	1.12
4	2.11
5	0.91
6	0.62
7	2.28
8	3.82
9	3.38
10	0.50
11	1.29
12	1.59
13	2.20
14	2.35
15	1.74
16	4.64
17	3.49
18	0.76
19	1.75
20	0.72
21	2.85
22	1.08
23	1.37
24	1.26
25	1.58
26	1.58
27	1.57
28	3.06
29	2.30
30	2.92
31	2.27
32	1.61
33	1.70
34	3.77

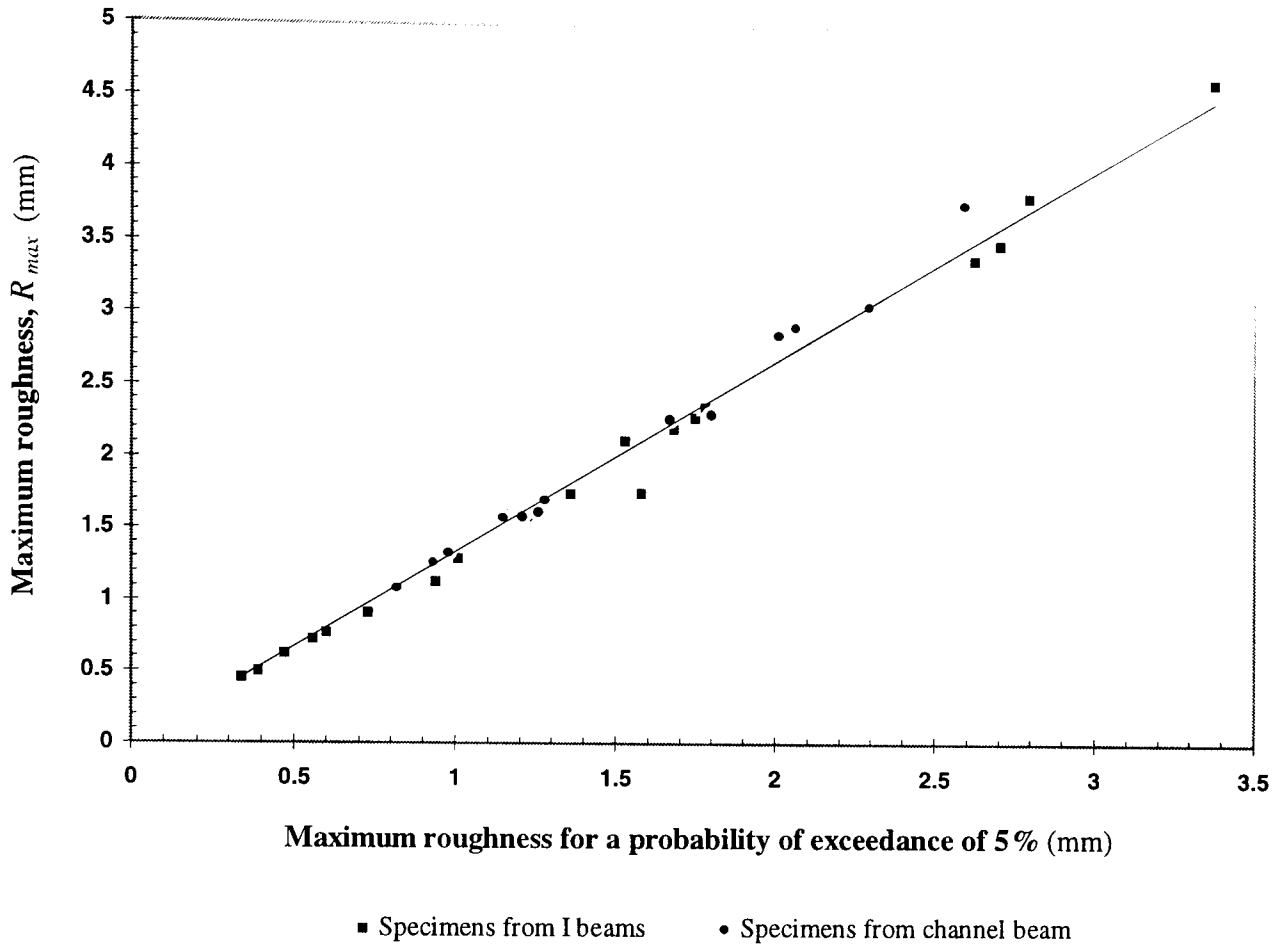

Figure 4.8 Maximum roughness versus 5% probability of exceedance of roughness of each corroded specimen.

4.9 Summary and conclusions

The main aspects that are associated with corrosion penetration have been identified and discussed in this chapter. The review has helped us to identify the factors which may increase the corrosion penetration of steelwork in long-term. From the previous studies carried out in the field of corrosion penetration, it has been observed that corrosion penetration follows a power function. The values of A and B in the power function for different types of steels in different environments have been obtained from tests carried out in the UK. In order to help to develop a relation for average penetration and maximum roughness (pitting corrosion), the following assumptions are made with regard to the corroded specimens:

1. The power function has been used because the results obtained by others during the last two decades for a variety of steels at different environments were well represented by the power function.

2. The value of A has been taken as 90.74 for industrial environments, which is the average value of tests carried out at different types of industrial sites in the UK.

3. The value of B has been calculated based on the average penetration measurements of corroded specimens weathered for nearly 40 years.

4. The method of average measurement has been used in this study instead of the mass loss method.

These assumptions have been used as the basis for the development of average maximum roughness in terms of exposure time.

It has been observed that the types of data collected for A and B in industrial sites of the UK and USA are different. The higher values of A and B indicate that the corrosion penetration was much higher in the UK sites than the USA sites. The primary reason for the higher penetration at the English sites appeared to be the combination of sulphur pollution and the longer period of relative humidity. Indeed, McKenzie (1978) reported that when the tests were carried out in the UK, the air was sufficiently humid over 80% of the testing period. Also it is evident from equation 4.4 that the degree of corrosion penetration increases with the atmospheric sulphur dioxide. At the British sites, the corrosion penetrations for the weathering steel in all environments and the mild steel in industrial sites, appeared to be higher than at the American sites (see Tables 4.1 and 4.4).

It has been observed and also noted by Kayser (1988) that the parameter A is only an algebraic multiplier in the equations of corrosion penetration and maximum roughness. The exponent B as shown in Tables 4.1 and 4.4, would have a significant effect in the equations of corrosion penetration and maximum roughness, but its effects may decrease as exposure time increases. However, it can be concluded that the parameter B is an important factor in the assessment of corrosion penetration.

Several estimate methods for determining the average corrosion penetration and maximum roughness were investigated in this study. It has been observed that mass loss

method by itself is not a satisfactory procedure for determination of extent of pitting. The relationships developed in this study showed a good accuracy for predicting the average maximum roughness. Long-term data have been used (the specimens were in service for nearly 40 years). The average maximum roughness compared very well with Copson's method and with Albrecht's data. Therefore, the function which has been developed can be used to predict the average pit depth of corroded steelwork structures. These equations, 4.9 and 4.11 will be used to estimate the remaining fatigue life of corroded structural members and components due to uniform and pitting corrosion in terms of exposure time in Chapter 7.

A statistical analysis for maximum roughness measurements was carried out using normal and log-normal distribution probability density functions. It was found that the log-normal distribution function fits the equivalent of the histogram (plotted from experimental data) better than the normal distribution function. The 5% probability of exceedance for all of the corroded specimens was at 3.24 mm.

CHAPTER V

FATIGUE ASSESSMENT

5.1 Introduction

The two main causes of deterioration of steel structures are fatigue and corrosion. The main aspects that are associated with corrosion of steel structures have been discussed in Chapters 2 and 4. A particular point of interest in this chapter is the brief review of fatigue concepts and an investigation into the mechanism by which corrosion pitting may reduce the fatigue life of steel structures.

Fatigue is the phenomenon in which a repetitively loaded structure fractures at a load less than its ultimate static strength. Any variation in the loading experienced by a member, no matter how small or infrequent, should be considered as fatigue loading. Fatigue failure may occur in as little as a few hundred, or as many as several millions load applications. This is the case for bridges which are subjected to loading by millions of heavy goods vehicles per year and for offshore structures which are subjected to wave loading. Fatigue is a very common problem in welded steel structures because of the presence of microscopic flaws in the weld metal (Smith 1988).

The first study of metal fatigue is believed to have been conducted around 1829 by a German mining engineer by the name of Albert (Suresh 1991). Interest in the study of fatigue began to expand with the increasing use of ferrous structures, particularly bridges in railway systems. Wohler (1871) conducted systematic investigations of fatigue failure in railroad axles for the German Railway Industry. He observed that the strength of steel axles subjected to cyclic loads was appreciably lower than their static strength. Wohler's studies included fatigue tests on full-scale axles and on a variety of structural components used in small machines under bending, torsion and axial loading conditions.

Extensive efforts have been undertaken over the years in characterizing the fatigue behaviour of metals along the lines of Wohler.

Fatigue failure can be defined as the number of cycles to reach a pre-defined failure criterion. Simple fatigue failure starts from a single crack and propagates until ultimate failure occurs. A compound fatigue failure results when the origin of the fatigue crack propagates from two or more locations and propagates, and their joint effects cause the total failure (Frank et al 1963). It has been pointed out by Maddox (1991) that positive damage such as sudden collapse, or excessive deflection can be induced if the crack is permitted to propagate to some critical size. The fatigue strength, which is the value of stress corresponding to failure after a given number of cycles, is generally below the yield strength. This means that cracks are able to initiate and propagate at stresses in the elastic region, stresses normally used for design.

Assessment of the fatigue capacity of steel bridges is further complicated by the need for rehabilitation or for extending the life of old and deteriorated bridges. Many old riveted steel bridges in different countries approach their hundredth birthdays, or even more, and very often there is no reason to put them out of service (Brandes 1990). The replacement of all these bridges far exceeds the available financial resources. In several cases replacement would be the least acceptable option because many of the bridges are of historical importance (Kim et al 1988). Sobanjo et al (1994) recently reported that as of 30 June 1988 about 41% of the United States inventoried bridges were classified as either structurally deficient or functionally obsolete. Each year, about 1,200 bridges reach the end of their design life (Yazdani et al 1990). Most of them must be strengthened, repaired or reconstructed to ensure an acceptable level of safety considering present and future traffic conditions. An evaluation of accumulated fatigue damage and the safe remaining life of a bridge will dictate the proper course of action to mitigate any potential hazard. Because of the limited amount of funds and the high cost of reconstruction, the concept of using structural rehabilitation and maintenance for the possible extension of the service life of existing structures is very attractive, and needs to be exploited to the fullest extent.

There is a voluminous literature in the field of fatigue. Problems associated with the fatigue of welded structures and bridges have been extensively reviewed by Gurney (1979), Fisher (1984) and Maddox (1991). The combined action of both corrosion and fatigue, known as corrosion fatigue on offshore structures have been investigated by Sawant et al (1989) and Ramachandra Murthy et al (1993 and 1994).

Research is continuing into the fatigue assessment of corroded steelwork structures. Hiam et al (1978) conducted fatigue tests on low carbon automotive steels and obtained results which have application to deteriorating bridges. Corrosion pits of various depths were induced in test specimens and a correlation between cycles to failure and pit depth was observed. Specimens which experienced pitting caused by under-vehicle exposure for two winters were also tested.

Considerable research regarding the fatigue resistance of weathering steel has been conducted by Albrecht et al (1980). The work was primarily concerned with the effect of weathering on the fatigue life of ASTM 588 (weathering steel) with welded stiffeners and attachments. A 40 percent decrease in fatigue life due to weathering was reported for a transverse stiffener detail. The decrease in fatigue life was attributed to rust pitting. Friedland et al (1982) observed that two years of continuous weathering, prior to stress cycling, reduced the fatigue life of specimens with stiffeners by 19 percent, as compared to non-weathered control specimens.

In a subsequent investigation Albrecht (1983) combined the losses due to weathering with an estimate of the effect of corrosion fatigue on the crack propagation life, obtained by Barsom and Novak (1977). The result was an expression for the percentage loss in total fatigue life as a function of the fatigue notch factor, k_f, which is a particular value for each fatigue category. That expression was then used to obtain new proposed AASHTO allowable fatigue design stress ranges to account for the anticipated losses in fatigue life caused by weathering. Kitagawa et al (1983) presented a statistical characterisation of the corroded surface of unnotched corrosion fatigue samples. It was concluded that increases in the cyclic stress level or the number of load cycles caused the formation of corrosion pits on the surface.

The effect of corrosion on the fatigue capacity of steel bridge beams was considered by Albrecht et al (1990). Albrecht proposed that three factors influence the fatigue life of corroded beams: firstly, the reduction in section modulus, due to loss of thickness of flanges and webs, resulting in higher stress; secondly, the effect of stress concentration in the vicinity of corrosion pits; and thirdly, the increased crack growth rate in a corrosive environment. He carried out tests on a number of corroded beams and produced an empirical formula to take account of the effect of pitting. Kulicki et al (1990) suggested a method by which the remaining fatigue life of corroded structural members may be estimated on the basis of visual inspection.

The main objectives of this chapter are:

1. To review briefly the fatigue concepts and the relevant research carried out in the field of fatigue assessment of corroded steelwork structures.
2. To test in the laboratory the fatigue failure of corroded steel specimens obtained from a structure which had been in service for nearly 40 years.
3. To investigate the fatigue capacity of corroded steelwork compared with the normal fatigue life of various classes of structural detail as classified in BS 5400, the UK code for fatigue.
4. To consider the application of the results for existing corroded steel bridges.

5.2 Fatigue process

The fatigue process can be divided into three phases: (1) the crack initiation phase; (2) the sub-critical crack propagation phase; (3) the fracture phase. The sub-critical crack propagation phase is considered to be the most important period in the engineering fatigue-resistant design, since it takes about 95% of the total fatigue life in many cases, especially for bridge structures.

Usually in laboratory tests, the cyclic stresses are the results of axial forces, shear forces, bending moments, and torsion which are applied in the form of a sine wave. This simple form of cyclic stress used in testing is shown in Figure 5.1. It can be described by several

parameters such as: σ_m (Mean stress), σ_r (Stress range), σ_{max} (Maximum stress or Upper limit stress), σ_{min} (Minimum stress or Lower limit stress), and σ_a (Stress amplitude or Alternating stress).

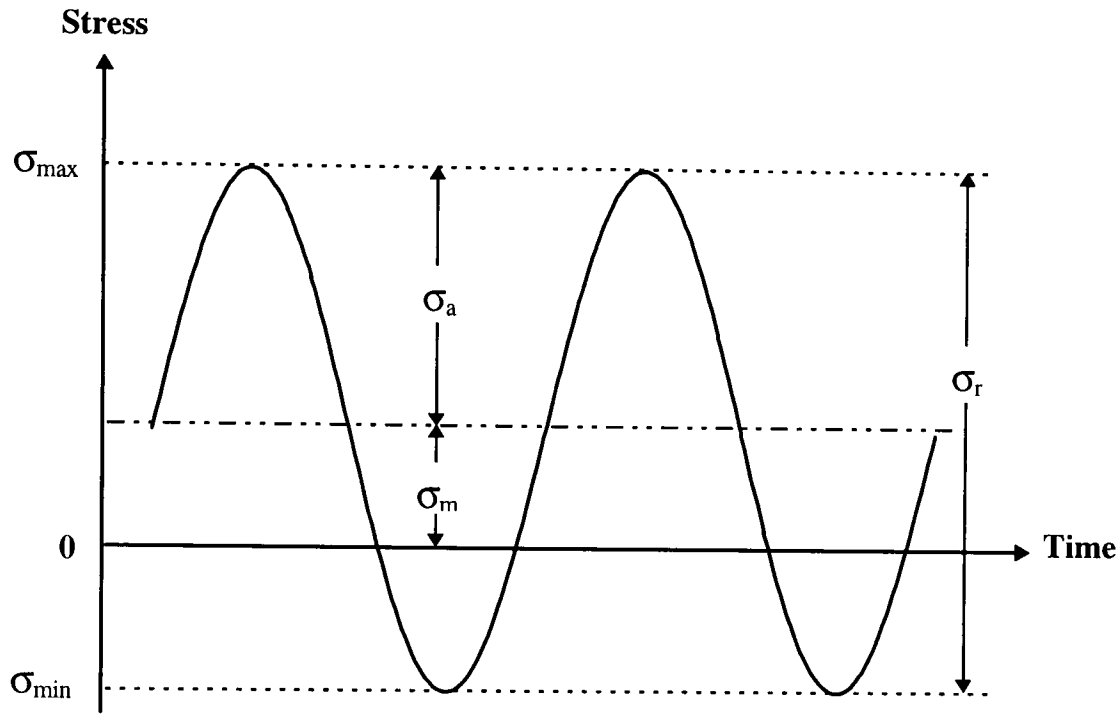

Figure 5.1 Terminology used to describe the stress parameters which affect fatigue life.

5.3 Assessment methods for fatigue life

There are two basic approaches for assessing the fatigue life of structural components of existing bridges (Simpson 1992). The first method is based on fracture mechanics which considers the growth rate of an existing defect at each stage in its propagation. This is based on the observed relationship between the stress intensity factor and the rate of growth of fatigue cracks. The second, which is currently in general use, relies on empirically derived relationships between applied stress ranges and fatigue life. This is called the *S-N* approach. Both methods are explained in this chapter.

5.3.1 Fatigue crack growth rate

Fatigue crack growth rate is the main factor which determines the fatigue life of a steel structure. Paris et al (1961) were the first to suggest that the increment of fatigue crack

advance per stress cycle, *da/dN*, could be related to the range of the stress intensity factor, ΔK, during constant amplitude cyclic loading. The rate of crack growth of a fatigue crack subjected to constant amplitude stress reversals is expressed in terms of crack length increment per cycle, *da/dN*. Values of *da/dN* for different loading conditions are determined from experimentally determined changes in crack length over a certain number of prior fatigue cycles. The crack growth rate, *da/dN* is related to the range of stress intensity factor, ΔK. The stress intensity factor is a measure of the stress distribution in the vicinity of a crack tip and it can be expressed as follows:

$$\Delta K = K_{max} - K_{min} \tag{5.1}$$

where K_{max} and K_{min} are the maximum and minimum values, receptively, of the stress intensity factor during a fatigue stress cycle. For an edge-cracked fatigue test specimen they can be evaluated in the following manner:

$$K_{max} = Y\sigma_{max}\sqrt{\pi a} \tag{5.2}$$

$$K_{min} = Y\sigma_{min}\sqrt{\pi a} \tag{5.3}$$

$$\Delta K = Y\Delta\sigma\sqrt{\pi a} \tag{5.4}$$

$$\Delta\sigma = \sigma_{max} - \sigma_{min} \tag{5.5}$$

where Y is a geometrical factor dependent upon the ratio of crack length, a, to the width of the specimen, w. The Paris equation, is derived based on linear elastic fracture mechanics and known as the simplest relation for fatigue evaluation process. He showed that the fatigue crack growth increment *da/dN* is related to the stress intensity factor range by the power law relationship

$$\frac{da}{dN} = C(\Delta K)^n \tag{5.6}$$

where a = crack length, N = number of cycles, ΔK = range of stress intensity factor, C and n are material constants or crack propagation constants which have to be determined for the relevant material. The exponent, n, is usually in the range 3 to 4. It is important

that ΔK should be known accurately if meaningful crack growth predictions are to be made.

5.3.1.1 Corrosion fatigue crack propagation

The concepts of fracture mechanics have been used extensively by different researchers to explore mechanical, microstructural and environmental relationship between the alternating stress intensity factor range, ΔK, and the crack growth rate, (da/dN). The results from such work serve two basic functions. In the first place, they increase understanding of the mechanics of fatigue. Second, they provide a rational basis for predicting fatigue lifetimes and failure.

Yazdani and Albrecht (1983) collected and analysed over 3500 data points for crack growth rate in mild steel, high strength low alloy steel, weathering steel, and quenched and tempered steel specimens tested in three different environments such as laboratory air, distilled water and a 3% saline solution. Most corrosion fatigue crack propagation data came from a National Cooperative Highway Research Program project (Barsom et al 1977) and a Federal Highway Administration project funded at Lehigh University (Robert et al 1986). The remainder of the data came from Klingerman et al (1973) and Mayfield et al (1982).

After an extensive statistical analysis of the effects of type of steel, loading, environment, and testing laboratory, Yazdani and Albrecht (1989), calculated the crack growth rates for mild and high strength low alloy steels, weathering steel, and quenched and tempered steels. The mean regression analysis for the region II data from the four studies mentioned above were used. It was found that the variable and constant amplitude loading data for all mild and high strength low alloy steels in air could be lumped together, because statistically the difference between data sets were insignificant. Therefore, the crack growth rate equations for mild and high strength low alloy (HSLA) steels in air is given by:

$$\left(\frac{da}{dN}\right)_{air} = 1.537\times10^{-12}(\Delta K_{eff})^{3.334} \tag{5.7}$$

Only Barsom et al (1977) measured crack growth rate for mild and high strength low alloy steels in aqueous environments. All aqueous data were combined into one set and the following formula resulted from the mean regression analysis:

$$\left(\frac{da}{dN}\right)_{aq} = 4.161\times10^{-12}(\Delta K_{eff})^{3.279} \tag{5.8}$$

where *da/dN* is crack growth rate in (m/cycle) and ΔK_{eff} is effective stress intensity factor range in (MPa$\sqrt{m}$).

The difference between the crack growth rates for mild steel and high strength low alloy steels in air and in aqueous environments was found to be significant. The cracks grew faster in aqueous environments than in air.

The following equations were given to calculate the crack growth rate for quenched and tempered steels in air and aqueous environments:

in air $$\left(\frac{da}{dN}\right)_{air} = 2.265\times10^{-11}(\Delta K_{eff})^{2.534} \tag{5.9}$$

in aqueous environment $$\left(\frac{da}{dN}\right)_{aq} = 6.002\times10^{-11}(\Delta K_{eff})^{2.420} \tag{5.10}$$

The fatigue life reduction due to the aqueous environment (K_e) is the ratio of the crack growth rates. The fatigue strength reduction factor is given by *n*-th root of the fatigue life reduction factor (Albrecht et al 1990).

$$K_e = \left(\frac{(da/dN)_{aq}}{(da/dN)_{air}}\right)^{1/n} \tag{5.11}$$

Where n = slope constant in plot of crack growth rate versus range of stress intensity factor and is the average exponent of both equations of mild steel and high strength low alloy steels in air and in aqueous environments ($n \approx 3.3$).

The equations developed for air and aqueous environments for each group of steels, plotted in Figure 5.2, are nearly parallel. At the lowest stress intensity factor range, ΔK = 14.8 MPa$\sqrt{m}$, at which corrosion fatigue crack propagation rates were measured by Albrecht et al (1990), it was found that cracks grew faster in aqueous environments than in air by a factor of 2.3 for mild and high strength low alloys steels, and by a factor of 1.9 for quenched and tempered steels. Both sets of equations indicate that structural details on bare weathering steel bridges have shorter crack propagation lives than those on painted steel bridges. In fact the air lines should be used for painted steel structures; the aqueous lines for bare steel structures such as those built from weathering steels. This conclusion applies to all types of details.

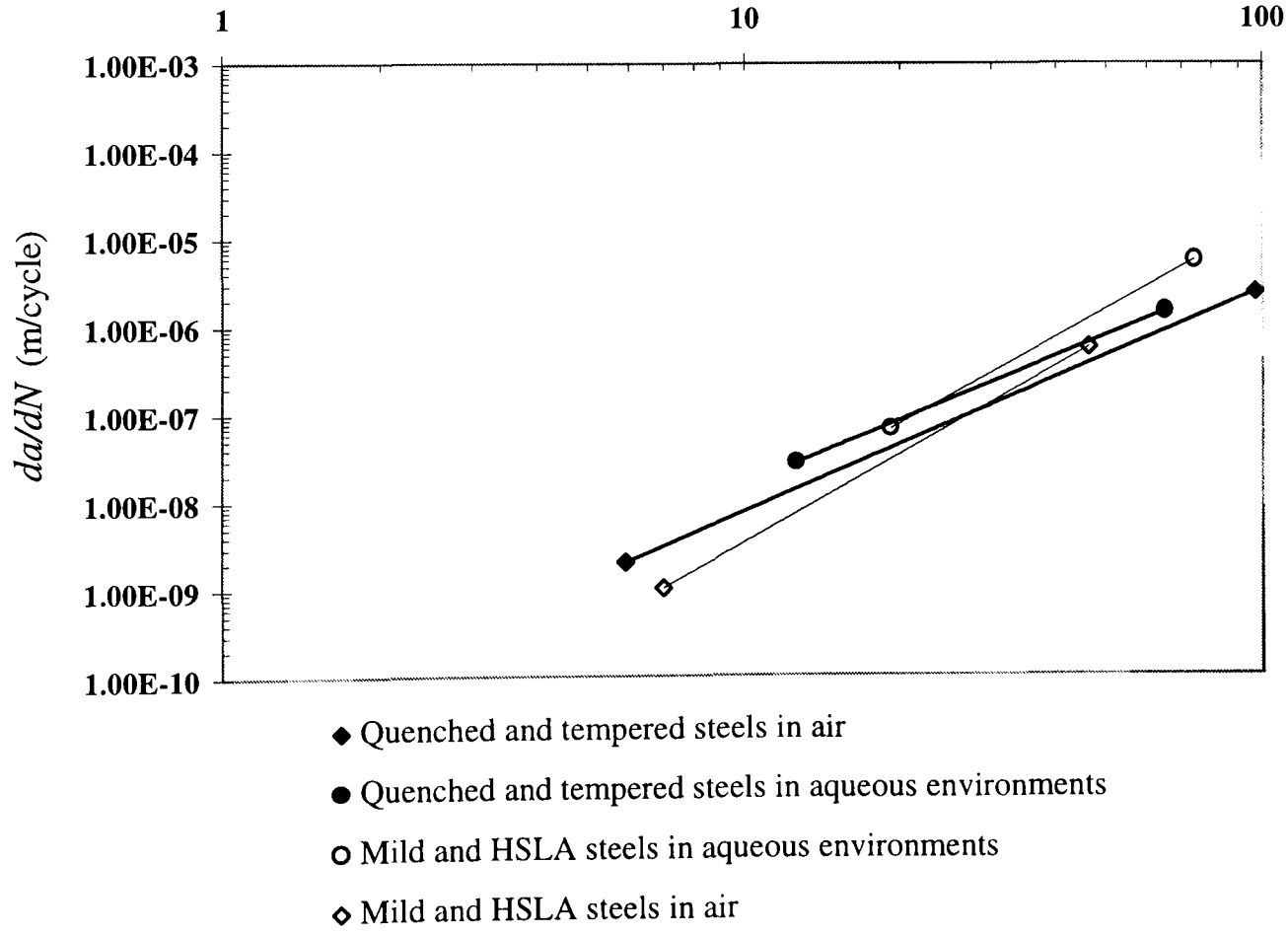

Figure 5.2 Mean regression lines for crack propagation rates of structural steels tested in air and aqueous environments.

5.3.2 *S-N* Curves

The most common form of presentation of fatigue data is the *S-N* curve, where the total cyclic stress range (σ_r) is plotted against the number of cycles to failure (*N*). Usually these curves are obtained experimentally (sufficient specimens are tested for statistical analysis to determine both mean fatigue strength and its standard deviation). Fatigue experiments show that the *S-N* curve line in log base consists of two straight lines: one is a slope, the other is a line parallel to the horizontal axis, as shown in Figure 5.3.

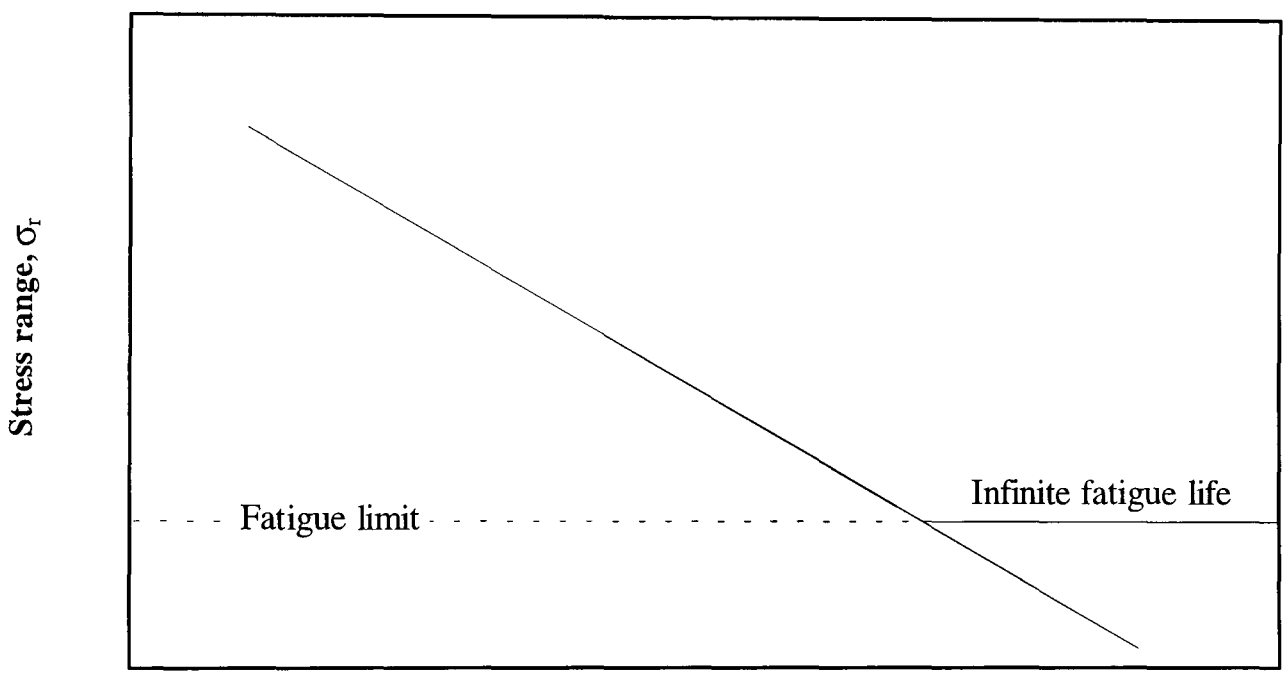

Figure 5.3 *S-N* curve (Hu Qiao et al 1995).

In the *S-N* curve shown in Figure 5.4, at first the stress which can be applied repeatedly decreases as the number of cycles increases, but the curve then flattens out and a comparatively small decrease in stress brings about a large increase in the number of cycles which can be withstood. For plain ferrous material (mild steel) it has been found that, after about 2-5 million cycles, the curve is almost parallel to the (*N*) axis, indicating that at a very slightly smaller stress the specimen would have an infinite life. This limiting stress is called the endurance limit or the fatigue limit of the material. It is assumed that the stresses below the fatigue limit do not produce fatigue damage.

However, research shows that stress below the fatigue limit does contribute to fatigue damage under complex loading (Schutz et al 1989). In order to take account of the effect of small stresses, Buxbaum (1983) extend the sloping line of the *S-N* curve to the fatigue limit at the same slope, as shown in Figure 5.3. For the other materials, and for specimens containing stress concentrations, the endurance limit is usually less well defined and corresponds to a life considerably in excess of 2-5 million cycles found for mild steel. Indeed, the *S-N* curve becomes progressively flatter as *N* increases (Gurney 1979).

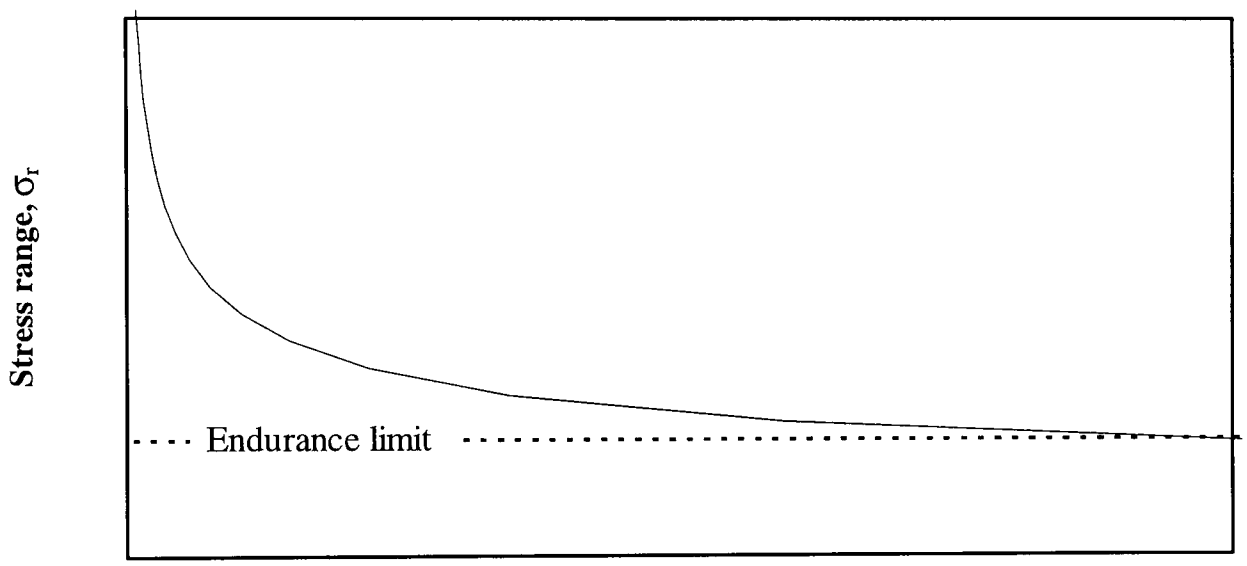

Figure 5.4 Typical *S-N* curve (Gurney 1979).

It has been found empirically that the results of fatigue tests follow a power-law relationship between stress and cycles. Therefore the curve in Figure 5.4 can be expressed as

$$N = K/(\sigma_r)^m \tag{5.12}$$

Logarithmic scales are conventionally used for both axes and the resulting curve is usually very nearly a straight line. In order to have the *S-N* curves in log-log plot, the following equation may obtained by taking the log of both sides of equation 5.12

$$\log N = \log K - m \log \sigma_r \tag{5.13}$$

where N = number of cycles to failure, σ_r = applied stress range, K = the constant term relating to the mean-line of the statistical analysis results, and m = inverse slope of the mean-line log σ_r - log N curve. The curves have been established empirically from a large number of small-scale laboratory tests.

The British Standards Institution prepared a detailed code of practice for fatigue assessment of welded steel bridges (BS 5400: Part 10, 1980). Fatigue assessment of welded steel structures depends on stress range and not on mean stress. In welded steel structures this is justified on account of the existence of tensile residual stress which ensure that the real stresses pulsate downwards from yield stress in tension (Gurney 1979).

For the purpose of fatigue design, constructional details are grouped in eight classes designated as B, C, D, E, F, F2, G, and W. Their mean values are listed in Table 5.1 and are plotted on log scales in Figure 5.5. Details of these classes are given in BS 5400: Part 10, (1980). The sketches in Table 5.1 give an approximate indication of where fatigue may be expected to occur.

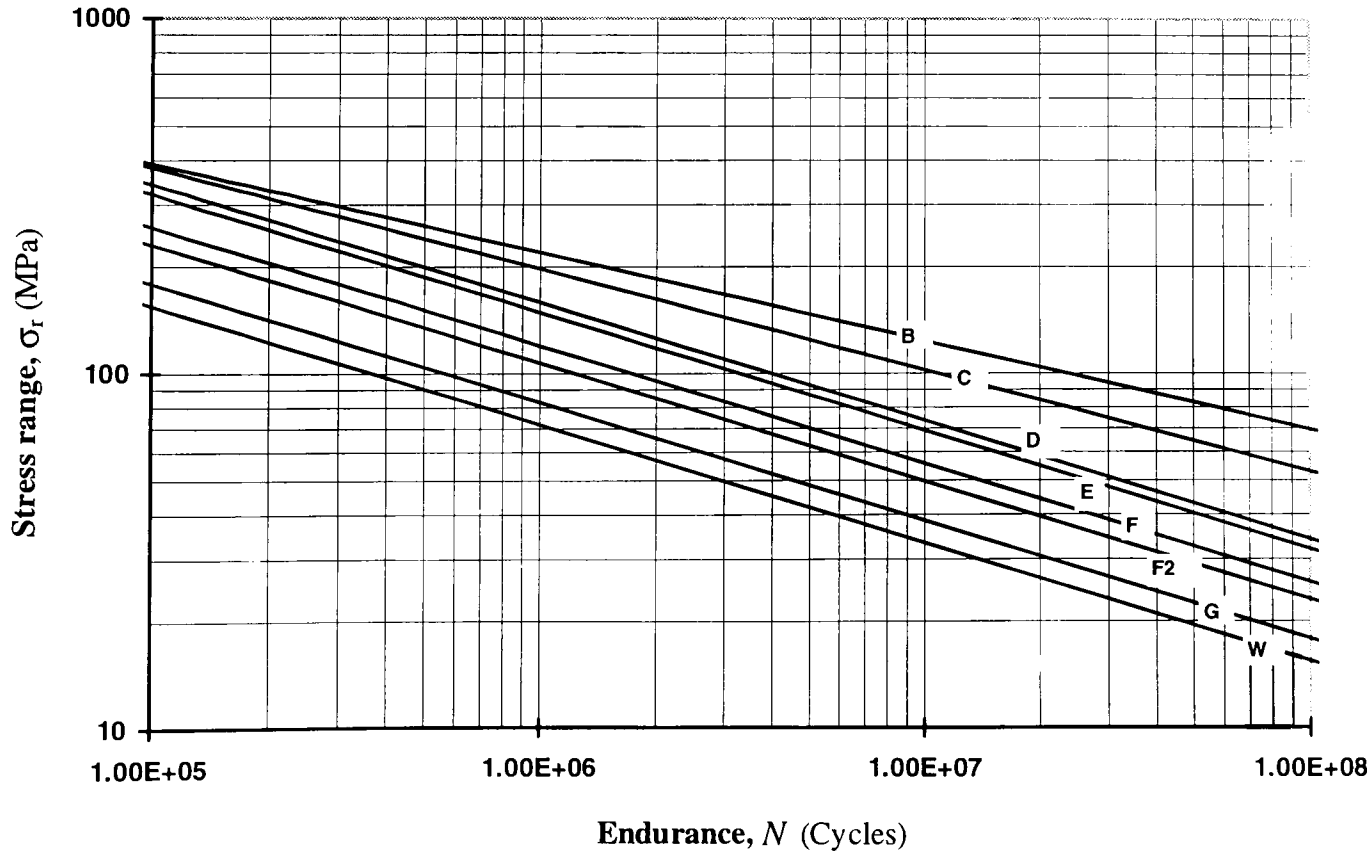

Figure 5.5 Mean S-N curves on a basis of log σ_r versus log N (BS 5400, 1980).

Table 5.1 Classification of welded structural detail based on mean-line σ_r-N relationship (BS 5400: Part 10, 1980).

Class	Detail Class	K	m	Typical crack location
B	Plain steel in as-rolled condition, or with cleaned surfaces and any flame-cut edges subsequently ground or machined	2.34×10^{15}	4.0	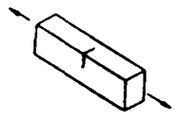
C	Butt or fillet welds, loaded parallel with their length and made by automatic process with no stop-start positions	1.08×10^{14}	3.5	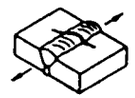
D	Butt welds loaded perpendicular to their length and made in the shop in the shop in the flat position	3.99×10^{12}	3.0	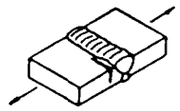
E	Parent metal at the end of a weld connecting a stiffener diaphragm or other attachment to a girder web in a region of combined bending and shear	3.29×10^{12}	3.0	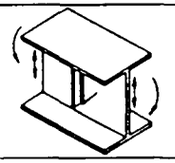
F	Fillet weld or T-butt weld with full penetration and any undercutting at the corners of the member dressed out by local grinding	1.73×10^{12}	3.0	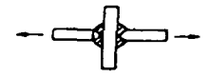
F2	Joint made with partial penetration welds with any undercutting dressed out by local grinding as above	1.23×10^{12}	3.0	
G	Parent metal at the toes or ends of butt or fillet welded attachments on corners of a stressed member	0.57×10^{12}	3.0	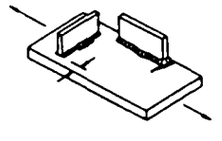
W	Weld metal in load-carrying joints made with fillet or partial penetration welds, with the welds either transverse or parallel to the direction of applied stress (based on nominal shear stress on the minimum weld throat area	0.37×10^{12}	3.0	

5.4 Damage accumulation

The flaws and discontinuities which are introduced by welding or corrosion serve as "damage sites" in structural components (Zuraski 1986). For many years, the vast majority of fatigue tests were carried out under constant amplitude loading, and designers were faced with the problem of how to use the resulting data to predict fatigue life under the wide range of variable amplitude load histories encountered in service. Evidently some method of assessing the effect of variable amplitude loading is required. Therefore the investigation of fatigue under varying stress amplitude came to be known as the study of cumulative damage because of early interest in how fatigue damage accumulated at various stress levels.

It has been pointed out by Yamada et al (1989) that the basic parameters affecting fatigue damage are the type of structural details, the stress ranges and the number of cycles. Since bridge structures are subjected to loads at variable times and with different characteristics and magnitude, variable amplitude type of loading results. The effects of variable stresses are normally accounted for by applying a cumulative damage rule. Although many rules have been proposed, the most widely used is the Miner (1945) linear cumulative damage rule. This states that the fatigue damage from any particular stress range is directly proportional to the number of cycles applied at that stress. For a particular stress range, $(\sigma_r)_1$, the constant amplitude endurance, N_1, is a measure of the available damage that is required to cause failure and therefore the fatigue damage as a result of $(\sigma_r)_1$, applied for n_1 cycles, is a fraction (n_1/N_1) of that needed to cause failure. Failure occurs under a sequence of different stresses when the sum of all the ratios (n/N) equals unity. This may be expressed as

$$\frac{n_1}{N_1}+\frac{n_2}{N_2}+\frac{n_3}{N_3}+\cdots\cdots\cdots=\sum\frac{n_i}{N_i}\leq 1 \qquad (5.14)$$

where values of N_i are taken from the appropriate design S-N curve for each value of $(\sigma_r)_i$ as shown in Figure 5.6.

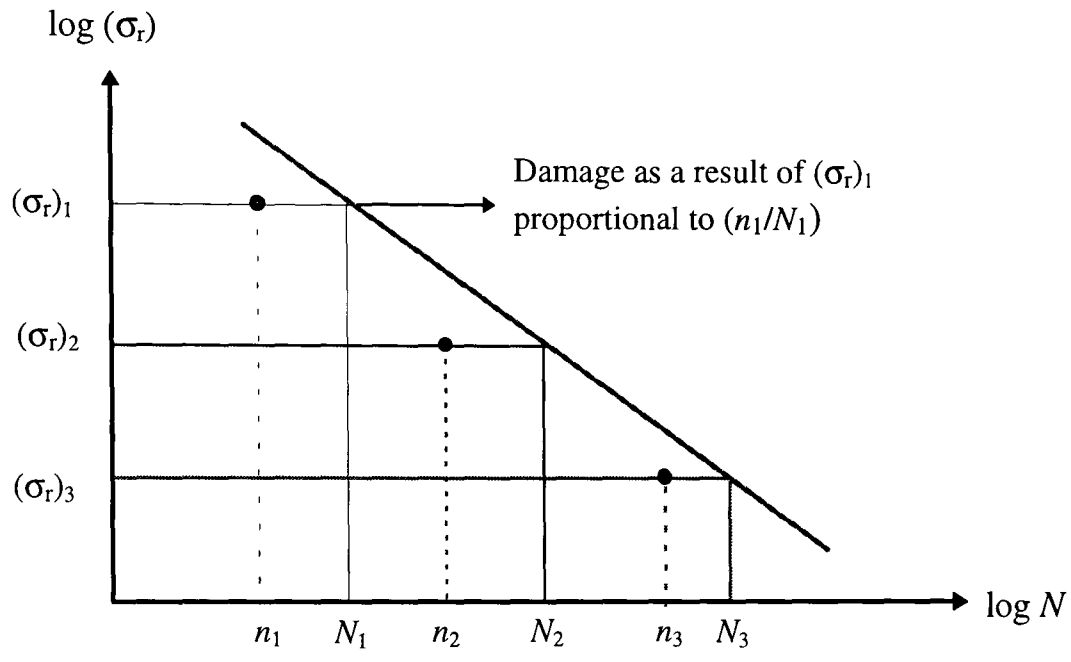

Figure 5.6 Application of Miner's rule.

It may be noted that N_i can be expressed in terms of $(\sigma_r)_i$ and the constants m and K given in Table 5.1.

$$N_i = K/(\sigma_r)_i^m \tag{5.15}$$

so that Miner's rule could be stated as

$$\sum(\sigma_r)_i^m n_i = K \quad \text{at failure} \tag{5.16}$$

or

$$\sum(\sigma_r)_i^m n_i \le K \quad \text{for survival} \tag{5.17}$$

The fatigue damage due to a block of n_i cycles at $(\sigma_r)_i$ is proportional to $(\sigma_r)_i^m n_i$. It was generally though that Miner's rule more accurately describes fatigue damage of structural components whose life consists mainly of crack initiation, but it also describes with success fatigue damage of structural components whose life is dominated by crack propagation.

One of the main difficulties in assessing fatigue life under variable amplitude or random loading is to determine the number of cycles occurring within each stress range. Various methods of calculating equivalent cyclic spectra have been devised (Gurney 1979), such as 'rainflow' counting, 'reservoir' counting, range pair, level crossing and peak counting methods. However, the most widely adopted in practice are the 'rainflow' method and the 'reservoir' method.

5.5 Experimental work

As mentioned in Chapter 3, test specimens were cut from the flanges, the webs and the stiffeners of four corroded mild steel beams. Forty one corroded specimens were selected at random from different locations of the beams and prepared for tests. Four of the specimens were machined smooth and were used for static tests and the remaining thirty seven for cyclic tests.

5.5.1 Static tests

One standard smooth surfaced specimen as shown in Figure 3.13 was chosen from each beam for a static test to obtain tensile strength, and hence to set the load range for the cyclic tests. The specimens were held in shackles with pins at the end in order to ensure axial loading. The results of all of the tests are summarised in Table 5.2. It can be seen that the strength of the steel from beams 2 and 3 were found to be identical. The table records the following:

σ_y = yield stress

σ_u = ultimate stress at maximum load achieved.

Table 5.2 Summary of tensile test results.

Beam number	σ_y (MPa)	σ_u (MPa)
1	310	430
2	330	540
3	330	540
4	310	541

5.5.2 Cyclic tests

Thirty seven specimens were subjected to dynamic axial loading in a servo-hydraulic fatigue machine as shown in Figure 5.7. Fully reversed sinusoidal loading with zero mean stress was applied in dry laboratory air. Seventeen were tested at constant stress range of 350 MPa at a frequency of 10 Hz. The stress range of 350 MPa was well below the yield strength and related to the first specimen which was loaded with ± 15 kN. Three of these were machined smooth before testing. The load for subsequent specimens was determined so that the stress range at the deepest point of penetration was 250 MPa for eighteen of them and 200 MPa for the remaining two. It was observed during the cyclic test that two of the specimens tested at stress range of 200 MPa did not fail up to $n_1 = 3183700$ cycles. Then it was decided to double the loading. Finally, the specimen failed at the deepest point of penetration at $n_2 = 446100$ cycles. This procedure was repeated with the second specimen which failed at $n_2 = 633900$ cycles. Miner's rule and fatigue power law were applied respectively to determine an equivalent value for N.

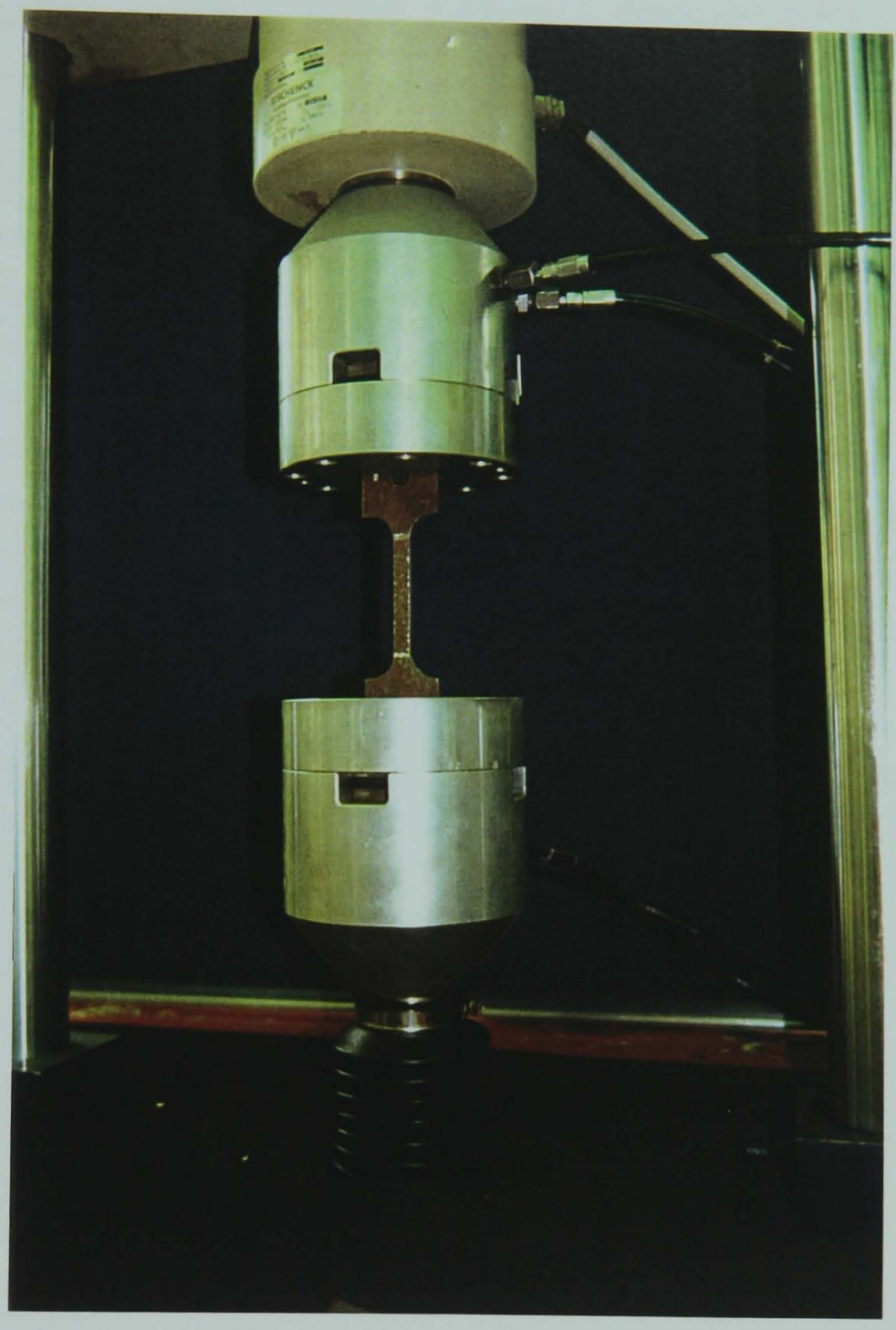

Figure 5.7 Specimen loaded by a servo-hydraulic fatigue machine.

5.5.2.1 Results of fatigue tests

The results of the fatigue tests for all specimens are recorded in Table 5.3.

Table 5.3 Results of fatigue tests and the location of rupture of specimens.

Specimen number	R_{max} (mm)	σ_r (MPa)	N (Cycles)	$log\ N$ (Cycles)	Location of rupture from the deepest point of penetration
1	0.34	200	36,900,000	7.56	at the deepest point
2	1.20	200	23,525,000	7.37	2 mm from the deepest point
3	0.94	250	506,200	5.70	at the deepest point
4	1.53	250	990,900	6.00	at the deepest point
5	0.73	250	1,843,500	6.27	1 mm from the deepest point
6	0.47	250	795,200	5.90	at the deepest point
7	1.75	350	40,960	4.61	3 mm from the deepest point
8	2.79	350	990	3.00	at the deepest point
9	2.62	350	15,590	4.19	at the deepest point
10	0.39	350	244,690	5.39	1 mm from the deepest point
11	1.01	350	298,170	5.47	7 mm from the deepest point
12	1.15	350	161,660	5.21	6 mm from the deepest point
13	1.68	350	24,790	4.39	at the deepest point
14	1.78	350	25,420	4.41	at the deepest point
15	1.36	350	15,570	4.19	2 mm from the deepest point
16	3.37	350	3,360	3.53	4 mm from the deepest point
17	2.70	350	38,640	4.59	at the deepest point
18	0.60	350	94,180	4.97	1 mm from the deepest point
19	1.58	350	218,940	5.34	at the deepest point
20	0.56	350	241,750	5.38	at the deepest point
21	2.01	250	512,090	5.71	at the deepest point
22	0.82	250	1,479,890	6.17	1 mm from the deepest point
23	0.98	250	969,380	5.99	at the deepest point
24	0.93	250	1,116,900	6.05	1 mm from the deepest point
25	1.23	250	770,800	5.89	1 mm from the deepest point
26	1.21	250	870,960	5.96	9 mm from the deepest point
27	1.15	250	560,300	5.75	8 mm from the deepest point
28	2.29	250	389,010	5.59	2 mm from the deepest point
29	1.80	250	594,100	5.77	at the deepest point
30	2.06	250	463,070	5.66	3 mm from the deepest point
31	1.67	250	634,200	5.80	at the deepest point
32	1.26	250	676,080	5.83	at the deepest point
33	1.28	250	741,300	5.87	at the deepest point
34	2.59	250	268,000	5.43	1 mm from the deepest point
35*	0.00	350	8,255,880	6.92	smooth specimen
36*	0.00	350	1,318,970	6.12	smooth specimen
37*	0.00	350	525,930	5.72	smooth specimen

5.5.2.2 Crack initiation and propagation

Cracks initiated and propagated in a direction perpendicular to the loading direction. The cracks of the corroded specimens initiated from single pits, the transition between crack initiation and rupture being very quick. It was observed that often multiple cracks propagated independently of each other and then joined to cause the final fracture. The rupture of corroded specimens under test occurred at or within 9 mm of the deepest point of penetration (see Table 5.3). In general the location of the deepest point of penetration seemed to give a good approximation to where the rupture occurred.

5.6 Fatigue assessment of corroded steelwork specimens

As yet there is no simple relationship between the magnitude of structural defects due to corrosion pitting and the corresponding reduction in fatigue life. There is an urgent need for a method to estimate the remaining fatigue life of members weakened by pitting corrosion. Therefore, one of the particular points of interest in this chapter is to see how depth of corrosion pitting might affect and reduce the fatigue life of steel structures. In order to demonstrate this the fatigue endurance and the fatigue performance of corroded specimens has been compared with fatigue capacity of various classes of structural detail in their new condition.

5.6.1 Classification of corroded steelwork specimens using *S-N* curves

In this section an attempt is made to classify corroded specimens in a way corresponding to the detailed classes in BS 5400: Part 10 (1980), the UK code for fatigue design. The result of fatigue tests for stress range of 350 MPa are plotted against the maximum roughness, R_{max}, as shown in Figure 5.8. Superimposed on this graph are the corresponding mean fatigue lives at 350 MPa for different classes of structural detail as classified in BS 5400: Part 10. It should be noted that five corroded specimens performed better than class B. This was repeated for specimens tested at 250 and 200 MPa and are shown in Figures 5.9 and 5.10.

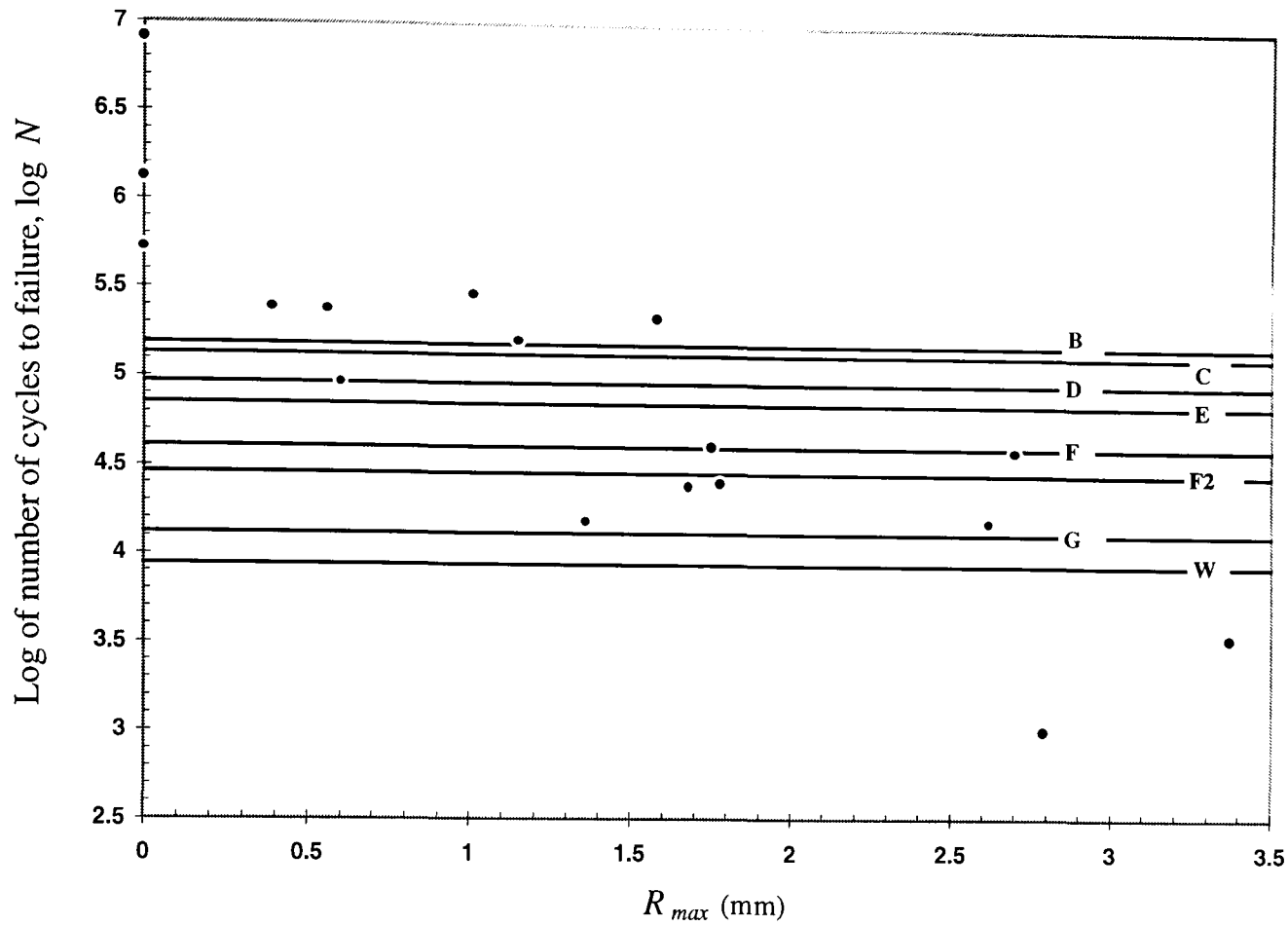

Figure 5.8 Maximum roughness, R_{max} versus log of number of cycles to failure, log N at stress range of 350 MPa.

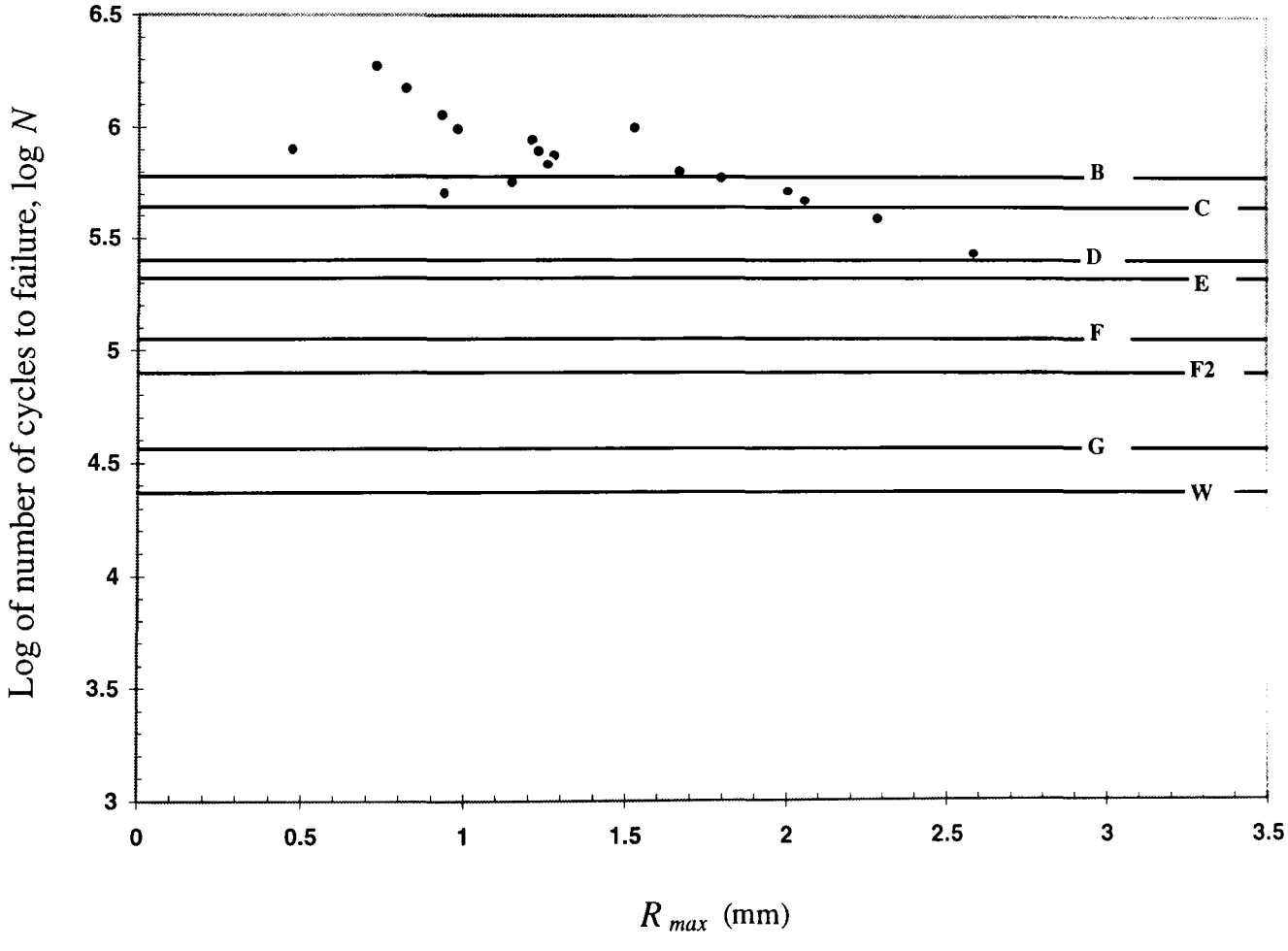

Figure 5.9 Maximum roughness, R_{max} versus log of number of cycles to failure, log N at stress range of 250 MPa.

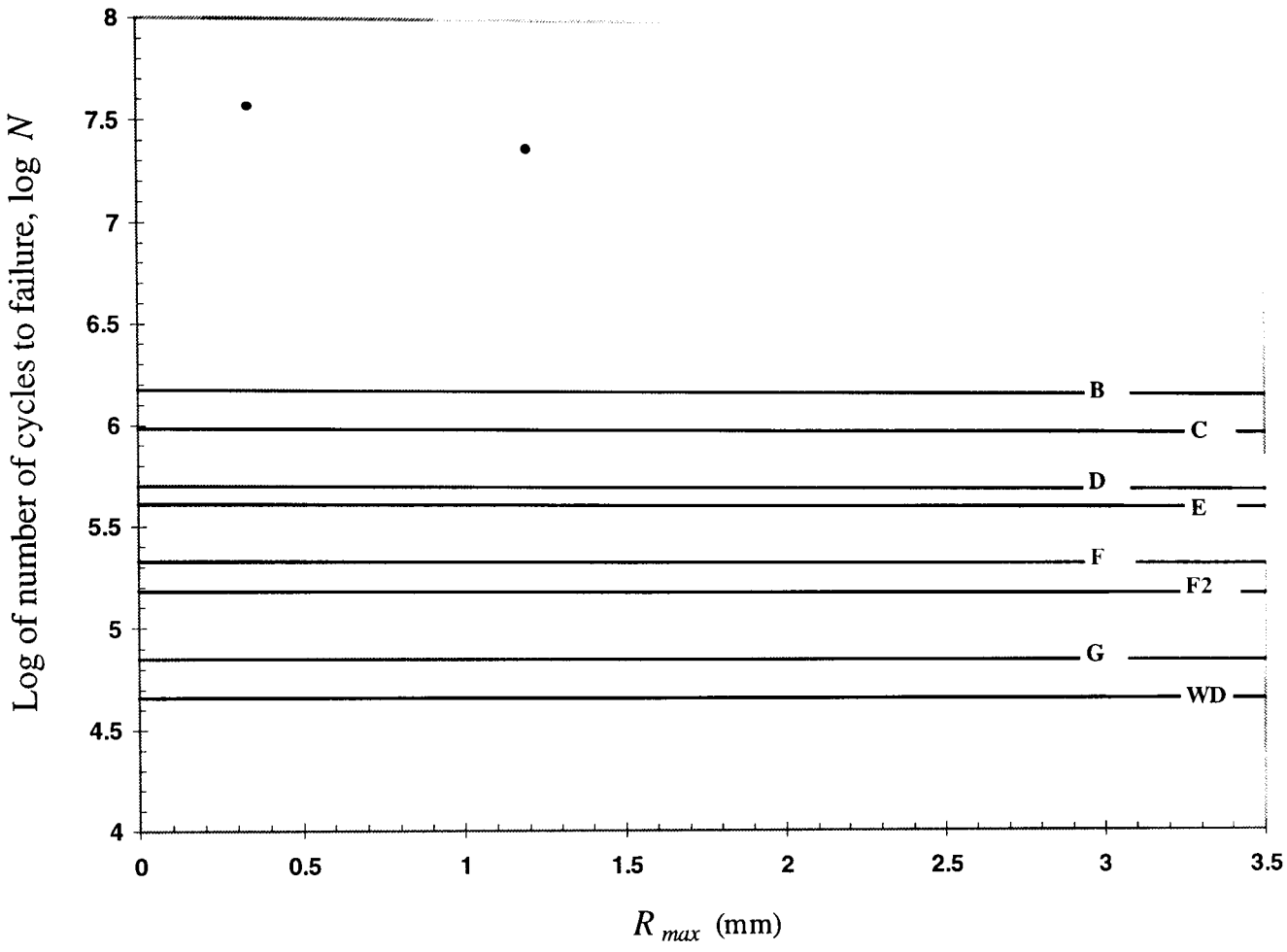

Figure 5.10 Maximum roughness, R_{max} versus log of number of cycles to failure, log N at stress range of 200 MPa.

The fatigue performance of corroded steel specimens may be compared with different classes of structural detail by considering the fatigue power law. Equation 5.12 may be used to calculate the constant K for all the fatigue specimens based on their number of cycles to failure and stress ranges listed in Table 5.3. The value of m in the fatigue power law relationship was taken to be 4.0 for class B or better, 3.5 for class C, and 3.0 for class D and below. The calculated values are listed in Table 5.4.

Table 5.4 Classification and the fatigue performance of corroded steel specimens.

Specimen number	R_{max} (mm)	S_d (mm)	σ_r (MPa)	N (Cycles)	Detail class	m	log K
1	0.34	0.067	200	36,900,000	better than B	4.00	16.77
2	1.20	0.226	200	23,525,000	better than B	4.00	16.57
3	0.94	0.112	250	506,200	C	3.50	14.10
4	1.53	0.357	250	990,900	better than B	4.00	15.59
5	0.73	0.110	250	1,843,500	better than B	4.00	15.86
6	0.47	0.090	250	795,200	better than B	4.00	15.49
7	1.75	0.324	350	40,960	F	3.00	12.24
8	2.79	0.630	350	990	W	3.00	10.63
9	2.62	0.465	350	15,590	G	3.00	11.83
10	0.39	0.064	350	244,690	better than B	4.00	15.57
11	1.01	0.170	350	298,170	better than B	4.00	15.65
12	1.15	0.271	350	161,660	B	4.00	15.38
13	1.68	0.317	350	24,790	G	3.00	12.03
14	1.78	0.349	350	25,420	G	3.00	12.04
15	1.36	0.232	350	15,570	G	3.00	11.82
16	3.37	0.775	350	3,360	W	3.00	11.16
17	2.70	0.483	350	38,640	F	3.00	12.22
18	0.60	0.101	350	94,180	D	3.00	12.61
19	1.58	0.105	350	218,940	better than B	4.00	15.52
20	0.56	0.098	350	241,750	better than B	4.00	15.56
21	2.01	0.515	250	512,090	C	3.50	14.10
22	0.82	0.159	250	1,479,890	better than B	4.00	15.76
23	0.98	0.210	250	969,380	better than B	4.00	15.58
24	0.93	0.202	250	1,116,900	better than B	4.00	15.64
25	1.23	0.215	250	770,800	better than B	4.00	15.48
26	1.21	0.227	250	870,960	better than B	4.00	15.53
27	1.15	0.261	250	560,300	C	3.50	14.14
28	2.29	0.469	250	389,010	D	3.00	12.78
29	1.80	0.304	250	594,100	C	3.50	14.16
30	2.06	0.522	250	463,070	C	3.50	14.06
31	1.67	0.366	250	634,200	B	4.00	15.39
32	1.26	0.217	250	676,080	better than B	4.00	15.42
33	1.28	0.254	250	741,300	better than B	4.00	15.46
34	2.59	0.717	250	268,000	D	3.00	12.62
35*	0.00	0.00	350	8,255,880	Smooth spec.	4.00	17.09
36*	0.00	0.00	350	1,318,970	Smooth spec.	4.00	16.29
37*	0.00	0.00	350	525,930	Smooth spec.	4.00	15.90

5.6.2 Comparison of fatigue performance of corroded steel specimens with different classes of structural detail

The fatigue performance of all the specimens was plotted in terms of log K against maximum roughness, R_{max}, as shown in Figure 5.11. The mean line of these results was then used to obtain the value of R_{max} which corresponded to each of the structural detail classes. For example, the fatigue curve intersects class C at a value of R_{max} = 1.60 mm. This is shown in Figure 5.11. This procedure was repeated for all fatigue classes and the results are given in Table 5.5. Furthermore, this procedure was repeated using the standard deviation, S_d, as the measure of roughness (see Figure 5.12) and is also included in Table 5.5.

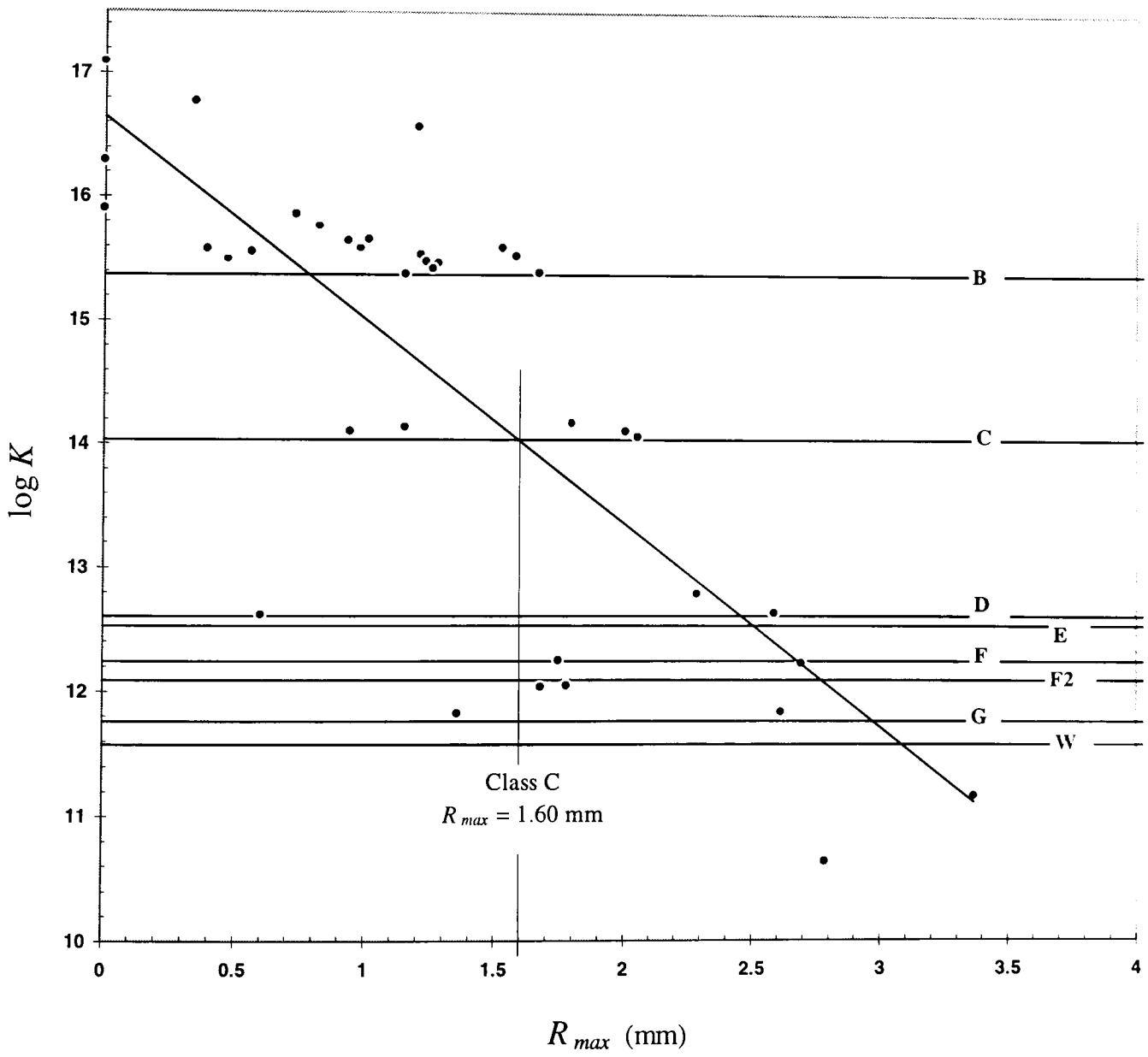

Figure 5.11 Comparison of fatigue life of corroded specimens with the BS 5400 classes.

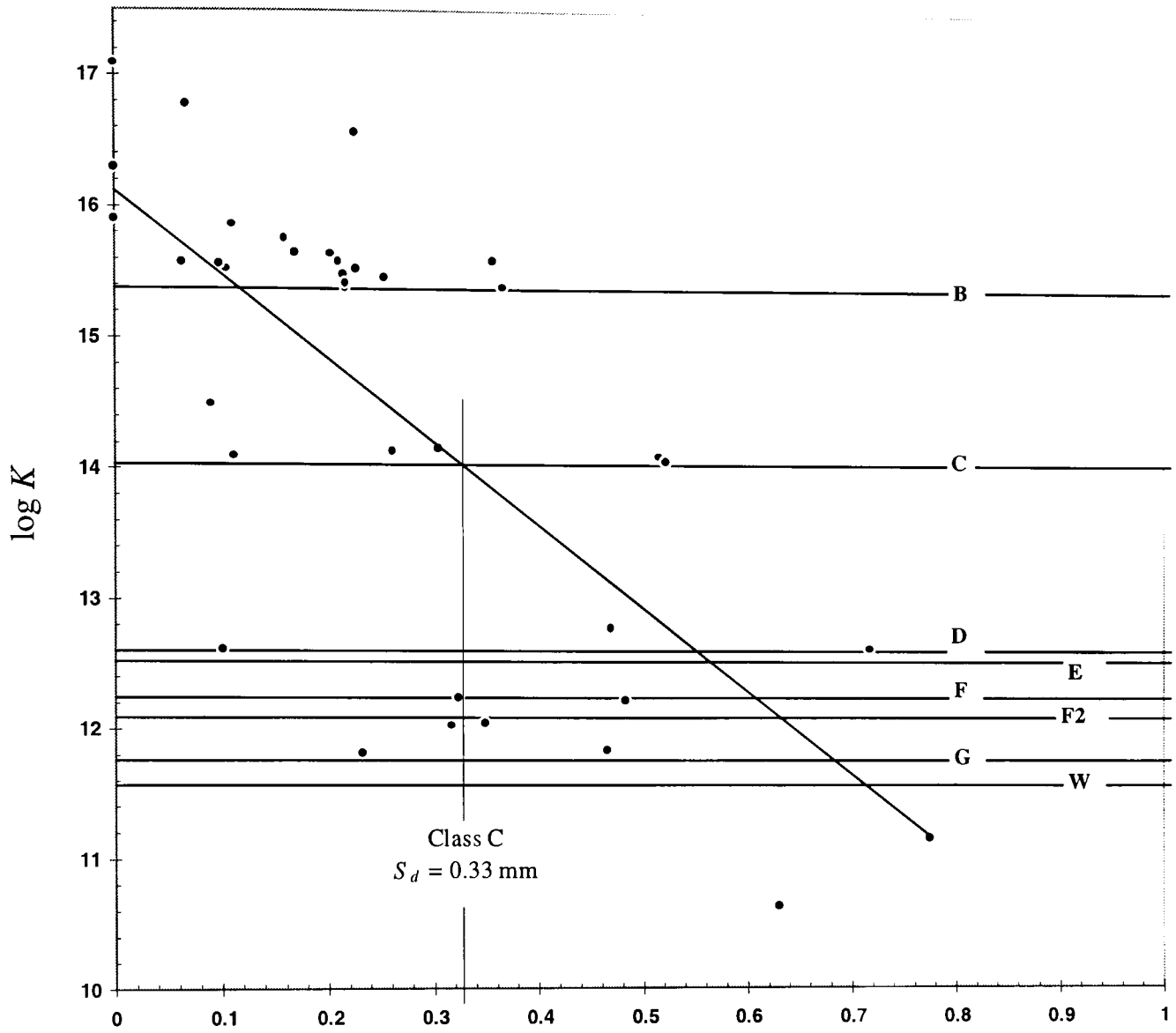

Figure 5.12 Comparison of fatigue life of corroded specimens with the BS 5400 classes.

Table 5.5 Fatigue life of new steelwork detail classes compared with corroded steelwork of equivalent roughness.

Detail class	log K	m	Equivalent R_{max} (mm)	Equivalent S_d (mm)
B	15.37	4.0	0.75	0.12
C	14.03	3.5	1.60	0.33
D	12.60	3.0	2.45	0.55
E	12.52	3.0	2.55	0.57
F	12.24	3.0	2.70	0.61
F2	12.09	3.0	2.78	0.63
G	11.76	3.0	2.95	0.68
W	11.57	3.0	3.10	0.71

5.6.3 Correlation between fatigue endurance and roughness measurement

In order to investigate the correlation between fatigue endurance and the roughness measurement, the results of the fatigue tests for different stress ranges are plotted against the maximum roughness, R_{max}, as shown in Figures 5.8, 5.9 and 5.10. The results of the fatigue tests showed that there was a significant reduction of fatigue life with corrosion roughness, using maximum roughness as the most appropriate measure. It was clear that this was caused by the "notch factor" due to corrosion pitting. It was found possible to relate the effect on fatigue life of pit depth, or maximum roughness, to classes of structural detail as used in fatigue codes. It can be observed from Figure 5.11 that most of the samples were worse than class B and if the maximum pit depth was greater than 1.60 mm they were worse than class C.

5.7 Application of this study for existing corroded steel bridges

It has been observed in Chapter 3, that the linear relation between maximum roughness and overall corrosion depth provides a convenient tool for the assessment of corrosion damaged bridges. When the corrosion penetration of a corroded steel member has been established, this provides a good approximation to maximum pit depth using Figure 3.18(a) from which the equivalent detail class may be obtained from Table 5.5. The equivalent corrosion detail class may then be compared with the detail classes at the location of maximum stress in the structure. Figure 5.13 shows the steps necessary to predict the remaining fatigue life of corrosion damaged steel structures.

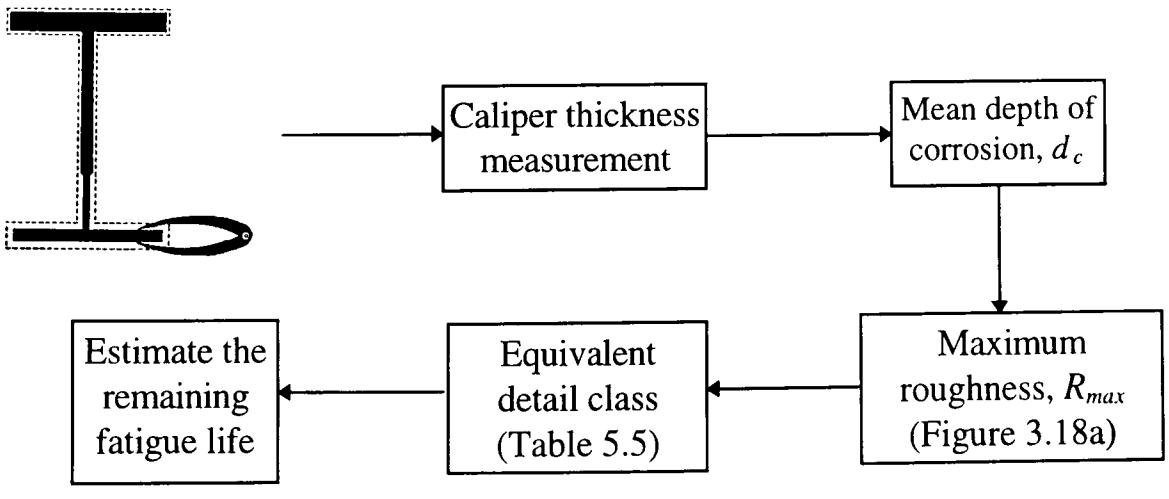

Figure 5.13 Procedures for predicting the remaining fatigue life.

5.8 Summary and conclusions

The concepts of fatigue which are relevant to the fatigue assessment of corroded steel structures have been discussed in this chapter. The brief literature review has shown the importance of corrosion in assessing fatigue life. The effects of pitting corrosion are investigated with how this form of corrosion affects the fatigue life of steel bridges.

The analysis of data provided by roughness measurement in Chapter 3 and fatigue test of corroded steel specimens in this chapter have helped us to identify the relationships between the fatigue endurance and pitting corrosion. It has been observed from the results of fatigue tests that the fatigue life depends largely on the applied stress range. Also it has been found that there is reduction in fatigue life of corroded steel specimens with depth of corrosion pitting which is due to the "notch factor" effect. Fatigue cracks in corroded specimens initiated from the deepest pits and rupture occurred at or within 9 mm of the deepest point of penetration.

A further indication of how corrosion pitting might affect the fatigue life of steel structures has been carried out by comparing the fatigue performance of corroded steel specimens against the maximum roughness. The mean regression line through the data points shows a considerable reduction in fatigue performance as pit depth increased. The mean line through the data points was used to determine the power law coefficient, K, in terms of maximum roughness, R_{max}. It can be used to estimate the remaining fatigue life of corroded structural members and components due to pitting corrosion. However, reduced fatigue life due to corrosion pitting may be related to classes of structural detail as used in design codes for fatigue.

The linear relation between the overall depth of corrosion and maximum roughness provides the simplest method for the assessment of corrosion damaged steel bridges. This method can indirectly give the quantitative relationship between the pitting corrosion and the corresponding remaining fatigue life of corrosion damaged steel structures by measuring loss of thickness.

CHAPTER VI

DEVELOPMENT OF FATIGUE NOTCH FACTOR DUE TO CORROSION

6.1 Introduction

Fatigue failure often starts at geometrical discontinuities such as holes or notches (Ahmad et al 1994). Fountain et al (1968) emphasized that all beams and structural members fall into the notch category even if they are composed solely of rolled material with no attachments. It has been reported by Fisher et al (1974) that cracks generally initiate from discontinuities in the flange surface that are apparently introduced by the normal rolling operation or by locally adhered scale. In practice, many steel structures exhibit these problems which may be a feature of construction or created by corrosion. It is, therefore, not surprising that much effort has been devoted to study of the fatigue behaviour of many forms and sizes of notch in a wide range of engineering materials. However, the particular point of interest in this chapter is to consider the effect of corrosion.

The fatigue strength of corroded steel removed from the tension flange of 77 years old truss stringers was examined by Zuraski et al (1984). A strength of 30 ksi for zero to maximum fatigue loading was observed at a life of one million cycles. In addition, it was shown that the fatigue strength reduction factor may be used to obtain a quantitative assessment of the effects of corrosion induced defects on fatigue strength.

Out et al (1984) investigated the extreme life fatigue behaviour of four weathered and deteriorated steel railroad bridge stringers. The sections, with riveted built-up cross sections, had been in service for 80 years. The fatigue resistance of a corroded region of a tension flange was observed to depend on the severity of the corrosion and the loss of

cross-sectional area. The author noted, however, that the degree of severity could not be accounted for by considering loss of area alone. Surface roughness and the associated stress concentration is a major factor in creating a fatigue detail that is more severe than might otherwise be anticipated.

In Chapter 4, it was mentioned that steel bridges are susceptible to pitting corrosion when subjected to severe environments. The pits which result from pitting corrosion can be dangerous because they extend into the metal, showing little external evidence of their existence, and are usually confined to a point or small area. The presence of pits increases stress in members and components from which cracks often develop. In practice, any fatigue life assessment must include an understanding of the effects of notch geometry and the associated stress field on both the crack formation and subsequent propagation phase of life.

It was noted by Yao et al (1995) that notches are one of the main factors that control the fatigue strength of structures. He pointed out that the problem of finding a brief and economical derivation for fatigue notch factor or fatigue strength reduction factor, k_f, had not been solved, because it is rather like a black box, with many factors that are difficult to determine. The most commonly accepted definition of fatigue notch factor is the ratio of the fatigue strength of a smooth specimen to that of a notched specimen under the same experimental conditions and the same number of cycles (Kuhn et al 1991).

The amount of published work on fatigue notch factor due to corrosion is limited. Albrecht et al (1990) identified three significant factors which contribute to the total reduction in fatigue strength of a corroded member. The first is the stress concentration effect of the rust pits which act as stress raisers that may lead to rapid crack initiation, k_p; the second is to the loss in cross-sectional area due to corrosion of the member in the plane of the crack which will increase the nominal stress range, k_c; and the third is the environmental effect, k_e. Accordingly, the fatigue notch factor or fatigue strength reduction factor is equal to the product of all factors. However, for simplicity Albrecht combined these factors as a single factor, known as the fatigue strength reduction factor.

This factor is an appropriate parameter for quantifying the effect of corrosion deterioration on fatigue strength which can be calculated for each specimen on the basis of applied stress range and the number of cycles to failure. In this study the results obtained for roughness measurements of corroded steelwork in Chapter 3 and cyclic tests in Chapter 5 may be used to develop the required relationships for fatigue notch factor.

The main goals in this chapter are:

1. To review the main aspects that are associated with stress concentration created by corrosion.
2. Development of a function which could represent fatigue notch factor in terms of average corrosion penetration by using different detailed thickness measurements such as the maximum roughness and the standard deviation of roughness.
3. Development of a relation for fatigue notch factor in terms of exposure time.
4. To investigate the fatigue notch factor of corroded steelwork compared with the fatigue notch factor of various classes of structural detail as classified in BS 5400, the UK code for fatigue.

6.2 Stress concentrations

Stress concentrators are almost inevitable in practical engineering structures and components (Burdekin 1985). Since the very beginning of fatigue testing, the known effects of stress concentrations on fatigue strength have been well documented. Stress concentration is the localisation of high stresses in the vicinity of a hole, notch, pit, groove or other discontinuity and measured by stress concentration factors. Some of the conditions created by corrosion can result in stress concentration and may control the fatigue life of structures. Stress concentration factors are obtained mathematically or experimentally by such means as photoelasticity or precision strain gauges (Hetenyi 1950). A comprehensive review on the subject of stress concentrations can be found in Smith (1988). Three types of stress concentration factors have been identified by Kulicki

et al (1990): elastic stress concentration factors, effective stress concentration factors and fatigue stress concentration factors.

6.2.1 Elastic stress concentration factors

The elastic or theoretical stress concentration factor, k_t, is defined as the ratio of the maximum local stress to the average stress, calculated based on net section. It assumes linear elastic behaviour of the material. In the last two to three decades a large amount of material on stress concentration has become available by Peterson (1974), Roark (1965), and Roark et al (1989). In order to illustrate the effect of geometry on the theoretical stress concentration factor, k_t, consider an elliptical hole with its major axis perpendicular to the load. The stress concentration factor at its edge is

$$k_t = 1 + \frac{2R_L}{R_S} \tag{6.1}$$

where R_L is the large radius and R_S is the smaller radius of the ellipse. For large values of R_L/R_S, k_t can be approximated by

$$k_t \cong 2\left(\frac{R_L}{R_o}\right)^{1/2} \tag{6.2}$$

where R_o is the radius at the end of major axis. This expression shows that k_t will increase with the length of the hole, R_L, and approach infinity for a very sharp corner, as R_o approaches zero.

It has been pointed out by Osgood (1970) that as long as the stress at the notch root is in the elastic region, the stress concentration factor can be calculated from the geometry of the notch alone. In most practical cases, however, steel will behave in a ductile manner and yield ahead of the stress concentration. The plastic yielding and the resulting redistribution of stress, which may even occur in relatively brittle materials, causes stress concentrations to have less effect on strength than might be expected from considering

elastic stresses only. The practical significance of stress concentration will depend on factors such as the type of metal and the type of loading. Peterson (1974) produced many diagrams for the elastic stress concentration factor according to different notch geometries.

6.2.2 Effective stress concentration factors

In the case of ductile materials, the theoretical stress concentration factor, k_t, has very little practical significance when evaluating static strength. For loadings beyond yielding, k_t becomes meaningless and the use of effective stress concentration factor, k_{eff}, is more appropriate. The effective stress concentration factor takes into account plastic yielding and redistribution of stress. It approaches unity as the load increases and the whole section is at yield stress. Thus, stress concentrations in ductile materials will not greatly reduce their static strength. Other criteria, however, may be affected such as deformation, stability, or fatigue. In most cases the structural steel used on bridges has good ductility. In the case of brittle materials under static loading, only limited yielding may take place and the effective stress concentration factor, k_{eff}, will approach the k_t factor.

In some cases such as impact loading, low temperature, or conditions of high restraint such as might be found in thick plates, ductile materials may behave in a brittle manner in the presence of severe notches. These cases can be evaluated using fracture mechanics methods. In most practical cases, however, corrosion will not result in the type of very severe notches which would require a fracture mechanics approach.

6.2.3 Fatigue notch factors

The effect of stress concentrations on fatigue resistance can be quantified by using a fatigue stress concentration factor or fatigue notch factor. The most commonly accepted definition of fatigue notch factor is the ratio of the fatigue strength of a smooth specimen to the fatigue strength of a specimen with stress concentration under the same experimental conditions and the same number of cycles (Sandor 1972).

Plentiful experimental results show that the fatigue notch factor is related to a number of factors, including material properties, material inherent defects, size and geometry of specimen, stress gradient, loading type and number of loading cycles. A notch-sensitive factor, q, has been introduced by Soderberg (1950) to indicate the sensitivity of materials to notches:

$$q = \frac{k_f - 1}{k_t - 1} \tag{6.3}$$

where k_f is the fatigue notch factor and k_t is the theoretical stress concentration factor. However, notch sensitivity is able to relate the fatigue notch factor, k_f, to the theoretical stress concentration factor, k_t (Peterson 1974). The value of q varies from 0, for no stress concentration effect (when $k_f = 1$), to 1.0, for full theoretical effect (when $k_f = k_t$). Several methods for calculating k_f from k_t have been proposed which can be found in Heywood (1952) and Roark et al (1989).

It is important to emphasise that there are many limitations to the evaluation of fatigue notch factors and that they cannot be applied with confidence to all situations. At present, the most reliable way to estimate the effects of stress concentration created by corrosion on fatigue strength is through full-scale fatigue tests on the actual conditions, if possible. This is particularly so in the case of corrosion, since it is very difficult to define a clear transition of notch radius. The actual surface or boundary of a corroded section is very irregular with small and sharp notches.

6.3 Stress concentration analysis for pits in different types of steel

Stress concentrations are not usually important in ductile materials but can be the cause of failure due to fatigue or brittle fracture in certain conditions (Righiniotis 1992). It has been pointed out by Albrecht et al (1990) that pits normally appear with different shapes in different steels. The pits in weathering steel beams were found to have steeper walls and at times flat bottoms, while those in the carbon steel beam had a more rounded profile. Therefore, there is a big difference between the stress concentration due to their

geometrical shape. In order to illustrate the effect of geometry on the theoretical stress concentration factor, k_t, a pit with depth of 1.5 mm and a width of 1 mm was modelled as a notch at the centre of a plate as shown in Figure 6.1. The plate had a unit width, depth of 8.0 mm, 60 mm length, and was loaded axially. For the purpose of analysis, the finite element package ANSYS 5.1 was used. The analysis was carried out using a two-dimensional 6 node triangular solid structural elements and plane stress.

The details of each notch shape and their related stresses at the root and 0.5 mm below are listed in Table 6.1. For carbon steel a U shape notch with depth of 1.5 mm and root radius of 0.5 mm was considered and the maximum stress at the root of notch was found to be 562 MPa. For weathering steel a V notch with the same depth as the carbon steel notch, but a root radius 0.2 mm was considered and the maximum stress at the root of notch was found to be 799 MPa. In practice steel will behave in a ductile manner and will yield before this stress occurs. It can be seen from the results that the concentration effect increases as the radius and angle of the notch decrease and as the depth increases. However, with sharp notches it becomes inaccurate to calculate the stress concentration elastically. The sharpness of the notch affects the value of the elastic stress concentration factor near the fatigue limit. It has been shown by many tests that the use of the full theoretical value of k_t in fatigue design will generally give results on the safe side (Osgood 1970).

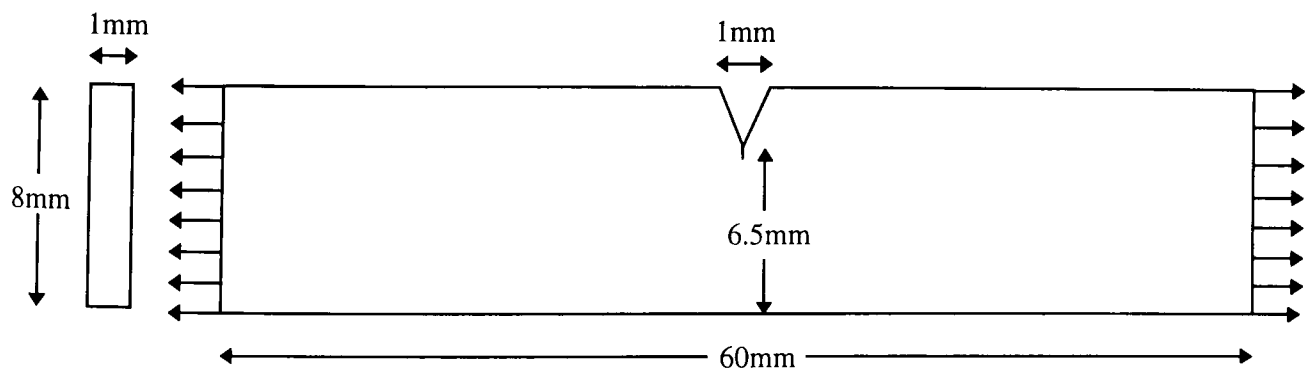

Figure 6.1 Dimensions and loading of plate modelled for ANSYS.

Table 6.1 Results of stresses for different pit shapes.

Shape of pit	Pit depth (mm)	Radius of pit at the root (mm)	Stress at the root of pit (MPa)	Stress at 0.5 mm below the root (MPa)
	1.5	0.0	∞	181
	1.5	0.2	799	193
	1.5	0.5	562	206

6.4 Methods of calculating fatigue notch factor

The presence of discontinuities or pits on the surface of steel structural members due to corrosion can result in a lower S-N curve. The reason for this is the stress concentration at the root of the pit which promotes the initiation of cracks which reduce the fatigue life. The effect of stress concentrations on fatigue resistance can be quantified by using a fatigue stress concentration factor or fatigue notch factor.

Two approaches for determining fatigue notch factors can be considered. The first requires testing smooth specimens, then utilising the Neuber's rule (1961) to calculate the fatigue notch factor based on the number of cycles to failure for corroded specimens. The second involves a comparison between test results for corroded specimens and a mean regression line for stress range versus cycles to failure in plain rolled beams. The regression line which was used in the comparison is the same one used in BS 5400: Part 10 (1980) for allowable stress range for class B (plain rolled beam) fatigue detail. Further discussion regarding the second approach is presented in this section.

The severity of various classes of structural detail in BS 5400: Part 10 (1980) can be expressed in terms of fatigue notch factors, k_f, before considering corrosion. It is more meaningful to select the fatigue strength of the plain rolled beam as the reference line for

which the fatigue notch factor is then defined as unity, $k_f = 1.0$. The fatigue notch factor for any other class x is then equal to the ratio between the stress ranges for the class B and class x means at a fixed number of cycles, as shown in Figure 6.2.

$$k_f = \frac{\sigma_{r,B}}{\sigma_{r,x}} \tag{6.4}$$

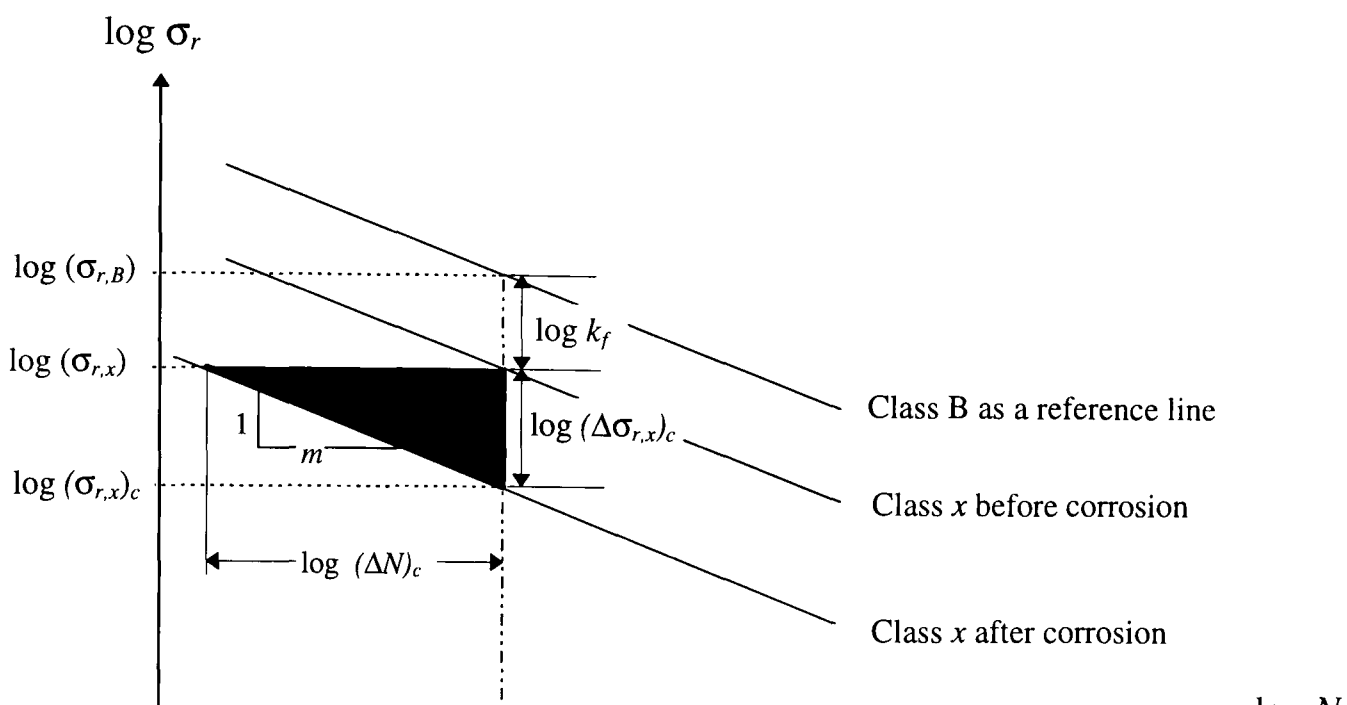

Figure 6.2 Definition of fatigue notch factor and computation of loss in stress range and fatigue life.

Since the slopes of the eight mean regression S-N lines vary, the fatigue notch factors were computed at 500,000 cycles of loading, which is about the logarithmic mean of the number of cycles to failure of the beams tested in two studies by Fisher et al (1970 and 1974) that form the basis of the design requirement in the Standard Specification of Highway Bridges. This reference (N = 500,000 cycles) is about midway on the range of N for which test data exist and has been used extensively by different authors (Zuraski 1986, Kulicki et al 1990 and Albrecht et al 1981, 1984, 1988, 1990 and 1994). Therefore, the calculations are not significantly affected by variations. Setting N = 500,000 and substituting the values of K and m for each class into the fatigue power law relationship gives the stress ranges for different classes listed in Table 6.2. Dividing

these stress ranges into 262 MPa, the stress range for class B yields k_f in accordance with equation 6.4 (see Table 6.2 and Figure 6.2).

Table 6.2 Calculation of fatigue notch factors for mean lines of BS 5400.

Detail Class	K	m	σ_r at 500,000 cycles	k_f at 500,000 cycles
B	2.34×10^{15}	4.0	262	1.00
C	1.08×10^{14}	3.5	241	1.09
D	3.99×10^{12}	3.0	200	1.31
E	3.29×10^{12}	3.0	189	1.39
F	1.73×10^{12}	3.0	151	1.74
F2	1.23×10^{12}	3.0	135	1.94
G	0.57×10^{12}	3.0	105	2.50
W	0.37×10^{12}	3.0	91	2.88

6.5 Calculation of fatigue notch factor for corroded specimens

Fatigue notch factor due to corrosion, k_{fc}, can be defined as the ratio of the stress range of a non-corroded base metal, $(\sigma_{r,x})$, to the stress range of the same metal with corrosion, $(\sigma_{r,x})_c$, under the same experimental conditions.

$$k_{fc} = \frac{(\sigma_{r,x})}{(\sigma_{r,x})_c} \tag{6.5}$$

Where $(\sigma_{r,x})$ is the mean stress range for class x at a reference number of cycles. This can be calculated by substituting the number of cycles to failure, N, into the fatigue power law equation. The value of $(\sigma_{r,x})_c$, represents the stress range which has been applied to the corroded specimen in the plane of crack. This relationship is illustrated in Figure 6.2, where the equation is evaluated at the mean cycle life for a group of specimens tested at a given stress range. In this study the base metal has been taken as class B and the values of $(\sigma_{r,B})$ have been calculated and listed in Table 6.3 by using the following equation as fatigue power law:

$$(\sigma_{r,B}) = \left(\frac{K}{N}\right)^{1/m} \tag{6.6}$$

Where K is the constant term relating to the mean-line of the results and m is the inverse slope of the mean-line log σ_r - log N curve. The values of K and m were taken to be 2.34×10^{15} and 4.0 respectively for class B. It should be noted, that the specimens performed better than class B. These had a notch factor of less than 1.0, and were included in the regression analysis.

Table 6.3 Calculation and results of fatigue notch factor.

Specimen number	d_c (mm)	R_{max} (mm)	S_d (mm)	$(\sigma_{r,B})_c$ (MPa)	N (Cycles)	$(\sigma_{r,B})$ (MPa)	k_{fc}
1	0.13	0.34	0.067	200	36,900,000	89	0.45
2	1.59	1.20	0.226	200	23,525,000	100	0.50
3	0.19	0.94	0.112	250	506,200	260	1.04
4	1.23	1.53	0.357	250	990,900	220	0.88
5	1.71	0.73	0.110	250	1,843,500	189	0.76
6	0.09	0.47	0.090	250	795,200	233	0.93
7	2.28	1.75	0.324	350	40,960	489	1.40
8	1.83	2.79	0.630	350	990	1270	3.63
9	1.25	2.62	0.465	350	15,590	622	1.78
10	0.13	0.39	0.064	350	244,690	313	0.90
11	0.16	1.01	0.170	350	298,170	298	0.85
12	0.38	1.15	0.271	350	161,660	347	1.00
13	1.61	1.68	0.317	350	24,790	554	1.58
14	2.31	1.78	0.349	350	25,420	551	1.57
15	2.34	1.36	0.232	350	15,570	623	1.78
16	2.68	3.37	0.775	350	3,360	914	2.61
17	1.93	2.70	0.483	350	38,640	496	1.42
18	1.58	0.60	0.101	350	94,180	397	1.13
19	1.61	1.58	0.105	350	218,940	322	0.92
20	1.06	0.56	0.098	350	241,750	314	0.90
21	2.06	2.01	0.515	250	512,090	260	1.04
22	1.26	0.82	0.159	250	1,479,890	199	0.80
23	1.34	0.98	0.210	250	969,380	222	0.89
24	1.12	0.93	0.202	250	1,116,900	214	0.86
25	1.19	1.23	0.215	250	770,800	235	0.94
26	1.23	1.21	0.227	250	870,960	228	0.91
27	1.52	1.15	0.261	250	560,300	254	1.02
28	2.05	2.29	0.469	250	389,010	279	1.12
29	1.64	1.80	0.304	250	594,100	251	1.00
30	2.16	2.06	0.522	250	463,070	267	1.07
31	1.56	1.67	0.366	250	634,200	246	0.98
32	1.46	1.26	0.217	250	676,080	243	0.97
33	1.39	1.28	0.254	250	741,300	237	0.95
34	2.06	2.59	0.717	250	268,000	301	1.20

6.5.1 Fatigue notch factor in terms of corrosion penetration

Further investigation was carried out to develop a relation for fatigue notch factor, k_{fc} in terms of average corrosion penetration, d_c. Two approaches were considered. The first requires measurements of the average corrosion penetration, d_c, the standard deviation of roughness, S_d, and the calculation of fatigue notch factor, k_{fc} based on the fatigue test. The second involves the same procedures, except instead of standard deviation of roughness, S_d, measurement is required of the maximum roughness, R_{max}. Further discussion regarding these methods for the development of the fatigue notch factor, k_{fc}, is given in the next section.

The fatigue notch factor for corroded specimens was calculated and plotted against standard deviation, S_d as shown in Figure 6.3. The following equation was produced from Figure 6.3 based on a mean regression line through the data points with the intercept of 1.0 calculated with the least-square-fit method:

$$k_{fc} = 1 + 0.99\, S_d \tag{6.7}$$

The fatigue notch factor of a corroded member by having measurements on average corrosion penetration is given by

$$k_{fc} = 1 + 0.2\, d_c \tag{6.8}$$

The fatigue notch factor for corroded specimens was plotted against maximum roughness, R_{max} as shown in Figure 6.4. The following equation was produced from Figure 6.4 based on a mean regression line through the data points with the intercept of 1.0 calculated with the least-square-fit method:

$$k_{fc} = 1 + 0.2\, R_{max} \tag{6.9}$$

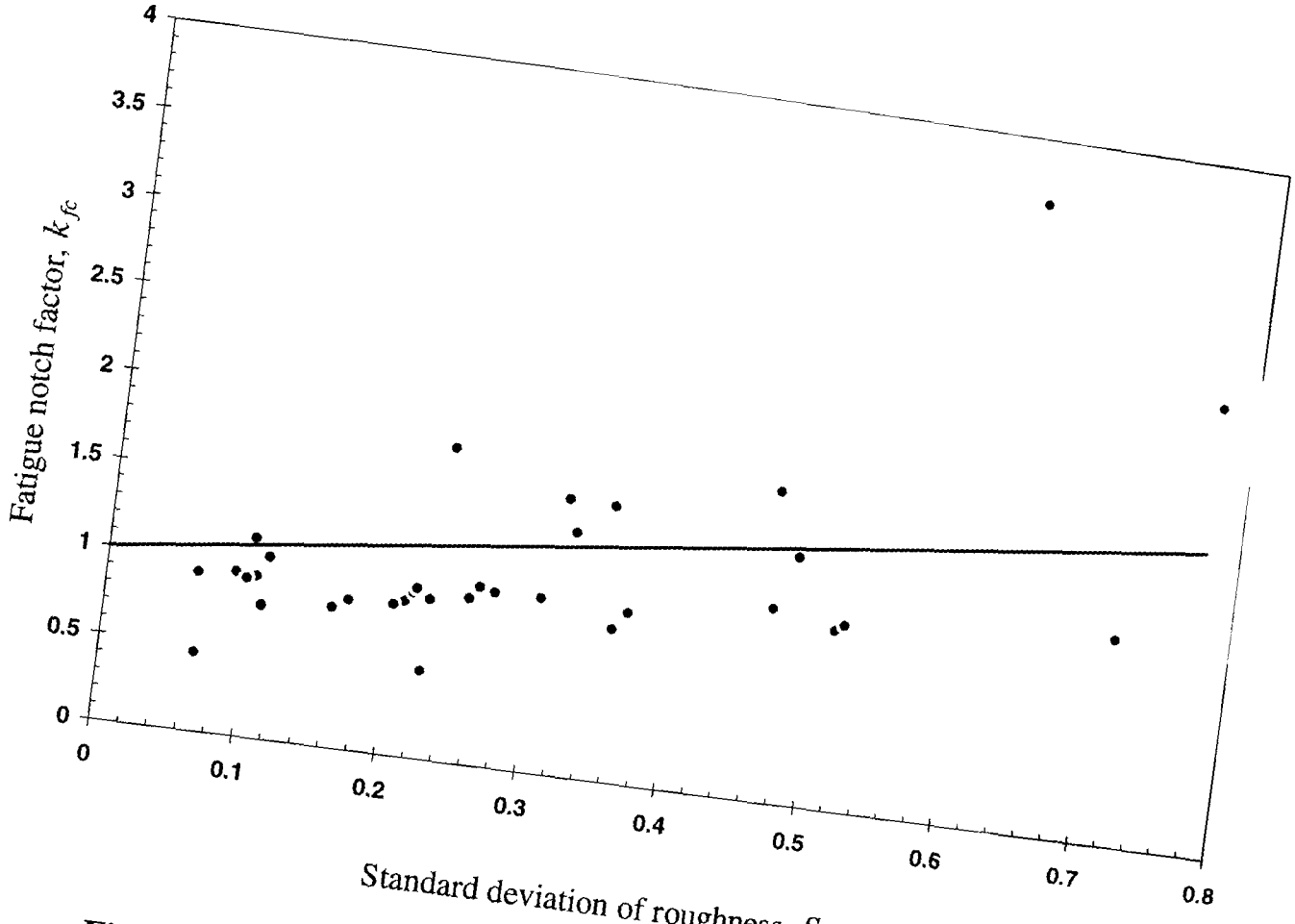

Figure 6.3 Fatigue notch factor versus standard deviation of roughness.

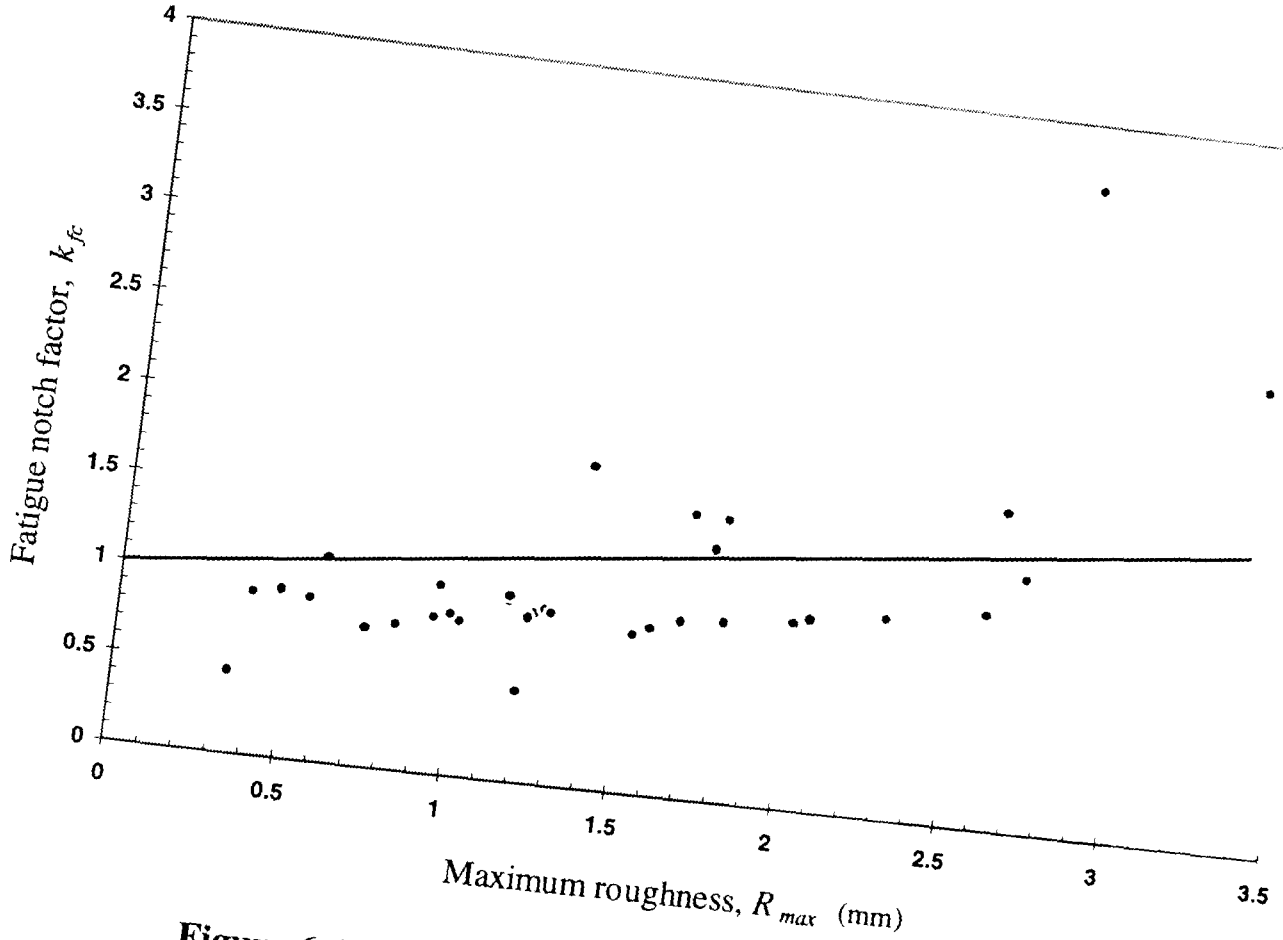

Figure 6.4 Fatigue notch factor versus maximum roughness.

6.5.2 Fatigue notch factor in terms of the exposure time

An attempt has been made to develop a relation for fatigue notch factor in terms of the exposure time. In Chapter 4, the following relationship was developed for corrosion penetration in terms of exposure time:

$$d_c = 90.74 t^{0.75} \tag{6.10}$$

In order to relate the effect of exposure time, t, to fatigue notch factor, k_{fc}, average corrosion penetration, d_c, from equation 6.10 has been substituted into equation 6.8.

$$k_{fc} = 1 + 0.018 t^{0.75} \tag{6.11}$$

Equation 6.11 can be used to calculate the fatigue notch factor of a corroded specimen or a member at any given exposure time in years.

6.6 Comparison of the fatigue notch factor with BS 5400 classes

The relationship developed for fatigue notch factor in terms of corrosion penetration (equation 6.8) is plotted in Figure 6.5. Superimposed on this graph are the corresponding fatigue notch factor for different classes of structural detail as classified in BS 5400: Part 10 (1980), the UK code for fatigue design (see Table 6.2). This equation was then used to obtain the equivalent value of d_c which corresponded to each of the structural detail classes. For example the fatigue notch factor curve intersects class F at a value of $d_c = 3.75$ mm. This is shown in Figure 6.5. This procedure was repeated for all classes and the results are given in Table 6.4.

Based on the results of the present study, two cases are possible, depending on whether the fatigue notch factor due to corrosion is smaller or greater than that of a given type of detail. If the fatigue notch factor due to corrosion is smaller than the fatigue notch factor for non-corroded detail, $k_f \geq k_{fc}$, then the fatigue notch factor of the detail, k_f, will

govern. If, on the other hand, $k_{fc} \geq k_f$, the fatigue notch factor due to corrosion, k_{fc}, will govern.

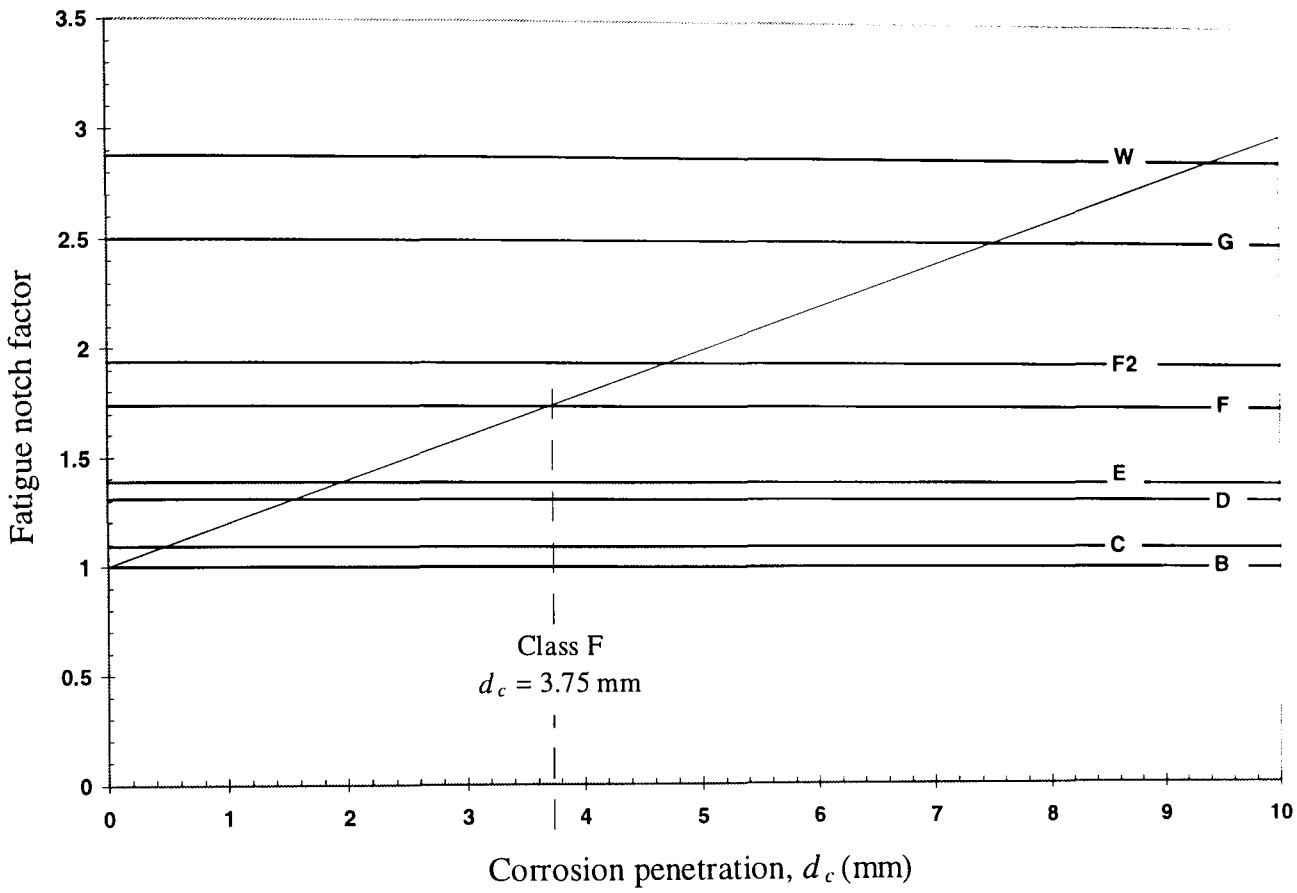

Figure 6.5 Comparison of the relation developed for fatigue notch factor in terms of corrosion penetration with BS 5400 classes.

Table 6.4 Fatigue notch factor of new steelwork detail classes compared with corroded steelwork of equivalent corrosion penetration.

Detail class	log K	m	k_f at 500,000 cycles	Equivalent d_c (mm)
B	15.37	4.0	1.00	0.00
C	14.03	3.5	1.09	0.40
D	12.60	3.0	1.31	1.65
E	12.52	3.0	1.39	1.95
F	12.24	3.0	1.74	3.75
F2	12.09	3.0	1.94	4.75
G	11.76	3.0	2.50	7.50
W	11.57	3.0	2.88	9.40

6.7 Summary and conclusions

The geometrical discontinuities which create stress concentrations and are frequently responsible for providing the origin of fatigue crack formation in engineering structures have been discussed. The brief survey of fatigue notch factors has showed that they play very important part in the estimation of fatigue life and fatigue strength of structures. It has been found from the conclusion of several authors that the most direct and reliable way of defining this parameter is by experiment. The stress results from finite element analysis shows that for the same depth stresses at the root of the pit in weathering steel are higher than in carbon steel.

Two methods have been investigated for calculating the fatigue notch factor. While one method was based on the Neuber's rule, the other was based on the mean stress range for class B as the reference line. The second method is widely used in building and bridge design because the fatigue strength of plain rolled beams is a convenient reference line for which the fatigue notch factor is defined as unity. It has been found that the fatigue notch factor is an appropriate parameter for quantifying the effect of corrosion deterioration on fatigue life and a comparison between the fatigue notch factor developed for corrosion penetration and the fatigue notch factor for a particular class should be made and the one of higher magnitude governs.

In this study, two relationships developed for calculating fatigue notch factor which can be used for the assessment of corroded steel structures. The first is in terms of average corrosion penetration which increased on average with the average corrosion penetration and the second is in terms of exposure time. The assessment of the remaining fatigue life of existing corroded steel structures, in terms of fatigue notch factor, requires only information of the average corrosion penetration or the time of exposure at the time of the assessment. In particular, the relation of fatigue notch factor in terms of exposure time gives a direct, accurate, and quantifiable assessment of corroded members and it needs only the time of weathering.

CHAPTER VII

REMAINING FATIGUE LIFE OF CORRODED STEEL STRUCTURES

7.1 Introduction

There is a large number of steel structures where structural members and components are corroded and where corrosion has been concealed by paint and may not be visually identifiable. Their present capacity may not satisfy design code requirements because most codes deal only with the design of new structures and the effects of uncertain problems such as corrosion are often not mentioned. Apart from fatigue, the most common problem for all steel bridges is deterioration due to corrosion since it appears to be the most important degradation mechanism in determining the remaining life of these structures. In bridges, the combined action of corrosion and fatigue, known as corrosion fatigue, causes considerable reduction in the life of the structure.

The deterioration of steel bridges due to corrosion is serious and upgrading them to an adequate condition may be very expensive (Hendawi 1994). Effects of fatigue in steel bridges was investigated in Chapter 5. Experimental work on the remaining fatigue life of corroded steel and weldments was conducted at the University of Maryland by Friedland et al (1982). The fatigue test results showed a significant reduction of the fatigue life in welded specimens which was mainly due to the formation of pits. The reliability of corroded steel bridges was studied by Kayser (1988). He pointed out that the effects of corrosion on the dynamic loading of a bridge can be significant in two ways. The first is that corrosion gradually reduces the stiffness of the structural members. The natural frequency of a bridge is proportional to its structural stiffness and the frequency response will have some influence on the dynamic impact factor. The second possible effect of corrosion on dynamic loading is the change in structural

boundary conditions due to locking up of the joints, bearing and hinges. In general, the change in boundary conditions from pinned to fixed will cause the structure to be inherently stiffer with higher natural frequencies

Albrecht et al (1984) conducted an in-depth study on the performance of weathering steel bridges and some on the performance of carbon steel. From the test results concerning the reduction in fatigue resistance of weathering steel a general conclusion was drawn that corrosion reduces the fatigue life of components, and the approximate loss of fatigue life can range quite widely depending on the type of detail.

The overall aim of this chapter is to develop an assessment method that can be used to make reliable estimates of the remaining fatigue life of corrosion damaged steel bridges using thickness loss and particularly pit depth provided by measurement or visual inspection, or by considering the time of exposure.

The specific objectives of this chapter are:

1. To develop relationships for fatigue life of members or components subjected to corrosion in terms of maximum roughness and exposure time.
2. To develop a procedure to estimate the cumulative fatigue damage.
3. To provide a numerical example to examine the sensitivity of various factors affecting cumulative damage.
4. To consider the application of structural reliability to the assessment of corrosion damaged steelwork.

7.2 Fatigue life assessment

In the past two decades, deterioration in steel structures has received increased attention as a cause of strength reduction and possible collapse. In fact, several bridge failures as mentioned previously have been attributed to various material degradation processes. Kulicki et al (1990) suggested that the remaining fatigue life of corroded structural members may be estimated simply on the basis of visual inspection or by using an

empirical formula given by Albrecht et al (1990) based on the fatigue tests of some corroded weathering and carbon steel beams in the laboratory.

In general, fatigue life cannot be estimated accurately from the results of visual examination alone because it is not dependent on the remaining thickness alone, but also on the amount of pitting present (Albrecht et al 1990). However, it was found in Chapter 3, that pitting is proportional to loss of thickness. Members cannot be removed from a bridge in service, although Kulicki et al (1990) reports the possibility of removing minor non-critical members for testing.

However, as yet there is no simple relationship between the magnitude of structural defects due to corrosion (pitting corrosion) and the corresponding reduction in fatigue life. There is an urgent need for a method to estimate the remaining fatigue life of members weakened by pitting corrosion. In Chapter 5, we have seen that a correlation exists between the corrosion penetration and fatigue life of corroded specimens. Therefore, it may be possible to develop a procedure for estimating the remaining fatigue life of corroded bridge beams based on this information.

7.2.1 Fatigue life in terms of maximum roughness

An attempt has been made to develop a relation for fatigue life, N, of members subjected to pitting corrosion in terms of average maximum roughness, R_{max}. The fatigue power law was used to calculate the constant term relating to the mean-line results K, for all the fatigue specimens tested in the laboratory (see Chapter 5, Table 5.4). Then the fatigue performance of all the specimens was plotted in terms of log K against maximum roughness, R_{max}, as shown in Figure 7.1.

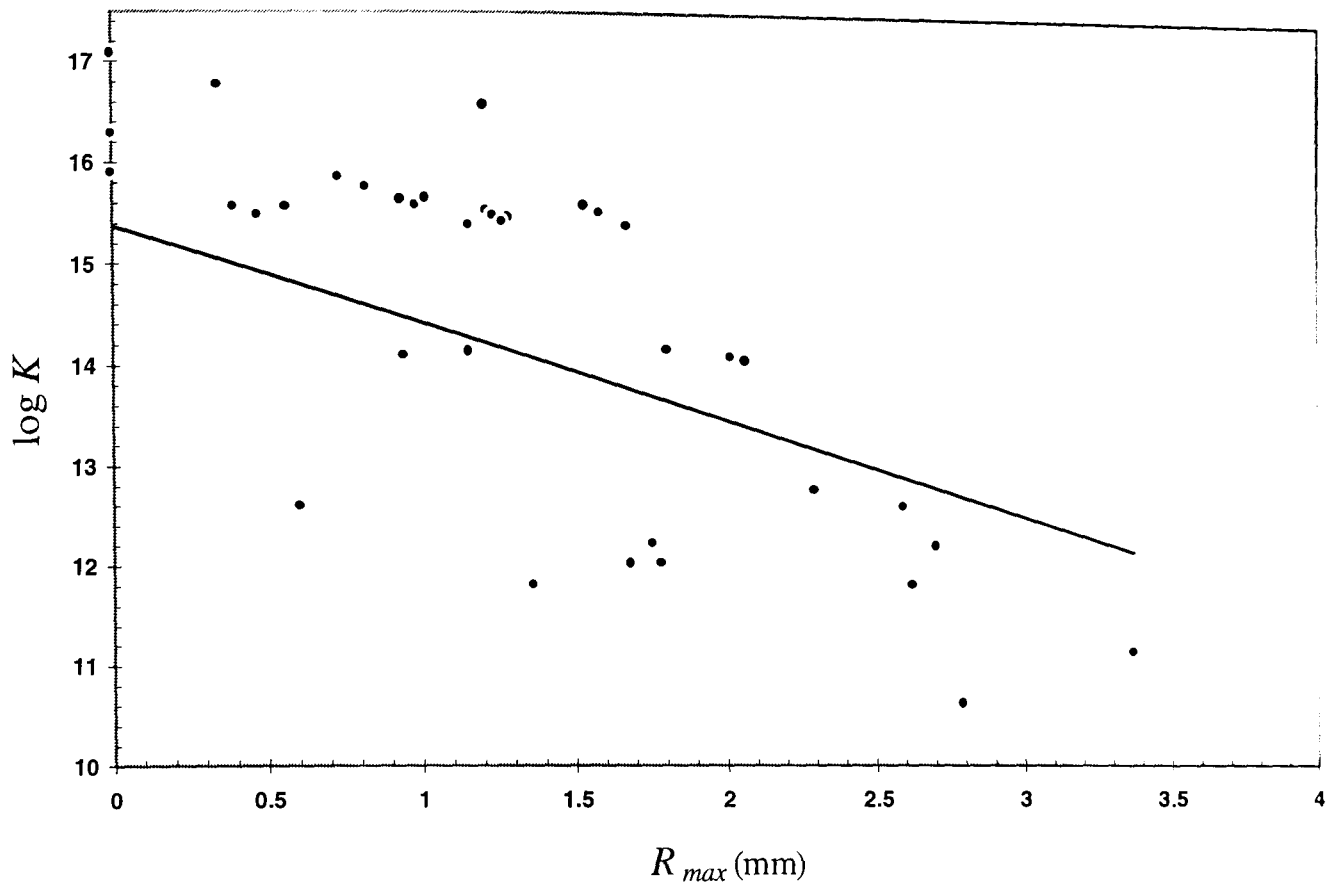

Figure 7.1 Fatigue performance of corroded specimens versus maximum roughness.

The following equation has been produced based on a mean regression line through the data points:

$$\log K = 15.37 - 0.95 R_{max} \tag{7.1}$$

Equation 7.1 can be written alternatively as:

$$K = 10^{(15.37 - 0.95 R_{max})} \tag{7.2}$$

The overall fatigue life of the specimens can be calculated from the following relation by substituting equation 7.2 into the fatigue power law:

$$N = \frac{10^{(15.37 - 0.95 R_{max})}}{(\sigma_r)^m} \tag{7.3}$$

7.2.2 Fatigue life in terms of exposure time

An attempt has been made to develop a relation for fatigue damage of members subjected to corrosion in terms of exposure time. In this way the fatigue performance of all the specimens was plotted in terms of log K against average depth of corrosion, d_c as shown in Figure 7.2.

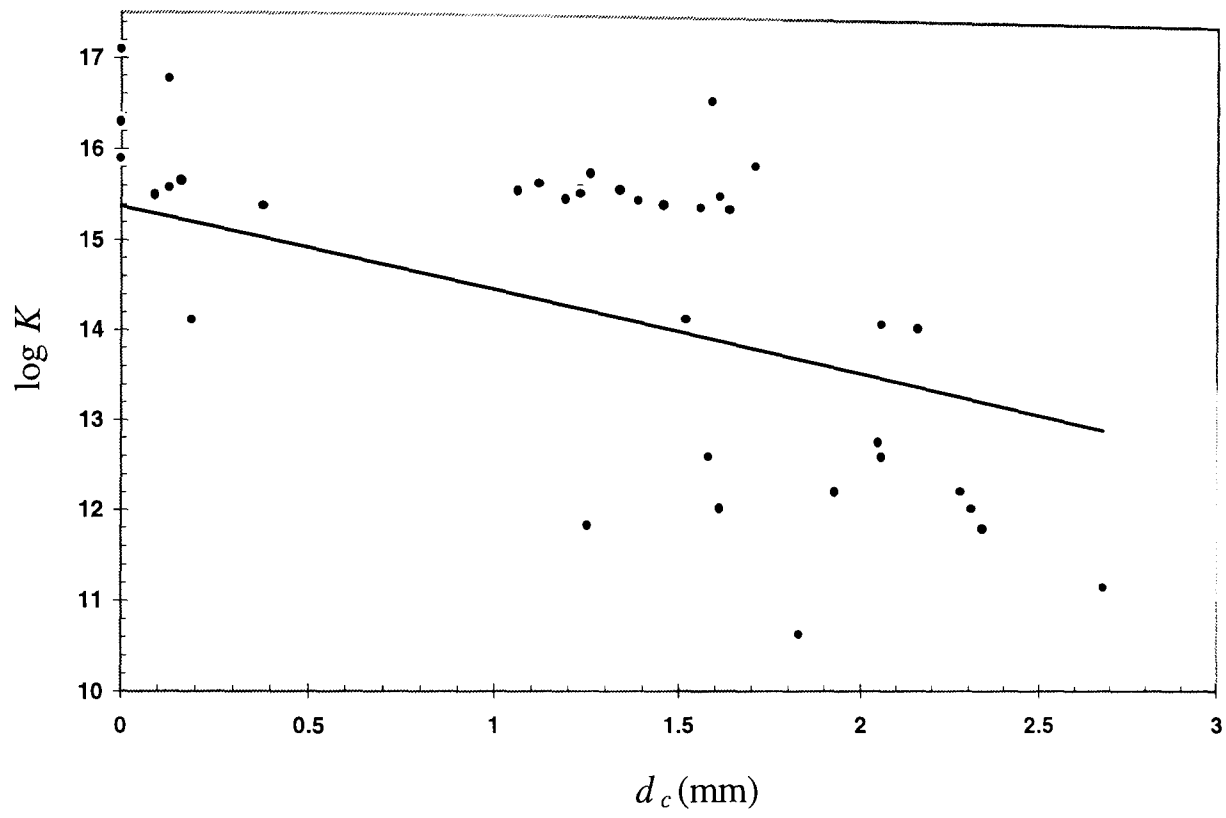

Figure 7.2 Fatigue performance of corroded specimens versus depth of corrosion penetration.

The following equation has been produced based on a mean regression line through the data points:

$$\log K = 15.37 - 0.91 d_c \tag{7.4}$$

Equation 7.4 can be written alternatively as:

$$K = 10^{(15.37 - 0.91 d_c)} \tag{7.5}$$

The following corrosion decay model has been developed in Chapter 4 for corrosion penetration in terms of exposure time in units of microns:

$$d_c = 90.74\, t^{0.75} \tag{7.6}$$

The fatigue performance of corroded specimens, K, can be expressed in terms of exposure time by substituting equation 7.6 into 7.5.

$$K(t) = 10^{(15.37 - 0.083 t^{0.75})} \tag{7.7}$$

The overall fatigue life of fatigue specimens in terms of exposure time can be obtained by substituting equations 7.7 into the fatigue power law:

$$N(t) = \frac{10^{(15.37 - 0.083 t^{0.75})}}{(\sigma_r)^m} \tag{7.8}$$

7.2.3 Cumulative fatigue damage

Since bridge structures are subjected to loads at variable times and with different characteristics and magnitude, a random variable amplitude type of loading results. Miner's rule provides a means of accounting for random variable loading. Miner's rule is given by

$$\sum \frac{n_i}{N_i} \leq 1 \tag{7.9}$$

where n_i is the number of cycles applied of a stress range for which the maximum life under constant amplitude loading is N_i. Failure occurs under a sequence of different stresses when the sum of all the ratios (n/N) equals unity. As mentioned before, the main point is to develop a relation for total fatigue damage (TFD) of corroded steel bridges in

terms of exposure time. Therefore, the terms in Miner's rule the relation for fatigue damage (FD) can be expressed as:

$$\mathrm{FD} = \frac{r\,dt}{N(t)} \tag{7.10}$$

In relation 7.10, over a period of time (dt) there are (rdt) cycles of loading where (r) is the number of load applications per year and $N(t)$ is represented by equation 7.8.

The total fatigue damage (TFD) over a life-time of T years due to general vehicle loading and progress of corrosion can be expressed as follows:

$$\mathrm{TFD} = \int_0^T \frac{r\,dt}{N(t)} \leq 1 \tag{7.11}$$

Equation 7.8 has been substituted into equation 7.11 and the total fatigue damage over all vehicles is as follows:

$$\mathrm{TFD} = \int_0^T \Sigma \left(\frac{r(\sigma_r)^m}{10^{(15.37-0.083t^{0.75})}} \right) dt \leq 1 \tag{7.12}$$

where TFD = total fatigue damage, r = number of load applications per year, σ_r = stress range due to the applied vehicle in units of MPa, t = time in units of year, and m = inverse slope of the mean-line log σ_r - log N curve.

7.3 Vehicle load spectrum

The commonly used term "load spectrum" means a load distribution, either derived from a sample of measurements by a statistical analysis (e.g. histogram) or defined by a theoretical or fitted probability distribution function of the loads. In both cases, the load spectrum may be used to simulate a time history of the loads or to calculate a load effect

distribution. It is especially useful for fatigue calculations of steel bridges under traffic loads, because the distribution of stress ranges will affect the overall damage.

An example of a conventional load spectrum is given by so-called "fatigue convoys" used for fatigue calculations of steel bridges. A "fatigue convoy" is a set of a few lorries or concentrated loads, with given gross weights, axle loads, axle and vehicle spacings and number of passages for each vehicle. For any element of the bridge, such as a cross-beam or a stiffener, the application of the load convoy on the bridge deck results in a stress variation time history. The stress cycle amplitudes may then be counted by the "rainflow" or "reservoir" method and the fatigue damage or the expected life-time of the structure may be computed.

There is a 25 band spectrum of commercial vehicles listed in Table 11 of BS 5400: Part 10, 1980. These statistics are from data of more than 18 years ago. It is well known that since that period there have been substantial increases in the types, weights and number of lorries on the UK roads. Therefore, a field survey was carried out by the author to collect new data relating to the types and the numbers of heavy vehicles from a local major highway, the M32. The data was collected at different hours over 6 separate days. From these results the equivalent number of vehicles in each group per million was calculated. The full details and the data for each of the vehicles are shown in Table 7.1. In this survey two types of new vehicles, 5A-H and 6A-H, which are not mentioned in the design code for fatigue assessment, have been observed. The details of the new vehicles are shown in Figure 7.3. This information was provided by the Loading Section of Highways Agency (Fenn 1997). The results showed that in the period between 1980 and 1997 in most of the cases there was a big increase in the number of lorries on the UK roads.

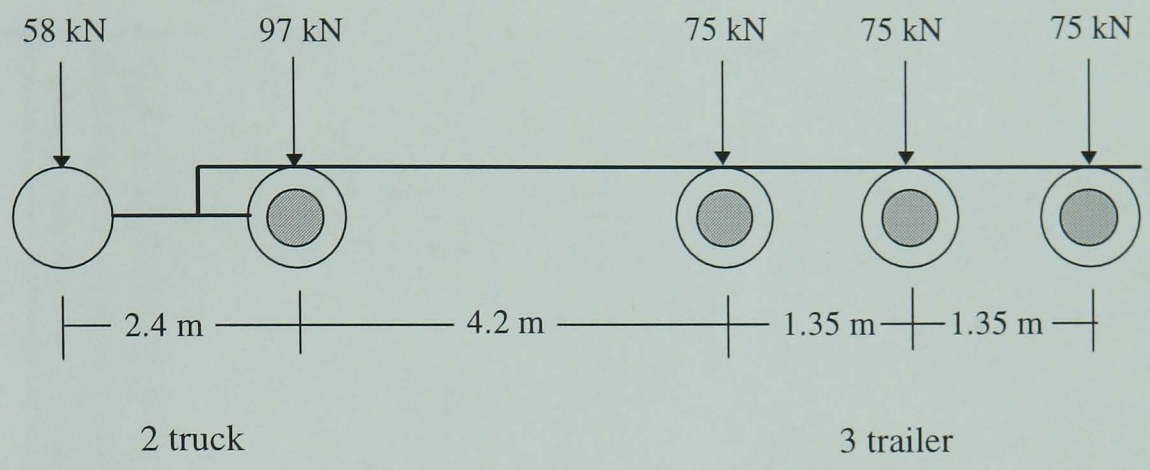

(a) Details of 5A-H (new) vehicle.

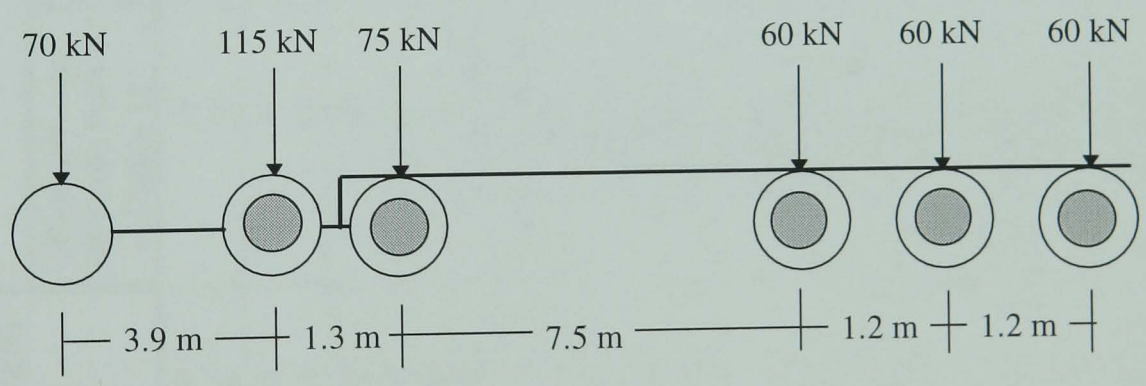

(b) Details of 6A-H (new) vehicle.

Figure 7.3 Details of new vehicles (Fenn 1997).

Table 7.1 Comparison of the data provided by BS 5400: Part 10 and the data obtained from the field survey for different types of vehicles.

Vehicle designation	Total weight (kN)	No. in each group per million vehicles			
		Data given by BS 5400: Part 10 (Table 11)	Data obtained from field inspection	Percentage difference between BS 5400 and field inspection data	Proportion of total vehicles in each group from field inspection
18GT-H	3680	10	10*	--	0.00001
18GT-M	1520	30	30*	--	0.00003
9TT-H	1610	20	20*	--	0.00002
9TT-M	750	40	40*	--	0.00004
7GT-H	1310	30	30*	--	0.00003
7GT-M	680	70	70*	--	0.00007
7A-H	790	20	750	Increased over 100%	0.00075
6A-H (new)	440	Not included	52500	(new)	0.0525
5A-H (new)	380	Not included	85900	(new)	0.0859
5A-H	630	280	4100	Increased over 100%	0.0041
5A-M	360	14500	21400	+47	0.0214
5A-L	250	15000	7900	-47	0.0079
4A-H	335	90000	29000	-68	0.029
4A-M	260	90000	29000	-68	0.029
4A-L	145	90000	10450	-88	0.01045
4R-H	280	15000	36700	Increased over 100%	0.0367
4R-M	240	15000	36000	Increased over 100%	0.036
4R-L	120	15000	21100	+41	0.0211
3A-H	215	30000	10200	-66	0.0102
3A-M	140	30000	9400	-69	0.0094
3A-L	90	30000	6900	-77	0.0069
3R-H	240	15000	31600	Increased over 100%	0.0316
3R-M	195	15000	30800	Increased over 100%	0.0308
3R-L	120	15000	18600	+24	0.0186
2R-H	135	170000	183500	+8	0.1835
2R-M	65	170000	182500	+8	0.1825
2R-L	30	180000	191500	+6	0.1915

* These types of vehicles were not observed in the field survey therefore the same numbers as listed in Table 11 of BS 5400: Part 10 used.

7.4 Evaluation of corroded steel bridge

The objective in this section is to examine the performance of corroded steel girder bridges using the corrosion model developed in Chapters 4 and 5. For this purpose a simply supported composite welded plate girder bridge with uniform cross section has been designed in order to present an approach to quantifying the remaining fatigue life due to corrosion.

7.4.1 Design of steel bridge

As mentioned in the previous section a simply supported composite welded plate girder bridge has been designed for this study using the ultimate limit state design method (see Appendix A). The design is according to the BS 5400 and the Department of Transport specification (Iles 1991). The general arrangement of the simply supported composite welded plate girder bridge is showing in Figure A.1. The girders are fabricated of mild steel (this was because the roughness and fatigue data was obtained from mild steel samples). Data regarding span length, width, loading and material properties are given in the design data. For this analysis of the remaining fatigue life, it has been assumed that the measured data on the corrosion specimens relates to the designed composite bridge. Full details of the design of bridge are given in Appendix A.

7.4.2 Fatigue assessment of the bridge at different paint interval times

The effectiveness of the paint system to protect steel structures from corrosion depends on the paint system material, environmental factors and structural details. Dutems (1987) believed that on the average a bridge is painted every 22 years. With mild steel, the expanding rust continuously destroys the adhesive bond between the paint and the steel surface. In this study the paint-cycles which have been assumed for a steel bridge over a life-time of 120 years are listed in Table 7.2. It can be seen that shorter paint life is assumed as the life-time increases because there is a discontinuity between the previous and the new painting-cycles of localized areas.

Table 7.2 Painting-cycles for a life-time of 120 years.

Life-time (Years)	Painting and corroding cycles
0-25	Painted
25-45	Corroded
45-65	Painted
65-80	Corroded
80-95	Painted
95-105	Corroded
105-120	Painted

The next step was to determined the numbers of load applications to the bridge per year. In order to achieve this the number of vehicles that are assumed to travel along each lane of the bridge per year has been taken from Table 1 of the BS 5400: Part 10 (1980). Since it has been assumed the bridge is a two lane single carriageway and may be used for all purposes, therefore, the number of vehicles per lane per year is $n_c = 0.5\times10^6$. The number of each group of vehicles applied to the bridge per year were obtained from the information in Table 7.1.

The next step is to investigate the total cumulative fatigue damaged of the steel bridge for a life-time of 120 years. Therefore, each type of vehicle in Table 7.1 was placed on the simple span bridge in such a way as to produce the maximum effect, (M_{max}). The maximum bending stress range at the top of the bottom flange, where corrosion is usually most severe, has been calculated for each type of vehicle and its value listed in Table 7.3.

Equation 7.12 was used for each group of vehicle loading by substituting the required values. The total fatigue damage for each vehicle over a life-time of 120 years was calculated, taking into account the paint-cycles above. The results of this calculation are listed in Table 7.3. It may be observed that the largest fatigue damage is caused by 6A-H (new) group which is similar to the standard fatigue vehicle as recommended by BS

Table 7.3 Calculations of maximum bending, maximum stress, number of vehicles applied in each group per year and cumulative fatigue damaged in each group of vehicles for a life-time of 120 years.

Vehicle designation	Total weight (kN)	M_{max} (kN.m)	σ_r (MPa)	No. of vehicles in each group per year	Cumulative fatigue damage in each group of vehicles for a life-time of 120 years
18GT-H	3680	7433	212.4	10	0.0104
18GT-M	1520	2669	76.3	30	0.0005
9TT-H	1610	6810	194.6	20	0.0147
9TT-M	750	2994	85.5	40	0.0011
7GT-H	1310	4347	124.2	30	0.0037
7GT-M	680	2269	64.8	70	0.0006
7A-H	790	2938	84.0	900	0.0229
6A-H (new)	440	1598	45.7	61800	0.1380
5A-H (new)	380	1386	39.6	101100	0.1272
5A-H	630	1982	56.6	4800	0.0245
5A-M	360	1492	42.6	25200	0.0425
5A-L	250	1049	30.0	9300	0.0038
4A-H	335	1409	40.3	34200	0.0462
4A-M	260	1075	30.7	33900	0.0154
4A-L	145	584	16.7	12300	0.0005
4R-H	280	1232	35.2	43200	0.0339
4R-M	240	1156	33.0	42300	0.0257
4R-L	120	578	16.5	24900	0.0009
3A-H	215	1097	31.3	12000	0.0059
3A-M	140	546	15.6	11100	0.0003
3A-L	90	417	11.9	8100	0.00008
3R-H	240	1183	33.8	37200	0.0249
3R-M	195	955	27.3	36300	0.0103
3R-L	120	581	16.6	21900	0.0008
2R-H	135	671	19.7	216000	0.0166
2R-M	65	327	9.30	214800	0.0008
2R-L	30	144	4.10	225300	0.00003
					TFD = 0.573

5400: Part 10 (1980). The overall fatigue damage can be obtained by adding the fatigue damage of all bands of vehicles together, giving a total of 0.573 in dry air. The same procedure was repeated to calculate the total fatigue damage by assuming that the bridge was protected by paint in the first time interval (0-25 years) and was unpainted thereafter. In this case the overall fatigue damage in 120 years life-time was 3.15. It should be noted that at a life-time of 97 years the total fatigue damage is unity. The overall cumulative fatigue damage against the time for both cases is plotted in Figure 7.4.

The cumulative damage has been calculated for a typical class D detail where the web is welded to the flanges. It can be seen that the value of its cumulative damage is 0.828 which indicates that it is more critical than the relatively well maintained case. The same procedure can be repeated for the weld stiffener detail which is more severe because it is classified as class F.

The effects of corrosion fatigue on total fatigue damage can be considered by calculating the environment factor. It has been mentioned in Chapter 5 (section 5.3.1.1) that the fatigue life reduction due to the aqueous environment (K_e) is the ratio of the crack growth rates in aqueous to the air environments. If the structure is to be painted a factor of $K_e = 1.0$ may be used. Otherwise the environment factor can be calculated based on the procedure suggested by Albrecht et al (1990) and explained in detail in section 5.3.1.1. It was found that the cracks grew faster in aqueous environments than in air by a factor of 2.3 for mild steel. Consequently, using equation 5.11 the environment factor is $K_e = (2.3)^{1/3.3} = 1.29$. This factor can be used directly in equation 7.12 in order to take into account of the effects of corrosion fatigue. Hence, the form of this equation for the total fatigue damage over all vehicles is as follows:

$$\mathrm{TFD} = \int_0^T \Sigma \left(\frac{r(K_e \sigma_r)^m}{10^{(15.37-0.083t^{0.75})}} \right) dt \leq 1 \qquad (7.13)$$

The overall cumulative fatigue damage against the life-time for both cases in dry air and aqueous environment are plotted in Figures 7.4 and 7.5.

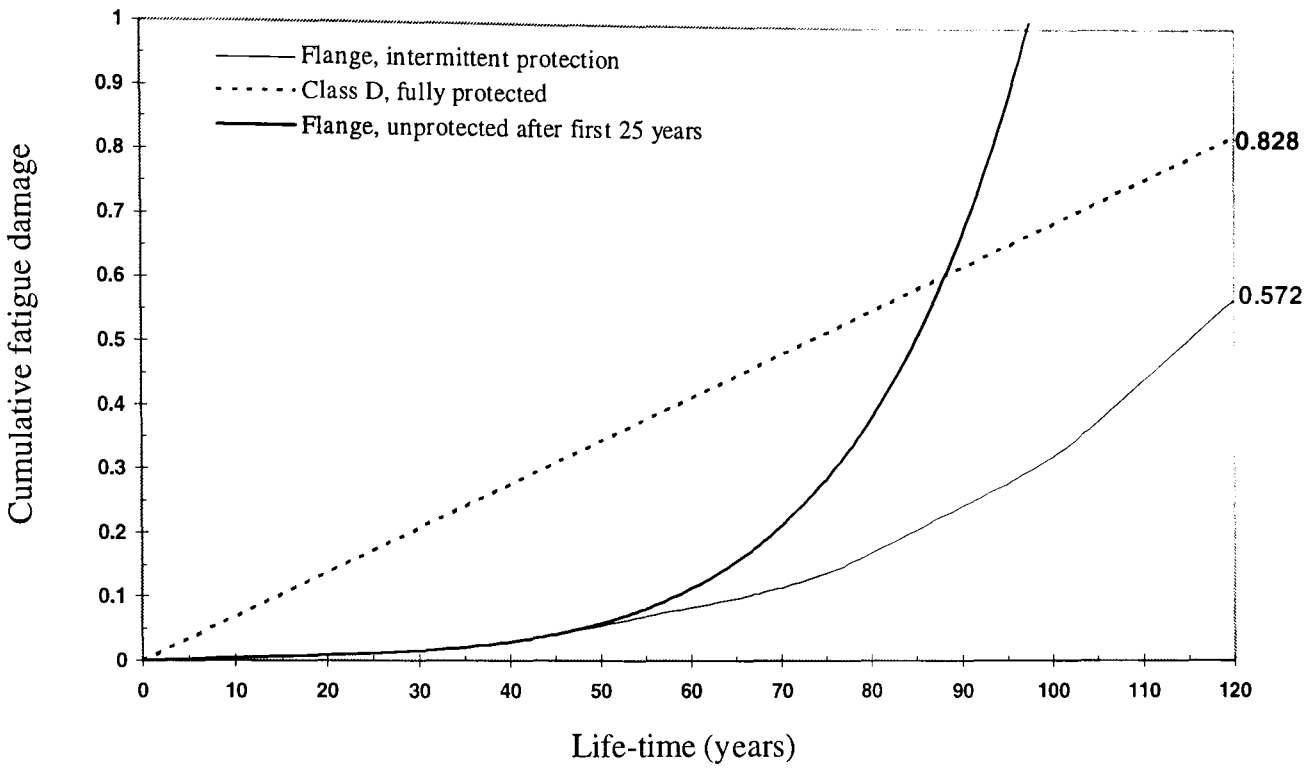

Figure 7.4 Cumulative fatigue damage versus life-time in dry air.

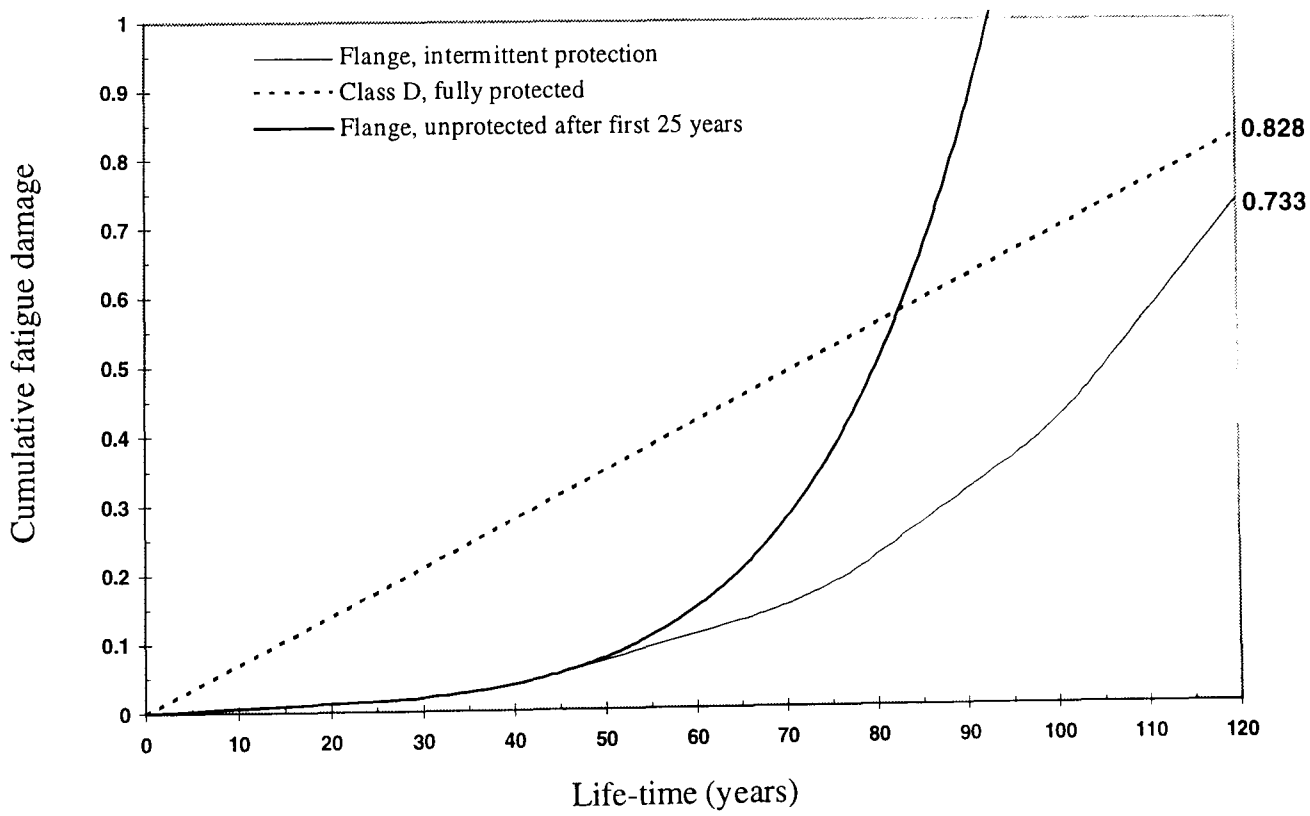

Figure 7.5 Cumulative fatigue damage versus life-time in aqueous environment.

7.5 Probabilistic reliability assessment

The remaining life and hence the level of safety of steel structures diminishes with time due to corrosion damage. It should be clear from the discussion in this thesis so far, and from the data presented, that there are many sources of randomness and uncertainty in the fatigue performance of corroded steel structures. The rate of corrosion is often non-uniform and difficult to predict. Roughness and pitting is highly irregular with substantial scatter in measured data. There is also scatter in the results of fatigue tests. The location of corrosion damage is dependent on uncertain factors such as design of details and local micro-climates. The vulnerability of structures to specific damage location is highly uncertain. Traffic loading is a random variable, not to mention the changes in load spectra with time. There are wide variations in the quality of bridge maintenance and painting frequency. Reliability analysis provides a framework for incorporating some of the uncertainties and in particular load spectra and the randomness inherent in corrosion roughness and in results of fatigue tests.

The theory of structural reliability has been developed to provide an appropriate method of analysis of structural safety. The main purposes of reliability theory is to find the probability of failure, or the reliability function of a structure in a prescribed load environment during its service life. Since Freudenthal (1956) first introduced the concept of probability of failure, the area of Probabilistic Risk Assessment has attracted the attention of many researchers and structural engineers (e.g. Blockley, Cornell, Ditlevsen, Hasofer, Melchers, Moses, Rackwitz and Thoft-Christensen). A great number of methods have been developed to evaluate structural reliability.

The main aim in this section is to examine the effects of corrosion damage on the reliability of a steel plate girder bridge using the data obtained from roughness measurement and fatigue tests of corroded specimens.

The first step was to take the fatigue life against depth of corrosion data (see section 5.6.2). The fatigue performance is shown in Figure 7.6 in terms of log K against mean depth of corrosion, d_c. To take account of the randomness inherent in the fatigue data,

the mean curve is given together with the curves for mean plus one standard deviation and the mean minus one standard deviation. It should be noted the mean curve shown here is the true mean of all the fatigue data. This is different from Figure 7.2 where the mean line was anchored to log $K = 15.37$ which is class B.

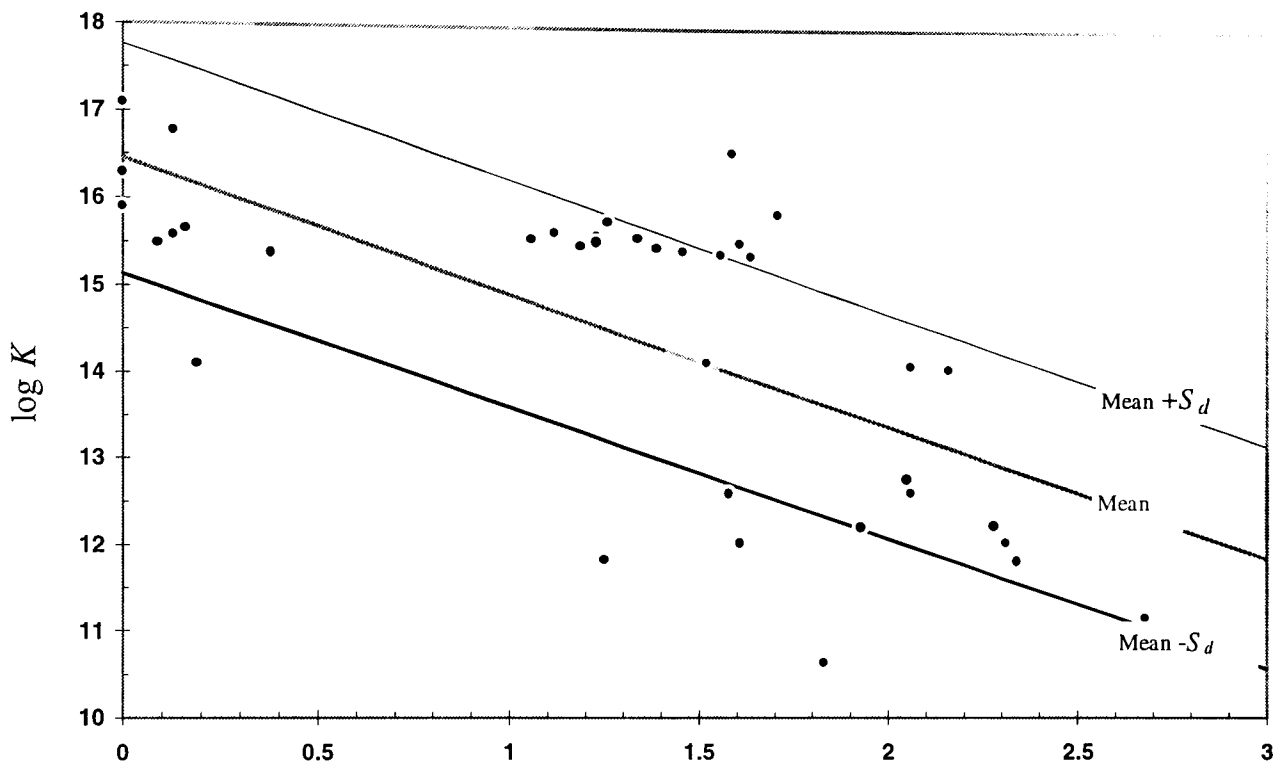

Figure 7.6 Fatigue performance of corroded specimens versus mean depth of corrosion penetration.

The next step was to use equation 7.12 to calculate the cumulative damage over the life of the bridge using the painting intervals in Table 7.2 and vehicle spectrum in Table 7.3. This was done for the mean fatigue curve and was repeated for the mean $+S_d$ and mean $-S_d$. These curves are shown in Figure 7.7.

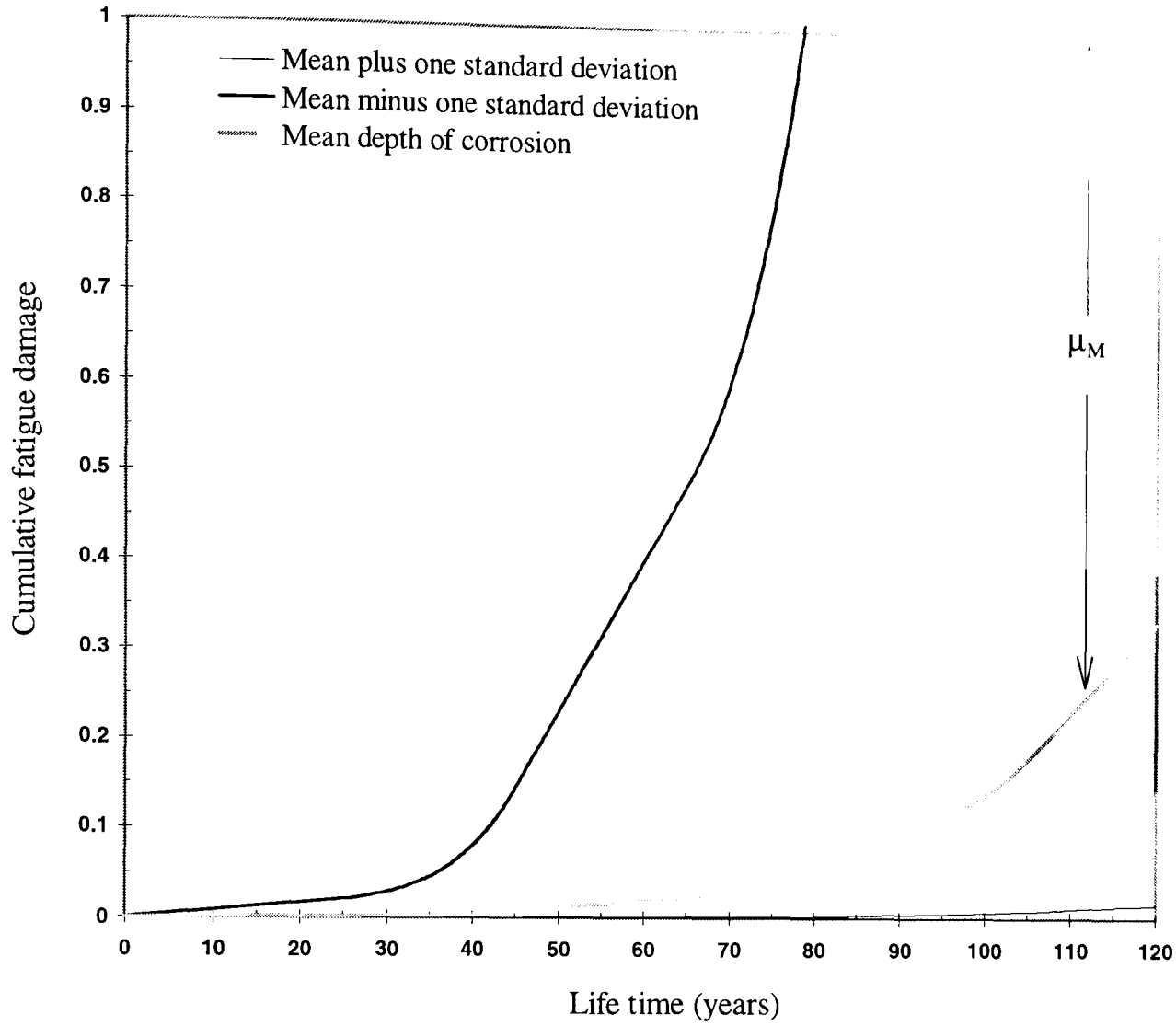

Figure 7.7 Cumulative fatigue damage versus life (mean; mean $+S_d$ and mean $-S_d$).

The reliability index, β, for a structure can be expressed in terms of the mean and standard deviation of structural performance (Cornell 1969) as follows:

$$\beta = \frac{\mu_R - \mu_S}{\sqrt{(S_R)^2 + (S_S)^2}} = \frac{\mu_M}{S_M} \tag{7.14}$$

where

μ_R = mean resistance

μ_S = mean stress

μ_M = mean margin between resistance and applied stress

S_R = standard deviation of resistance

S_S = standard deviation of stress

S_M = standard deviation of the margin

In the case of cumulative damage we will interpret the margin, at a particular time in the life of the bridge, as the difference between a cumulative damage of 1.0 and the cumulative damage of the mean line at that specific time. This is shown in Figure 7.7.

The standard deviation of the margin cannot be determine directly because there is a non-linear relation between the deviation in log K and the corresponding deviation in the total fatigue damage. Therefore, the following simplified procedure was adopted.

If we consider the results of a number of fatigue tests carried out on a corroded sample, of a specified age, we can express the fatigue life of a single test by $(K + e_K)$, where K is the mean value of the constant in the fatigue power law and e_K is the error in the single test. If this same sample were subjected to the traffic load spectrum and corrosion history as if it was part of a bridge, then its total fatigue damage up to the that point in time would be given by

$$\mathrm{TFD} + e_{\mathrm{tfd}} = \int_0^T \Sigma \left(\frac{r(\sigma_r)^m}{(K + e_K)} \right) dt \qquad (7.15)$$

This is equivalent to equation 7.12 except that it takes account of an experimental error in K. Abbreviating the expression for the integral above, the error in the total fatigue damage can be written

$$e_{\mathrm{tfd}} = \int_{e_K} - \mathrm{TFD} \qquad (7.16)$$

It would be possible to calculate a sequence of values of e_{tfd} corresponding to values of e_K generated randomly on a Monte Carlo basis and conforming to the distribution of experimental scatter. In this way the standard deviation of TFD could be calculated approximately from the root mean square error as follows:

$$S_{\mathrm{tfd}} = \sqrt{\frac{1}{n} \Sigma \left(\int_{e_K} - \mathrm{TFD} \right)^2} \qquad (7.17)$$

where n is the number of simulations. For simplicity it is proposed that a good approximation may be obtained from only two calculations, one using $e_K = +S_K$ and the other using $e_K = -S_K$, where S_K is the experimental standard deviation in K. Hence

$$S_{tfd} = \sqrt{\frac{1}{2}\left\{\left(\int_{+S_K} - \mathrm{TFD}\right)^2 + \left(\int_{-S_K} - \mathrm{TFD}\right)^2\right\}} \qquad (7.18)$$

Since the performance margin ($\mu_M = 1 - \mu_{tfd}$) the standard deviation of the margin is the same as equation 7.18. Hence the reliability index, β, can be calculated from equation 7.14. In this way the reliability index was calculated over a period extending from 45 years to 120 years. Prior to 45 years it was found that the values of β are very high and are not included in the graph. This follows the approach adopted by others (Zhao et al 1996). The results are shown in Figure 7.8.

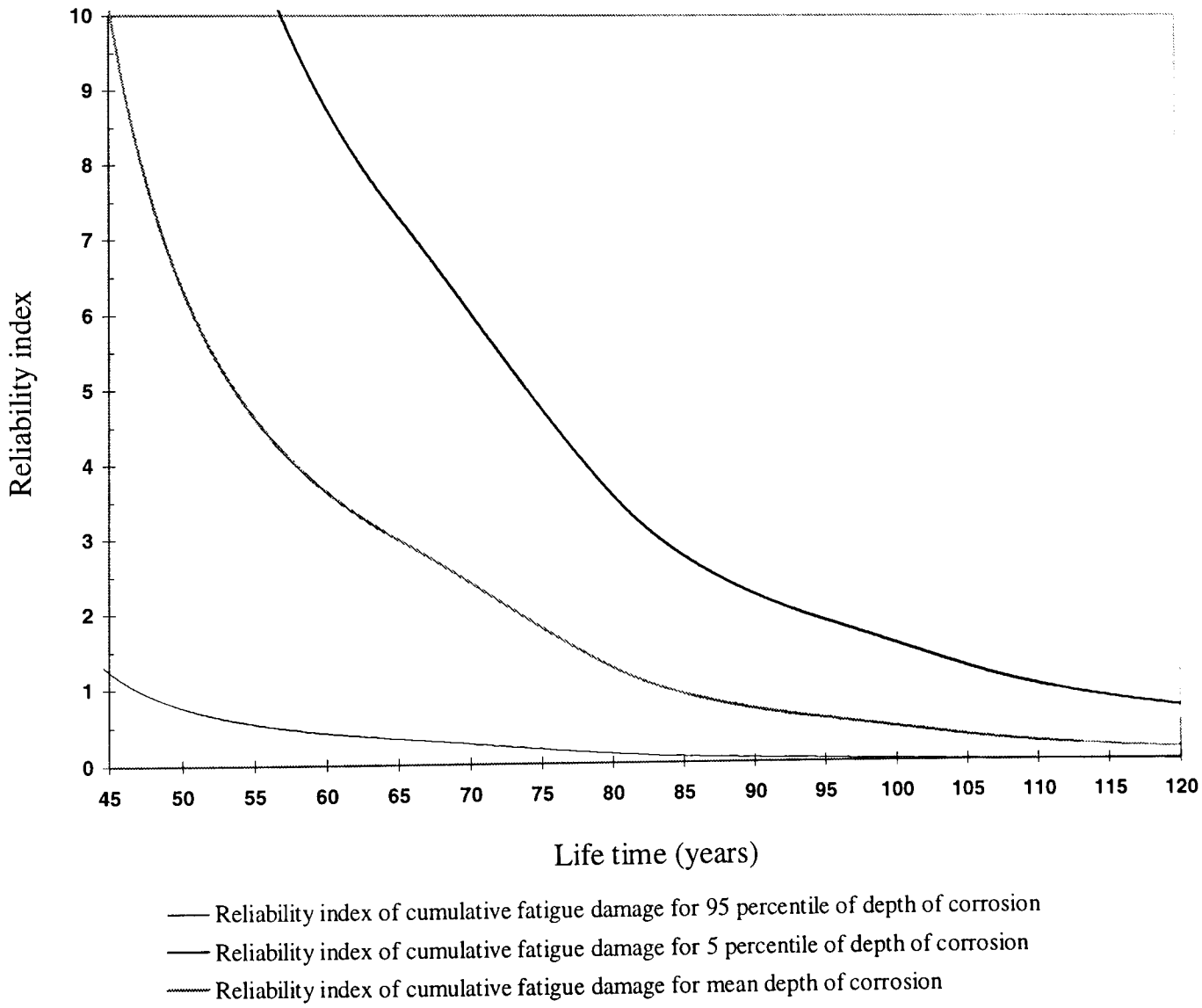

Figure 7.8 Reliability index of cumulative fatigue damage.

The whole procedure was repeated but using the 5 percentile and the 95 percentile values of d_c according to the measurements made in Chapter 3. The curves of β for these additional cases are also shown in Figure 7.8. In this way it was possible to make an assessment of the effects of randomness in corrosion roughness and randomness in fatigue data. Studies by other researchers in the field of reliability have indicated that a value for the index less than about 4 or 5 is some cause for concern. This might not be so significant in the case of fatigue damage which is progressive.

7.6 Summary and conclusions

The analysis of the data provided by roughness measurement and fatigue tests of corroded steel specimens have been used to develop an assessment method to calculate the remaining fatigue life of corroded steel structures. The relationships developed in this study are in terms of thickness loss or pit depth provided by measurement or using the time of exposure. A procedure was developed for calculating the cumulative damage over the life of a steel bridge. This took account of progressive corrosion damage which would occur during periods when the paint system was defective. It also took account of changes in load spectra which have occurred over the years. The procedure for calculating cumulative fatigue damage has been used for different cases of painting intervals. It was observed that when the bridge is painted the cumulative fatigue damage is linear with time and when it started to corrode the slope of cumulative fatigue damage increased non-linearly with time. The knowledge obtained from the assessment of cumulative fatigue damage in different cases indicates that maintenance is essential in existing steel bridges to keep them in service. The analysis was repeated taking account of randomness in the roughness profile and in results of fatigue tests. A procedure was developed for calculating the reliability index over the life of the bridge. It was shown that the reliability index for onset of fatigue failure falls below 4 after about 55 years.

CHAPTER VIII

CONCLUSIONS AND RECOMMENDED RESEARCH

8.1 Conclusions

The deterioration of steel structures has become a very important issue. The condition of all steel structures is subjected to decay with time, due to various factors. The first is the environment. Parts of the structure exposed to wind and rain or in which water or dirt may become trapped will eventually begin to corrode. Another factor is fatigue which is the growth of microscopic cracks in parts of structure due to repeated loading on bridges. For steel girder bridges, apart from fatigue, the most serious form of deterioration is corrosion. The deterioration is often aggravated by inadequate maintenance. Corrosion reduces the static load capacity of girder bridges because of loss of section. Roughness caused by corrosion pits also results in additional stress concentration which may reduce fatigue life further due to the "notch factor" effect. There is a need for a more accurate assessment method which can be used to predict the penetration and remaining fatigue life of existing corroded steel bridges due to pitting corrosion.

The electrochemical process and various forms of corrosion have been discussed along with how these occur on steel bridges and what factors contribute to their occurrence and prevention. The effects of corrosion on steel bridges at the initial stage may be taken as uniform. As the exposure time increases pitting corrosion may occur particularly on top of the bottom flange where water and debris can accumulate due to leakage from expansion joints or the spray created by underpass traffic.

Techniques for measuring corrosion penetration and roughness were reviewed. A technique similar to stylus methods using two displacement transducers was

developed for measurement of surface roughness of corroded specimens in this investigation. It had some potential advantages in accuracy and speed of measurement for the measurement of roughness of existing corroded steel bridges on site. It was concluded that none of the methods investigated are entirely satisfactory for roughness measurement of corroded steelwork directly but can be used to measure the variation in thickness and therefore roughness indirectly using the methods developed for analysis of roughness during this research. The analysis of the data provided by roughness measurement showed that there is linear relation between the depth of corrosion and the degree of roughness or pitting. In particular, it was found that the standard deviation of roughness correlates well with the largest corrosion pits. Furthermore, the linear relation between maximum roughness and overall corrosion depth provides a convenient tool for the assessment of corrosion damaged bridges. The depth of corrosion correlated with roughness parameters for beams from different sites.

The factors which may increase the corrosion penetration of steelwork in the long-term have been identified. The corrosion penetration with time may be predicted by a power function (equation 4.5), but it will be very approximate when applied to a real situation, as the equation was obtained using experimental data from small test coupons. The most sensitive parameter in the corrosion penetration model is the loss exponent B. Variation in B from one environment to another significantly changes the rate of corrosion penetration. These parameters were gathered from the experiments carried out in different environments in the UK. The higher values of A and B indicate that the corrosion penetration was much higher in the UK sites than the USA sites because the air was significantly humid over 80% of the testing period. The relationships developed in this study showed good accuracy for predicting the average maximum roughness. The average maximum roughness compared very well with Copson's method and with Albrecht's data. Therefore, the function which has been developed can be used to predict the average pit depth of corroded steelwork structures. A statistical analysis for maximum roughness measurements was carried out and it was found that the log-normal distribution function fits the data satisfactorily.

The relationship between the fatigue endurance and pitting corrosion was obtained by roughness measurement and fatigue tests of corroded steel specimens. The results of fatigue tests showed that the fatigue life depends on the applied stress range and the irregularity of the corroded surface. Also there was a well correlated reduction in fatigue life of corroded steel specimens with depth of corrosion pitting due to the "notch factor" effect since fatigue cracks in the corroded specimens initiated from the deepest pits and rupture occurred at or within 9 mm of the deepest point of penetration. A considerable reduction in fatigue performance occurred as pit depth increased. The reduced fatigue life due to corrosion pitting may be related to classes of structural detail as used in design codes for fatigue. The linear relation between the overall depth of corrosion and maximum roughness provides the simplest method for the assessment of corrosion damaged steel bridges. This method can indirectly give the quantitative relationship between pitting corrosion and the corresponding remaining fatigue life of corrosion damaged steel structures by measuring loss of thickness.

The results from finite element analysis using ANSYS (a finite element package) suggested that, for the same depth, stresses at the root of the pit in weathering steel are higher than in carbon steel. The fatigue notch factor is an appropriate parameter for quantifying the effect of corrosion deterioration on fatigue life. The fatigue notch factor developed for corrosion penetration may be compared with the fatigue notch factor for a particular class and the one of higher magnitude governs. Based on the data provided from roughness measurement and fatigue tests two relationships were developed for estimating fatigue notch factor which can be used for the assessment of corroded steel structures. The first is in terms of average corrosion penetration and the second is in terms of exposure time. The assessment of the remaining fatigue life of existing corroded steel structures, in terms of fatigue notch factor, requires only information of the average corrosion penetration or the time of exposure at the time of the assessment.

The analysis of the data provided by roughness measurement and fatigue tests of corroded steel specimens have been used to develop a procedure for assessing the

cumulative fatigue damage of steel bridges in terms of exposure time, stress range, and number of vehicles per year. It was observed from the numerical example that when a bridge is protected by paint work the cumulative fatigue damage is linear but when it starts to corrode the slope of cumulative fatigue damage curve increases non-linearly with the time of exposure. This demonstrated the importance of the continued maintenance of steel bridges. The cumulative damage due to corrosion of a class B detail on a poorly maintained bridge was more severe than a well maintained class D detail. The influence of an aqueous environment on more rapid corrosion fatigue was also investigated. A procedure was developed for calculating the reliability index over the life of the bridge and it was found that the reliability index for onset of fatigue failure falls below 4 after about 55 years.

8.2 Suggestions for further research

1. Further research into the corrosion penetration of actual bridges is needed. These studies should investigate the relationship between corrosion and bridge design and local environment. There is a need to develop a convenient tool for on-site measurement of corrosion penetration and roughness, and use it in the assessment of a number of actual bridges.

2. Corrosion fatigue tests of typical welded joints under conditions representative of bridge service environments are required. These should include large specimens, realistic cycling rates, variable amplitude loading and intermittent spray. *S-N* data, in addition to crack growth rate data should be obtained for typical detail classes. In this case the effect of corrosion on the total life (crack initiation and propagation) can be determined.

3. There are many uncertainties in the assessment of steel bridges affected by corrosion. These include: uncertainties surrounding maintenance and re-painting cycles; uncertainties concerning the influence of the environment and design of details on the corrosion rate; variability of heavy vehicle traffic loads; the wide scatter in roughness data itself. There is a need to consider probabilistic methods in the assessment of ageing steel bridges.

REFERENCES

Abbott E. J and Firestone F. A (1933)

Specifying Surface Quality, Mechanical Engineering, Vol. 55, pp. 569-572.

Abbott E. J and Goldschmidt E (1937)

Surface Quality, Mechanics Engineering, Vol. 59, pp. 813-825.

Ahmad H. Y and Yates J. R (1994)

An Elastic-Plastic Model for Fatigue Crack Growth at Notches, Journal of Fatigue and Fracture of Engineering Materials & Structures, Vol. 17, No. 6, pp. 651-660.

Albrecht P and Friedland I. M (1980)

Fatigue Tests of 3-Year Weathered A588 Steel Weldment, Journal of the Structural Division, Proceedings of the American Society of Civil Engineers, Vol. 106, No. ST5, pp. 991-1003.

Albrecht P and Simon S (1981)

Fatigue Notch Factors for Structural Details, Journal of the Structural Division, Proceedings of the American Society of Civil Engineers, Vol. 107, No. ST7, pp. 1279-1296.

Albrecht P (1983)

Fatigue Design Stresses for Weathering Steel Structures, Corrosion Fatigue: Mechanics, Metallurgy, Electrochemistry, ASTM STP 801, Crooker T. W and Leis B. N. Eds., American Society for Testing and Materials, pp. 445-471.

Albrecht P and Naeemi A. H (1984)

Performance of Weathering Steel in Bridges, National Cooperative Highway Research Program, Report 272, Transportation Research Board, National Research Council. Washington, D.C.

Albrecht P and Sidani M (1987)

Fatigue Strength of 8-Year Weathered Stiffeners in Air and Salt Water, National Cooperative Highway Research Program, Report 10-22/1, Department of Civil Engineering, University of Maryland, College Park, Maryland.

Albrecht P (1988)

Fatigue Strength of A588 Steel Beams, Department of Civil Engineering, University of Maryland, College Park, Maryland.

Albrecht P and Gouping X (1988)

Fatigue Strength of Long-Term Weathered Rolled Beam, Maryland Department of Transportation.

Albrecht P, Coburn S. K, Wattar F. M, Tinklenberg G. L and Gallagher W. P (1989)

Guidelines for the Use of Weathering Steel in Bridges, National Cooperative Highway Research Program, Report 314, Transportation Research Board, National Research Council, Washington, D.C.

Albrecht P, Shabshab C. F, Li W and Wright W (1990)

Remaining Fatigue Strength of Corroded Steel Beams, International Association for Bridge and Structural Engineering Workshop, Vol. 59, pp. 71-84.

Albrecht P and Lee H (1991)

Evaluation of Rating Numbers for Atmospheric Corrosion Resistance of Weathering Steel, Journal of Testing and Evaluation, Vol. 19, No. 6, pp. 429-439.

Albrecht P and Shabshab C. F (1994)

Fatigue Strength of Weathered Rolled Beam Made of A588 Steel, Journal of Materials in Civil Engineering, Proceedings of the American Society of Civil Engineers, Vol. 6, No. 3, pp. 407-428.

Alm L. O (1977)

Rut Formation in Road Surfaces, Drawbacks, Critical Rut Depth and Method of Measurement, VTI Report, National Road and Traffic Research Institute, Fack, Linkoping, Sweden.

American Society for Metals (ASM 1976)

Ultrasonic Inspection, Metals Handbook, Eighth Edition, Ed. Boyer H. E, American Society for Metals, Metals Park, Ohio, Vol. 11, pp. 161-198.

American Standard Association (1955)

Surface Roughness, Waviness and Lay, American Standard Association, ASA, Vol. 46.

Anon (1983)

Rusted Supports Snap, Drop Old Bridge Span, Engineering News-Record.

Anon (1984)

State Blamed for Failure, Engineering News-Record, Vol. 213, No. 1, p. 27.

ASTM, G1 (1981)

Standard Practice for *Preparing, Cleaning, and Evaluating Corrosion Test Specimens*, ASTM Designation: G1, American Society for Testing and Materials, 1981 Annual Book of ASTM Standards, Part 10, pp. 829-834.

ASTM, G16 (1981)

Standard Recommended Practice for *Applying Statistics to Analysis of Corrosion Data*, ASTM Designation: G16, American Society for Testing and Materials, 1981 Annual Book of ASTM Standards, Part 10, pp. 880-901.

ASTM, G46 (1981)

Standard Recommended Practice for *Examination and Evaluation of Pitting Corrosion*, ASTM Designation: G46, American Society for Testing and Materials, 1981 Annual Book of ASTM Standards, Part 10, pp. 1005-1014.

ASTM, E797 (1983)

Standard Practice for *Measuring Thickness by Manual Ultrasonic Pulse-Echo Contact Method*, ASTM Designation: E797, American Society for Testing and Materials, 1983 Annual Book of ASTM Standards, Vol. 03.03, pp. 721-727.

Bakht B and Csagoly P. F (1979)

Bridge Testing, Research Report No. 79-10, Ministry of Transportation and Communications of Ontario, Ontario, Canada.

Ballard D. B and Yakowitz H (1969)

Mechanism Leading to the Failure of the Point Pleasant, West Virginia Bridge, Part 3, National Bureau of Standards Report No. 9981 to United State Bureau of Public Roads.

Barsom J. M and Novak S. R (1977)

Sub-Critical Crack Growth in Steel Bridge Members, National Cooperative Highway Research Program, Report 181, Transportation Research Board, National Research Council, Washington, D.C.

Barwell F. T (1956)

Lubrication of Bearings, Published by Butterworths Scientific, London.

Bass G. G and Fuchs J. M (1963)

Wave Scattering of Electromagnetic Waves from Rough Surfaces, Macmillan, New York.

Beckmann P and Spizzichino A (1963)

The Scattering of Electromagnetic Wave from Rough Surfaces, Pergamon, Oxford.

Beckwith T. G, Marangoni R. D and Lienhard J. H (1993)

Mechanical Measurements, Fifth Edition, Published by Addison-Wesley Publishing Company, Reading, New York.

Bellenoit J. R, Yen B. T and Fisher J. W (1984)

Stresses in Hanger Plates of Suspended Bridge Girders, Transportation Research Record 950, National Research Council, Washington D.C., pp. 20-23.

Bendat J. S and Piersol A. G (1986)

Random Data; Analysis and Measurement Procedures, Second Edition, Published by John Wiley & Sons, New York, pp. 14-20.

Bengough G. D and Wormwell F (1935)

Special Report for Corrosion Committee, Iron and Steel Institute, Vol. 3, p. 168.

Bennett J (1994)

Introduction to Surface Roughness, Optical Society of America, Washington D.C.

Bennett J. M and Mattsson L (1989)

Introduction to Surface Roughness and Scattering, Optical Society of American, Washington D.C.

Bennett J. M, Elings V and Kjoller K (1993)

Recent Developments in Profiling Optical Surfaces, Allied Optics, Vol. 32, No. 19, pp. 3442-3447.

Berry M. V and Hannay J. H (1978)

Topography of Random Surfaces, Nature, Vol. 271, p. 573.

Bhushan B (1990)

Tribology and the Mechanics of Magnetic Storage Devices, Springer, New York.

Bhushan B (1995)

Handbook of Micro/Nanotribology, Published by CRC Press, p. 82.

Binning G, Rohrer H, Gerber C and Weibel E (1982)

Surface Studies by Scanning Tunnelling Microscopy, Physics Review Letters, Vol. 49, pp. 57-61.

Blackman R. B and Tukey J. W (1958)

The Measurement of Power Spectra, New York, Dover Publications.

Blessing G. V and Eitzen D. G (1988)

Ultrasonic Sensor for Measuring Surface Roughness, in Surface Measurement and Characterization, Bennett J. M, Edited by Proceedings of the Society of Photo-Optical Instrumentation Engineers, Vol. 1009, pp. 281-289.

Blessing G. V, Slotwinski J. A, Eitzen D. G and Ryan H. M (1993)

Ultrasonic Measurements of Surface Roughness, Journal of Applied Optics, Vol. 32, No. 19, pp. 3433-3437.

Bohenenkamp K, Burgmann G and Schwenk W (1973)

Investigations of the Atmospheric Corrosion of Plain Carbon and Low Alloy Steels in Sea, Country and Industrial Air, Stahl und Eisen, Vol. 93, No. 22, pp. 1054-1060.

Bowden F. P and Tabor D (1950)

The Friction and Lubrication of Solids, Part I, Oxford.

Bragard A. A and Bonnarens H. E (1982)

Prediction at Long-Terms of the Atmospheric Corrosion of Structural Steels from Short-Term Experimental Data, Atmospheric Corrosion of Metals, ASTM STP 767, pp. 339-358.

Brandes K (1990)

Crack Growth Tests to Assess the Remaining Fatigue Life of Old steel Bridges, International Association for Bridge and Structural Engineering Workshop, Vol. 59. pp. 103-109.

Briant C. L (1985)

Metallurgical Aspects of Environmental Failures, Material Science Monographs. Vol. 12, Elsevier, Amsterdam, pp. 31-47.

Brockenbrough R. L (1983)

Consideration in the Design of Bolted Joints for Weathering Steel, AISC Engineering Journal, American Institute of Steel Construction, Vol. 20, No. 1, pp. 40-45.

Broderick R. F (1985)

Harvard Bridge Eyebar Failures, Proceedings of the Failure Analysis Program at the International Conference And Exposition of Fatigue, Corrosion Cracking, Fracture Mechanics and Failure Analysis: Salt Lake City, Utah.

BS 1134 (1961)

Centre-Line-Average Height Method for the Assessment of Surface Texture, British Standards Institution, London.

BS 4360 (1990)

Specification for Weldable Structural Steels, British Standards Institution, London.

BS 5400 (1980)

Steel, Concrete and Composite Bridges, Part 10, Code of Practice for Fatigue, British Standards Institution, London.

Burdekin F. M (1985)

Engineering Design Against Fracture at Stress Concentrators. Materials Science and Technology, Vol. 1, No. 1, pp. 487-493.

Burdekin F. M (1993)

Non-Destructive Testing of Structural Steelwork. Proceedings of the Institution of Civil Engineers, Structures and Buildings, Vol. 99, pp. 85-95.

Burrill L (1986)

Superintendent of Bridge Inspection Division Michigan Department of Transportation, Private Communication, January 1986.

Buxbaum O (1983)

Vergleich der Lebensdauervorhersage nach dem Kerbgrundkonzept und dem Nennspannungskonzept, LBF Bericht FB-169, LBF, Darmstadt.

Byers W. G (1979)

Structural Details and Bridge Performance, Journal of the Structural Division, Proceedings of the American Society of Civil Engineers, Vol. 105, No. ST7, pp. 1393-1404.

Caber P. J (1993)

Interferometric Profile for Rough Surfaces, Applied Optics, Vol. 32, No. 19, pp. 3438-3441.

Chaka R. J (1979)

The Design and Development of a Highway Speed Road Profilometer, Transaction of Society of Automotive Engineers, Section 1, Vol. 87, Paper No. 780064, pp. 200-204.

Champion F. A (1964)

Corrosion Testing Procedures, Edited by Chapman and Hall, London.

Champion F. A (1965)

Corrosion Testing Procedures, Second Edition, John Wiley & Sons, New York, p. 205.

Chandler K. A and Kilcullen M. B (1970)

Corrosion Resistant Low-Alloy Steels, A Review with Particular Reference to Atmospheric Conditions in the United Kingdom, British Corrosion Journal, Vol. 15. No. 1, pp. 24-32.

Charlton P. C (1996)

Evaluation Current Option for Non-Destructive Testing, Bulk Liquid Storage Tank Conference, London.

Chen C. M, Froning M. H and Verink E. D (1976)

Crevice Corrosion and Its Relation to Stress Corrosion Cracking, Stress Corrosion New Approaches, ASTM STP 610, American Society for Testing and Materials, pp. 289-307.

Choate P and Walter S (1981)

America in Ruins-The Decaying Infrastructure, Duke University Press, Durham, NC, 1983, (Originally by the Council of State Planning Agencies, 1981).

Coburn S. K (1974)

Enhancing the Performance of Offshore Steel Structures, Offshore Technology Conference, Paper No. OTC 2139, Texas, pp. 1081-1110.

Coburn S. K (1978)

Increasing Container Service Life with Painted USS COR-TEN Steel, Container Technology, Vol. II, Proceedings of Second Container Technology Conference, Brighton, England, pp. 177-199.

Cohen D. K, Caber P. J and Brophy C. P (1992)

Rough Surface Profiler and Method, US Patent 5,133,601.

Congleton J, Olieh R. A and Parkins R. N (1982)

Corrosion Fatigue Crack Nucleation in 1.5Mn-0.5Si Steel, Metal Technology, Vol. 9. pp. 94-103.

Cooper D. R. C (1983)

High-Speed Profilometer Measurements on the Rut Humber Bridge, Transport and Road Research Laboratory, TRRL Laboratory Report 794, Pavement Design and Maintenance Division, Highways and Structures Department, Crowthorne, UK.

Copson H. R and Larrabee C. P (1959)

Extra Durability of Paint on Low-Alloy Steels, ASTM Bulletin, American Society for Testing and Materials.

Copson H. R (1960)

Long-Time Atmospheric Corrosion Tests on Low-Alloy Steels, American Society for Testing and Materials, Vol. 60, pp. 650-667.

Cornell C. A (1969)

A Probability Based Structural Code, Journal of American Concrete Institute, Vol. 66, No. 12, pp. 974-985.

Courtel R and Tichvinsky L. M (1963)

A Brief History of Friction, Mechanical engineering, Part I, pp. 55-59.

Creath K (1988)

Phase-Shifting Interferometry Techniques, in Progress in Optics, Wolf E, Edited by Elsevier, New York, Vol. 26, pp. 357-373.

Crews D. L (1976)

Interpretation of Pitting Corrosion Data from Statistical Prediction Interval Calculations, Galvanic and Pitting Corrosion: Field and Laboratory Studies. ASTM STP 576, pp. 217-230.

Culp J. D and Tinklenberg G. L (1980)

Interim Report on Effect of Corrosion on Steel Bridges of Unpainted A588 Steel and Painted Steel Types, Michigan Department of State Highways and Transportation, Testing and Research Division, Lansing, Michigan.

Cygnus Instruments Ltd (1992)

Ultrasonic Inspection of Weathering Steel, Technical Report, the Cygnus Instruments Limited, Cygnus House, 30 Prince of Wales Road, Dorchester, Dorset, England.

Cygnus Instruments Ltd (1996)

Saving Time on Bridge Inspections, Insight, The Journal of British Institute of Non-Destructive Testing, Vol. 38, No. 11, pp. 772-773.

Davidson M, Kaufman K, Mazor I and Cohen F (1987)

An Application of Interference Microscopy to Integrated Circuit Inspection and Metrology, in Integrated Circuit Metrology, Inspection and Process Control, Monahan K. M, Edited by Proceedings of the Society of Photo-Optical Instrumentation Engineers, Vol. 775, pp. 233-247.

Dexter S. C (1986)

Biologically Induced Corrosion, Edited by National Association of Corrosion Engineers, Houston.

Dickerson R. S and Mace D. G. W (1976)

A High-Speed Profilometer (Preliminary Description), Department of the Environment, Transport and Road Research Laboratory, TRRL Laboratory Report SR 182 UC, Crowthorne, UK.

Dovey R. R (1991)

Non-Contact Surface Measurement Shows Broad Applications, Metallurgia, Vol. 58, p. 462.

Dowson D (1979)

History of Tribology, Published by Longman, London and New York.

Drury J. C (1997)

Corrosion Monitoring and Thickness Measurement-What Are We Doing Wrong?, Insight, The Journal of British Institute of Non-Destructive Testing, Vol. 39, No. 1, pp. 17-20.

Dupuy O (1968)

High-Precision Optical Profilometer for the Study of Micro-Geometrical Surface Defects, Proceedings of the Instrumentation for Mechanical Engineers, Vol. 182, Part 3K, pp. 255-259.

Dutems C (1987)

Anti-Corrosion Protection Investigation Concerning Cost and Service Life, Proceeding of the US European Workshop on the Rehabilitation of Bridges, Paris, France.

Dyson A (1978)

Hydrodynamic Lubrication of Rough Surfaces- A Review of Theoretical Work, Surface Roughness Effects in Lubrication, Edited by Dowson, Taylor, Godet and Berthe, pp. 61-70.

Elliott A. L (1969)

Bigger Bridge Loads Coming: Will we be Ready?, Civil Engineering, Vol. 39, pp. 52-53.

Ellis O. B and LaQue F. L (1951)

Area Effects in Crevice Corrosion, Corrosion, Vol. 7, No. 11, pp. 362-364.

Ernst H and Merchant M. E (1940)

Surface Friction of Clean Metals-A Basic Factor in the Metal Cutting Process, Proceedings of a Special Summer Conference on Friction and Surface Finish, Tech. Press, M.I.T.

Evans U. R (1963)

An Introduction to Metallic Corrosion, Second Edition, Edward Arnold Ltd.. London.

Evans U. R (1981)

An Introduction to Metallic Corrosion, Third Edition, Edward Arnold Ltd., London.

Federal Highway Administration (1982)

Safe Life Design for Bridges, Annual Progress Report, Project 5L, Federally Coordinated Program of Research and Development in Highway Transportation, Federal Highway Administration, Office of Research, Development and Technology.

Federal Highway Administration (1984)

Highway Bridge Replacement and Rehabilitation Program, Fifth Annual Report to Congress, Federal Highway Administration (FHWA).

Fenn J (1997)

Private Communication with Loading Section of Highways Agency in London.

Fisher J. W, Frank K. H, Hirt M. A and McNamee B. M (1970)

Effect of Weldments on the Fatigue Strength of Steel Beams, NCHRP Report No. 102, Transportation Research Board, National Research Council, Washington, D.C.

Fisher J. W, Albrecht P. A, Yen B. T, Klingerman D. J and McNamee B. M (1974)

Fatigue Strength of Steel Beams with Welded Stiffeners and Attachments, NCHRP Report 147, Transportation Research Board.

Fisher J. W (1984)

Fatigue and Fracture in Steel Bridges, Third Edition, John Wiley & Sons, Inc., pp. 8-32.

Fontana M. G (1987)

Corrosion Engineering, McGraw-Hill Book Company, New York, Third Edition, pp. 12-152.

Fountain R. S, Munse W. H and Sunbury R. D (1968)

Specifications and Design Relations, Journal of the Structural Division, ASCE, Vol. 94, No. ST 12, pp. 2751-2767.

France W. D (1972)

Crevice Corrosion of Metals, Localized Corrosion Case of Metal Failure, American Society for Testing and Materials, ASTM STP 516, pp. 162-200.

Frank R and Stone J (1963)

Metal Fatigue and Its Recognition, Engineering Division, Bulletin No. 63-1, Bureau of Safety, Civil Aeronautics Board.

Freudenthal A. M (1956)

Safety and Probability of Structural Failure, Trans. of ASCE, Vol. 121, pp. 1337-1397.

Friedland I. M, Albrecht P and Irwin G. R (1982)

Fatigue of Two-Years Weathered A588 Stiffeners and Attachments, Journal of the Structural Division, ASCE, Vol. 108, No. ST 1, pp. 125-144.

Gaythwaite J (1981)

The Marine Environment and Structural Design, Von Nostrand Reinhold Company, New York.

Grattesat G (1982)

Rating and Evaluation of Remaining Life of Bridges, Maintenance, Repair and Rehabilitation of Bridges, International Association for Bridge and Structural Engineering Symposium, pp. 75-89.

Greenwood J. A and Williamson J. B. P (1966)

Contact of Nominally Flat Surfaces, Proceeding of Royal Society, London, Vol. A295, pp. 300-319.

Greenwood J. A and Williamson J. B. P (1977)

Development in the Theory of Surface Roughness, Pare VI(i), Surface Roughness Effects in Lubrication, Edited by Dowson D, Taylor C. M, Godet, M and Berthe D, Proceedings of the 4th Leeds-Lyon Symposium on Tribology, pp. 167-177.

Gurney T. R (1979)

Fatigue of Welded Structures, Second Edition, Cambridge University Press, Cambridge, UK.

Guttman H and Sereda P. J (1968)

Measurement of Atmospheric Factors Affecting the Corrosion of Metals, Metal Corrosion in the Atmosphere, ASTM STP 435, pp. 326-359.

Haesing J (1961)

Determining Surface Finish of Workpieces by Means of Surface Standards, Microtecnie, Vol. 15 pp. 24-28.

Hahin C, South J. M, Mohammadi J and Polepeddi R. K (1993)

Accurate and Rapid Determination of Fatigue Damage in Steel Bridges, Journal of Structural Engineering, ASCE, Vol. 119, No. 1, pp. 150-168.

Halliday J. S (1955)

Surface Examination by Reflection Electron Microscopy, Proceedings of Institution of Mechanical Engineers, Vol. 169, No. 38, p. 177.

Halling J (1975)

Principles of Tribology, Published by Macmillan Press, London and Basingstoke.

Halmshaw R (1991)

Non-Destructive-Testing, Second Edition, Edward Arnold, London.

Harries J. E (1990)

Journal of the Institute of Metals, London, Vol. 6, No. 10.

Hasunuma H (1966)

Statistical Characteristic of Surface Profile, Bulletin, Japan Society Precision Engineers, Vol. 1, No. 4, pp. 205-211.

Haynie F. H and Upham J. B (1974)

Correlation Between Corrosion Behaviour of Steel and Atmospheric Pollution Data, Corrosion in Natural Environments, American Society for Testing and Materials, ASTM STP 558, pp. 33-51.

Haynie F. H, Spence J. W and Upham J. B (1978)

Effects of Air Pollutants on Weathering Steel and Galvanised Steel, A Chamber Study, Atmospheric Factors Affecting the Corrosion of Engineering Metals, ASTM STP 646, American Society for Testing and Materials, pp. 30-47.

Hearn G and Testa R. B (1991)

Modal Analysis for Damage Detection in Structures, Journal Structural Engineering, Proceedings of the American Society of Civil Engineers, Vol. 117, No. 10, pp. 3042-3063.

Hendawi S. A (1994)

Structural System Reliability with Applications to Bridge Analysis and Optimisation, Ph.D Thesis, Department of Civil Engineering, University of Colorado.

Henry J. J and Hegmon R. R (1975)

Pavement Texture Measurement and Evaluation, Edited in Rose J. G "Surface Texture Versus Skidding: Measurements, Frictional Aspects, and Safety Features of Tire-Pavement Interactions," ASTM STP 583, 3-17, American Society for Testing and Materials.

Herbsleb G and Schwenk W (1985)

The Influence of Dynamic Mechanical Parameters on Stress Corrosion Cracking of Steel-A Review, Corrosion, Vol. 41, No. 8, pp. 431-437.

Hetenyi M (1950)

Handbook of Experimental Stress Analysis, John Wiley, New York.

Heywood R. B (1952)

Designing by Photoelasticity, Chapman and Hall Ltd.

Hiam J. R and Pietrowski R (1978)

The Influence of Forming and Corrosion on the Fatigue Behaviour of Automotive Steel, SAE Technical Paper No. 780040, Society of Automotive Engineers, pp. 132-140.

Hill G. V (1985)

Tower Bridge; Keeping Corrosion at Bay, Materials Performance, pp. 78-79.

Hirt M. A (1982)

Remaining Fatigue Life of Bridges, Maintenance, Repair and Rehabilitation of Bridges, International Association for Bridge and Structural Engineering Symposium, pp. 113-129.

Ho S. K, White R. M and Lucas J (1990)

A Vision System for Automated Crack Detection in Welds, Measurement Science Technology, Vol. 1, pp. 287-294.

Hondros E. D (1971)

Tribology, Published by Mills & Boon Limited, London, pp. 26-27.

Hopwood T and Havens J. H (1984)

Corrosion of Cable Suspension Bridges, Research Report UKTRP-84-84, Kentucky Transportation Research Program, University of Kentucky, pp. 70.

Hsiong W (1978)

Repair of Poplar Street Complex Bridge in East St. Louis, Transportation Research Record 664: Bridge Engineering, Vol. 1, Transportation Research Board, National Research Council, Washington, D.C.

Hudak S. J and Page R. A (1983)

Analysis of Oxide Wedging During Environment Assisted Crack Growth, Corrosion, Vol. 39, No. 7, pp. 285-290.

Hu Qiao and Xu Hao (1995)

Two-Parameter Nominal Stress Approach, International Journal of Fatigue, Vol. 17, No. 5, pp. 339-341.

IJsseling F. P (1980)

Electrochemical Method in Crevice Corrosion Testing, British Corrosion Journal, Vol. 15, Editor, Brasher, D. M, The Metal Society, London, pp. 51-69.

Iles D. C (1991)

Design Guide for Simply Supported Composite Bridges, The Steel Construction Institute, Berkshire, UK.

Jacobson R. D, Wilson S. R, Al-Jumaily G. A, McNeil J. R, Bennett J. M and Mattsson L (1992)

Microstructure Characterisation by Angle-Resolved Scatter and Comparison to Measurements Made by Other Techniques, Applied Optic, Vol. 31, pp. 1426-1435.

Jaske C. E, Broek D, Slater J. E and Anderson W. E (1978)

Corrosion Fatigue of Structural Steels in Seawater and for Offshore Applications, Corrosion Fatigue Technology, ASTM STP 642, Craig Jr., Crooker T. W and Hoeppner D. W, American Society for Testing and Materials, pp. 19-47.

Johnson K (1992)

Corrosion Resistance, Steel Designers' Manual, Owens G. W and Knowles P. R, 1992, The Steel Construction Institute, Fifth Edition, Edited by Blackwell Scientific Publications, London, pp. 998-1019.

Jolic K. I, Nagarajah C. R and Thompson W (1994)

Non-Contact, Optically Based Measurement of Surface Roughness of Ceramics, Measurement Science and Technology, Vol. 5, pp. 671-684.

Jordan P. G and Still P. B (1982)

Measurement of Rut Depths in Road Surfaces by the TRRL High-Speed Profilometer, Transport and Road Research Laboratory, TRRL Laboratory Report 1037, Construction and Maintenance Division, Highways Department, Crowthorne, UK.

Karpenko G. V and Vasilenko I. I (1979)

Stress Corrosion Cracking of Steels, Freund Publishing, Tel-Aviv, Israel.

Kayser J. R, Malinski T and Nowak A. S (1987)[1]

Corrosion Damage Models for Steel Girder Bridges, Effect of Damage and Redundancy on Structural Performance (Edited by Frangopol, D. M), Presented at the ASCE 1987 Convention, Atlantic City, pp. 9-22.

Kayser J. R and Nowak A. S (1987)[2]

Evaluation of Corroded Steel Bridges, Structures Congress Related to Bridge and Transmission Line Structures, American Society of Civil Engineers, Orlando, Florida, pp. 35-47.

Kayser J. R and O'Neil M. A (1987)[3]

The Inspection of Steel Bridges for Corrosion, Paper No. IBC-87-32, Proceedings of Fourth International Bridge Conference, Pittsburgh, Pennsylvania, pp. 154-157.

Kayser J. R (1988)

The Effect of Corrosion on the Reliability of Steel Girder Bridges, Ph.D Thesis, Department of Civil Engineering, University of Michigan.

Kayser J. R and Nowak A. S (1989)

Capacity Loss Due to Corrosion in Steel-Girder Bridges, Journal of Structural Engineering, ASCE, Vol. 115, No. 6, pp. 1525-1537.

Kilcullen M. B and McKenzie M (1979)

Weathering Steel, Proceeding of the Conference, Corrosion in Civil Engineering, Institution of Civil Engineers, London.

Kim J. B, Brungraber R. J and Kun R. H (1988)

Recycling Bridges, Civil Engineering, pp. 58-59.

Kitagawa H, Fujita T and Miyazawa K (1978)

Small Randomly Distributed Cracks in Corrosion Fatigue, Corrosion Fatigue Technology, ASTM STP 642, Craig H. L, Crooker T. W and Hoppner D. W, American Society for Testing and Materials, pp. 98-114.

Kitagawa H, Tsuji K, Hisada T and Hashimoto Y (1983)

An Analysis of Random Pits in Corrosion Fatigue: A Statistical Three-Dimensional Evaluation of an Irregularly Corroded Surface, Corrosion Fatigue: Mechanics, Metallurgy, Electrochemistry, ASTM STP 801, Crooker T. W and Leis B. N, pp. 147-158.

Klingerman D. J and Fisher J. W (1973)

Threshold Crack Growth in A36 Steel, Fritz Engineering Laboratory Report No. 386.2, Lehigh University, Bethlehem, Pennsylvania.

Knofel D (1978)

Corrosion of Building Materials, Van Nostrand Reinhold Company, New York, London.

Knotkova C. D, Vlckova J and Honzak J (1982)

Atmospheric Corrosion of Weathering Steels, Atmospheric Corrosion of Metals, ASTM STP 767, pp. 7-44.

Kohon T, Ozawa N, Miyamoto K and Musha T (1988)

High Precision Optical Surface Sensor, Applied Optic, Vol. 27, pp. 103-108.

Kont J. F (1982)

Chemical and Mechanical Aspects of Crack Initiation and Growth in Interactive Environments, Metal Technology, Vol. 9, pp. 86-93.

Komp M. E (1987)

Atmospheric Corrosion Ratings of Weathering Steels-Calculations and Significance, Journal of Materials Performance, Vol. 26, No. 7, pp. 42-44.

Krautkramer J and Krautkramer H (1975)

Ultrasonic Testing of Materials, Published by Spring-Verlag, Berlin Heidelberg and New York, Third Edition.

Kuhn P and Hardraht H. F (1991)

An Engineering Method for Estimating the Notch-Size Effect in Fatigue Tests on Steel, NACA TN2805, Langley Aeronautical Laboratory, Washington.

Kulicki J. M, Prucs Z, Sorgenfrei D. F and Mertz D. R (1990)

Guidelines for Evaluating Corrosion Effects in Existing Steel Bridges, National Cooperative Highway Research Program, Report 333, Transportation Research Board, National Research Council, Washington, D.C.

Lange D. A, Jennings H. M and Shah S. P (1993)

Analysis of Surface Roughness using Confocal Microscopy, Journal of Materials Science No. 28, pp. 3879-3884.

Larrabee C. P (1941)

The Effect of Specimen Position on Atmospheric Corrosion Testing of Steel, Transactions of Electrochemical Society, Vol. 85, pp. 297-303.

Larrabee C. P and Coburn S. K (1961)

The Atmospheric Corrosion of Steels as Influenced by Changes in Chemical Composition, First International Congress on Metallic Corrosion, London, pp. 276-285.

Larrabee C. P (1966)

Corrosion Resistance of High-Strength Low Alloy Steels as Influenced by Composition and Environment, U.S. Steel Corporation, Research and Development Laboratory.

LeDoux F. S, Levine A. S and Kamp R. N (1983)

New York State Department of Transportation Bridge Inspection and Rehabilitation Design Program, Transportation Research Record 899, pp. 35-43.

Lee B. S and Strand T. C (1990)

Profilometry with a Coherence Scanning Microscope, Applied Optic, Vol. 29, pp. 3784-3788.

Legault R. A and Leckie H. P (1974)

Effect of Alloy Composition on the Atmospheric Corrosion Behaviour of Steel Based on a Statistical Analysis of the Larrabee-Coburn Data Set, Corrosion in Natural Environments, ASTM STP 558, American Society for Testing and Materials, pp. 334-347.

Lichtenstein A. G (1983)

Remaining Useful Life of Bridges, Draft Proposal Submitted to the ASCE Committee on Steel Bridges.

Lindley T. C, McIntyre P and Trant P. J (1982)

Fatigue Crack Initiation at Corrosion Pits, Metals Technology, Vol. 9, pp. 135-142.

Lister N. W and Addis R. R (1978)

Field Observation of Rutting and Practical Implications, Paper Presented at the Symposium on Rutting in Asphalt Concrete Pavements, Annual Meeting of the Transportation Research Board, Washington D.C.

Luk F, Huynh V and North W (1989)

Measurement of Surface Roughness by a Machine Vision System, Journal of Physics, Society of Instrumentation, Vol. 22, pp. 977-980.

Maddox S. J (1991)

Fatigue Strength of Welded Structures, Second Edition, Woodhead Publishing Ltd, Cambridge, UK.

Majumdar A and Bhushan B (1990)

Role of Fractal Geometry in Roughness Characterization and Contact Mechanics of Surfaces, ASME Journal of Tribology, Vol. 112, pp. 205-216.

Manning D. G (1984)

Accelerated Corrosion in Weathering Steel Bridges, Canadian Structural Engineering Conference, Canadian Steel Construction Council, Willowdale, Ontario.

Martin L. H and Purkiss J. A (1992)

Structural Design of Steelwork to BS 5950, First Edition, Edward Arnold, London.

Matsumoto M and Okada S (1994)

Effects on Corrosion Deterioration of Steel Bridge by Typhoon, Report, Department of Civil Engineering, Kyoto University, Japan.

Mayfield M. E and Maxey W. A (1982)

Weld Zone Characteristics, NG-18 Report No. 130, American Gas Association, Arlington, Virginia.

McCool J. I (1987)

Relating Profile Instrument Measurements to the Functional Performance of Rough Surfaces, Journal of Tribology, Vol. 109, pp. 264-270.

McCrum R. L, Arnold C. J and Dexter R. P (1985)

Current State Report Effects of Corrosion on Unpainted Weathering Steel Bridges, Testing and Research Division, Research Report No. R-1255, Michigan Department of Transportation, Lansing.

McKenzie M (1978)

The Corrosion Performance of Weathering Steel in Highway Bridges, Transport and Road Research Laboratory, TRRL Laboratory Report 857, Bridge Construction Division, Structures Department, Crowthorne, UK.

McKenzie M (1981)

Monitoring of Weathering Steel Structures- the Induction Ultrasonic Thickness Tester, Transport and Road Research Laboratory, TRRL Laboratory Report 677, Bridge Construction Division, Structures Department, Crowthorne, UK.

McKenzie M (1990)

The Corrosion of Weathering Steel Under Real and Simulated Bridge Decks, Transport and Road Research Laboratory, TRRL Research Report 233, Bridge Construction Division, Structures Department, Crowthorne, UK.

Miner M. A (1945)

Cumulative Damage in Fatigue, Transaction of American Society of Mechanics. Journal of Applied Mechanics, Vol. 67, No. 3, pp. 159-164.

Moore D. F (1969)

A History of Research on Surface Texture Effects, Wear, Vol. 13, pp. 381-412.

Myers N. O (1962)

Characterisation of Surface Roughness, Wear: An International Journal on the Science and Technology of Friction, Lubrication and Wear, Vol. 5, pp. 182-189.

Naeemi A. H and Albrecht P (1984)

Atmospheric Corrosion of Weathering Steel, 9th International Congress on Metallic Corrosion Proceeding, Vol. 1, Toronto, Canada.

Nakayama Y (1972)

Durability of Paint on Atmospheric Corrosion Resistant Steels, Chemical Abstracts, Vol. 76.

National Cooprative Highway Research Program, NCHRP (1979)

Bridge Deck Joint-Sealing Systems, Evaluation and Performance Specification, NCHRP Report 204, Transportation Research Board, National Research Council, Washington, D.C.

National Cooprative Highway Research Program, NCHRP (1982)

NCHRP Research on bridge Engineering, Research Results Digest, No. 132, p. 2.

Nayak P. R (1973)

Random Process Model of Rough Surface in Plastic Contact, Wear, Vol. 26, pp. 305-333.

Neuber H (1961)

Theory of Stress Concentration for Shear-Strained Prismatical Bodies with Arbitrary Non-Linear Stress-Strain Law, Journal of Applied Mechanics. Transactions of the ASME, Vol. 28, pp. 544-550.

Ogilvy J. A (1991)

The Theory of Wave Scattering from Random Rough Surfaces, Hilger. Bristol, UK.

Osgood C. C (1970)

Fatigue Design, John Wiley & Sons, New York and Toronto.

Out J. M. M, Fisher J. W and Yen B. T (1984)

Fatigue Strength of Weathered and Deteriorated Riveted Members, Transportation Research Record 950, Vol. 2, Transportation Research Board, pp. 10-22.

Owen J. V (1990)

Are Lasers Measuring Up?, Manufacturing Engineering, pp. 60-67.

Owens G. W and Knowles P. R (1992)

Corrosion Rate, Steel Designers' Manual, The Steel Construction Institute, Fifth Edition, Edited by Blackwell Scientific Publications, London.

Papoulis A (1965)

Probability Random Variable and Stochastic Processes, McGraw-Hill, New York.

Pardue W. M, Beck F. H and Fontana M. G (1961)

Propagation of Stress Corrosion Cracking in a Magnesium-Base Alloy as Determined by Several Techniques, Transaction of the American Society of Metals, Quarterly 54, pp. 539-549.

Paris P. C, Gomez M. P and Anderson W. E (1961)

A Rational Analytical Theory of Fatigue, The Trend in Engineering, Vol. 13, No. 1, pp. 9-14, University of Washington, Seattle, Washington.

Parsons D (1978)

Beam Cracks Close 39th Street Bridge, Daily Press, Newport News, Hampton, Virginia.

Payer J. H and Staehle R. W (1971)

Localized Attack on Metal Surfaces, Corrosion Fatigue: Chemistry, Mechanical and Microstructure, National Association of Corrosion Engineers, Conference at the University of Connecticut, pp. 211-269.

Pearce J. T. H (1997)

Corrosion-a Layman's Guide, Insight, The Journal of British Institute of Non-Destructive Testing, Vol. 39, No. 1, pp. 10-16.

Peterson R. E (1974)

Stress Concentration Factors, John Wiley & Sons, New York.

Porter R (1996)

Thickness Measurement of Hull Structures, Lloyds Register, Paper Presented at the British Institute of Non-Destructive Testing Seminar.

Porter R (1997)

Ultrasonic Thickness Surveys on Tankers and Bulk Carriers, Insight, The journal of the British Institute of Non-Destructive Testing, Vol. 39, No. 1, pp. 21-23.

Posey C. J (1946)

Measurement of Surface Roughness, Mech. Eng., Vol. 68, pp. 305-306.

Press W. H, Teukolsky S. A, Vetterling W. T and Flannery B. P (1992)

Numerical Recipes, Second Ed., Cambridge University Press, New York.

Purvis R. L and Berger R. H (1983)

Bridge Joint Maintenance, Transportation Research Record, No. 899, pp. 1-10.

Ramachandra Murthy D. S (1993)

Corrosion Fatigue Behaviour of Steel Tubular Joints of Offshore Structures, Ph.D thesis, Anna University, Madras, India.

Ramachandra Murthy D. S, Madhava Rao A. G and Santhakumar A. R (1994)

Corrosion Fatigue of Stiffened Offshore Steel Tubular Joints, Journal of Structural Engineering, ASCE, Vol. 120, No. 7, pp. 1991-2010.

Reece B (1995)

Advanced Video Measurement System, Brian Reece Scientific Limited, Berkshire.

Righiniotis J (1992)

Tension Members, Steel Designers' Manual, Owens, G. W and Knowles, P. R, 1992, The Steel Construction Institute, Fifth Edition, Edited by Blackwell Scientific Publications, London, p. 352.

Roark R. J (1965)

Formula for Stress and Strain, Fourth Edition, McGraw-Hill, New York.

Roark R. J and Young W. C (1989)

Formula for Stress and Strain, Sixth Edition, McGraw-Hill, New York.

Roberts R, Irwin G. R, Fisher J. W, Chen G, Chakravarti P, Ma Z. Z and Yen B. T (1986)

Corrosion Fatigue Characteristics of Bridge Steels, Vol. I, Executive Summary, Federal Highway Administration, Report FHWA/RD-86/165, Washington, D.C.

Roderick R. L and Truell R (1952)

The Measurement of Ultrasonic Attenuation in Solid by the Pulse Technique and some Results in Steel, Journal of Applied Physics, Vol. 23, No. 2, pp. 232-237.

Rowe L. C (1974)

Measurement and Evaluation of Pitting Corrosion, Galvanic and Pitting Corrosion-Field and Laboratory Studies, ASTM STP 576, pp. 203-216.

Sandor B. I (1972)

Fundamental of Cyclic Stress and Strain, University of Wisconsin Press, Madison, WI.

Sarveswaran V (1996)

Remaining Capacity of Corrosion Damaged Steel Structures, Ph.D Thesis, Department of Civil Engineering, University of Bristol, UK.

Sawant S. S, Wagh A. B and Venugopalan V. P (1989)

Corrosion Behaviour of Mild Steel in Offshore Waters of the Arabian Sea, Corrosion Prevention and Control, Scientific Surveys Ltd., Bucks, England, pp. 44-47.

Sayles R. S and Thomas T. R (1978)

Surface Topography as a Non-Stationary Random Process, Nature, Vol. 271, pp. 431-434.

Scantlebury J. D, Callow L and De Sousa J. D (1980)

Inhibition of the Corrosion of Mild and low-Alloy Steel by Zinc Phosphate Pigments, Corrosion and Protection Centre, University of Manchester Institute of Science and Technology, Manchester, England.

Scheffey C. F and Cayes L. R (1974)

Model Tests of Modes of Failure of Joint C13N of Eyebar Chain, Point Pleasant Bridge Investigation, Federal Highway Administration Report No. FHWA-RD-74-19, Department of Transportation, Washington, D.C.

Schlesinger G (1942)

Surface Finish, Institute of Production Engineers, London.

Schmitt R. J and Mathay W. L (1967)

Tests Show Performance of Low Alloy Steel in Chemical Plant Environments, Material Protection, Vol. 6, No. 9, pp. 37-42.

Schorsch H (1958)

Gutebestimung an Technichen Oberflachen, Wissenschaftliche, Stuttgart.

Schutz W and Heuler P (1989)

Advances in Fatigue Science and Technology, Proceedings of the NATO Advanced Study Institute, Eds. Branco C. M and Rosa L. G, Klueven Academic Publishers, Dordrecht, Portugal, pp. 177-219.

Scully J. C (1966)

The Fundamentals of Corrosion, First Edition, Pergamon Press Ltd., Oxford, London, pp. 156-186.

Scully J. C (1990)

The Fundamentals of Corrosion, Third Edition, Pergamon Press Ltd., Oxford, England.

Sereda P. J (1974)

Weather Factors Affecting Corrosion of Metals, Corrosion in Natural Environments, ASTM STP 558, pp. 7-22.

Silk M. G (1984)

Ultrasonic Transducer for Non-Destructive Testing, Published by Adam Higler, Bristol.

Silk M. G, Stonehamm A. M and Temple J. A. G (1987)

The Reliability of Non-Destructive Inspection, Published Adam Higler, Bristol.

Simpson R (1992)

Fatigue, Steel Designers' Manual, Owens, G. W, Knowles, P. R, 1992. The Steel Construction Institute, Fifth Edition, Edited by Blackwell Scientific Publications. London, pp. 226-241.

Slomba A. F, Hull-Allen C. G, Takacs P. Z, Evans C. J and Bennett J. M (1992)

Flatness Intercomparison Measurements Made on an Optical Flat, In Optical Fabrication and Testing Workshop, Vol. 24, Optical Society of American Technical Digest Series, Washington D.C.

Smith J. W (1988)

Vibration of Structures (Applications in Civil Engineering Design), Chapman and Hall Ltd (UK), pp. 300-320.

Smith J. W (1993)

Mechanical Properties of Samples of Structural Steel Affected Severely by Corrosion, Report No. UBCE/JWS/93/01, Department of Civil Engineering, University of Bristol.

Sobanjo J. O, Stukhart G and James R. W (1994)

Evaluation of Projects for Rehabilitation of Highway Bridges, Proceedings of the American Society of Civil Engineers, Journal of Structural Engineering, Vol. 108, pp. 81-99.

Soderberg C. R (1950)

Handbook of Experimental Stress Analysis, Edited by Hetenyi M, see (Chapter 10, Working Stresses), pp. 449-450.

Stanke F. E and Liang K. K (1991)

Profiling High-Angle Surfaces with Focused Transducers and Time-of-Flight Measurements, Proceedings of IEEE 1990, Ultrasonic Symposium, McAvoy B. R Edited by Institute of Electrical and Electronics Engineers, New York, 1991, pp. 1053-1056.

Stanley R. P, Snowden C and Hayward J. D (1995)

Extending the Useful Life of Tower Bridge in London, International Association for Bridge and Structural Engineering Symposium, Vol. 73/1, pp. 83-88.

Stewart D and Tulloch D. S (1968)

Principles of Corrosion and Protection, Published by Macmillan Press Ltd., London.

Still P. B and Jordan P. G (1980)

Evaluation of the TRRL High-Speed Profilometer, Department of the Environment, Transport and Road Research Laboratory, TRRL Laboratory Report LR 992, Crowthorne, UK.

Suresh S (1991)

Fatigue of Materials, Published by Cambridge University Press, Cambridge, UK.

Talysurf Handbook

Operator's Handbook, Talysurf 10, Rank Taylor Hobson, England, p. 7.

Thomas T. R (1975)

Recent Advances in the Measurement and Analysis of Surface Microgeometry, Wear, Vol. 33, pp. 205-233.

Thomas T. R (1982)

Rough Surfaces, Longman, New York.

Townsend H. E and Zoccola J. C (1982)

Eight Year Atmospheric Corrosion Performance of Weathering Steel in Industrial, Rural, and Marine Environments, Atmospheric Corrosion of Metals, ASTM STP 767, American Society for Testing and Materials, pp. 45-59.

Tsukizoe T and Hisakado T (1968)

On the Mechanism of Contact Between Metal Surfaces, Part 2. Transactions of ASME. Vol. 90E, p. 81.

Tsukizoe T (1970)

Metrology, Yohkendo, Tokyo, Japan, pp. 180-199.

Uhlig H. H (1973)

Distinguishing Characteristics of Pitting and Crevice Corrosion, Materials Protection and Performance, Vol. 12, No. 2, pp. 42-44.

Underwood E. E (1989)

Proceedings of the 7th International Conference on Fracture, Edited by Salama K, Pergamon Press, Oxford, p. 3391.

Van Eijnsbergen J. F. H (1979)

Weathering Steels Versus Ordinary Structural Steels as a Base for Paints, Cargo Systems International, Vol. 5, No. 6, pp. 101-103.

Whitehouse D. J (1996)

Optical Methods in Surface Metrology, Published by Society of Photographic Instrumentation Engineers.

Whitehouse D. J (1997)

Surface Metrology, Measurement Science and Technology, No. 8, pp. 955-972.

Williams D. A (1996)

Remote Monitoring of Crack Growth, Report No. 96/47, Department of Mechanical Engineering, University of Bristol, Bristol.

Williamson J. B. P (1967)

Topography of Solid Surfaces, Interdisciplinary Approach to Friction and Wear, Proceedings of a NASA-Sponsored Symposium, San Antonio, Texas, pp. 85-179.

Wohler A (1871)

Tests to Determine the Force Acting on Railway Carriage Axles and the Capacity of Resistance of the Axles, Engineering, Vol. 11, p 199.

Yamada K (1983)

Japanese Experience on Weathering Steel Bridges, Department of Civil Engineering, Nagoya University.

Yamada K, Kato M, Kondo A and Ishizaki H (1989)

Fatigue Assessment of Orthotropic Steel Decks of Box Girder Bridges, Pacific Structural Steel Conference, STEEL 2000, Gold Coast.

Yao W, Xia K and Gu Y (1995)

On the Fatigue Notch Factor, International Journal of Fatigue, Vol. 17, No. 4, pp. 245-251.

Yatchmenoff B and Compton R. D (1990)

Ceramic Surface-Analysis Using Optical Sections, Journal of American Ceramic Society Bulletin, Vol. 69, No. 8, pp. 1307-1310.

Yazdani N and Albrecht P (1983)

Crack Growth Rates of Structural Steels in Air and Aqueous Environments, Civil Engineering Report, University of Maryland, College Park, Maryland.

Yazdani N and Albrecht P (1989)

Crack Growth Rates of Structural Steels in Air and Aqueous Environments, Journal of Engineering Fracture Mechanics, Vol. 32, No. 6, pp. 997-1007.

Yazdani N and Albrecht P (1990)

Probabilistic Fracture Mechanics Application to Highway Bridges, Engineering Fracture Mechanics, Vol. 34, pp. 969-985.

Zhao Z and Haldar A (1996)

Bridge Fatigue Damage Evaluation and Updating using Non-Destructive Inspections. Engineering Fracture Mechanics, Vol. 53, No. 5, pp. 775-788.

Zuraski P. D and Johnson J. E (1984)

Research on the Remaining Life in Steel Bridges, ASCE Speciality Conference on Probabilistic Mechanics and Structural Reliability, Berkeley, CA, pp. 414-418.

Zuraski P. D (1986)

The Remaining Life in Deteriorated Steel Deck-Girder Highway Bridges, Ph.D Thesis, Department of Civil and Environmental Engineering, University of Wisconsin.

Appendix A

Design of simply supported composite welded plate girder bridge

As mentioned in Chapter 7 a simply supported composite welded plate girder bridge with uniform section was designed in order to investigate the applicability of the relationships developed for the remaining fatigue life of corroded steelwork structures.

Design data

General

Span	33 m
Skew	32^{o}
Carriageway	5.5 m wide (2 lanes)
Surfacing	100 mm thick minimum (including waterproofing)
Footways	1.5 m wide each side
Location	Central UK
Design life	120 years

Loading

Live loads:	HA	2 lanes (full loading on each lane)
	HB	30 units
	Footway	5 kN/m^2 (5 × 0.8 with HA or HB)
Unit weights:	Concrete	25 kN/m^3
	Surfacing	24 kN/m^3

Formwork:	0.5 kN/m^2 allowable for possible permanent formwork
Temperature:	Minimum shade air temperature -18^{o}C
Wind:	Maximum mean hourly wind speed 28 m/s

Design parameters

Steel (grade 50)	σ_y = 355 N/mm^2
	E_s = 205,000 N/mm^2
Concrete (grade 40)	σ_{cu} = 40 N/mm^2
	E_{cs} = 31,000 N/mm^2
	E_{cl} = 15,500 N/mm^2
Reinforcement (grade 40)	σ_{ry} = 460 N/mm^2
	E_r = 200,000 N/mm^2

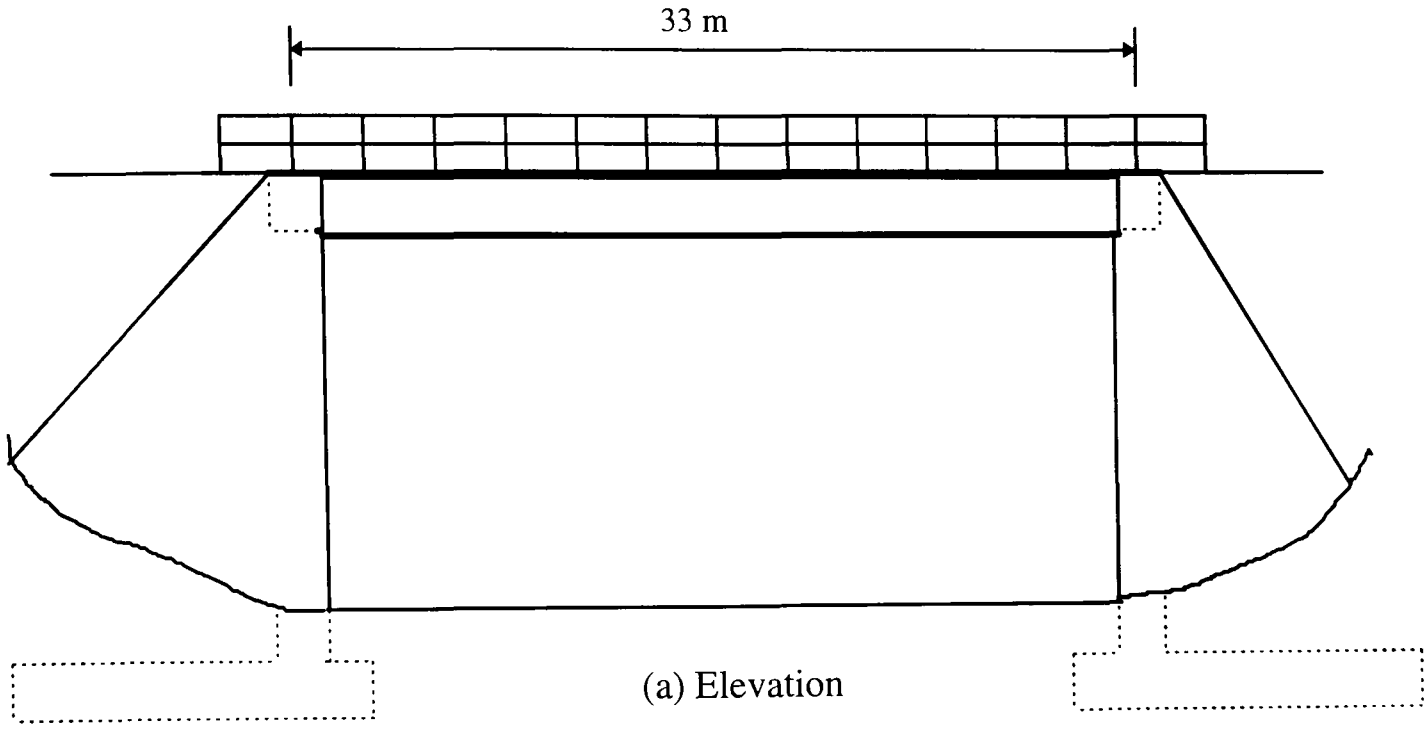

(a) Elevation

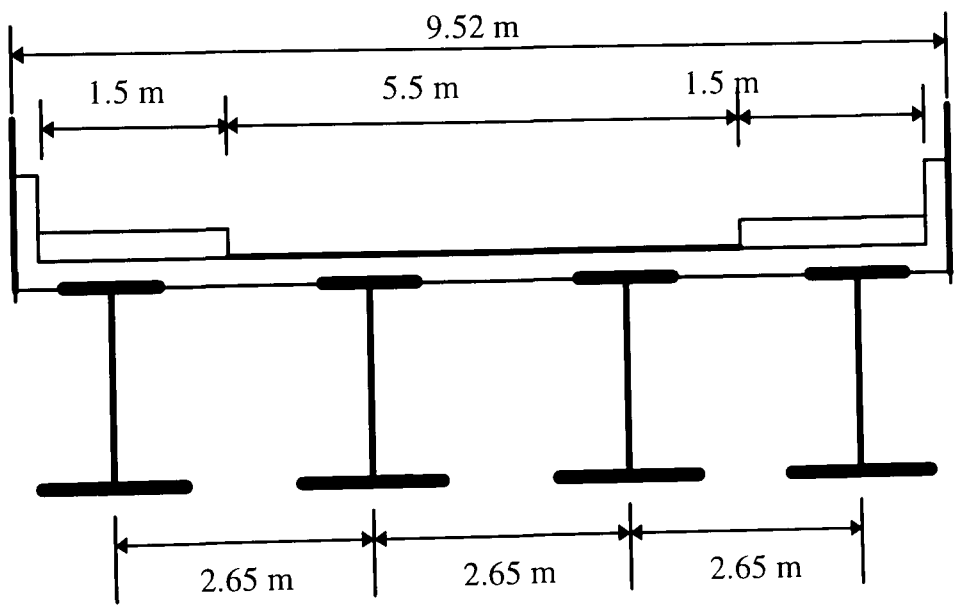

(b) Cross-section of composite steel girders and concrete deck of the bridge

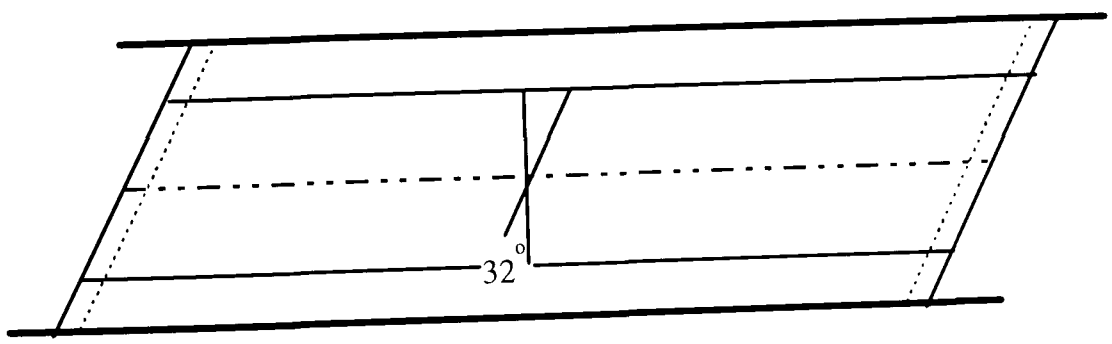

(c) plan

Figure A.1 Details of composite steel girder bridge.

Design moments

The maximum bending moments for the design of beams have been calculated based on ultimate limit state design method.

Exterior Girder

The total dead load due to the self weight of plate girder, deck, footway, road surfacing, parapet, fascia and formwork is

$W_{DL} = 33.7$ kN/m

and the total bending moment due to the overall dead load is

$M_{DL} = 4587$ kN.m

The total ultimate limit state of live load bending moment due to HA loading which is a uniformly distributed load and HB loading which is an abnormal heavy vehicle (see BS 5400: Part 2, 1978) are

$M_{HA} = 1024$ kN.m

$M_{HB} = 1261$ kN.m

The bending moment due to the live load of footway is

$M_{FT} = 1006$ kN.m

In the design usually one of the values of HA or HB will be used, the one which has the highest value. Therefore, the maximum total bending moment for the design of exterior girder, $(M)_{Ext}$ is as follows:

$$(M)_{Ext} = (M_{DL})_{Ext} + (M_{HB})_{Ext} + (M_{FT})_{Ext}$$

$$= 4587 + 1261 + 1006$$

$$= 6854 \text{ kN.m}$$

Interior Girder

The total dead load due to the self weight of plate girder, deck, footway, road surfacing, parapet, fascia and formwork is

W_{DL} = 37.75 kN/m

the total bending moment is

M_{DL} = 5139 kN.m

The total ultimate limit state of live load bending moment due to HA loading and HB loading are

M_{HA} = 6321 kN.m

M_{HB} = 6188 kN.m

The bending moment due to the live load of footway is

M_{FT} = 220 kN.m

In the design usually one of the value of HA or HB will be used, the one which has the highest value. Therefore, the maximum total bending moment for the design of interior girder, $(M)_{Int}$ is as follows:

$$(M)_{Int} = (M_{DL})_{Int} + (M_{HA})_{Int} + (M_{FT})_{Int}$$

$$= 5139 + 6321 + 220$$

$$= 11680 \text{ kN.m}$$

Design of plate girder sizing

The value of design bending moment for interior girder is greater than exterior girder because it is more heavily loaded. Therefore, the dimensions of the interior girder have been determined based on its maximum bending $(M)_{Int}$ = 11680 kN.m. The same section

size will be adopted for the exterior girders. The girder dimensions are shown in Figure A.2.

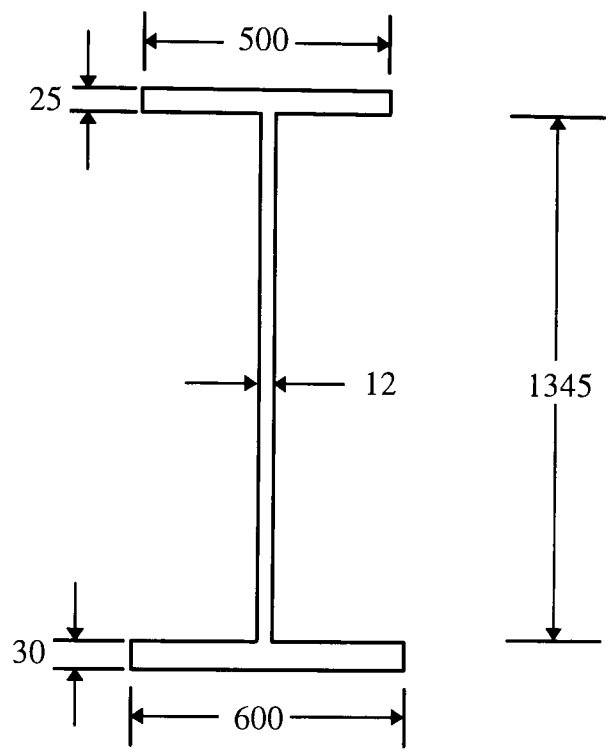

Figure A.2 Dimensions of girder (all dimensions are in millimetres)

The important properties of the section are the section modulus, S, and the second moment of area, I. The value of I is determined on the basis of the transformed section. The transformed section is calculated by transforming the effective concrete slab area into an equivalent steel area. This transformation is accomplished by dividing the effective width of the slab by the value of the modular ratio of steel to concrete ($\alpha = E_s/E_c$). The value of α for long-time dead loads is greater than the α for short-term loading such as live load and impact. The following section properties are calculated from transformed effective width of the slab from Figure A.3, based on the short-term loading ($\alpha = 6.60$):

$\overline{y} = 417$ mm $\quad y_c = 197$ mm $\quad S_c = 0.208$ m^3

$I = 0.041$ m^4 $\quad y_T = 1203$ mm $\quad S_T = 0.0341$ m^3

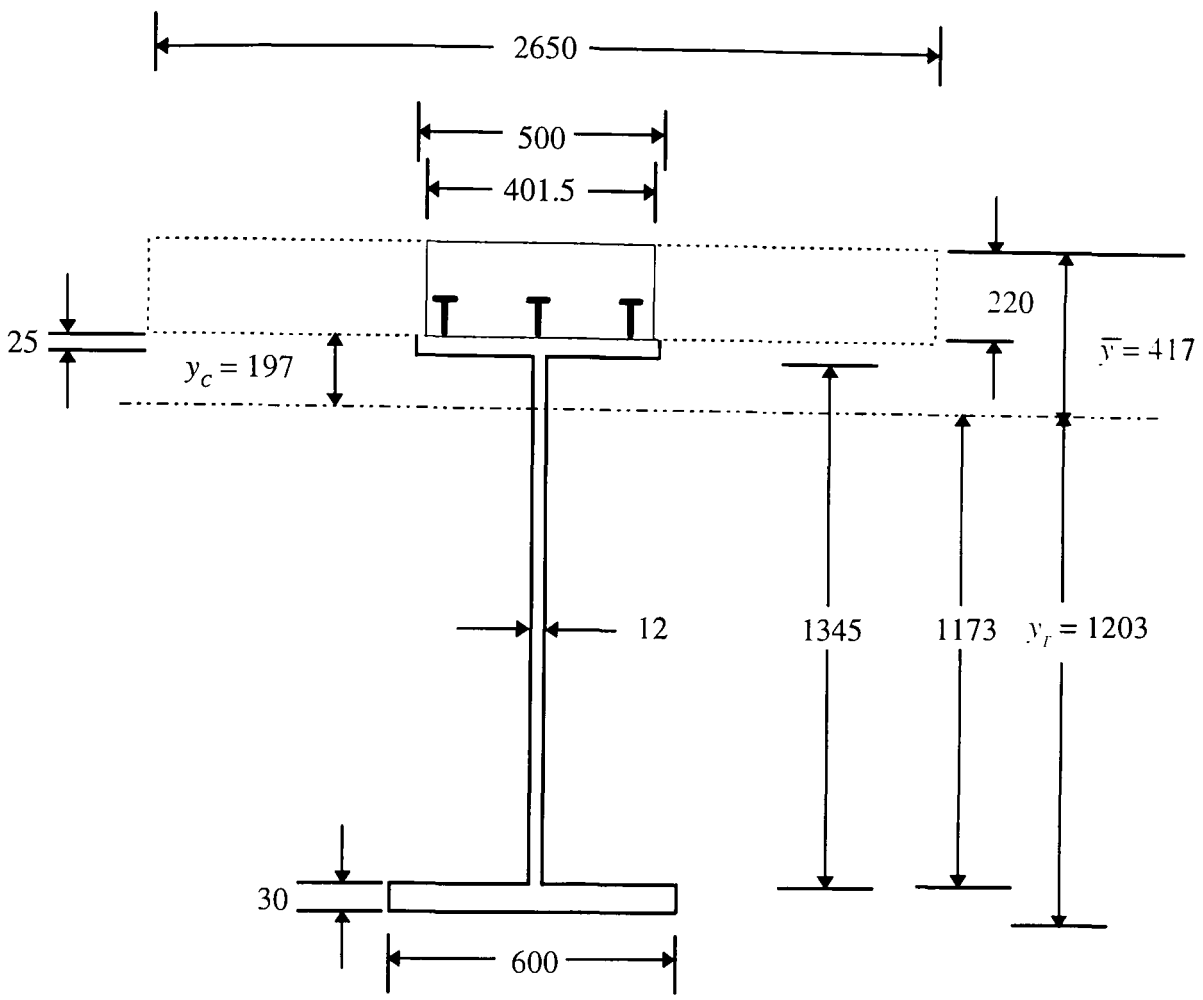

Figure A.3 Cross-section of composite section for interior girder (all dimensions are in millimetres).

In order to investigate the plastic resistance of the composite section, short-term modulus has been used since the section is compact (BS 5400: Part 3/9.3.7). The position of the neutral axis is determined such that there are equal and opposite force above and below it at ultimate limit state. It was found that the position of neutral axis is just within top flange. The new section properties were calculated based on the new position of the neutral axis. The total moment of resistance in bending was found to be as follows:

interior girder $(M_R)_{Int} = 12037$ kN.m

exterior girder $(M_R)_{Ext} = 11810$ kN.m

Table A.1 Bending moments at midspan of interior girder due to the applied loads at ultimate limit state.

Applied loads	Factor for ultimate limit state	Bending moment (kN.m)	Factored bending moment (kN.m)
Live load (HB)	1.30	2438	does not govern
Live load (2 lanes HA)	1.50	2681	4022
Live load (footway)	1.50	402	603
Dead load (steel girder)	1.05	513	539
Dead load (slab)	1.15	1985	2283
Dead load (asphalt)	1.75	592	1036
Dead load (footway, parapet and formwork)	1.20	784	941
Total			9424

The following design checks have been carried out according to BS 5400:

a) shear in webs and connectors (studs),

b) web buckling,

c) transverse bracing at the supports,

d) intermediate transverse bracing between the main girders and

e) bearing stiffeners.

See Iles (1991) for detail design calculations.

Fatigue assessment

An attempt has been made to verifying the remaining fatigue life of corroded steel bridges by using the empirical formula developed in term of pit depth. Therefore, a simply supported composite welded plate girder bridge with uniform cross section has been designed in order to present an approach to quantifying the remaining fatigue life due corrosion. The design is according to the BS 5400 and the Department of Transport specification (a summary of the design procedure is given in separate section).

The only regions of simply supported highway bridges which are likely to need to be considered for fatigue are the tension flange in midspan when there are welded attachments or bolt holes, the shear connectors and the bearing stiffeners. Fatigue detail classification relates to the potential defect at welds, holes or other discontinuities. The greater the defect the lower the stress range which can be tolerated for a given fatigue life. A complete range of classification is given in Table 17 of BS 5400: Part 10.

The continuous longitudinal butt weld, as in the web-to-flange joint of a beam (plate girder), presents no change of shape in the way of the main bending stress field and gives good fatigue strength. In this type of welds cracking usually initiates on the weld surface at stop and start positions, with automatic welding even these blemishes are absent. Therefore, in order to fabricate the plate girders, it has been assumed that continuous longitudinal butt welds were used (manually) to weld the flanges to the web. According to the BS 5400: Part 10, the fabricated steel girders can be classified as class D for fatigue assessment and the following values can be considered:

$K = 3.99 \times 10^{12}$

$m = 3.0$

The shear stud are considered as class S for fatigue assessment and the following values can be considered:

$K = 2.13 \times 10^{23}$

$m = 8.0$

There is a possible stress reversal at the midspan of the simply supported plate girder due to the vehicle loading. The maximum values of bending moment due to each vehicle listed in Table 7.3 are calculated then the stress range on the critical zone of the tension flange (at the weld, top of the bottom flange) has been computed based on the non-corroded modulus of section, S_T, for short-term design.